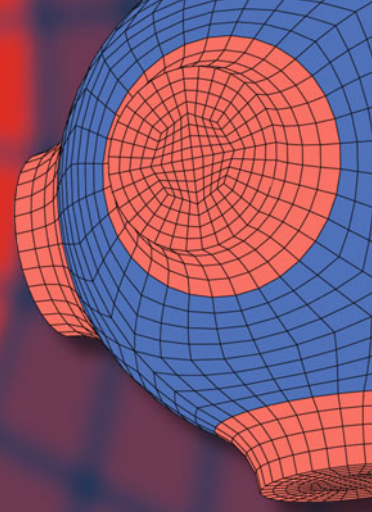Rocco Furferi
Rodorico Giorgi
Kate Seymour
Anna Pelagotti *Editors*

The Future of Heritage Science and Technologies

Materials Science

Springer

Advanced Structured Materials

Volume 179

Series Editors

Andreas Öchsner, Faculty of Mechanical Engineering, Esslingen University of
Applied Sciences, Esslingen, Germany

Lucas F. M. da Silva, Department of Mechanical Engineering, Faculty of
Engineering, University of Porto, Porto, Portugal

Holm Altenbach , Faculty of Mechanical Engineering, Otto von Guericke
University Magdeburg, Magdeburg, Sachsen-Anhalt, Germany

Common engineering materials are reaching their limits in many applications, and new developments are required to meet the increasing demands on engineering materials. The performance of materials can be improved by combining different materials to achieve better properties than with a single constituent, or by shaping the material or constituents into a specific structure. The interaction between material and structure can occur at different length scales, such as the micro, meso, or macro scale, and offers potential applications in very different fields.

This book series addresses the fundamental relationships between materials and their structure on overall properties (e.g., mechanical, thermal, chemical, electrical, or magnetic properties, etc.). Experimental data and procedures are presented, as well as methods for modeling structures and materials using numerical and analytical approaches. In addition, the series shows how these materials engineering and design processes are implemented and how new technologies can be used to optimize materials and processes.

Advanced Structured Materials is indexed in Google Scholar and Scopus.

Rocco Furferi · Rodorico Giorgi · Kate Seymour ·
Anna Pelagotti

Editors

The Future of Heritage Science and Technologies

Materials Science

Springer

Editors
Rocco Furferi 🆔
Ingegneria Industriale
Università di Firenze
Firenze, Italy

Rodorico Giorgi 🆔
Dipartimento di Chimica 'Ugo Schiff'
University of Florence
Florence, Italy

Kate Seymour 🆔
Stichting Restauratie Atelier Limburg
Maastricht, The Netherlands

Anna Pelagotti 🆔
European Commission, Bruxelles
Italian National Council of Research
Seconded to the European Research
Council
Firenze, Italy

Preface and Acknowledgements

This book presents a selection of contributions, dealing with the application of Mechanical Engineering in the field of Cultural Heritage, presented at the *3rd Florence Heri-Tech International Conference*, held on May 16–18, 2022, in Firenze, Italy.

Organized under the patronage of the University of Florence with the support of the Department of Industrial Engineering, *Florence Heri-Tech* gathered researchers and experts in the field of "heritage science and related technologies" to disseminate their recent research at an international level as well as to draw new inspiration. The Conference was part of the *2022 Florence International Biennial for Art and Restoration*, an international event attracting prestigious institutions and companies and creating a unique opportunity to bring together the academic world with industry.

The overarching goal of *Florence Heri-Tech* is to promote European mobility and cooperation among researchers, students, and practitioners, to further Europe's growth as a multicultural society, and to promote the idea that scientific-cultural research must be an important part of society. Furthermore, the Conference intends to foster international networks between universities, training institutions, and businesses in order to foster long-term partnership prospects.

More than 80 experts, coordinated by General Chairs and supported by a high-level Technical and Scientific Committee, were involved in the review process, which led to the selection of 22 papers (out of 101 papers submitted at the Conference and 146 abstracts received by the Scientific Committee). The overall number of authors involved was 154. Contributions focus on multi-disciplinary and interdisciplinary research concerning the use of innovative materials, methods, and technologies for documenting, managing, preserving, and communicating cultural heritage.

The editors would like to personally thank everyone participating in the review process for their dedication and skill at the service of the Conference. Special appreciation goes to the members of the Technical and Scientific Committees who made it possible for the Conference to take place.

The Conference prestige was enhanced by the participation of Honorary Chairs: Prof. Dei, Prof. Baglioni, Prof. Bonsanti, Prof. Cappellini, Prof. Cather, Prof. Ciatti, Prof. Colombini, Prof. Rodrigues, Prof. Santos, and Prof. Sgamellotti. General Chairs

extend their thanks to all authors, speakers, and those persons whose labor, financial support, and encouragement made the Florence Heri-Tech event possible.

Florence, Italy   Rocco Furferi
Florence, Italy   Anna Pelagotti
Maastricht, The Netherlands   Kate Seymour
Florence, Italy   Rodorico Giorgi

Organization Committee

General Chairs

Rocco Furferi, Lapo Governi, Yary Volpe, Rodorico Giorgi, University of Florence
Anna Pelagotti, Executive Agency of the European Research Council
Kate Seymour, Stichting Restauratie Atelier Limburg (SRAL), Maastricht

Organizing Committee

Elena Amodei, Lucia Maranzana
Francesco Gherardini, University of Modena
Rocco Furferi, University of Florence

Honorary Chairs

Piero Baglioni, University of Florence
Giorgio Bonsanti, University of Florence
Vito Cappellini, University of Florence
Sharon Cather, The Courtauld Institute of Art, London
Marco Ciatti, Opificio delle Pietre Dure, Florence
Maria Perla Colombini, CNR-ICVBC. National Research Council of Italy, Institute
for the Conservation and Valorization of Cultural Heritage
Luigi Dei, Rector of the University of Florence
Jose Delgado Rodrigues, Laboratorio Nacional De Engenharia Civil, Lisbon
Mauro Matteini, Former Director of ICVBC, Istituto per la Conservazione e la
Valorizzazione dei Beni Culturali—CNR
Mario Primicerio, University of Florence

Pedro Santos, Fraunhofer Institute for Computer Graphics Research IGD, Darmstadt
Antonio Sgamellotti, University of Perugia

Technical and Scientific Committee

Hani M. Al Huneidi, International Cultural Heritage Specialist, Jordan
Fabrizio Argenti, Department of Information Engineering, University of Florence
Carla Balocco, Industrial Engineering Department, University of Florence
Umberto Berardi, Canada Research Chair, Ryerson University
Francesco Bianconi, Department of Engineering, University of Perugia
Michele Bici, Department of Mechanical and Aerospace Engineering of Sapienza, University of Rome (Italy)
Francesco Buonamici, Department of Industrial Engineering, Unifi
Andrea Camilli, Soprintendenza per i Beni Archeologici della Toscana, Department Member
JoAnn Cassar, University of Malta
Duccio Cavalieri, Department of Biology, University of Florence
Angelo Corallo, Department of Innovation Engineering, Unisalento
Sidney Cheung, The Chinese University of Hong Kong, Hong Kong
Corinna Del Bianco, Director of the International Institute Life Beyond Tourism and Adviser of the Romualdo Del Bianco Foundation
Alberto Del Bimbo, Department of Information Engineering, University of Florence
Luca Di Angelo, Department of Industrial Engineering University of L'Aquila
Fabio Bruno, Department of Mechanical Energetics and Management Engineering, University of Calabria
Leila Es Sebar, Ph.D. in Metrology, Politecnico di Torino
Federica Fernandez, IEMEST, Istituto EuroMediterraneo di Scienza e Tecnologia, Director of Department NIMA
Francesco Ferrise, Department of Mechanics Polytechnic of Milan
Marco Fioravanti, Agrifood Production and Environmental Sciences Agriculture, Food and Forestry Systems University of Florence
Bernard Frischer, Department of Informatics, Indiana University
Leire Garmendia Arrieta, Faculty of Engineering in Bilbao University of the Basque Country (UPV/EHU)
Francesco Gherardini, Department of Engineering "Enzo Ferrari", University of Modena and Reggio Emilia
Giacomo Goli, Agrifood Production and Environmental Sciences Agriculture, Food and Forestry Systems, University of Florence
Gabriele Guidi, Department of Mechanics Polytechnic of Milan
Susan Hazan, Coordinator, Israel Consortium for Digital Heritage
Ernesto Iadanza, University of Florence

Luca Lanzoni, Architect and Urban Planner, International Expert/Lead Expert in the Field of Cultural Heritage Enhancements, UPCT Polytechnical University of Cartagena, Spain

Mariangela Lazoi, Department of Innovation Engineering, Unisalento

Susan Macdonald, Getty Conservation Institute, Los Angles

Tomas Markevicius, University of Amsterdam

Pedro Martín Lerones, Heritage Area Manager, CARTIF Technology Center, Spain

Nina Olsson, Art Conservation, Portland, Oregon, USA

Alessandro Patelli, Department of Physics and Astronomy "Galileo Galilei", University of Padua

Anselmo Pavia, Applied Computer Group, Computer Science Department, Federal University of Maranhão, Brazil

Marcello Pellicciari, University of Modena and Reggio Emilia

María Jesús Peñalver Martínez, Department of Architecture and Building Technology, Universidad Politécnica de Cartagena

Vincenzo Armando Razionale, University of Pisa Department of Civil and Industrial Engineering

Alessandro Ridolfi, Department of Industrial Engineering at the University of Florence

Cristiano Riminesi, Scienze del patrimonio culturale. Studio e sviluppo di tecniche e metodologie per la conservazione dei beni culturali, CNR Italian National Research Council

Kate Seymour, Stichting Restauratie Atelier Limburg, Maastricht, The Netherlands

Alba Patrizia Santo, Earth Sciences Department of University of Florence

Piero Tiano, Institute for the Conservation and Valorization of Cultural Heritage (ICVBC)

Grazia Tucci, Department of Civil, Constructional, and Environmental Engineering

Francesca Uccheddu, Department of Industrial Engineering, University of Florence

Vaccaro, Vincenzo, Opera del Duomo, Florence

Contents

Methods and Instruments for the Conservation Diagnosis and Treatment

Governance Methods for Cultural Heritage

Chapter 1
Prioritization Methodology for Resilience Enhancement of Historic Areas Facing Climate Change-Related Hazards

Estibaliz Briz ⬤**, Leire Garmendia** ⬤**, Laura Quesada-Ganuza** ⬤**,**
Ane Villaverde ⬤**, Irantzu Alvarez** ⬤**, and Aitziber Egusquiza** ⬤

Abstract It is demonstrated that climate change is leading to intense and frequent extreme events. As a consequence, the impact on cultural heritage has increased, accelerating its deterioration. Climate-related hazards that can affect historic areas are dependent on both the nature of the risk and the specific characteristics of the heritage that is under threat, as well as the inherent vulnerability of the geographical environment and historic area. Conservation interventions at historic sites are generally focused on improving their resilience and minimizing any long-term deterioration of materials and works of art. However, conservation interventions are rarely focused on responding to the threat of sudden damage during emergency management phases. In these scenarios, a quick response is crucial when selecting the most appropriate intervention from the different solutions and the very many factors that they may take into account. The aim of this research is to develop a multi-criteria prioritization methodology that supports the intervention decision. The prioritization methodology entailed the consideration of specific scenarios and hazard types and their characteristics and the application of MIVES methodology together with the analytical

E. Briz (✉) · L. Garmendia · L. Quesada-Ganuza · A. Villaverde
Department of Mechanical Engineering, University of the Basque Country UPV/EHU, Plaza Ingeniero Torres Quevedo, 48013 Bilbao, Spain
e-mail: estibaliz.briz@ehu.eus

L. Garmendia
e-mail: leire.garmendia@ehu.eus

L. Quesada-Ganuza
e-mail: laura.quesada@ehu.eus

A. Villaverde
e-mail: ane.villaverde@ehu.eus

I. Alvarez
Department of Graphic Design and Engineering Projects, University of the Basque Country UPV/EHU, Rafael Moreno "Pitxitxi", 48013 Bilbao, Spain
e-mail: irantzu.alvarez@ehu.eus

A. Egusquiza
TECNALIA, Basque Research and Technology Alliance (BRTA), Parque Tecnológico De Bizkaia, Astondo Bidea, Edificio 700, 48160 Derio, Spain
e-mail: aitziber.egusquiza@tecnalia.com

hierarchy process (AHP). Technical, socioeconomic, cultural, and environmental aspects were then weighted to produce a prioritization index for decision-making in response to each scenario.

Keywords Cultural and natural heritage · Climate change · Hazards · Adaptive solutions · Prioritization methodology

1.1 Introduction

It is a fact that atmospheric greenhouse gas emissions are a major contributory cause of climate change. The rise in global mean surface temperature is evidence of climate change, and it is likely that the limit of 1.5 °C in relation to pre-industrial periods will have been exceeded at the end of the twenty-first century [1]. In 2019, global average temperature increased by 1.1 °C compared to pre-industrial levels [2]. This value is very close to the limit of 1.5º with respect to pre-industrial levels for the end of the twenty-first century [1]. In 2014, the fifth report from the Intergovernmental Panel on Climate Change (IPCC) [3] was published. According to the IPCC report and considering the RCP8.5 scenarios, average mean temperature increases of 2 °C and 3.7 °C were, respectively, estimated for 2065 and for 2100; however, according to the data published in 2021 for the sixth IPCC report [4], average mean temperature increases of 2.4 °C and 4.4 °C are estimated for 2065 and 2100, respectively, considering the same scenario. Rising sea levels represent another climate change impact. In 2019, an 87.6 mm increase in sea levels was recorded in comparison with the sea levels recorded in 1993 [5]. In the fifth IPCC report, the estimated average values of rising sea levels for 2065 and 2100 were, respectively, 0.3 m and 0.63 m [3]; nevertheless, data published in 2021 that reported estimated sea level rises of 0.45 m and 0.9 m, respectively, for those same two years are even more discouraging.

In October, the climate change summit was held in Glasgow with the aim of reaching agreements to mitigate this situation. However, the pledges at that summit will be insufficient to achieve the objective defined in the Paris Agreement that set a limit of 1.5 °C with respect to pre-industrial levels before the end of twenty-first century. Based on new announcements at the summit, the experts estimated that we are now on a path toward temperature rises between 1.8 and 2.4 °C [6].

Considering the data that the experts have published, extreme weather and climate events are foreseen, such as heavy precipitation, heat waves, and droughts of increasing intensity and frequency.

Cultural and natural heritage are important for understanding human history and identity; unfortunately, it is threatened by many natural hazards caused by climate change. Evidence of the value attached to cultural and natural heritage is the different projects financed by the European Union through the EU Horizon 2020 program, such as SHELTER, HYPERION, ARCH, and Pro-tecCH2save [7–10]. Different heritage management methods have been developed within these projects. In addition, interventions at different levels and both guides and tools have been developed that will

be of assistance to the various decision-making bodies for the preservation of both cultural and natural heritage and to enhance their resilience against extreme climate change-related weather events.

When an intervention is needed, various indicators of a diverse nature must be defined in order to select the most sustainable solution that will not affect the value of the asset. These indicators are related to cost, invasiveness of the solution, damage to the heritage, CO_2 emissions, etc. It is a task that complicates any comparison of all the possible solutions on the same scale that must be implemented to improve the resilience of historic areas facing climate change-related hazards. Moreover, stakeholders of varied profiles participate in the decision-making process, adding this aspect to the difficulty of ensuring objective and sustainable decisions [11].

The very diverse criteria under analysis can be processed with a multi-criteria decision-making (MCDM) method, in which all of these criteria are combined, to produce an objective and sustainable assessment. The integrated value model for sustainable evaluation (MIVES from the Spanish acronym) implements the value function in the MCDM methodology, obtaining a standardized index with which solutions with indicators of a different nature may be compared [12, 13], thereby facilitating the selection the most sustainable solution. A choice of suitable indicators will make it possible to quantify the degree of sustainability of each action and select the most sustainable and resilient one, analyzing the entire value chain throughout its useful life.

In the present study, the results of work developed in the SHELTER project that is currently in progress are summarized. The aim of the study is to enhance the resilience and to promote the sustainable reconstruction of historic areas to cope with climate change and natural hazards on the basis of different possible solutions that are prioritized. The prioritization is based on MIVES methodology which uses a multi-attribute utility theory and a multi-criteria decision-making, including the value function definition and assigning weights by means of the analytic hierarchy process (AHP) [14, 15]. This methodology provides a prioritization index (PI) for each solution in a ranking that facilitates the decision-making process.

1.2 Prioritization Methodology Development

MIVES is based on a multi-criteria methodology that enables to compare indicators of different nature. The methodology first evaluates the model and, then, generates the different alternatives. This procedure makes possible to evaluate each alternative objectively. The outcome is an objective index for each alternative with which they are ranked. MIVES methodology together with AHP was used for the development of the prioritization methodology in five steps:

1. *Definition of the requirements tree.* The information is organized into a hierarchical structure. In this case, there are two levels of information. The top and the lowest levels are, respectively, defined with criteria and with indicators. Figure 1.1 defines the requirements tree used for the prioritization of the solutions. The tree is firstly defined with the prioritization criteria and then the indicators to evaluate each criterion. Four criteria were considered as follows: type of adaptive solution criterion, technical criterion, cultural/natural preservation criterion, and circular economy criterion. These criteria were designed to collect relevant aspects (cultural, technical, social, environmental, and economic) that can be improved through the implementation of emergency solutions that support sustainable development [16, 17].
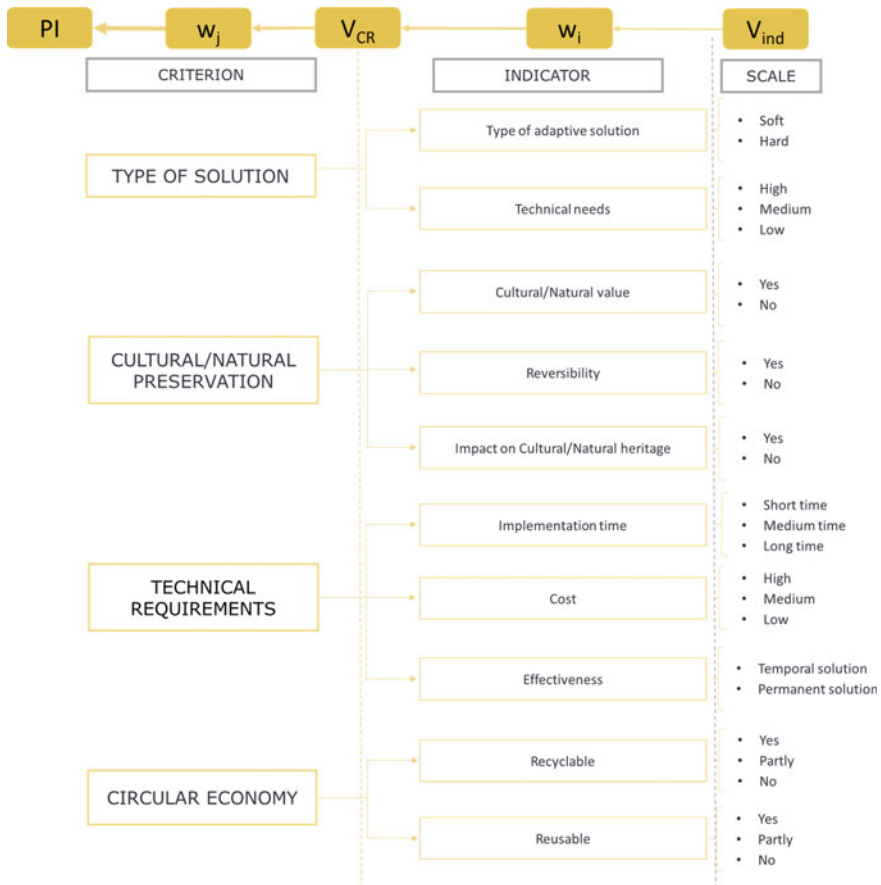
Fig. 1.1 Requirement tree for the development of MIVES

2. *Assignation of value functions to each indicator*. A qualitative scale of indicators is defined in Fig. 1.1. In this step, the qualitative value is turned into a quantitative value through a value function (V_{ind}). The value function, defined by Eqs. (1.1) and (1.2), is a dimensionless standardization mechanism with which the different dimensional variables can be defined whose values vary between 0 and 1 [18, 19]. Different alternatives are shown in Fig. 1.2 for the definition of the indicator value function considering its nature.

$$V_{ind} = B \cdot \left[1 - e^{-k_i \left(\frac{|x - x_{min}|}{C_i} \right)^{P_i}} \right] \tag{1.1}$$

$$B = \frac{1}{1 - e^{-k_i \left(\frac{|x_{max} - x_{min}|}{C_i} \right)^{P_i}}} \tag{1.2}$$

where

x_{min} and x_{max}	minimum and maximum reference points on the indicator scale (0 and 1, respectively)
x	response to the assessed alternative between x_{min} and x_{max}
P_i	shape factor curve (concave: <1; convex and "S" shaped >1 and straight $\approx$ 1)
C_i	abscissa value corresponding to the inflection point on a curve where $P_i > 1$
k_i	C_i point ordinate
B	standardization factor.
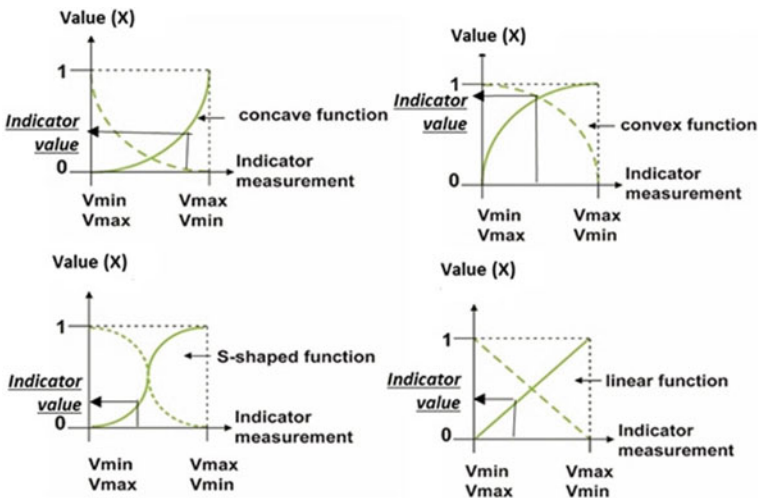
Fig. 1.2 Possible shapes of value function curves

A panel of experts with different backgrounds was assembled for the definition of the value function shape, and the results were validated in discussion with stakeholders with different backgrounds. Table 1.1 summarizes the indicator values after applying Eq. (1.1). The corresponding value was assigned to each solution, depending on the qualitative value that had previously been assigned.

Table 1.1 Value of each indicator from the value function equation

Type of solution		
Type of AS	Soft	1
	Hard	0
Technical requirement	High	0
	Low	1
Cultural/natural preservation		
Impact on cultural value	Yes	0
	No	1
Reversibility	Yes	1
	No	0
Impact on protected CH	Yes	0
	No	1
Technical requirements		
Implementation time	Short time	1
	Medium time	0.5
	Long time	0
Cost	Low	1
	Medium	0.56
	High	0
Effectiveness	Temporal solution	0
	Permanent solution	1
Maintenance	None	1
	Low	1
	Medium	0.53
	High	0
Circular economy		
Recyclable	Yes	1
	Partly	0.68
	No	0
Reusable	Yes	1
	Partly	0.68
	No	0

ALTERNATIVE VALUE	←	CRITERIA WEIGHT	←	CRITERIA VALUE	←	INDICATOR WEIGHT	←	INDICATOR VALUE
• $Pi = \sum_j w_j \cdot V_{Crit.j}$		• w_j		• $V_{Crit.j} = \sum_{ind} w_i \cdot V_{ind}$		• w_i		• V_{ind}
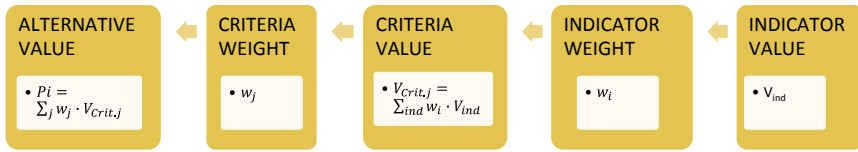
Fig. 1.3 MIVES workflow for the definition of the PI of each alternative

3. *Assignation of weight.* A survey was administered to participants who assigned a weight to each criterion and indicator, in order to assign an objective weight to both the criteria and the indicators. The survey was shared with a panel of experts with different backgrounds; the experts were selected based on a purposive sampling technique with which an interviewee assumed to possess ample information on the problem under investigation was selected, based on personal knowledge and professional experience [20]. The scale used in the survey for evaluating the importance of each criterion and indicator ranged from 1 (extremely insignificant) to 9 (extremely important).

4. *Pairwise comparative matrix.* MIVES uses the relative weight of criteria and indicator. In the previous step, a weight was defined from this value for each criterion/indicator, and a pairwise comparative matrix was then defined to obtain a relative weight for each criterion/indicator.

5. *Definition of the prioritization index for each solution.* Once all the information of the requirements tree (Fig. 1.1) had been collected, the last step was to apply MIVES (Fig. 1.3) to obtain the prioritization index (PI) of each alternative.

1.2.1 Survey Results for the Definition of the Relative Weight

Table 1.2 sums up the results of the survey and the relative weights obtained with the AHP methodology. Three different options were considered depending on the radius of action of the solution that may be needed. These options were asset scale (when the protection of the asset is needed); urban scale (when a protective solution is implemented at an urban scale); and territory scale (when the solution is implemented not only to protect the assets at an urban level, but also other architectures/artifacts in the landscape scale). A global analysis of the data obtained for the relative weights showed a balance between the importance of the circular economy and cultural/natural preservation when compared with technical requirements and type of solution criteria.

Analyzing Table 1.2, it may be seen that the relative importance of each criterion/indicator differs depending on the scale. The importance of the type of solution and the technical criteria was almost the same for the three scales (the highest deviation was 6.4% when comparing territory scale and urban scale). Cultural/natural preservation was the most important criterion for experts working at territory level and at asset level, but more important for the first one. Finally, the circular economy

Table 1.2 Survey results and relative weight of each criterion/indicator

	Territory scale		Urban scale		Asset scale	
	Survey	w	Survey	w	Survey	w
Type of solution	6.533	0.251	8.000	0.267	7.500	0.256
Type of adaptive solution	6.800	0.505	7.000	0.467	7.500	0.498
Technical needs	6.667	0.495	8.000	0.533	6.500	0.502
Cultural/natural preservation	7.533	0.289	8.000	0.267	8.500	0.276
Cultural/natural value	7.333	0.342	8.000	0.364	8.500	0.329
Reversibility	6.600	0.307	7.000	0.318	7.500	0.340
Cultural/natural heritage	7.533	0.351	7.000	0.318	9.000	0.331
Technical requirements	6.667	0.256	8.000	0.267	6.500	0.252
Implementation time	6.067	0.329	9.000	0.409	5.000	0.334
Cost	5.400	0.292	6.000	0.273	4.000	0.302
Effectiveness	7.000	0.379	7.000	0.318	7.500	0.364
Circular economy	5.333	0.205	6.000	0.200	6.000	0.216
Recyclable	5.733	0.483	4.000	0.364	6.500	0.495
Reusable	6.133	0.517	7.000	0.636	5.000	0.505

was the least important at any scale, with a more notorious difference at territory level. When comparing natural/cultural preservation with the circular economy, the greatest difference was observed on a territorial scale (40%).

1.3 Results of the Prioritization Methodology

The prioritization methodology was applied to a portfolio of solutions that includes numerous solutions to counter natural hazards arising from climate change. Each solution collects the information related to each indicator of the requirement tree (see Fig. 1.1). This information is used to identify the solutions that better contribute to resilience enhancement of cultural and natural historic areas and their preservation. The solutions respond to those hazards that can potentially have the greatest impact on cultural/natural heritage (heatwaves, flooding, earthquakes, subsidence, wildfires, and storms) [11, 21–24], and they are planned as part of the emergency phase which includes preparedness and response. Figure 1.4 shows an example of a solution data sheet.

Table 1.3 collects the results of the prioritization index obtained after applying MIVES, as schematized in Fig. 1.3, to some flood-related solutions. As previously mentioned, relative weights depend on the required scale of action, according to which, there are three possibilities (asset scale, urban scale, and at territory level). The

Adaptive solution	Temporary flood protection systems: Sandbags (buildings)			Prioritization Index	0.872	♪helter	
DRM phase	☑ Emergency	☐ Prevention	☑ Preparedness	☐ Response	☐	Recovery & BBB	
Hazard	☐ Heat waves	☑ Flooding	☐ Earthquakes	☐ Subsidence	☐	Wildfires ☐ Storm	
Action Scale	Building	Function (1)	Building protection	Function (2)			
Type of AS	Soft	Architectural and engineering solutions		Technical requirement	Low		
Impact on cultural value:	No			Reversibility	Yes		
Impact on protected CH	No						
Building:	☐						
Façade	☐ Material	☐ Components	☐ Carpentry	☐ Colour/finishing			
Roof:	☐ Material	☐ Volumetry	☐ Components				
Structure:	☐ Material	☐ Structural system					
Public zone:	☐ Pavement/material	☐ Natural species	☐ Path/Gradient	☐ Park / natural environment			
Implementation time	Short time	Pictures					
Cost	Low						
Effectiveness	Temporal solution						
Maintenance	Low						
Recyclable	Yes						
Reusable	Partly						

Fig. 1.4 Example of a solution data sheet

first three solutions are implemented at building level and only protect the building. The others are implemented at district level, often close to the river that is prone to overflowing; however, the protection level can be at territory scale, district scale, and asset scale.

Analyzing the solutions at building level, the PI of the first solution was 0.872 and the second solution was slightly superior at 0.908. Both have almost the same indicator value with the difference in the case of the first one that only part is reusable and the other is wholly reusable. The third solution, as it is not recyclable, had the lowest PI (0.801). Many building owners may not have the knowledge to compare possible solutions, and they will often choose the most resilient option when implementing the solutions; this methodology shows the most suitable solution, the solution with the highest PI value (in this case the second one).

Table 1.3 Prioritization index for some flooding solutions

	Adaptive solution	Prioritization index		
		Territory scale	Urban scale	Asset scale
1	Temporary flood protection systems: sandbags (buildings)			0.872
2	Temporary flood protection systems: shields and panels (building)			0.908
3	Installation of check systems and pumps (building)			0.801
4	Temporary flood protection systems: container systems	0.868	0.873	0.872
5	Temporary flood protection systems: free-standing and frame barriers	0.903	0.915	0.908
6	Installation of check systems and pumps	0.729	0.77	0.725

Regarding the other three solutions, the best solution considering any of the three scales is the fifth one (free-standing and frame barriers). This solution guarantees cultural/natural preservation, and it is both reusable and recyclable. In the case of the container system solution, only one part is reusable and the last one is not recyclable.

Analyzing the results summarized in Table 1.3, it is clear that the methodology yields better scores for those solutions that better contribute to both natural and cultural preservation and to the fight against climate change.

1.4 Conclusion

Both cultural and natural heritage are under threat from climate change-related hazards, the magnitude, and the frequency of which are foreseen to increase. Conservation interventions in historic area sites are generally focused on enhancing resilience considering the long-term deterioration of the materials and the works of art.

In an emergency situation, the preservation of historic value is not always considered, and the solutions tend to be focused on reducing the impact of the emergency. However, the consideration of different dimensions (technical needs, type of solution, cultural/natural preservation, and circular economy) within the multi-criteria methodology that has been developed is used to assess their relative importance. The results have shown that traditional decision-making criteria (i.e., technical needs, cost implementation time, etc.) are as important as cultural/natural value preservation criteria and circular economy criteria.

Decision-makers usually have to manage despite a lack of information and background to evaluate all these aspects. (What aspect should be considered? How important is each one?) The methodology developed in this research work provides decision-makers with a robust ranking of solutions that best fit all criteria.

References

1. Masson-Delmotte V, Zhai P, Pörtner H-O, Skea J, Shukla P, Pirani A (2018) Global warming of 1.5 °C. An IPCC special report on the impacts of global warming of 1.5 °C above pre-industrial levels and related global greenhouse gas emission pathways. In: The context of strengthening the global response to the threat of climate change. IPCC
2. World Meteorological Organization (2020) World Meteorological Organization. [Online]. Available: https://public.wmo.int/en/media/press-release/wmo-confirms-2019-second-hottest-year-record. Last accessed: 23 Nov 2021
3. IPCC (2014) Climate change 2014: synthesis report. In: Contribution of working groups I, II and III to the fifth assessment report of the intergovernmental panel on climate change. IPCC, Geneva, Switzerland
4. IPCC (2021) Summary for policymakers. In: Masson-Delmotte V, Zhai P, Pirani A, Connors SL, Péan C, Berger S, Caud N, Chen Y, Goldfarb L, Gomis MI, Huang M, Leitzell K, Lonnoy E, Matthews JBR, Maycock TK, Waterfield T, Yelekçi O, Yu R, Zhou B (eds) Climate change 2021: the physical science basis. Contribution of working group I
5. Lindsey R (2021) climate.gov. [Online]. Available: https://www.climate.gov/news-features/understanding-climate/climate-change-global-sea-level. Last accessed: 23 Nov 2021
6. European Commission (2021) European Union. [Online]. Available: https://ec.europa.eu/commission/presscorner/detail/en/ip_21_6021. Last accessed: 23 Nov 2021
7. https://shelter-project.com/ [Online]. Last accessed: 23 Nov 2021
8. https://www.hyperion-project.eu/. [Online]. Last accessed: 23 Nov 2021
9. https://savingculturalheritage.eu/. [Online]. Last accessed: 23 Nov 2021
10. https://www.interreg-central.eu/Content.Node/ProteCHt2save.html. [Online]. Last accessed: 1 Dec 2021
11. Quesada-Ganuza L, Garmendia L, Roji E, Gandini A (2021) Do we know how urban heritage is being endangered by climate change? A systematic and critical review. Int J Disaster Risk Reduction 65:102551
12. Cuadrado J, Zubizarreta M, Roji E, Larrauri M, Álvarez I (2016) Sustainability assessment methodology for industrial buildings: three case studies. Civ Eng Environ Syst
13. Oses U, Rojí E, Cuadrado J, Larrauri M (2018) Multiple-criteria decision-making tool for local governments to evaluate the global and local sustainability of transportation systems in Urban Areas: case study. J Urban Plann Dev 144(1):04017019
14. Saaty TL (2008) Decision making with the analytic hierarchy process. Int J Serv Sci 1(1):83–98
15. Saaty TL, Vargas LG (2012) The seven pillars of the analytic hierarchy process. In: Models, methods, concepts and applications of the analytic hierarchy process, pp 23–40
16. Ornelas C, Miranda Guedes J, Breda-Vázquez I (2016) Cultural built heritage and intervention criteria: a systematic analysis of building codes and legislation of Southern European countries. J Cult Heritage 20:725–732

17. Pickard R (2010) A comparative review of policy for the protection of the architectural heritage of Europe. Int J Heritage Stud 349–363
18. Alarcon B, Aguado A, Manga R, Josa A (2011) A value function for assessing sustainability: application to industrial buildings. Sustainability 3:35–50
19. Piñero I, San-José JT, Rodríguez P, Losánez MM (2017) Multi-criteria decision-making for grading the rehabilitation of heritage sites. Application in the historic center of La Habana. J Cult Heritage 26:144–152
20. Ritchie J, Lewis J (2003) Qualitative research practice: a guide for social science students and researchers. AGE Publications
21. McBean G, Ajibade O (2009) Climate change, related hazards and human settlements. Environ Sustain 1:179–186
22. Cacciotti R, Kaiser A, Sardella A, De Nuntiis P, Drdácký M, Hanus C, Bonazza A (2021) Climate change-induced disasters and cultural heritage: optimizing management strategies in Central Europe. Clim Risk Manage 32:100301
23. Calheiros T, Pereira M, Nunes J (2021) Assessing impacts of future climate change on extreme fire weather and pyro-regions in Iberian Peninsula. Sci Total Environ 14233
24. Maio R, Ferreira TM, Vicente R (2018) A critical discussion on the earthquake risk mitigation of urban cultural heritage assets. Int J Disaster Risk Reduction 27:239–247

Chapter 2
Specific Risk Maps for Cultural Heritage Materials and Airborne Pollutants: An Open Data Approach to Risk-Based Management

Giada Bartolini, Anna De Falco, Francesca Giuliani, Renato Iannelli, and Carlo Resta

Abstract A number of hazards threaten the preservation of our built heritage; among these, air pollution, causing soiling, flaking, corrosion, and more on the surface of our monuments. Notwithstanding the anthropogenic nature of this hazard, which should make it one of the first and easiest to tackle at the source, intervention is usually limited to inspection and restoration by the stakeholders managing each artefact. In an effort to simplify and rationalize the definition of intervention priorities, we investigated an approach to assess the variability (both geographical and chronological) of the risk that airborne pollutants pose to heritage materials, thus orienting a risk-based management strategy. Maps of specific risk (here defined as a product of hazard and vulnerability) are produced for each material by combining climate reanalysis and air quality data with dose-response functions, quantifying the detrimental effects of pollutants. The process uses QGIS, is completely open source and as such, it can easily be expanded and integrated with external scripts. Tuscany has been employed as a case study to test the effectiveness of the approach. A first analysis of the areas of higher specific risk and of the most influential pollutants for each material showed a predominant role of SO_2, which concentration is higher near hubs of maritime transportation. The average specific risk of the region was also compared with literature-based thresholds, which in most cases were not surpassed. Finally, historical variability was assessed, highlighting a general decline of specific risk, in Tuscany, in the years 2000–2019.

G. Bartolini · R. Iannelli · C. Resta (✉)
Department of Energy, Systems, Territory and Construction Engineering (DESTeC), University of Pisa, Largo Lucio Lazzarino, 56126 Pisa, Italy
e-mail: carlo.resta@ing.unipi.it

A. De Falco · F. Giuliani
Department of Civil and Industrial Engineering (DICI), University of Pisa, Largo Lucio Lazzarino, 56126 Pisa, Italy

15

2.1 Introduction

Cultural heritage (CH) is threatened by several hazards. Among these, air pollution is attracting much interest in the light of its link to climate change issues. The topic has been investigated within several European projects, such as the MULTI-ASSESS (2002–2005) and CULT-STRAT (2004–2007) projects [1], which proposed models and methodologies to estimate the performance of CH materials in polluted environments. On these grounds, further research regarded practical examples of the assessment and prediction of the effects of air pollution on CH materials on different geographical scales [2, 3]. In these works, maps illustrate the susceptibility of some materials of UNESCO cultural sites in Europe [2], and the likelihood of corrosion damage at a city level at the town of Madrid with its heritage artefacts [3], providing a useful evaluation for policy makers and local heritage managers to understand the need for interventions. Furthermore, an International Co-operative Programme on effects of air pollution on materials, including historic and cultural monuments (ICP Materials), was initiated in 1985 with the aim of collecting the main findings of various official projects on climate change issues, including trends, UNESCO case studies, contribution to the mapping manual, and functions for quantitative evaluation of the effects of multi-pollutants and climate parameters on materials of CH [4].

The global concentration of air pollution, as the number of its sources, has critically grown in the last century, despite a slightly positive trend (induced by emission regulation) being observed in the last twenty years [5]. Many deterioration patterns registered on historical materials are directly and indirectly induced by pollution [6], with different effects for stone [7], metals [8], or even glass [9].

The effects of airborne pollutants on CH materials can be quantitatively evaluated through dose-response functions, which constitute a link between the concentration of pollutants and climatic parameters, such as temperature, relative humidity, rain (dose), and their effect on materials (response) [10]. Within this framework, two main types of deterioration processes are designated through the generic terms *corrosion* and *soiling*. Here, corrosion stands for an unwanted reduction of mechanical strength or aesthetic value usually caused by a combination of physical, biological, and chemical damage mechanisms, with a predominance of the last. Although many materials are affected by corrosion, its effects on stone are the most severe [1]. Corrosion is described in terms of either material Mass Loss (ML, measured in $g\,m^{-2}$) for metals, or surface Recession (R, measured in μm) for stone materials. Soiling generally indicates the blackening effect on stones (loss of reflectance of white surfaces) or the loss of light transmission in glass due to the formation of removable layers of airborne pollutant. Glass soiling is measured using the haze parameter, corresponding to the ratio between the diffuse and the direct transmittance of light through the glass [1]. Thus, a higher haze value corresponds to more opaque glass.

As a side note, it is worth noting that soiling is different from the formation of black crusts on stones, which involve irreversible changes to the materials' chemical composition. A similar terminology muddle is not infrequent. It affects, too, the term "corrosion", which, within the field of CH restoration, is only used for selected materials.

The present research employs the above mentioned dose-response functions, together with geographically distributed data regarding pollutant concentration and relevant climate parameters, to build maps of the deterioration rate to which materials are subject in the Italian Region of Tuscany. These can be thought of as maps of the specific risk to which CH assets are exposed under the chemical threat posed by airborne pollutants. The choice to evaluate specific risk at the regional level differentiates the work from existing ones in the literature and has a twofold objective: to identify the sources of potential high-risk areas, and to supply a tool that can be used by regional policy makers in charge of enacting planning actions and regulations over the area.

2.2 Materials and Methods

2.2.1 Risk Definition

Literature defines risk as the combination of the probability of occurrence of relevant events and their potential consequences on people, environment, and physical assets [11]. According to this definition, risk can be modelled by three components: Hazard (H), Exposure (E), and Vulnerability (V):

$$R = H \times E \times V. \tag{2.1}$$

Hazard refers to the possible occurrence of physical events that may influence the exposed assets. Exposure refers to the inventory of assets in the hazardous area, expressed in terms of their value (either tangible or not). Vulnerability is the liability of assets to be influenced by the considered hazards.

Within the scope of the present work, air pollutants represent the considered hazard, while dose-response functions, detailing chemical effects on heritage materials, can be used to quantify vulnerability. Exposure would then be a quantification of projected losses due to a given degree of material alteration. As such, it is asset-dependent, and could be evaluated by the stakeholders tasked with the preservation of each artefact. Hazard and vulnerability can instead be defined geographically, once spatial distributions of the relevant parameters are available. We can define a specific risk as a product of hazard and vulnerability:

$$SR = H \times V , \tag{2.2}$$

or pollutant concentration and relevant dose-response function. Maps of specific risk, developed during this research, represent quantitatively the hazardous conditions in which a given material verses within the considered area and timeframe.

Table 2.1 Employed dose-response functions for sheltered and unsheltered materials

Material	Dose-response function
Sandstone	$R = 2.0[SO_2]^{0.52}e^{f(T)} + 0.028\,Rain[H^+]$ $f(T) = 0$ when $T \leq 10\,°C,$ $f(T) = -0.013(T - 10)$ otherwise $\quad$ (2.3)
Limestone	$R = 4.0 + 0.0059[SO_2]Rh_{60}$ $\quad + 0.054\,Rain[H^+]$ $\quad + 0.078[HNO_3]Rh_{60} + 0.0258[PM_{10}]$ (2.4)
Carbon steel	$R = 6.5 + 0.178[SO_2]^{0.6}Rh_{60}e^{f(T)}$ $\quad + 0.166\,Rain[H^+] + 0.076[PM_{10}]$ $f(T) = 0.15(T - 10)$ when $T < 10\,°C,$ $f(T) = -0.054(T - 10)$ otherwise $\quad$ (2.5)
Zinc	$R = 0.49 + 0.066[SO_2]^{0.22}e^{0.018Rh + f(T)}$ $\quad + 0.0057\,Rain[H^+] + 0.192[HNO_3]$ $f(T) = 0.062(T - 10)$ when $T < 10\,°C,$ $f(T) = -0.021(T - 10)$ otherwise $\quad$ (2.6)
Cast bronze	$R = 0.15 + 0.000985Rh_{60}e^{f(T)}$ $\quad + 0.00465\,Rain[H^+] + 0.00432PM_{10}$ $f(T) = 0.060(T - 11)$ when $T < 11\,°C,$ $f(T) = -0.067(T - 11)$ otherwise $\quad$ (2.7)
Modern glass	$Haze = \frac{0.2529[SO_2] + 0.1080[NO_2] + 0.1473PM_{10}}{(1 + 382/t)^{1.86}}$ $\quad\quad$ (2.8)

2.2.2 Dose-Response Functions and Relevant Parameters

Deterioration rates of construction materials can be calculated using dose-response functions, as delivered from the two ICP Materials exposure programmes.

Relevant pollutants are mainly sulphur dioxide (SO_2), nitrogen dioxide (NO_2), and nitric acid (HNO_3), as well as the particulates PM_{10}. Their concentration and spatial distribution are the object of several monitoring programmes [12]. To the degradation of materials also concur some climatic parameters, in particular, the annual average temperature, the total annual precipitation depth, the annual average relative humidity, and finally the average annual rain acidity. Materials, taken from the aforementioned ICP exposure programmes and factored in the present research are: Portland limestone, white dolomitic Mansfield sandstone, carbon steel, zinc, cast bronze, and modern glass.

Dose-response functions for an SO_2 dominating scenario in unsheltered and sheltered conditions are available as a result of the ICP 8-years exposure programme (1987–1995) [13], while ones for multi-pollutant scenario derive from the 4-year exposure programme (1997–2001) [10]. When available, multi-pollutant-scenario functions are to be preferred to the SO_2 dominating ones. They are better suited to describe the current worldwide situation, characterized by decreasing levels of

SO_2 and increasing levels of traffic, resulting in higher concentrations of multiple pollutants [1].

To quantify corrosion, surface recession (R [μm]) is considered. For sandstone, R is calculated through the dose-response function for the SO_2 dominating scenario, since it is the only available. For the remaining materials, dose-response functions for the multi-pollutant scenario are instead employed. Functions used in the present work are summarized in Table 2.1. Here:

R is the surface recession or corrosion depth (μm);

Rh is the annual average relative humidity (%);

Rh_{60} = Rh − 60 when Rh > 60, 0 otherwise (%);

Rain is the annual amount of precipitation (mm year^{-1});

T is the annual average temperature (°C);

[X] is the annual average concentration of compound X (μg m^{-3});

[H$^+$] is the annual average H$^+$ concentration in rain (mg l^{-1});

t is the time of exposure (days). In the following, this is taken to be one year (365 days).

2.2.3 Acceptable Rate of Deterioration

It is useful to compare damage to the materials with thresholds from literature, to assess its gravity. Corrosion rate targets can be found in the 2009 *Indicators and Targets for Air Pollution Effects* report by the Working Group on Effects of the United Nations' Executive Body for the Convention on Long-Range Transboundary Air Pollution [14]. Within the report, "non-binding, aspirational" [14] targets are proposed for corrosion rates in 2020 and 2050. The values of the corrosion or soiling rates (K_a) are set as in Eq. 2.9, in which K_b is the "background" corrosion or deterioration level, namely the lower 10-th percentile of the observed corrosion rates in the materials exposure programme (years 1987–1995) [4], and $n > 1$ is a multiplying factor.

$$K_a = n K_b \qquad (2.9)$$

The rates vary for each sample material, and the values for a 1-year exposure period ($n = 1$) are provided in [15]. The same document recommends setting n equal to 1.5, 2.0, and 2.5, although lower values can be used if the value of cultural assets is deemed to be significantly high. According to [14], the background rates can be amplified using $n = 2$ for the year 2050 and $n = 2.5$ for the year 2020, as summarized in Table 2.2.

The comparison between the actual deterioration values and the acceptable yearly rates enables evaluating the temporal variation of deterioration over time and eventually assessing the impact of emission-regulating policies on historical materials (see Sect. 2.3.3).

Table 2.2 Values of the acceptable rates according to [2, 15]

Material	Background ($n = 1$)	Year 2050 ($n = 2$)	Year 2020 ($n = 2.5$)
Limestone	3.2	6.4	8
Sandstone	2.8	5.5	7
Copper	0.32	0.64	0.8
Bronze	0.25	0.5	0.6
Zinc	0.45	0.9	1.1
Carbon steel and weathering steel	8.5	16	20

The rates are expressed in μm and referred to a 1-year exposure

2.2.4 Case Study

To test the application of the developed approach, we employed as a case study the region of Tuscany, in Italy. Three main arguments can be presented for this choice:

1. the distribution of air pollution-related specific risk has seldom been mapped at a regional scale;
2. at the regional scale, it is easier and more productive to pinpoint the locations with the highest risk concentrations; furthermore, the presence of areas where risk is above the admissible limit can more easily be linked to triggering factors;
3. analysis within regional boundaries supports regional policy makers, which can use its results as an aid to pursue emission reduction policies for the whole area.

Notwithstanding this choice of a case study, the whole area of Italy was employed to calculate risk-pollutant correlations (see Sect. 2.3.1). This was done to enlarge the data set on which correlations were calculated.

2.2.5 Data Sets and Calculations

As already mentioned, the creation of specific risk maps requires the use of climate and air pollution data. For the present work, we employed only freely accessible data from a number of sources, in order to assess the feasibility of a decision support approach built completely on open data. In cases when more than one source was available, our choices were mainly oriented by the ease of use and reliability of information for future access. Climate variables were obtained from the Copernicus ERA5 monthly averaged reanalysis data [12]. Pollutant concentration info were obtained from the Co-operative programme for monitoring and evaluation of the long-range transmission of air pollutants in Europe (EMEP) MSC-W modelled air concentrations and depositions [16], specifically type-1 and type-2 data. Type-1 data were employed for 2019 and type-2 data for 2000 and 2010. Finally, a Digital Elevation

Table 2.3 Covariance matrix: materials and average yearly air pollutant concentration

Materials	HNO$_3$	NO$_2$	PM$_{10}$	SO$_2$
Carbon steel	0.53	0.25	0.52	**0.81**
Cast bronze	0.36	0.14	**0.91**	0.6
Portland limestone	**0.95**	0.09	0.44	0.45
Modern glass	0.35	0.35	**0.88**	0.59
White Mansfield dolomitic sandstone	0.5	0.32	0.34	**0.88**
Zinc	**0.95**	0.15	0.33	0.50

Values in **bold** correspond to the most influential pollutants for each material

Model (DEM) of Tuscany was downloaded from the Regional open data platform [17]. Its original spatial resolution of 10 m was reduced to 250 m via downsampling.

Raw data were treated using QGIS software [18], which was also employed to produce specific risk maps.

2.3 Results and Discussion

2.3.1 Risk-Pollutant and Risk-Climate Correlations in Italy with 2019 Data

We first calculated specific risk maps for the entirety of Italy, using climate and air pollution data from 2019. Results are obtained in the form of geo-referenced raster images, with 0.1° pixel width both in latitude and longitude.

We then checked the maps for correlation against the geographical distribution of input values (i.e., climate and pollution data), by computing covariance values. Results highlight the most influential pollutants affecting each material. This was done over the entire area of Italy, instead of Tuscany (see Sect. 2.2.4).

Table 2.3 gives the covariance matrix obtained by comparison with air pollutant concentration. The single most influential pollutant for each material is highlighted.

Nitrogen dioxide constitutes the least threatening pollutant in the study area. Sulphur dioxide, inversely, emerges as the most influential one, representing in each case either the first or the second-most correlated factor. It is followed closely by particulate matter and nitric acid. The latter plays a clearly dominant role as a risk factor for limestone. This is unsurprising, as the high reactivity of Portland limestone to HNO$_3$ is well known and documented [19].

The relevant role of SO$_2$ allows us to take another step in the direction of result interpretation, by considering the main sources of sulphur dioxide emission. Figure 2.1 shows the distribution of average surface SO$_2$ concentration according to the
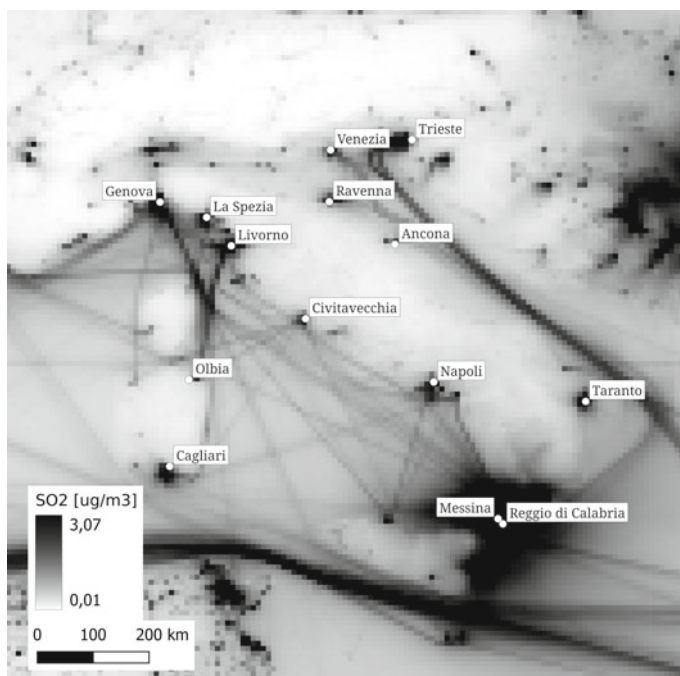
Fig. 2.1 Geographical distribution of average surface SO$_2$ concentration in 2019 over Italy. The main port cities are also indicated. Elaborated from EMEP data

EMEP 2019 data set, with the darkest areas corresponding to a higher presence of the pollutant. A clear correlation with maritime transport can be inferred, as highlighted by both the concentration of dark areas above port cities, and the evident traces of the busiest routes. This correlation, too, is a well-known fact [20, 21], and is of importance in the analysis of Tuscany specific risk maps, as explained in Sects. 2.3.2 and 2.3.3.

It should be noted that these results strictly hold only for the area under study and for 2019, but the procedure is of general validity. Analysing the relative influence of the different pollutants could prove helpful for stakeholders, for example by providing quantitative data to orient emission reduction policies.

As a related investigation, we proceeded to examine the correlation of specific risk with climate data, notwithstanding the fact that specific courses of action to alter climate factors are outside the usual boundaries of cultural heritage preservation. Table 2.4 gives the covariance matrix obtained by comparison of specific risk with climate maps. As with the previous one, values in bold indicate the highest covariance for a specific material.

At first glance, the negative correlation showed by precipitation (and in some cases by relative humidity) may appear wrong, considering that both are additive factors in the employed dose-response functions (cfr. Table 2.1). But the geographical nature of

Table 2.4 Covariance matrix: materials and yearly averages of climate parameters (same symbols as Sect. 2.2.2)

	Rh	*T*	Rain
Carbon steel	0.14	**0.54**	−0.43
Cast bronze	−0.27	**0.65**	−0.61
Portland limestone	0.35	**0.69**	−0.47
Modern glass	−0.33	**0.60**	−0.54
White Mansf. dolomitic sandstone	0.06	**0.44**	−0.34
Zinc	0.33	**0.71**	−0.46

Values in **bold** correspond to the most influential parameters for each material

the data has to be taken into account. A negative covariance value indicates only that rainy areas are less prone to material degradation. This may just as well be caused—as is probably the case—by a low influence of wet conditions on corrosion or soiling rates, together with a high influence of a hidden parameter (perhaps elevation) on rainfall, humidity, and pollutant concentration. More information on the subject is presented in the following section.

Within the study area and in 2019, the temperature is nevertheless the most influential parameter for all examined materials, with higher temperatures being the most detrimental. This information is of course of some concern when considering the global trend of rising temperatures, but a much more in-depth analysis would be necessary to assess the influence of climate change on the deterioration of cultural heritage.

2.3.2 Specific Risk Maps for Tuscany with 2019 Data

After an overall analysis of the impact of airborne pollutants in Italy in 2019, we restricted our scope to Tuscany. Figure 2.2 shows the geographical distribution of specific risk for different materials within the area of study, superimposed over a graphical representation of the region's Digital Elevation Map (DEM). To obtain the maps, we used climatic and air pollution data from 2019 (the most recent data available at the time of the study). Pixel size, as for the previous elaborations, is 0.1° for both latitude and longitude, corresponding here to a distance of about 10 kilometres.

The distribution of specific risk follows a similar pattern for all of the examined materials. Under identical exposure conditions, higher damage is to be expected in the area around Livorno, while the eastern and south-eastern portions of the Region are safer. As mentioned in the previous section, maritime transportation has a primary role in the production of air pollutants (in particular sulphur dioxide), so it comes as no surprise that the presence of a relevant port city in the region would be cause for
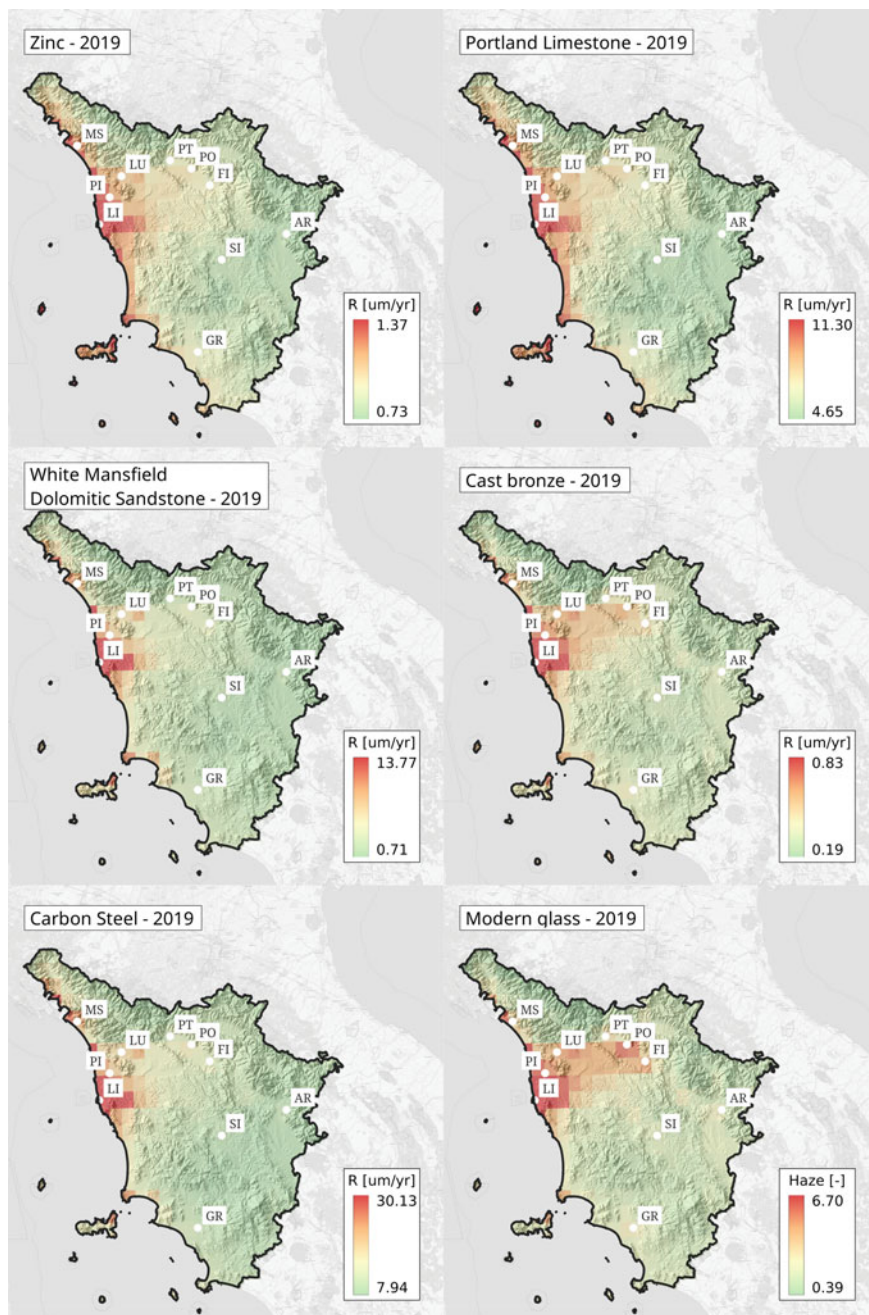
Fig. 2.2 Specific risk maps for Tuscany with 2019 data. Colour maps ranging between the 2nd and the 98th percentile of values. Minimum and maximum values explicitly indicated. The main cities are indicated through province codes. Base maps: Italian map from *OpenStreetMap*; DEM of Tuscany from *Regione Toscana* [17]

risk concentration. The whole northern coastal area appears to be affected as well. The second pole of specific risk can also be found in the city of Piombino, on the cape facing Elba island.

Observation of specific risk values in the medium range could lead to suggestive insights regarding the role of elevation, in Tuscany, as a protective agent against the causes of material degradation. In the northern part of the region, Apuane Alps seem to cut short the diffusion of airborne pollutants that cause the concentration of risk. Conversely, such a diffusion seems to be allowed in the area between the provinces of Pisa (PI on the map) and Florence (FI) by the absence of areas of significant elevation. This becomes particularly evident in the maps for cast bronze and modern glass. Unfortunately, the plain under investigation is also the site of many manufacturing activities, which density on the contrary is reduced in mountain areas. For this reason, a dedicated analysis would be necessary to pinpoint exactly the role played by elevation.

To gain better insight into the exact value and frequency of corrosion and soiling rates in the study area, Fig. 2.3 shows the histograms of specific risk values. The vertical axis has a logarithmic scale in order to better show the presence of the highest rate values, which would otherwise be hidden by the large prevalence of smaller ones. To overcome any interpretation issues that the choice of a logarithmic scale may cause, the mean is also indicated. As explained in Sect. 2.2.3, ICP Materials also set acceptable rates of deterioration for corrosion, with benchmarks at either 2020 or 2050. We thus compared the distribution of corrosion risk values with such limit rates.

For all examined materials subject to corrosion, the following two observations can be made:

- the mean value of the corrosion rate is well below the acceptable rates;
- the specific risk map includes small areas in which corrosion rates are greatly higher than the average, and which surpass the acceptable boundaries.

The latter observation, when compared with values on the map, leads to the identification, once again, of the area around Livorno as the most risk-prone. In that area, all ICP Materials-set limits are surpassed.

The analysis of histograms is clearly less intuitive than that of the maps, but it, too, should prove a useful tool for policy makers. The possibility to compare the full distribution of degradation rates against acceptable boundaries, instead of having to check the values of specific points on the map, empowers the user to assess the overall severity of the threat that air pollution poses to cultural heritage in the area.

2.3.3   Variability of Specific Risk in Tuscany Along the Years

The same analysis outlined in Sect. 2.3.2 can be repeated for different years in order to inspect the temporal variability of the specific risk in Tuscany. We applied the
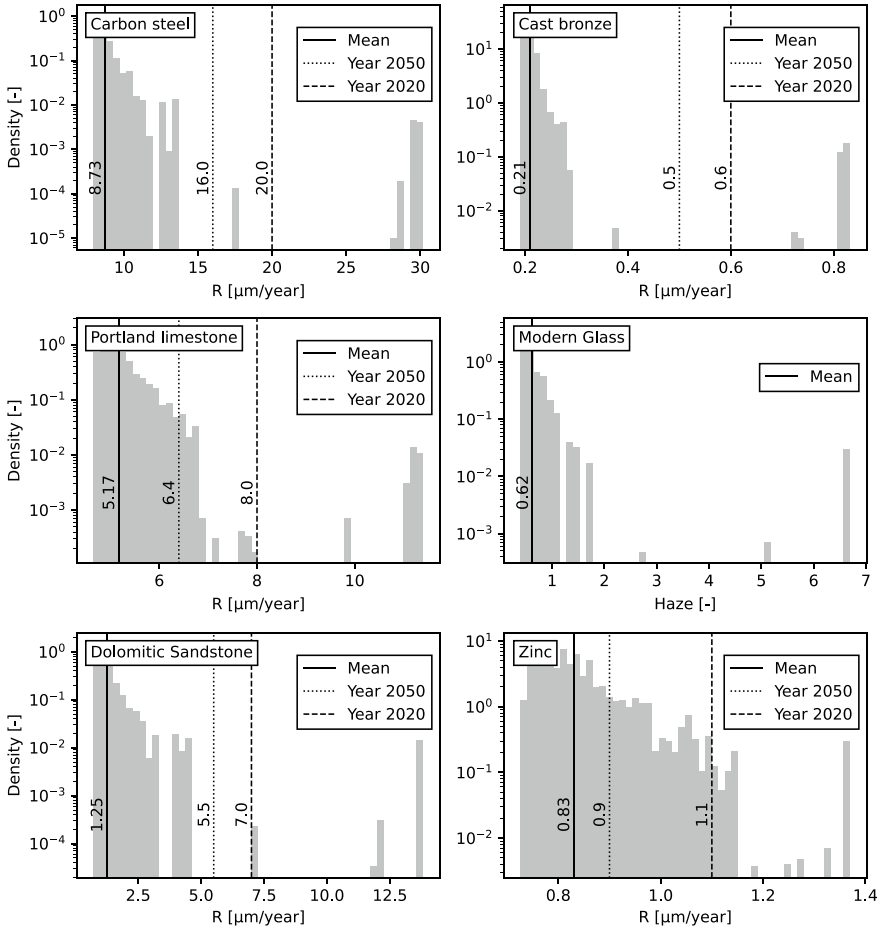
Fig. 2.3 Histograms of corrosion/soiling rate density in Tuscany in 2019. ICP materials-set accept-ability boundaries with reference at 2020 and 2050 are also indicated

exact same procedure using climate and pollution data from 2000 and 2010. Figure 2.4a shows how the mean value of specific risk for each material changed along the years; Fig. 2.4b shows instead the variation in the percentage of the region's area where specific risk surpasses the acceptable threshold for 2050.

The graphs are encouraging, exhibiting a clear reduction of specific risk. While mean values only show a small variation, the collapse in the percentage of the area above the 2050 threshold suggests that actions were taken to deal with the most extreme pollution concentrations. This kind of output should prove useful for policy makers since it allows to quantitatively represent the effect of emission reduction practices on the specific risk for CH.
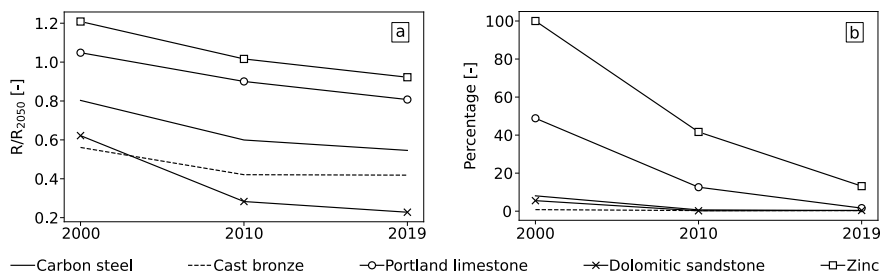
Fig. 2.4 Temporal variation of specific risk in Tuscany: **a** mean value with respect to the 2050 limit and **b** percentage of the regional area with specific risk surpassing the 2050 limit

2.4 Conclusions

The materials which make up our cultural heritage are susceptible to alteration and deterioration at the hands of airborne pollutants, which abundance is a direct consequence of an ever growing anthropic activity. Several studies delved into the matter, developing quantitative relationships between pollution and material damage (dose-response functions), and investigating the most at-risk heritage sites around the globe. In the present work, we employed open access data regarding pollutant concentration and climatic parameters, together with dose-response functions from ICP Materials, to investigate an approach that frames the problem as a spatial distribution of specific risk for cultural heritage. It aims to provide assistance to stakeholders and policy makers in prioritizing interventions and emission-regulating policies. After a preliminary evaluation of the correlation between pollutants, climatic parameters, and damage to a given material within the scope of the present work, we concentrated on the region of Tuscany, in Italy, as a case study. We produced maps representing the distribution of specific risk for cultural heritage materials in 2019, identifying two areas (near the cities of Livorno and Piombino, both maritime transportation hubs) as the most problematic ones. We also compared the distribution of risk with acceptable thresholds from literature, identifying the urgency of intervention. Finally, we applied the same analysis procedure to past data sets from 2000 and 2010, tracking the evolution of both the average risk in the region, and the percentage of areas surpassing the aforementioned acceptable thresholds. Results show an unequivocally positive trend, which may be the outcome of effective emission-regulating policies enforced, in the region, during the last twenty years.

References

1. Hamilton R, Kucera V, Tidblad J, Watt J (eds) (2009) The effects of air pollution on cultural heritage. Springer US, Boston, MA. https://doi.org/10.1007/978-0-387-84893-8
2. Spezzano P (2021) Mapping the susceptibility of UNESCO world cultural heritage sites in Europe to ambient (outdoor) air pollution. Sci Total Environ 754

3. de la Fuente D, Vega JM, Viejo F, Díaz I, Morcillo M (2013) Mapping air pollution effects on atmospheric degradation of cultural heritage. J Cult Heritage 14(2):138–145

4. Tidblad J, Kreislová K, Faller M, de la Fuente D, Yates T, Verney-Carron A, Grøntoft T, Gordon A, Hans U (2017) ICP materials trends in corrosion, soiling and air pollution (1987–2014). Materials 10(8):969

5. Fowler D, Brimblecombe P, Burrows J, Heal MR, Grennfelt P, Stevenson DS, Jowett A, Nemitz E, Coyle M, Liu X, Chang Y, Fuller GW, Sutton MA, Klimont Z, Unsworth MH, Vieno M (2020) A chronology of global air quality. Phil Trans R Soc A 378(2183):20190314

6. Vidal F, Vicente R, Mendes Silva J (2019) Review of environmental and air pollution impacts on built heritage: 10 questions on corrosion and soiling effects for urban intervention. J Cult Heritage 37:273–295

7. Vergès-Belmin V (2008) ICOMOS-ISCS: illustrated glossary on stone deterioration patterns, English-French version edn., no 15. Monuments and sites. ICOMOS, Paris

8. Tidblad J, Kucera V (2003) Air pollution damage to metals, vol 2. Imperial College Press, pp 227–247. https://doi.org/10.1142/9781848161283_0007

9. Al-Thani H, Koç M, Isaifan RJ (2018) A review on the direct effect of particulate atmospheric pollution on materials and its mitigation for sustainable cities and societies. Environ Sci Pollut Res 25(28):27839–27857

10. Kucera V, Tidblad J, Kreislova K, Knotkova D, Faller M, Reiss D, Snethlage R, Yates T, Henriksen J, Schreiner M, Melcher M, Ferm M, Lefèvre RA, Kobus J (2007) UN/ECE ICP materials dose-response functions for the multi-pollutant situation. Water Air Soil Pollut Focus 7(1–3):249–258

11. Cardona OD, van Aalst MK, Birkmann J, Fordham M, McGregor G, Perez R, Pulwarty RS, Schipper ELF, Sinh BT, Décamps H, Keim M, Davis I, Ebi KL, Lavell A, Mechler R, Murray V, Pelling M, Pohl J, Smith AO, Thomalla F (2012) Determinants of risk: exposure and vulnerability. In: Field CB, Barros V, Stocker TF, Dahe Q (eds) Managing the risks of extreme events and disasters to advance climate change adaptation. Cambridge University Press, Cambridge, pp 65–108. https://doi.org/10.1017/CBO9781139177245.005

12. ECMWF: European Centre for Medium-Range Weather Forecasts—ERA5 (Copernicus knowledge base). https://confluence.ecmwf.int/display/CKB/ERA5

13. Tidblad J, Kucera V, Mikhailov AA, Henriksen J, Kreislova K, Yates T, Stöckle B, Schreiner M (2001) UN ECE ICP materials: dose-response functions on dry and wet acid deposition effects after 8 years of exposure. In: Satake K, Shindo J, Takamatsu T, Nakano T, Aoki S, Fukuyama T, Hatakeyama S, Ikuta K, Kawashima M, Kohno Y, Kojima S, Murano K, Okita T, Taoda H, Tsunoda K, Tsurumi M (eds) Acid rain 2000. Springer, Netherlands, pp 1457–1462. https://doi.org/10.1007/978-94-007-0810-5_90

14. Working Group on Effects (2009) Indicators and targets for air pollution effects. Technical report 16, UN ECE

15. CLRTAP (2014) Guidance on mapping concentrations levels and deposition levels, Chapter II of manual on methodologies and criteria for modelling and mapping critical loads and levels and air pollution effects, risks and trends

16. EMEP (Co-Operative Programme for Monitoring and Evaluation of the Long-Range Transmission of Air Pollutants in Europe): MSC-W modelled air concentrations and depositions. https://emep.int/mscw/mscw_moddata.html

17. Regione Toscana: Altimetria 10 metri (2015) OpenData. http://dati.toscana.it/dataset/dem10mt

18. QGIS Development Team (2022) QGIS geographic information system. https://www.qgis.org/en/site/

19. Kirkitsos P, Sikiotis D (1995) Deterioration of pentelic marble, Portland limestone and baumberger sandstone in laboratory exposures to gaseous nitric acid. Atmos Environ 29(1):77–86

20. Viana M, Hammingh P, Colette A, Querol X, Degraeuwe B, de Vlieger I, van Aardenne J (2014) Impact of maritime transport emissions on coastal air quality in Europe. Atmos Environ 90:96–105

21. Ledoux F, Roche C, Cazier F, Beaugard C, Courcot D (2018) Influence of ship emissions on NOx, SO2, O3 and PM concentrations in a North-Sea harbor in France. J Environ Sci 71:56–66

Methods and Instruments for the Conservation Diagnosis and Treatment

Chapter 3
Satellite Radar Interferometry for Monitoring Historic Urban Fabric: Lucca and Florence Test Cities

Silvia Bianchini and **Davide Festa**

Abstract Satellite radar interferometric techniques are non-invasive remote sensing methods without material contact with manufacts and with high data sampling, so that they can be profitably used for measuring and periodically monitoring millimetric deformations of architectural structures without affecting their integrity. In particular, this work proposes a procedure for detecting and monitoring ground movements based on Synthetic Aperture Radar Interferometry (InSAR) data elaborated through Persistent Scatterers Interferometry (PSI) technique over historical built-up areas. We exploit PSI data extracted from medium resolution Sentinel-1 satellite images acquired in the time span 2014–2021 to analyse deformation patterns and potential instability of single building at local scale, with particular attention to Cultural Heritage structures. The analysis was performed on two test cities: Florence city, whose historic centre enclosed within the avenues that follow the old medieval walls is recognized as a World Heritage Site by UNESCO since 1982, and Lucca city, whose historic centre was submitted to the UNESCO Tentative List in 2006. Results demonstrate the potential use of remote sensing satellite technologies in measuring deformation phenomena on historical buildings, especially in areas affected by hydrogeological hazards, such as subsidence and slow-moving landslides. In particular, the outcomes of such PSI monitoring could be a useful tool to be considered for authorities in charge of environmental planning in addressing urban zoning regulations and prescribing maintenance and improvement of the heritage and historic city centre resilience.

Keywords Radar interferometry · Persistent scatterers · Monitoring · Historic city centre · UNESCO

S. Bianchini (✉) · D. Festa
Department of Earth Sciences, University of Florence, Florence, FI, Italy
e-mail: silvia.bianchini@unifi.it

D. Festa
e-mail: davide.festa@unifi.it

3.1 Introduction

Italy is a country with a high number of cultural assets included in the UNESCO World Heritage List (WHL), but at the same time, from a geological and geomorphological point of view, it is extensively affected by significant natural risks. Cultural heritage must not be considered separately from the environmental and natural context in which it is inserted, and from which possible causes of instability and deterioration may arise. Therefore, there is a strong requirement to better detect and study the extent and intensity of potential geological hazards that can affect cultural heritage, e.g. subsidence and landslides, before they create irreparable damage in order to provide operational priorities for protection, conservation, and sustainable use measures of the territory [1].

Satellite Synthetic Aperture Radar (SAR) interferometric techniques are non-invasive remote sensing methods without material contact with manufacts and with high data sampling (up to weekly frequency), so that they can be profitably used for measuring and periodically monitoring millimetric deformations of architectural structures without affecting their integrity. Multi-temporal SAR Interferometry (InSAR) techniques, e.g. Persistent Scatterer Interferometry (PSI), have been profitably used for measuring slow-moving ground deformations especially on urban areas where many radar targets can be retrieved as point measurements [2].

In scientific literature recent works have demonstrated the potential of satellite SAR remote sensing technologies in prospection of cultural sites and investigation of environmental, land surface and anthropogenic processes that can alter the condition of heritage assets [3–5]. Some PSI-based procedures have been implemented for assessing potential building deformation and settlement at local scale [6–12].

This work proposes a methodology for detecting and monitoring ground movements based on Synthetic Aperture Radar Interferometry (InSAR) data elaborated through Persistent Scatterers Interferometry (PSI) technique over historical built-up areas. In particular, PSI data from medium resolution Sentinel-1 (ESA, European Space Agency) satellite images referred to the time span 2014–2021 are exploited to analyse deformation patterns and potential instability at the local scale of single building on Florence city and Lucca city, whose historic urban centres are included in the UNESCO WHL and in the Tentative List, respectively.

3.2 Test Cities: Lucca and Florence

3.2.1 Florence City

The city of Florence was built on the site location of an Etruscan settlement and later it was an ancient Roman colony named Florentia. The city became a symbol of the Renaissance between the fifteenth and the sixteenth centuries, reaching high levels of economic and cultural development [13]. The present historic city centre covers

about 5 km^2 and is bounded by the remains of the fourteenth-century city walls, which are represented by enduring gates, towers, and fortresses. Through the city, the Arno River flows east and west, and several bridges connect its banks.

Geological and Geomorphological Setting. Florence is located in the Firenze-Prato-Pistoia alluvial plain, which is a northwest-southeast oriented intermontane basin, 45 km long and 10 km wide, with a mean altitude of 45 m above sea level [14, 15]. The alluvial plain is bounded by two ridges (geologically represented by two horsts) mostly made of calcareous-marly flysch associated with ophiolites and arenaceous flysch [16, 17]. The northern boundary of the plain is marked by a normal fault that makes the basin a half-graben. Hills southwards Arno River are gentle slopes made of marly-arenaceous flysch, whilst piedmont areas are composed of loose lacustrine and fluvial sediments [16]. The half-graben basin was formed by the sedimentation of clay, sandy clay, and peat from a lacustrine-swampy environment covered by more recent fluvial sediments [15, 18] (Fig. 3.1a).

The setting of Florence, surrounded by the Tuscan hills and bisected by the Arno River is threatened by several risks ascribable to geohazard factors, i.e. Arno floods, and landslide movements in the surrounding hilly areas, subsidence and ground motions due to recent tramway roadworks and high-speed train excavations. Thus, during its history, the Florence city centre has suffered many geohydrological disasters, such the flood of the Arno River in Florence occurred on 4th November 1966 [19], the riverbank failure in Lungarno Torrigiani in 2016, the Lungarno Diaz sinkhole in 2019 as well as the slope instability of San Miniato hill historically recorded and studied since the Renaissance [13].
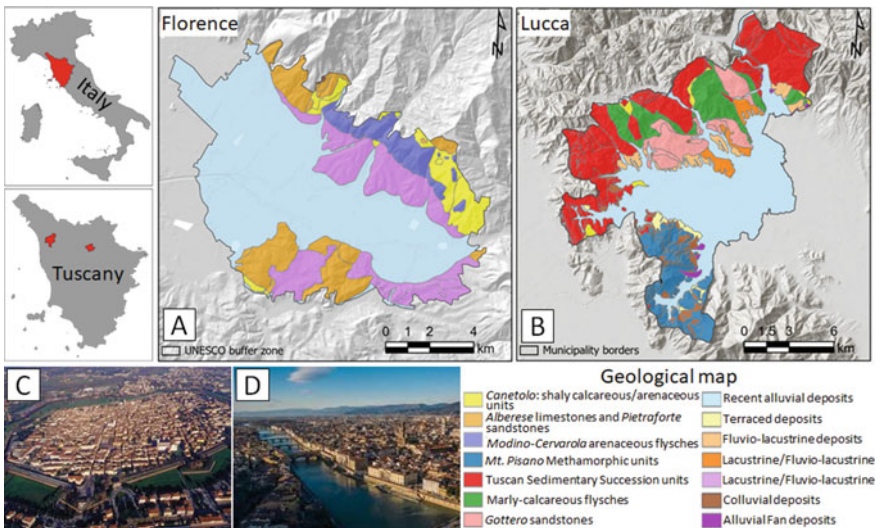
Fig. 3.1 Geographical location of Florence and Lucca cities; **a** and **b** Geological map of Florence and Lucca areas; **c** and **d** Photos of Florence and Lucca cities. *Sources*: www.intoscana.it

UNESCO World Heritage Site. The city centre, which is enclosed within the avenues that follow the old medieval walls, collects the most important cultural assets of Florence and in 1982 was recognized as a World Heritage Site by UNESCO. In particular, it includes historical urban built-up and many cultural and landscape assets that are subject to architectural and archaeological restrictions. Around the area of the city centre ascribed in the WHL UNESCO and known as *core zone*, a larger surrounding area was also traced, known as *buffer zone* extended up about 110 km^2 (Fig. 3.1a).

3.2.2 Lucca City

Lucca was an ancient Etruscan settlement that later became a Roman colony. In the Middle Ages, it was the second largest Italian city state after Venice with a republican constitution to maintain its independence for centuries. The walls enclosing the old town have remained intact since the sixteenth century, even as the city has expanded and modernized: the walls were originally built as a defensive barrier and, after they lost their military importance, they were converted into a pedestrian promenade, which stands as a street atop the walls connecting the ancient strongholds and gates, and embraces the historic city centre that extends up about 1.7 km^2.

Geological and Geomorphological Setting. Lucca is located in the Serchio River floodplain in the extensional intermontane tectonic basin that dissected the inner portion of the Northern Apennines in the late Miocene [20]. The alluvial plain derived from the gradual filling of a paleovalley entrenched during the sea level lowstand of the last glaciation. The stratigraphy of the Lucca alluvial plain is composed of a bedrock of arenaceous flysch, overlapped by lower lacustrine and fluvial continental deposits with coarse-grained gravel fluvial body and upper alluvial succession of fine-grained sandy deposits which represent paleochannel fill and overbanks, with minor palustrine to lacustrine deposits [21].

The Lucca alluvial plain developed over the centuries through the migration of the Serchio River, which followed a different path from the present one and which now streams north-westwards Lucca city. Across time, the Serchio River has caused several relevant floods. The oldest one dates back to 16th November 1812, when the river overflowed and the water reached the heights of the city walls, so that the left bank of the river was further raised up to protect the city. Recent flood events occurred in November 2000, December 2009 and July 2014 after heavy rainfall. On these dates, some landslides also took place, mostly debris flow and slides evolved in flows, which caused many damages especially to the road network throughout the Lucca municipality, which extends up about 185 km^2 (Fig. 3.1b).

UNESCO World Heritage Site. The historic walls of Lucca were built at the end of the 1500 s and are still intact nowadays, representing a highly valuable cultural resource. As they fulfil the criteria of authenticity and integrity for WHL inclusion

regarding both the urban structure and the presence of perfectly preserved monuments and architectural complexes, the historic Centre of Lucca have been proposed in the UNESCO Tentative List since 2006.

3.3 Materials and Methods

In this work we used Persistent Scatterer Interferometry (PSI) technique for qualitatively and quantitatively assessing slow-moving deformation of terrain and manufacts, with attention to the potential settlements of the urban fabric at local scale.

Persistent Scatterer Interferometry (PSI) is a multi-temporal radar interferometric technique that analyses long temporal series of satellite SAR images acquired from space-borne microwave sensors, and provides mean annual velocities and time series of ground deformation on dense grids of point-wise benchmarks, the so-called PS or Persistent Scatterers [2]. These radar targets are typically man-made structures (i.e. buildings, pylons, roadways, etc.) or natural elements (i.e. rocks) that exhibit stable and strong backscattered radar signal and coherence characteristics over the entire observation period so that are used to derive surface deformation. Recently, DS (Distributed Scatterers) approach was also developed (i.e. SqueeSAR technique, [22]) as a new SAR images elaboration to be used for areas with low population of PS targets, since it extracts information not only from point-like elements (PS), but also from distributed scatterers (DS) that show moderate coherence, low signal-to-noise ratio, but relatively stable reflection, usually corresponding to semi-natural, arid or debris areas with low vegetation.

The output of such SAR processing consists of sparse sets of points (PS and DS, generally called PSI data) each of which is provided with a velocity value (expressed in mm/year) estimated along the satellite acquisition Line Of Sight (LOS) and a time series of displacements, i.e. a plot that shows the displacement (in mm) of the radar target at the given date of acquisition [23] (Fig. 3.2).

The spatial resolution and density of radar data mainly depend on the microwave length of the radar signal and acquisition mode of the used sensor (e.g. microwave C-band Sentinel-1 sensor with cell size of medium resolution 5×20 m; microwave X-band, e.g. COSMO-SkyMed satellites, with cell size of high resolution 3×3 m).

3.3.1 Methodological Procedure

In building surveying, the assessment of conditions of manufacts is typically provided as a rate according to numbered classes as output to express the structural health of the structure, keeping it brief and informative [9, 24, 25].
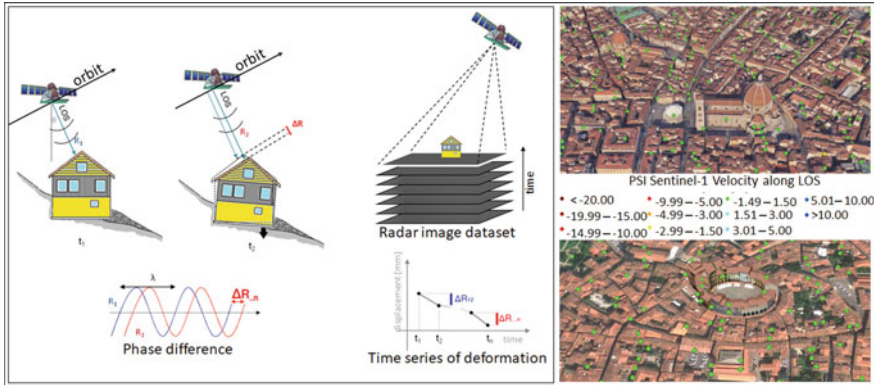
Fig. 3.2 Sketch of the basic principles of PSI radar interferometric technique (left); examples of spatial distribution of PSI targets on the test cities of Florence and Lucca (right)

In this work we propose a procedure that relies on PSI analysis for building-scale instability assessment by means of classification indexes, starting from experience of some previous works on this topic [9, 26]. Thus, the stability and potential deformation on urban fabric at the single manufact scale are analysed by considering ground deformation rates of PSI data on each building. The PS deformation estimates are converted into indexes whose range classes allow us to rate the instability of buildings due to structural or terrain deformation.

We consider a buffer area around individual manufact of some metres in order to avoid possible georeferencing shifts between buildings and PSI layers and to consider even PS that are not included within the building plain-edge, but that are the result of a backscattered radar signal, which could be even influenced by the structure itself, as a consequence of the metric resolution cell of space-borne radar images. We dimensioned this buffer area according to the spatial resolution of the employed SAR image, i.e. 5 m if using medium resolution C-band data.

Figure 3.3 shows the proposed set of indexes to classify the information content of PSI data and to rate the deformation conditions of buildings at the local scale: for each structure, PSI coverage and deformation rates are translated into the classification indexes.

In practise, we intersected the boundaries of buildings buffers with the PSI data falling within such areas, and we extracted 5 class values and thus the indexes. This downscaling rate is feasible when the PSI coverage over the structure is sufficient. PSI data in ascending and descending geometries were merged and considered as a unique dataset.

In particular we define the I_d Data Coverage Index to express the spatial distribution of PSI data covering the building to survey. This index is scored from E to A to signify poor PS to optimal coverage on an individual manufact.
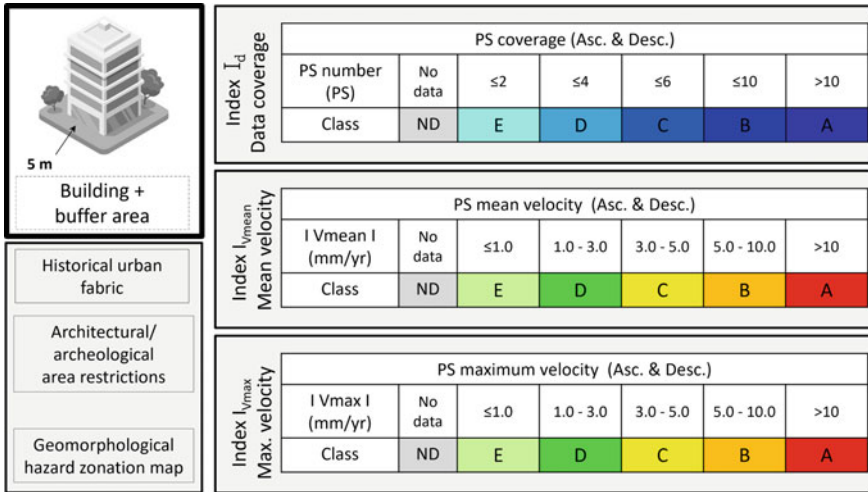
Fig. 3.3 Rating of PS coverage and instability indexes for building classification

The I_{vmean} Mean Velocity Index and the I_{vmax} Maximum Velocity Index are defined according respectively to the average value and the maximum value of the velocity ranges of PSI within the building buffers. The absolute value of velocities was considered since we merged deformation rates with negative and positive sign (which stands respectively for movements away and towards the satellite sensor) from ascending and descending orbits. The I_{vmean} and I_{vmax} indexes scored from E to A and are colour-coded from green to red (from 'stable structure' to 'critical deformation').

Values of 5 classes are dimensioned according to the PSI VLOS (velocities recorded along the LOS in mm/yr). It is worth to notice that the ranges of Class E, which means the most stable condition, was set as variable according to the standard deviation value (1.0 mm/yr) of the PSI population of SNT data, respectively.

The No Data (ND) class of each Index refers to building where no PS was identified within its buffer area boundaries.

3.3.2 Data on Test Cities

PSI ground deformation data used in this work on the two test cities consist of measures derived from Sentinel-1 (SNT) data on Florence city and Lucca city acquired in the spanning time 2014–2021 elaborated with the SqueeSAR technique [22] available in the framework of the on-going InSAR monitoring system financed by the Regional Government of Tuscany within the agreement 'Monitoring ground deformation in the Tuscany Region with satellite radar data' [12, 27].

The spatial distributions of PSI LOS velocities in descending orbit on Lucca and Florence cities are shown in Fig. 3.4. The negative sign stands for an increasing

distance of the target from the satellite sensor, whilst a positive sign means a movement towards the satellite. Within the PSI velocity, the stability threshold for distinguishing stable targets (displayed in a green colour) from moving ones is fixed at ±1.0 mm/yr. This velocity threshold is chosen according to the standard deviation values of the PS population and in agreement with stable threshold values already tested and adopted by the scientific community [6].

Sentinel-1 PSI data on Florence *buffer zone* show deformation rates within the stable range. An area of subsidence with ground motion rate of 4–5 mm/yr is recognized in Mercafir Olmatello area, due to urban-induced loading for recent construction of a Marshal and Police Officers School Complex. Some further areas present mean velocity values of 3–4 mm/yr in both ascending and descending orbit that demonstrate the presence of slight lowering motions, in correspondence of construction works for high-speed rail lines at Circondaria-Viale Corsica and Campo Marte station.

Sentinel-1 PSI data on Lucca municipality reveal some sparse ground movements with average velocity values of 5–6 mm/yr in areas involved in active or dormant landslides (e.g. landslides in Pieve Santo Stefano and Mutigliano NE of
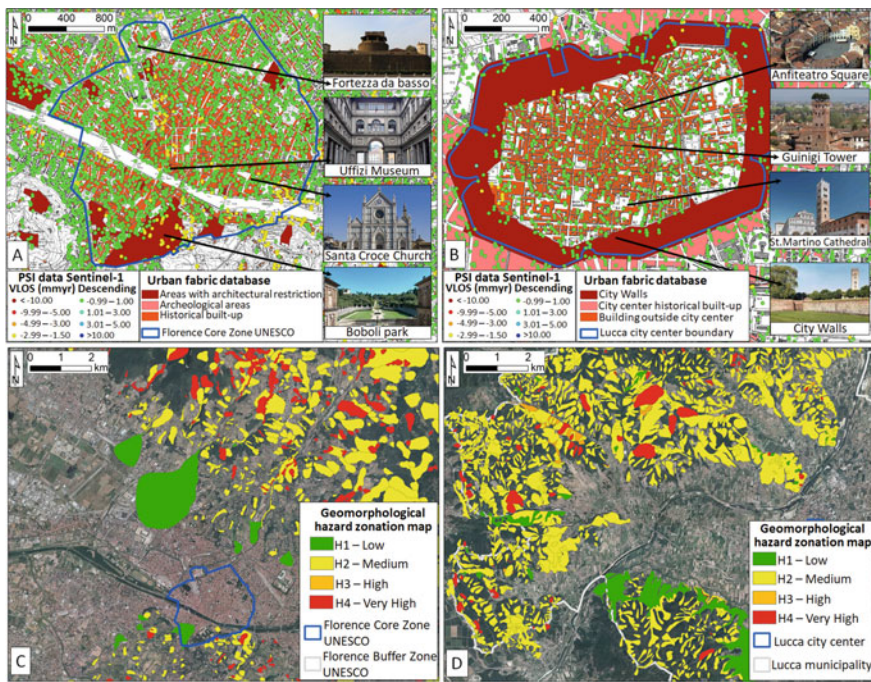
Fig. 3.4 **a** PSI data, urban fabric and photos of some CH sites of Florence city; **b** PSI data, urban fabric and photos of some CH sites of Lucca city; **c** Geomorphological hazard zonation map on Florence area; **d** Geomorphological hazard zonation map on Lucca municipality

Lucca city) or in areas characterized by very local subsidence phenomena probably due to groundwater pumping.

The urban fabric datasets consist of two different databases on Florence and Lucca cities: (i) The database on Florence city comprises the buildings included within the UNESCO buffer zone. It consists of 4040 manufacts, 877 of which located in the UNESCO Core zone, and it is composed of the whole historical built-up fabric, the archaeological areas, and the sites with architectural restrictions, i.e. parks, villas, castles, churches (Territorial Coordination Plan of Florence province—PTCP); (ii) The database on Lucca city comprises the buildings included within the Lucca municipality. It consists of 6848 manufacts: 4759 buildings are located within the historical city centre and are derived from the 1:2000 topographic map taken from the Regional website of Tuscany Region, 1 polygon refers to the wall embrace around the city centre and 2090 buildings are historical buildings located outside the city walls including i.e. churches, parks, and villas subject to architectural restrictions.

In order to characterize the geomorphological setting of the two test cities with particular regard to the hydrogeological hazard, we also acquired the geomorphological hazard zonation maps derived from regional landslide inventory map and from PAI (Hydrological setting Plan) referred to Arno and Serchio river basins. These zonation maps, provided by the River Basin District Authorities, classify the territory into 4 classes of landslide hazard-prone areas (named H1 to H4: moderate, medium, high, very high hazard).

3.4 Analysis and Results

The computation of the PSI data coverage and instability indexes for the built-up database of Florence city show that, by considering all the 4040 manufacts within the UNESCO buffer zone, 1106 structures (27% of the total amount) have no measurement points falling within their tolerance area (ND class); it is noteworthy that, given the medium resolution of the Sentinel-1 satellite, the manufacts are spatially small compared to the ground spatial resolution (5×20 m) of the satellite. An amount of 266 and 307 buildings were respectively in class A (7%) and B (8%) of the I_d Data Coverage Index (Table 3.1).

Results from the computation of the I_{vmean} Mean Velocity and the I_{vmax} Maximum Velocity Indexes show an overall stability of all the buildings within the Florence UNESCO buffer and core zones (Fig. 3.5). With regard to I_{vmean}, a percentage of 70% of manufacts (2821 buildings) fall into class E (mean velocity < 1.0 mm/yr), 3% (112 buildings) fall into class D (mean velocity < 3 mm/yr, which is a very low rate, still being nearly the minimum values exceeding the accuracy of the PSI technique). No building is detected to be in class B and A (Table 3.1). The one building in class C (mean velocity of 3–5 mm/yr) corresponds to Fattoria di Maiano complex nearby Fiesole, where descending PSI data show ground motion displacements downwards the slope.

Table 3.1 Coverage and instability indexes computed for Florence and Lucca built-up database

Index	ND	E	D	C	B	A
	Florence: 4040 buildings					
I_d data coverage (SNT)	1106 (27%)	1372 (34%)	665 (16%)	324 (8%)	307 (8%)	266 (7%)
I_{vmean} mean velocity	1106 (27%)	2821 (70%)	112 (3%)	1 (<0%)	0 (0%)	0 (0%)
I_{vmax} maximum velocity	1106 (27%)	2653 (66%)	277 (7%)	3 (<0%)	1 (<0%)	0 (0%)
	Lucca: 6848 buildings					
I_d data coverage (SNT)	3776 (55%)	1921 (28%)	502 (8%)	267 (4%)	228 (3%)	154 (2%)
I_{vmean} mean velocity	3776 (55%)	2958 (43%)	112 (2%)	1 (<0%)	1 (<0%)	0 (0%)
I_{vmax} maximum velocity	3776 (55%)	2728 (40%)	337 (5%)	4 (<0%)	2 (<0%)	1 (<0%)

Numbers and percentages refer to the amounts and % of the total of buildings in each Index class
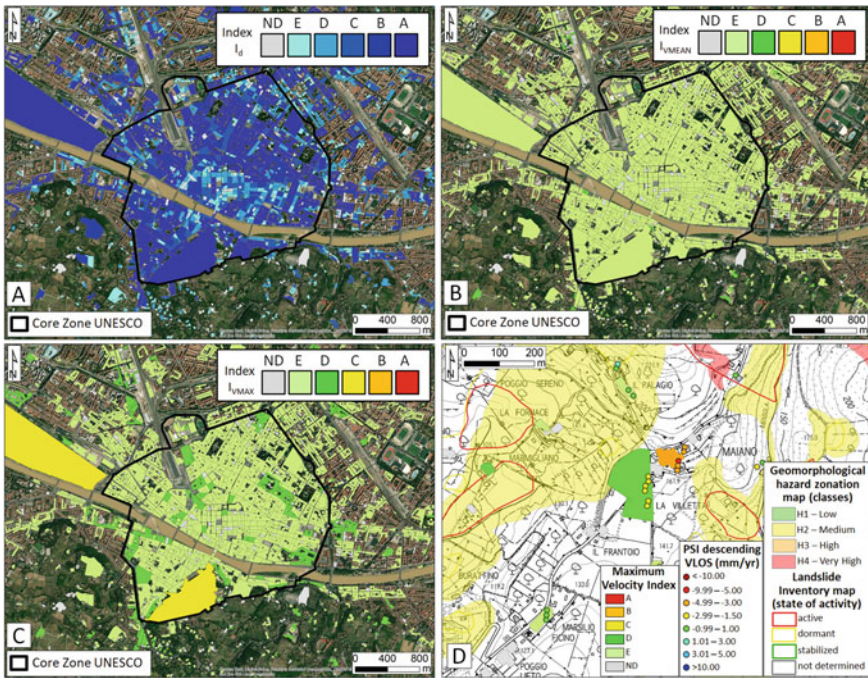
Fig. 3.5 **a** Data coverage index I_d on Florence UNESCO core zone; **b** Mean velocity index I_{vmean} on Florence UNESCO core zone; **c** Maximum velocity index I_{vmax} on Lucca city centre; **d** Maiano site

These terrain movements could derive from surface ground deformation related to slope instability of the area. It is worth to notice that an active rotational slide is mapped downhill in the regional inventory about 100 m southwards the complex and that in this area the geomorphological hazard class is H3 due to presence of potential erosional or gravitation mass movements; this zonation could be potentially enlarged uphill to include area where moving PSI data are detected on the Maiano complex (Fig. 3.5d).

With regard to I_{vmax}, data show similar results with I_{vmean} since 66% of buildings are in class E, 277 structures are in class D (7%), 3 in class C, and 1 in class B corresponding to the previously mentioned complex of Fattoria di Maiano. The three structures in class C correspond to Cascine Park, Boboli Park and a building in San Gaggio village southward Florence city centre: such category comes out due to the presence of one radar benchmark with yearly mean velocity of 3.1–3.5 mm/yr within each structure's buffer, but this should not be critical because in any case we are dealing with low and single deformation values.

Concerning the built-up database of Lucca city, the computation of the PSI data coverage and instability indexes reveal that information can be provided for 45% of the buildings since 55% has no PSI data within its buffer area (ND class). An amount of 1921 buildings (28% of the total) fall in class E of the Data Coverage Index, whilst remaining manufacts are distributed in the other classes. A percentage of 2% of buildings show more than 10 PS targets within their buffer area (Class A of I_d) (Table 3.1).

The Mean Velocity Index I_{vmean} and the Maximum Velocity Index I_{vmax} computed for the whole Lucca urban fabric database also show a general stability (Fig. 3.6). In particular, most of the historical buildings of city centre inside the wall embrace has no data, but the ones with PSI information, including the wall belt, primarily fall into class E and secondarily in class D of both instability indexes I_{vmean} and I_{vmax}. Outside the historical city centre, one main situation with high stability index (i.e. class B and A) can be highlighted: it is the Pieve Santo Stefano Church, NE of Lucca city, that reveals an average and maximum velocity of 6 mm/yr (Class B of I_{vmean}) and 15 mm/yr (class A of I_{vmax}), respectively. The manufact is located on a large active landslide already mapped in the regional landslide inventory. The area is classified in class H4 of the hazard zonation map. The moving PSI targets on the church and on other near edifices are located on the crown of the landslide, whose elevation ranges between 270 and 120 m, and show LOS velocity values up to 12.6 mm/yr (Fig. 3.6d).
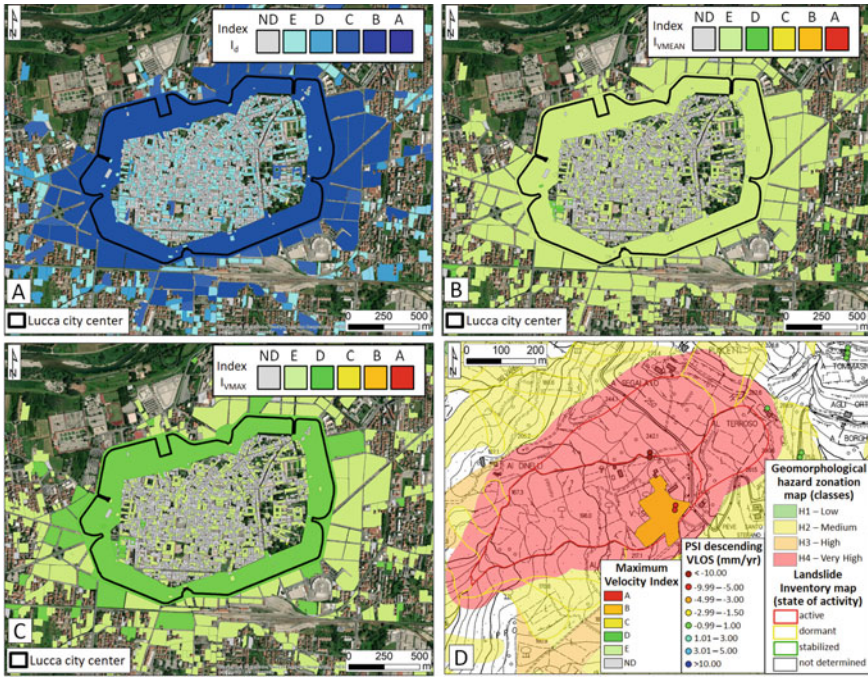
Fig. 3.6 **a** Data coverage index I_d on Lucca city centre; **b** Mean velocity index I_{vmean} on Lucca city centre; **c** Maximum velocity index I_{vmax} on Lucca city centre; **d** Pieve Santo Stefano Church

3.5 Discussion and Conclusions

The exploitation of satellite Earth Observation data can support the mapping and monitoring of the ground movements that could affect the urbanized heritage of the city by threatening its integrity and stability. Satellite remote sensing techniques are an efficient tool to this aim, given the need to adopt non-invasive techniques without direct contact with the objects of investigation in order not to damage them.

In this framework, the use of the space-based multi-temporal interferometric data from the EO Copernicus programme provides millimetric measurements of displacement over the territory for periodically and regularly monitoring ground deformations especially on urban areas. In particular, PSI data derived from systematic acquisitions of Sentinel-1 constellation every 6–12 days can scan the territory and rapidly point out the highest deformations rates and most hazardous sites over the historical and cultural heritage of cities and surrounding territories.

In this work, a novel set of PSI-based indexes are proposed to categorize the deformation conditions of manufacts at the local scale. For each building, PS coverage and deformation rates of PSI are converted into three classification indexes, named I_d (Data Coverage Index), I_{vmean} (Mean Velocity Index) and I_{vmax} (Maximum Velocity Index).

The methodological procedure to compute the classification indexes was purposely trained on PSI dataset from medium resolution Sentinel-1 SAR images.

It is worth to highlight that some choices in the proposed procedures are needed to be set by considering the type of satellite radar data we are using, referring to the spatial resolution of SAR imagery of the satellite. For instance, with regard to the Data Coverage Index (I_d), the number of radar benchmarks for defining each class should be set according to the used SAR satellite sensor: so, if radar data at high spatial resolution are employed, e.g. X-band COSMO-SkyMed (CSK) data with high density of retrieved radar targets, a higher number of PSI data should be defined with respect to the proposed ones for Sentinel-1 medium resolution data.

Likewise, the buffer area around each building should be dimensioned according to the cellsize of SAR radar image, i.e. 5 m if using medium resolution C-band data, as in our work, or lower values (e.g. 3 m) if exploiting higher spatial resolution X-band data. Furthermore, the exploitation of X-band radar data could allow retrieving information on a higher number of buildings and thus reducing the amount of manufacts in ND class.

The building instability rating proposed in this work can optimize the use of PSI datasets with regards to spatial distribution and velocity information at the manufact scale, since deformation rates are converted into outputs with colour-coded rates that surveyors and end-users can be familiar with and easy to be understood.

The test examples over the urban heritage of Florence and Lucca cities prove the suitability of the colour-coding rating system: surveyors could clearly recognize, even at small scale, the buildings that require attention and further analysis.

Overall, all the buildings of the built-up database within the Florence UNESCO buffer zone show stability and no critical situation is identified. On Lucca municipality, PSI data and computed instability Indexes also reveal stability over buildings within the historical city centre embraced within the wall belt and nominated in UNESCO Tentative List. A most critical situation was recognized by means of Indexes computation on the Pieve Santo Stefano Church, NE of Lucca city, which turns out to be classified in high classes (class A and B) of the Maximum Velocity Index I_{vmax} and Mean Velocity Index I_{vmean}, as located on the most hazard geomorphological zonation H4 due to the presence of a large mapped active landslide.

In conclusion, this PSI-based procedure applied to the built-up heritage of urban settings could be useful within the management plan as strategic and operational tool through which it is possible to monitor and protect cultural heritage sites. Moreover, it could be a valuable opportunity to consider and include an effective characterization of ground deformation rates and geohazards on the cultural heritage for its correct conditions assessment and for better planning where to establish proper interventions.

References

1. Themistocleous K, Danezis C, Frattini P, Crosta G, Valagussa A(2018) Best practices for monitoring, mitigation, and preservation of cultural heritage sites affected by geo-hazards: the results of the PROTHEGO project. In: Proceedings of 6th international conference on remote sensing and geoinformation of the environment, Paphos, Cyprus

2. Ferretti A, Prati C, Rocca F (2001) Permanent scatterers in SAR interferometry. IEEE Trans Geosci Remote Sens 39(1):8–20

3. Tapete D, Cigna F (2017) Trends and perspectives of space-borne SAR remote sensing for archaeological landscape and cultural heritage applications. J Archaeol Sci Rep 14:716–726

4. Tapete D, Cigna F (2019) COSMO-SkyMed SAR for detection and monitoring of archaeological and cultural heritage sites. Remote Sens 11:1326

5. Chen F, You J, Tang P, Zhou W, Masini N, Lasaponara R (2018) Unique performance of spaceborne SAR remote sensing in cultural heritage applications: overviews and perspectives. Archaeol Prospect 25(1):71–79

6. Bianchini S, Pratesi F, Nolesini T, Casagli N (2015) Building deformation assessment by means of persistent scatterer interferometry analysis on a landslide-affected area: the Volterra (Italy) case study. Remote Sens 7(4):4678–4701

7. Bru G, Herrera G, Tomás R, Duro J, de la Vega R, Mulas J (2010) Control of deformation of buildings affected by subsidence using persistent scatterer interferometry. Struct Infrastruct Eng 9:188–200

8. Sanabria MP, Guardiola-Albert C, Tomás R, Herrera G, Prieto A, Sánchez H, Tessitore S (2014) Subsidence activity maps derived from DInSAR data: Orihuela case study. Nat Hazards Earth Syst Sci 14:1341–1360

9. Pratesi F, Tapete D, Terenzi G, Del Ventisette C, Moretti S (2015) Rating health and stability of engineering structures via classification indexes of InSAR Persistent Scatterers. Int J Appl Earth Obs Geoinf 40:81–90

10. Margottini C, Spizzichino D (2014) The management of cultural heritage in sites prone to natural hazard. Mem Descr Carta Geologica d'Italia 96:415–430

11. Ciampalini A, Bardi F, Bianchini S, Frodella W, Del Ventisette C, Moretti S, Casagli N (2014) Analysis of building deformation in landslide area using multisensor PSInSAR™ technique. Int J Appl Earth Obs Geoinf 33:166–180

12. Bianchini S, Raspini F, Solari L, Del Soldato M, Ciampalini A, Rosi A, Casagli N (2018) From picture to movie: twenty years of ground deformation recording over Tuscany region (Italy) with satellite InSAR. Front Earth Sci 6:177

13. Morelli S, Pazzi V, Tofani V, Raspini F, Bianchini S, Casagli N (2021) Reconstruction of the slope instability conditions before the 2016 failure in an Urbanized District of Florence (Italy), a UNESCO world heritage site. In: Sassa K, Mikoš M, Sassa S, Bobrowsky PT, Takara K, Dang K (eds) Understanding and reducing landslide disaster risk. Springer, Cham, pp 449–455

14. Morelli S, Segoni S, Manzo G, Ermini L, Catani F (2012) Urban planning, flood risk and public policy: the case of the Arno River, Firenze, Italy. Appl Geogr 34:205–218

15. Capecchi F, Guazzone G, Pranzini G (1975) Il bacino lacustre di Firenze-Prato-Pistoia. Geologia del sottosuolo e ricostruzione evolutiva. Boll Soc Geol It 94:637–660

16. Coli M, Rubellini P (2007) Note di Geologia Fiorentina. Società Elaborazioni Cartografiche, Florence, Italy

17. Pandeli E (2008) La pianura di Firenze-Prato-Pistoia nel quadro dell'evoluzione geologica dell'Appennino settentrionale. In: Un piano per la Piana: idee e progetti per un parco. Unifi, Florence, Italy, pp 1–16

18. Briganti R, Ciufegni G, Coli M, Polimeni S, Pranzini G (2003) Underground florence: plio-quaternary geological evolution of the Florence area. Boll Soc Geol Ital 122:435–445

19. De Zolt S, Lionello P, Nuhu A, Tomasin A (2006) The disastrous storm of 4 November 1966 on Italy. Nat Hazard Earth Sys 6(5):861–879

20. Bisson M, Piccinini S, Zanchetta G (2011) A multidisciplinary GIS-based approach for mapping paleoriver migration: a case study of the Serchio River. GIScience Remote Sens 48(4):566–582
21. Nardi R, Nolledi G, Puccinelli A, Rossi F (1987) Geologia e idrogeologia della Pianura di Lucca. Geogr Fis Dinam Quat 10:132–160
22. Ferretti A, Fumagalli A, Novali F, Prati C, Rocca F, Rucci A (2011) A new algorithm for processing interferometric datastacks: SqueeSAR™. IEEE Trans Geosci Remote Sens 49:3460–3470
23. Crosetto M, Monserrat O, Cuevas-González M, Devanthéry N, Crippa B (2016) Persistent scatterer interferometry: a review. ISPRS J Photogramm Remote Sens 115:78–89
24. Salim NAA, Zahari NF (2011) Developing integrated building indicator system (IBIS) (a method of formulating the building condition rating). Procedia Eng 20
25. Wahida RN, Milton G, Hamadan N, Lah N, Mohammed AH (2012) Building condition assessment imperative and process. Procedia-Soc Behav Sci 65
26. Pratesi F, Tapete D, Del Ventisette C, Moretti S (2016) Mapping interactions between geology, subsurface resource exploitation and urban development in transforming cities using InSAR Persistent Scatterers: two decades of change in Florence, Italy. Appl Geogr 77:20–37
27. Raspini F, Bianchini S, Ciampalini A, Del Soldato M, Solari L, Novali F, Del Conte S, Rucci A, Ferretti A, Casagli N (2018) Continuous, semi-automatic monitoring of ground deformation using Sentinel-1 satellites. Sci Rep 8(1):1–11

Chapter 4
The Risk of Heat Waves to Historic Urban Areas. A GIS-Based Model for Developing a Risk Assessment Methodology

Laura Quesada-Ganuza , **Leire Garmendia** , **Irantzu Alvarez** ,
Estibaliz Briz , **Alessandra Gandini** , and **Marta Olazabal**

Abstract Climate change impacts such as extreme events and progressive global warming are threatening the conservation and livability of urban cultural heritage. Understanding climate risks on heritage should be part of policy and planning decision-making processes to increase resilience and sustainability of both social and built environmental systems. However, despite a large body of literature focusing on climate-related hazards, there is a noticeable knowledge gap regarding a holistic conceptualization of the risks in historic urban areas, which is particularly concerning in the case of the impacts of heat waves and heat urban island phenomena on urban heritage. The main goal of this study is to analyze and represent the interaction between urban spaces and heat waves via geographic information systems (GIS) data, considering the vulnerability of historic areas both as urban systems and as heritage areas. To frame a holistic approach, socioeconomic, cultural, governance (services

L. Quesada-Ganuza (✉) · L. Garmendia · E. Briz
Department of Mechanical Engineering, School of Engineering Bilbao, University of the Basque Country UPV/EHU, Plaza Ingeniero Torres Quevedo s/n, (48013) Bilbao, Spain
e-mail: laura.quesada@ehu.eus

L. Garmendia
e-mail: leire.garmendia@ehu.eus

E. Briz
e-mail: estibaliz.briz@ehu.eus

I. Alvarez
Department of Graphic Design and Engineering Projects, School of Engineering Bilbao, University of the Basque Country UPV/EHU, Rafael Moreno "Pitxitxi", (48013) Bilbao, Spain
e-mail: Irantzu.alvarez@ehu.eus

A. Gandini
TECNALIA, Basque Research and Technology Alliance (BRTA), Parque Tecnológico De Bizkaia, Astondo Bidea, Edificio 700, 48160 Derio, Spain
e-mail: alessandra.gandini@tecnalia.com

M. Olazabal
Basque Centre for Climate Change (BC3), Sede Building 1, 1st Floor Scientific Campus of the University of the Basque Country, (48940) Leioa, Spain
e-mail: marta.olazabal@bc3research.org

and resources), and physical (gathering tangible characteristics of all infrastructures, elements, and buildings) aspects of the system are taken into account. To this end, key performance indicators addressing relevant vulnerable elements of historic urban areas are identified for the development of a risk assessment methodology. Complementary and as foundation for the risk assessment, a categorization of vulnerability to heat waves is proposed for both buildings and urban spaces. Here, the gathering and processing of data for the development of a GIS-based model in the historic area of Bilbao, Basque Country is presented. This work aims to serve as a basis and reference for future holistic assessments of heatwaves risks in historic urban areas worldwide.

Keywords Historic urban areas · Climate change · Risk assessment · Vulnerability assessment · Key performance indicators

4.1   Introduction and Objective

As stated by the World Meteorological Organization (WMO) [26] Global warming increases with the twenty-first century being the warmest on record. The global warming is causing an increase in the frequency and strength of extreme events, among them heat waves are one of the main ones [12]. Urban areas and their surroundings record some of the maximum temperatures [13]. The larger urban areas will accumulate most of the world population in the near future (Considering the predictions for 2025 population) [25], being exposed to at least a mean of 2 °C above pre-industrial levels.

Heat waves are a cause of increase in mortality rates, with the population in urban areas being vulnerable to extremes in heat and relative humidity. The impact of heat waves can adversely affect not only the health of urban residents, well-being, and livelihoods, but also affects the urban ecosystems and infrastructures [27]. The AR5, the most recent special report from the Intergovernmental Panel on Climate Change (IPCC) [13], states that to increase the future resilience to climate change, urban areas and infrastructure are one of the systems in need of mayor transformation. There are certain urban characteristics that differentiate their response to the changing climate, namely, low permeability of the soil, density of population, higher concentrations of productive activities, and the specific construction materials. Cities suffer from specific microclimates because of the aforementioned characteristics that cause the heat island effect, resulting in higher temperatures, under the same climatic conditions, than the surrounding countryside [11].

Within cities, old quarters are the root of cultural identity and sense of place, concentrating important economic assets that make them very relevant. These historic urban areas have very specific characteristics that differentiate them when faced with changes in climate and extreme events [22]. Their distinct vulnerabilities are related to physical characteristics of the built and tangible assets, but also the complete cultural landscape, such as specific population patterns, tourism, or traditional socioeconomic

activities. Because of this, relevant heritage organizations such as ICOMOS and UNESCO have made climate change and risk prevention one of their primary focuses over the past decade [4, 18]. In conclusion, the risk that historic urban areas face with climate change and related extreme events and its assessment is a priority to guide future policy and research.

This paper is divided into four main sections. In the first three, the objective is to develop the indicators and categorization that will feed the data needed for the development of the GIS model that is explained on the last section of this work. The goal of the first section is to set the framework for the research work, setting goals, and developing a methodological approach. In the second part, key performance indicators for risk assessment methodologies are identified. These indicators address both the elements of historic urban areas as part of a system and the potential impact of prolonged heat waves. In the third part, a categorization is proposed for both buildings and urban spaces within historic urban areas regarding their vulnerability to heat waves. At last, the case study of Bilbao is presented, with the gathering and processing of data for the development of the aforementioned categorization of the area in a GIS model.

4.2 First Steps for a Risk Assessment Methodology

4.2.1 Framework and Methodological Approach

The lack of research on the heat wave vulnerability assessment for historic areas is a noticeable gap in knowledge [21]. Hence, the present study aims to assess the vulnerability of historic urban areas, considering their complexity as physical and socioeconomic entities, and to provide the framework for a risk assessment methodology. The main objective of this paper is to develop the first steps for the development of a holistic and multi-criteria methodology for risk assessment of historic urban areas toward heat waves and implement them in the case study of Bilbao. The future methodology should provide support for the prioritization of future adaptation actions, using a holistic perspective to identify vulnerabilities and risks in historic urban areas.

This research has a multi-scalar approach that considers both the buildings and the urban spaces. The proposed indicators and characterization are thought taking into consideration all kinds of urban areas, to promote their integration at city scale and not stay isolated in historical areas. Vulnerability and risk assessment methodologies are founded onto the use of individual or composite indicators that generate information about non-measurable conditions and enable to compare differently measured data [15]. To begin a risk assessment, the first steps are to define the objectives (why), what system is being analyzed (who/what; in this case the historic urban areas), the stressors/hazard (to what; in this case, heat waves) and the time horizon (when) [1, 8].

The main stressor or hazard in this case is heat waves that are characterized differently depending on the climate. As a general definition, the WMO guidance on heat-health warning (WMO-No.1142) defines heat waves as periods of unusually hot and dry or hot and humid weather that have a duration of at least two to three days and a discernible impact on human activities [14]. Therefore, heat waves can be characterized using two main indicators, temperature and relative humidity (RH); distinguishing between dry and humid heat waves [5]. Consequently, the development of exposure or vulnerability indicators must come from the analysis of the effects of high heat and low or high humidity on the elements that conform the system of a historic urban area.

When assessing heat waves in urban areas, the urban heat island phenomenon must be a primary consideration. This phenomenon shows how morphology of an urban area affecting its shading and ventilation, the technical characteristics of urban elements and materials, and the type and distribution of green spaces influence its intensity [16]. Urban geometry and materials influence wind flow, energy absorption, and the ability of surfaces to release long wave radiation back to space [10] causing the urban heat island effect.

As previously mentioned, this work defines historic urban areas addressing the system from the twofold perspective or an urban area and a historic area. The indicators derive mainly from literature review, either from and urban perspective, or weathering of historic materials. For a holistic approach, the assessment of every system needs to be addressed, distinguishing between social and economic, cultural, governance (services and resources), and physical (gathering tangible characteristics of all infrastructures, elements, and buildings).

For the present study, the workflow is proposed as follows: the first step is the collection of information to feed a multiscale data model, which in turn provides a statistical overview of the historical area and feeds the sample building categorization process explained in Sect. 4.4 of this paper, that composes the second step. The more complete information gathered during this process is basis for the last and third step of the vulnerability and risk assessment.

4.3 Key Performance Indicators

As guided by the foundation set in the previous section of this paper, the characterization of the potential impacts of heat waves and the urban heat island on the systems that conform the historic urban area will result in the indicators. The impact chain, therefore, is a result of the mentioned approach and its combination with the AR5 framework from the Intergovernmental Panel on Climate Change (IPCC) (Figs. 4.1 and 4.2).

Beginning with heat waves as the hazard, the main parameters for its characterization will be temperature, humidity, and sun exposure (short-wave solar radiation). The different variations in relative humidity can adversely affect traditional materials. Therefore, humidity cycles and shocks have to be considered [3].
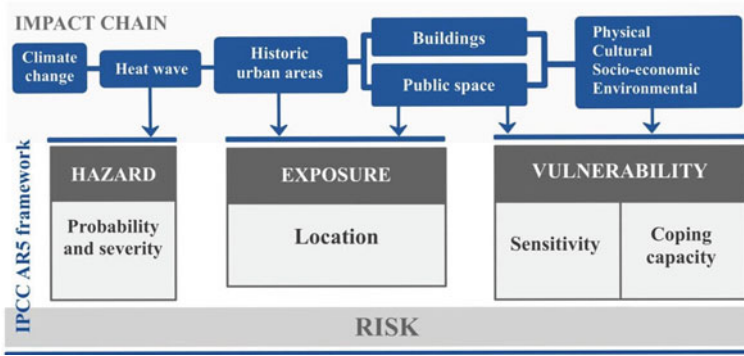
Fig. 4.1 Relation between IPCC AR5 framework for risk assessment and the proposed impact chain for historic urban areas
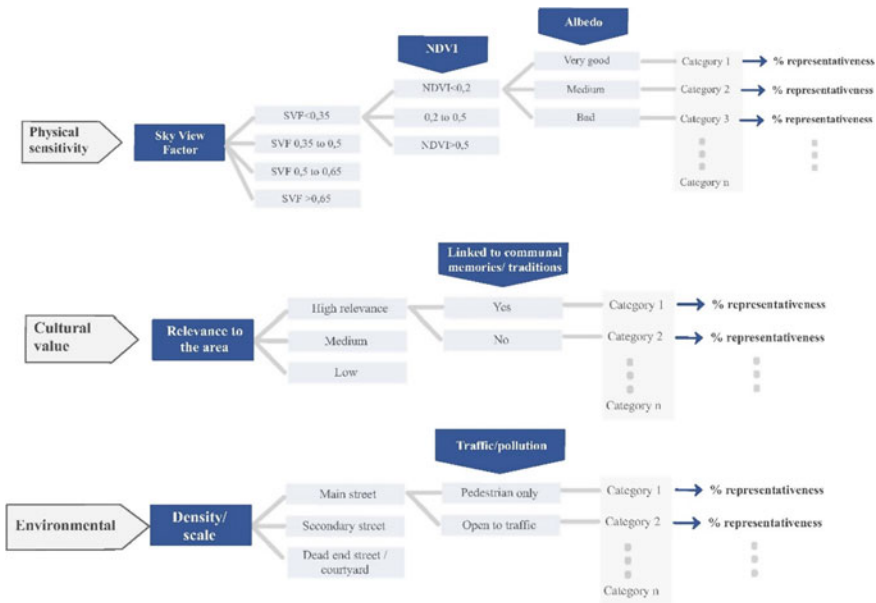
Fig. 4.2 Example of the proposal for the categorization process for public space

In the case of exposure, in regards to the buildings, sun exposure, or exposure to short-wave radiation, is the primary indicator. Hence, the number of daily hours during which the envelope is hit by solar radiation, that along with the orientation of the building results in the exposure of the different façades to the sun, in addition the shading of the surrounding buildings has to be taken into consideration. In the case of open public spaces, urban heat island indicators sky view factor (SVF) and normalized difference vegetation index (NDVI) have to be considered. The phenomenon

known as urban canyon is determined mainly by SVF [10], indicating the proportion of an urban space related to heat storage [6], also the NDVI uses satellite images to quantify the amount and quality of the vegetation. Along with these two main indicators, tropospheric ozone (O_3) levels and acoustic pollution appear in literature linked to heat. Literature indicates that conditions such as high temperature, intense solar radiations, and long sunshine hours, all specific meteorological characteristics linked to heatwaves [20], can cause an increase in ozone levels, with high ozone levels being dangerous for human health [23]. Regarding acoustic pollution, heat storage inside buildings can be higher in high street noise areas because of inhabitants tending to reduce ventilation with the goal of shielding themselves from the noise [19].

As with exposure, sensitivity indicators are divided between building and open spaces. The sensitivity of the buildings is divided among four aspects: social, physical, economic, and cultural sensitivity. Population density, age group, and socioeconomic data define social sensitivity. Physical sensitivity, on the other hand, is determined by the possible weathering of sensitive traditional materials under heat wave conditions [3] linked to their construction date and style, and the thermal characteristics of the materials, that is, albedo and thermal diffusivity. In the case of economic sensitivity, the indicators are based on the use of the building, considering either its productive use, residential, public, etc., or its relevance for tourism. Cultural sensitivity is defined by the link of the building either to communal memories or to rituals or traditions and its protection level. As for the sensitivity of public spaces to heat waves, the indicators are divided among its physical characteristics, in this case, albedo, its use, and its cultural value, regarding its link either to communal memories or to rituals and traditions.

Coping capacity indicators are divided between building and public space. For the assessment of social coping capacity within the buildings, healthcare access (distance to hospital and availability of hospital beds) and awareness of the population to the hazard (like the existence of emergency plans) are the main indicators, added to accessibility, in this case, the existence of elevator. In the case of open public spaces, accessibility for ambulances and firefighters is the main parameter considered.

4.4 Categorization of Historic Urban Areas

The step of categorization is very relevant in a risk assessment methodology when it comes to its replicability.

When assessing a large and varied stock of elements such as the ones that conform an urban area, a statistical approach is a good strategy, with the aim to describe all the assets using archetypes o sample assets. Archetypes include estimated statistical data whereas sample assets refer to real elements of the area that include measured data [2, 24]. To categorize an area, the methodology will be, therefore, a statistical overview of the characteristics of both buildings and open spaces, starting from samples and then extrapolating these results to elements of the same category, resulting in a

complete vulnerability assessment for the historic area. For this goal, it is necessary to create a limited number of samples that are a representation of almost every element under assessment of the historic urban area, taking into consideration data availability. Considering the approach used for the development of the indicators, the categories will reflect the vulnerabilities of both buildings and public space to heat waves, considering their cultural value, use, social, and constructive characteristics. Moreover, data should be as widely available as possible, in order to build a replicable model for different case studies [7, 9].

A main consideration during this process should be the balance between the amount of categories and their representativeness considering the relevance of the indicators, for this a minimum threshold is set to discard the less representative categories. Depending on the size and homogeneity that the area presents, the threshold should be set between 2 and 5% [7].

Following the groundwork set in the development of the indicators, building categorization will be divided between physical sensitivity, use, cultural value, and social sensitivity:

- Physical sensitivity: namely the correlation between the year of construction (divided into construction periods that have similar construction techniques/materials, and consequently, the same vulnerability to heat waves) and state of conservation of the building.
- Use: buildings main use, residential, industrial, public use or touristic use, while adding relevant added characteristics such as commercial use, the existence of touristic apartments in, or the sensitivity of its use to heat wave conditions.
- Cultural value: protection level of the buildings considering if it is linked or not to communal memories or traditions.
- Social sensitivity: population density is the main category in this area, adding the percentage of population older than 65.

In the characterization of public space, following physical sensitivity, cultural value, and environmental characteristics (Fig. 4.3) these parameters were chosen:

- Physical sensitivity: considers three subdivisions, starting with the sky view factor to predict the possible street canyons, and NVDI levels to measure the amount of vegetation and albedo of the spaces.
- Cultural value relevance of the space for the life in the area, then adding if it is linked or not to communal memories or traditions.
- Environmental characteristics: considers the density or scale of the space, distinguishing between main and secondary streets, and adding the parameter of the existence of traffic or if it is only pedestrian.

Fig. 4.3 The area selected as the case study, historic district of the city of Bilbao, and sectors of study

4.5 The Case Study of Bilbao and Development of the GIS Model for the Characterization

4.5.1 Bilbao's Old Quarters

Bilbao is located in the northwest of Spain with approximately 345.000 inhabitants. The area selected as the case study is the historic district of the city of Bilbao (See Fig. 4.4). For the present study, most of the historical and protection information has been gathered from the "PLAN ESPECIAL DE REHABILITACIÓN DEL CASCO VIEJO DE BILBAO" (Special Rehabilitation Plan for the Historic City Core of Bilbao) approved in 1998 with the goal of addressing the preservation and re-structuring of the old town.

The selected area is divided into six sectors, of those five falls into the study area. These sectors are differentiated according to the historical morphology and growth of the city. Sector 1 is the "Siete Calles" district, with a layout inherited from the tenth century in its configuration; from the sixteenth century in the palatial specialization of the head plots of the Ribera, and from the second half of the nineteenth century on its house typology. Perpendicular to the estuary, the streets are the organizing element, marking a buildable intermediate of 32 m with 5.50 m streets; such an organization is justified, both by a tradition inherited from the Roman grid, as for the evacuation of water and waste in medieval times. Although of secondary importance, 2.60 m wide cantons cut the building groups in "Apples" of irregular dimension. It is an area characterized by a row organization of the plots which measurement does not respond
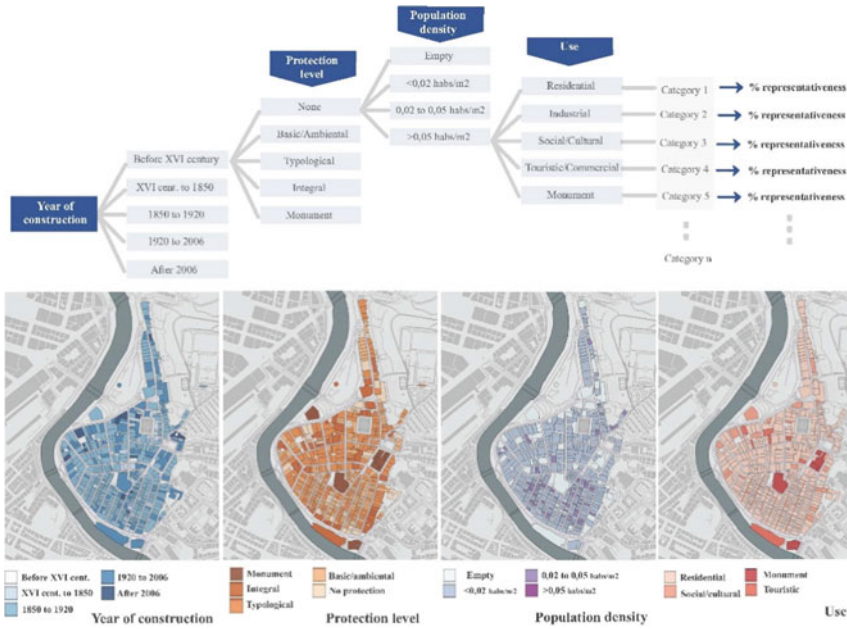
Fig. 4.4 Categorization process for buildings

to a fixed module, ranging from 3.50 to 4 m even six, subordinated to the capacity of the owner and to the technological constants of wood (main structural material historically) and superimposing in height the two uses of housing and commerce, or artisan workshop. Originally, the heart of the Old Quarter was surrounded by walls and consisted of three parallel streets. Later, it became necessary to take down the walls and build four streets perpendicular to the river, which along with the first three. Since 1979, this area has been a pedestrian precinct, with hundreds of commercial establishments, bars, and restaurants.

Sector 2 or Rondas is of typical appearance on the walled cities, within a dynamics of natural growth. The occupational type responds to the same logic, in a long and narrow plot, perpendicular to the wall, forming short-bottomed blocks with direct exits on both sides and entrance, from the inner city side. Currently, the original typologies have been replaced by new buildings of the late nineteenth and early twentieth centuries, allowing a greater use in height. Those replaced in the last century have six heights for the most part, while those of the twentieth century reach the seven heights.

Sector 3 (Ensanche Ribera y Plaza Nueva) originally urbanized during the seventeenth century, this was a land semi invaded by the tide, receiving the name of "Arenales". The Ordinances unified constructive criteria in a, materials and even cornices; façade reforms and additions unified the image of the city. Baroque—neoclassic plot characterized by buildings of oak wood structure as structural support facing the shortage of good stone quarries.

Sector 4 or Arrabales constitute axes of natural growth extramural, starting the settlements from the singular elements generators of the new plot. The type of plot is very varied, so a common norm cannot be drawn for this area.

Sector 6 (Sendeja-Epalza) area developed in the XIX whose parcel type is homogeneous in the block Sendeja-Epalza and more irregular in the front of Ascao. As the edge of this sector is the entire Mallona reserve, in his day concentrating certain "services" of the Villa (cemetery, walks, as well as garden spaces linked to convents), today an important green area for the city.

4.5.2 Building a GIS Model for Bilbao

The GIS model has been completed for the case study of Bilbao with semantic information available from public data sources. The data has been worked in two different ways, most of it has been collected from the Basque Government geographical information database (Geoeuskadi) and processed to automatically include in the data model; other data has been obtained from either satellite data (Copernicus) or through the Urban Multi-scale Environmental Predictor (UMEP) plugin for QGIS [17]. In addition to this, the data from the Special Rehabilitation Plan for the Historic City Core of Bilbao, namely the protection status of the buildings, has been introduced manually. As for Bilbao, not all the data mentioned in the previous steps was available. Hence, some of the parameters have simplified. They were not available: the state of conservation of the buildings, the age of the residents, as well as both indicators of the cultural value of public space. For this reason, in the case of the buildings, the social and physical characterization has been combined to provide a more specific statistical overview of the buildings.

As explained in Sect. 4.2 of this paper, the workflow (Fig. 4.1) first step is the collection of information and the building of a multiscale data model, which in turn provides a statistical overview of the historical area and feeds the sample building categorization process explained in Sect. 4.4 of this paper. The results of this process are divided between buildings and public space following the different aspects mentioned before.

Buildings
See Fig. 4.4

Because of the analysis, ten categories that have a representativeness over 2% are selected. As shown on Table 4.1, most of the buildings are from the period between 1850 and 1920, with basic or typological protection, residential, and with a low population density.

Table 4.1 Results of the categorization of the buildings for Bilbao

Year of construction	Protection	Population density (habs/m^2)	Use	Amount	% of representativeness
XVI century to 1850	Typological	< 002	Residential	18	344
1850 to 1920	Basic/ambiental	< 002	Residential	114	2180
1850 to 1920	Basic/ambiental	002–005	Residential	47	899
1850 to 1920	Typological	< 002	Residential	131	2505
1850 to 1920	Typological	002–005	Residential	21	402
1850 to 1920	Integral	< 002	Residential	19	363
1920 to 2006	none	0	Residential	14	268
1920 to 2006	none	< 002	Residential	34	650
1920 to 2006	Basic/ambiental	< 002	Residential	18	344
1920 to 2006	Typological	< 002	Residential	23	440
			TOTAL		8394

Public Space
See Fig. 4.5
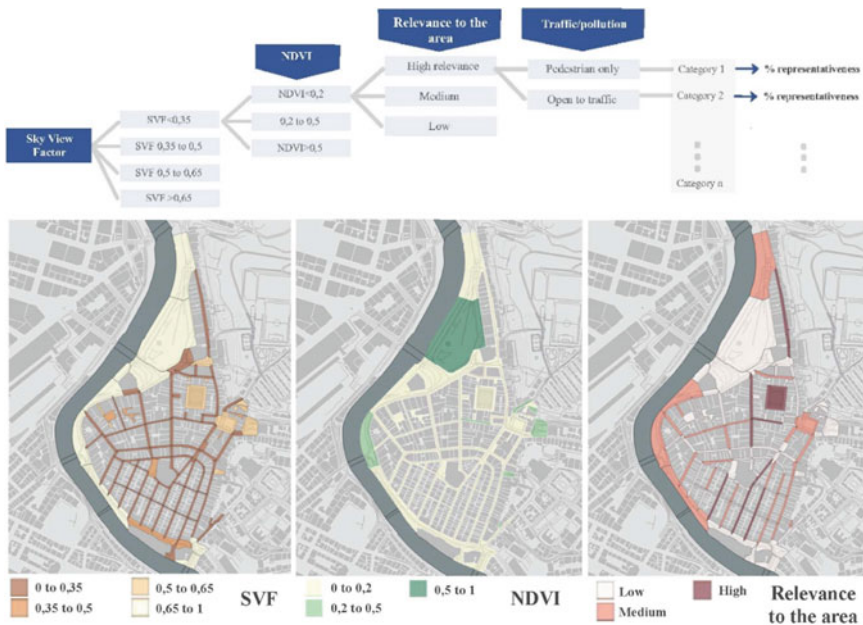
Fig. 4.5 Categorization process for public space for Bilbao

Table 4.2 Results of the categorization of the public space for Bilbao

SVF	NDVI	Relevance	Amount	Percentage Bilbao (%)
< 035	< 02	Low	45	4206
< 035	< 02	Medium	20	1869
< 035	< 02	High	9	841
035–05	< 02	Low	5	467
05–065	< 02	Low	6	561
05–065	02–05	Low	3	280
> 065	< 02	Low	4	374
> 065	< 02	Medium	4	374
			TOTAL	8972

For public space categorization results, eight categories compose nearly 90% of the representativeness as shown on Table 4.2 (with over 2%). The mayor three categories that gather most of the spaces are the ones with a low SVF that characterize the narrowest streets, with a low NDVI for the lack of green elements in those areas.

4.6 Conclusions

Even though climate change risk assessment is a very relevant and necessary topic for designing resilient cities, there is a noticeable gap in knowledge regarding heat wave vulnerability assessment for historic areas. This study presents the first steps for the development of a holistic and multi-criteria methodology for risk assessment of historic urban areas toward heat waves, displaying its application on a case study. The next step should be the identification of risks with a holistic perspective, in order to develop a full methodology that could help in the prioritization of future conservation and adaptation actions.

References

1. Apreda C, D´Ambrosio V, Di Martino F (2019) A climate vulnerability and impact assessment model for complex urban systems. Environ Sci Policy 93(Aug 2018):11–26. https://doi.org/10.1016/j.envsci.2018.12.016
2. Ballarini I, Corgnati S, Corrado V, Talà N (2011) Improving energy modeling of large building stock through the development of archetype buildings

3. Brimblecombe P, Grossi CM, Harris I (2011) Climate change critical to cultural heritage. Survival Sustain 195–205. https://doi.org/10.1007/978-3-540-95991-5

4. Cassar M, Young C, Weighell T, ICCROM, ICOMOS, Sheppard D, Bomhard B, Rosabal P, UNESCO (2007) Climate change and world heritage. Report on predicting and managing the impacts of climate change on world heritage and strategy to assist states parties to implement appropriate management responses (Colette A (ed))

5. Chen X, Li N, Liu J, Zhang Z, Liu Y (2019) Global heat wave hazard considering humidity effects during the 21st century. Int J Environ Res Public Health 16(9). https://doi.org/10.3390/ijerph16091513

6. Dirksen M, Ronda RJ, Theeuwes NE, Pagani GA (2019) Sky view factor calculations and its application in urban heat island studies. Urban Clim 30:100498. https://doi.org/10.1016/j.uclim.2019.100498

7. Egusquiza A, Prieto I, Izkara JL, Béjar R (2018) Multi-scale urban data models for early-stage suitability assessment of energy conservation measures in historic urban areas. Energy Buildings 164:87–98. https://doi.org/10.1016/j.enbuild.2017.12.061

8. GIZ (2013) Vulnerability assessments. Experiences of GIZ with vulnerability assessments at the local level. Enhanced reader. Deutsche Gesellschaftfür Internationale Zusammenarbeit (GIZ) GmbH. https://www.adaptationcommunity.net/download/va/vulnerability-guides-manuals-reports/giz-2013-en-vulnerability-assessment.pdf

9. Gandini A, Garmendia L, Prieto I, Álvarez I, San-José J-T (2020) A holistic and multi-stakeholder methodology for vulnerability assessment of cities to flooding and extreme precipitation events. Sustain Cities Soc 63. https://doi.org/10.1016/j.scs.2020.102437

10. Gartland L (2010) Heat islands: understanding and mitigating heat in urban areas. Earthscan

11. He B-J, Wang J, Liu H, Ulpiani G (2021) Localized synergies between heat waves and urban heat islands: implications on human thermal comfort and urban heat management. Environ Res 193:110584. https://doi.org/10.1016/j.envres.2020.110584

12. IPCC, Masson-Delmotte V, Zhai P, Pörtner H-O, Roberts D, Skea J, Shukla P, Pirani A, Moufouma-Okia W, Péan C, Pidcock R, Connors S, Matthews R, Chen Y, Zhou X, Gomis M, Lonnoy E, Maycock T, Tignor M, Tabatabaei M (2018) Global warming of 1.5 °C. An IPCC special report on the impacts of global warming of 1.5 °C above pre-industrial levels and related global greenhouse gas emission pathways, in the context of strengthening the global response to the threat of climate change

13. IPCC (2014) Climate change 2014: impacts, adaptation, and vulnerability. Part A: global and sectoral aspects. Contribution of working group II to the fifth assessment report of the inter-governmental panel on climate change. https://www.ipcc.ch/site/assets/uploads/2018/02/WGIIAR5-PartA_FINAL.pdf

14. Jarosińska D, Héroux M-È, Wilkhu P, Creswick J, Verbeek J, Wothge J, Paunović E (2018) Development of the WHO environmental noise guidelines for the European region: an introduction. Int J Environ Res Public Health 15(4):813. https://doi.org/10.3390/ijerph15040813

15. Kalisch A, Satapathy S, Porsché I, Rolker D, Bhatt S, Tomar S, Nair S (2014) A framework for climate change vulnerability assessments. CCARDESA. https://www.ccardesa.org/knowledge-products/framework-climate-change-vulnerability-assessments

16. Li D, Bou-Zeid E (2013) Synergistic interactions between urban heat islands and heat waves: the impact in cities is larger than the sum of its parts*. J Appl Meteorol Climatol 52(9):2051–2064. https://doi.org/10.1175/JAMC-D-13-02.1

17. Lindberg F, Grimmond C, Gabey A, Huang B, Kent C, Sun T, Theeuwes N, Järvi L, Ward H, Capel-Timms I, Chang Y, Jonsson P, Krave N, Liu D, Meyer D, Olofson F, Tan J, Wästberg D, Xue L, Zhang Z (2018) Urban multi-scale environmental predictor (UMEP): an integrated tool for city-based climate services. Environ Model Softw 99:70–87. https://doi.org/10.1016/j.envsoft.2017.09.020

18. Markham A, Osipova E, Lafrenz Samuels K, Caldas A (2016) World heritage and tourism in a changing climate. http://whc.unesco.org/%0Adocument/139944

19. Núñez Peiró M, Sánchez C, Sanz-Fernández A, Heredia M, López-Bueno J, Neila J, Linares C, Díaz J, Muñoz G (2020) Exposure and vulnerability towards summer energy poverty in the city of Madrid: a gender perspective. IN PRESS
20. Pyrgou A, Hadjinicolaou P, Santamouris M (2018) Enhanced near-surface ozone under heatwave conditions in a Mediterranean island. Sci Rep 8(1):9191. https://doi.org/10.1038/s41598-018-27590-z
21. Quesada-Ganuza L, Garmendia L, Roji E, Gandini A (2021) Do we know how urban heritage is being endangered by climate change? a systematic and critical review. Int J Disaster Risk Reduction 65:102551. https://doi.org/10.1016/j.ijdrr.2021.102551
22. Sabbioni C, Brimblecombe P, Cassar M, (Project), NA (2010) The atlas of climate change impact on European cultural heritage: scientific analysis and management strategies. In: EC cultural heritage research series, no 19. Anthem
23. Stedman JR (2004) The predicted number of air pollution related deaths in the UK during the August 2003 heatwave. Atmos Environ 38(8):1087–1090. https://doi.org/10.1016/j.atmosenv.2003.11.011
24. Swan LG, Ugursal VI (2009) Modeling of end-use energy consumption in the residential sector: a review of modeling techniques. Renew Sustain Energy Rev 13(8):1819–1835. https://doi.org/10.1016/j.rser.2008.09.033
25. UN-Habitat (2016) World cities report 2016: urbanization and development—emerging futures. https://unhabitat.org/world-cities-report
26. WMO (2013) WMO statement on the status of the global climate in 2012 (Issue 1108). http://www.wmo.int/pages/mediacentre/press_releases/documents/WMO_1108_EN_web_000.pdf
27. Zuo J, Pullen S, Palmer J, Bennetts H, Chileshe N, Ma T (2015) Impacts of heat waves and corresponding measures: a review. J Clean Prod 92:1–12. https://doi.org/10.1016/j.jclepro.2014.12.078

Chapter 5
A Non-destructive Archaeometric Study of a Hellenistic Gold Jewel

Check for updates

**Andrea Smeriglio, Giuseppe Elettivo, Simone Caputo,
Maria Caterina Crocco, Joseph John Beltrano, Antonello Nucera,
Marco Castriota, Vincenzo Formoso, Riccardo Cristoforo Barberi,
Armando Taliano Grasso, Giada Chiodo, and Raffaele Giuseppe Agostino**

Abstract The fonts on the technological processes used in the art of the ancient goldsmith are largely fragmentary and a continuous activity must be developed to describe those processes. Amongst them, the archaeometric studies recently are taken advantage of the innovative non-destructive techniques. Some of those allows to study

A. Smeriglio (✉) · S. Caputo · M. C. Crocco · J. J. Beltrano · A. Nucera · M. Castriota ·
V. Formoso · R. C. Barberi · R. G. Agostino
Dipartimento Di Fisica, STAR Lab IR, Università Della Calabria, Arcavacata Di Rende,
(Cosenza), Italia
e-mail: andrea.smeriglio@unical.it

S. Caputo
e-mail: simone.caputo@outlook.it

J. J. Beltrano
e-mail: joseph.beltrano@unical.it

A. Nucera
e-mail: antonello.nucera@unical.it

M. Castriota
e-mail: marco.castriota@fis.unical.it

V. Formoso
e-mail: vincenzo.formoso@fis.unical.it

R. C. Barberi
e-mail: riccardo.barberi@fis.unical.it

R. G. Agostino
e-mail: raffaele.agostino@fis.unical.it

G. Elettivo
GE STONES, Rose, (Cosenza), Italia

Università Di Bari, Bari, Italia

A. T. Grasso · G. Chiodo
ArToMed-Lab Dipartimento Di Culture, Educazione E Società, Università Della Calabria,
Arcavacata Di Rende, (Cosenza), Italia
e-mail: armando.taliano@unical.it

the whole body of a finding in terms of both used materials and traces of the technological processes put in place in its production process. The aim is twofold: on the one hand, we need to reveal the techniques and their relationship to the specific cultural milieu and, on the other hand, we can attempt to describe the exchange of raw materials needed for the production of such jewellery. Our study concerns the complete description of an archaeological finding consisting in a piece of Hellenistic gold jewellery embedding a precious stone. It was likely manufactured in the Greek colony of Taranto and discovered in Serre Boscose location in Cariati municipality (CS), Italy. This is a hilly area known in ancient times as Hylias, which was centred around fortified brettia city of Pruìia of Terravecchia (CS). The gold jewel was examined by means of the X-ray microtomography at the μTomo experimental station of STAR-facility (University of Calabria) to recover its internal structure and describe the details of the metal processing. This imaging technique allowed us to acquire the volumetric model of the finding and to characterize its internal structure with a resolution of 10 microns. Furthermore, the X-ray fluorescence spectrometry was used to analyse the elements of the constituent materials whilst the Raman spectroscopy was used to characterize the precious stone.

Keywords Hellenistic jewel · X-ray μCT · XRF spectroscopy · Raman spectroscopy · Archaeometry

5.1 Introduction

The study of ancient goldsmithing has acquired, over the years, a scientific value that goes beyond the artistic and aesthetic of the objects. The jewel, to which the value of "historical document" is attributed [1], represents the ideology of the age and it is strictly related to the power symbology. In addition, it has an ornamental function representing an important expression of culture.

In October 2010, during a topographical survey carried out in Cariati municipality (CS)—as part of a research project on ancient human settlements in the territory in Serre Boscose location (Fig. 5.1)-, we found a golden disk that was probably part of an earring. The location is a hilly area, not far from the coast and the Nicà river's mouth, known in ancient times as Hylias. According to the Greek historian Tucidide, in the 413 B.C. This river marked the boundary between Kroton and Thurii [2]. Several traces of human activity have been found in this area from the first half of the Iron age to the late-Imperial period, even though the Hellenistic age was the most important for its development. In fact, during this period, buildings and necropolis were created on the hills. This defenceless agglomeration, which gravitated on the near fortified brettia city of Pruìia of Terravecchia (CS), was used to control seaport placed at the Nicà river's mouth, connecting the coast with the inland areas [3]. Anyway, there have been already found others jewellery's objects in this area, like a golden ring related to electrum alloy coins of Carthaginian and Syracusans origin. A closet recovered in 1957 contained silver's coins of Corinth and of the most important Magno-Greek

mint [4]. Moreover, several gold's jewels have been found as part of female grave decoration [2].

The case of study consists of a golden round-shaped thin case (Ø 13 mm) with a twisted wire (Ø 0, 8 mm) which is welded on the outer edge. Next to it, there is a straight wire (Ø 0, 5 mm). The case inner bottom is decorated with an eight-petalled rosette which has a red gemstone in its centre. On the back there is a twisted threadlike ring that was used to attach a pendant to the disk, which was unfortunately lost. There are also visible traces of welding where likely the earring hanger was fixed. Finally, the case is slightly deformed and bruised as it can be noted in Fig. 5.2.

The documents regarding the round-shaped earrings with pendant typology, to which the artefact under investigation belong, provide a multitude of variant. It's possible to split the different types of earrings according to the relative position between the disk and the pendant and their size. Pier Giovanni Guzzo identified these
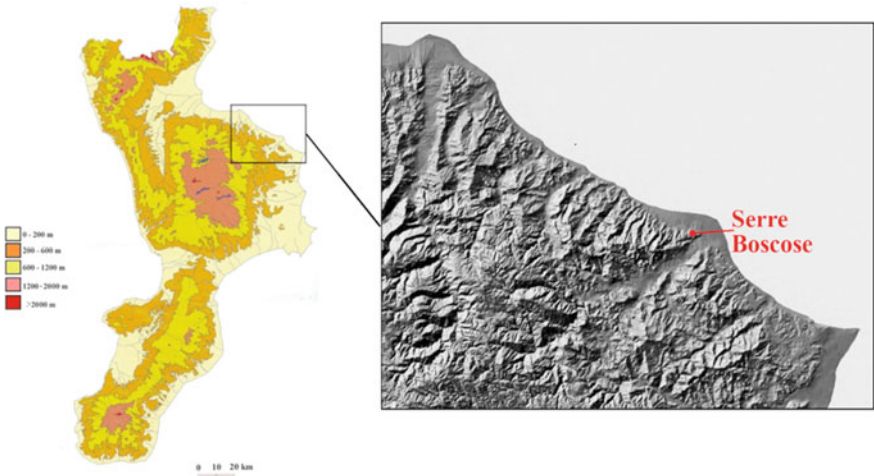
Fig. 5.1 Map of the Calabrian region in which Serre Boscose location is shown (in the inset)

Fig. 5.2 Back and front of the find under study

different variants in ten specific classes [5]. It's difficult to do a direct comparison with other manufacts of this type because they were made for a long period, until the Hellenism [6] and beyond. However, according to classification quoted above, our finding is part of class V type B2 [5]. Moreover, it is possible to perform a comparison with the gold's earring (n. inv. 1872.0604.562), that the British Museum bought from Alessandro Castellani in 1873 [7] and with the earrings kept in the Antikensammlung des Staatliche Museen of Berlins, that are made probably in Taranto between the III and the II century B.C. [8].

Some details, like the simple decoration and the presence of the red gemstone in its centre, suggests that the manufact found in Cariati belongs to the same period of the other earrings. In fact, it is known that the use of gemstones increases from the Hellenistic age to more recent times [6]. Probably the finding was produced in Taranto. Here have been found several gold jewels from the Hellenistic age, revealing the probable presence of goldsmith shops [9]. If this hypothesis is true, it confirms the relevant business relationships between the Bretti and the city of Taranto. There is evidence of this commercial interchange also in the period before the Hellenistic age [10] and in the period after the second Punic war, when, in 209 B.C., Taranto was conquered by Romans and so all its riches were confiscated [9].

The aim of this research is to expand the archeological investigation and to get more information about the manufacturing processes of the jewel. By means of non-destructive methodologies such as X-ray microtomography, X-ray fluorescence spectroscopy and Micro-Raman spectroscopy we have been able to study its morphology and the chemical composition of alloy and precious gem. The results allowed us to give hints on the production methodologies of the find.

5.2 Methods

5.2.1 X-ray Microtomography

The X-ray microtomography is a powerful technique to characterize the 3D microstructure of various samples. It is a non-destructive and non-invasive method that allows it to be applied in many research fields like biology, material science, cultural heritage [11, 12] and so on.

X-ray μ-CT investigations were performed at the μTomo experimental station of the STAR research infrastructure devoted to material science at the University of Calabria. The source features are well described in Lopez-Prat et al. [13]. In order to acquire the microtomographic images, the following parameters of X-ray source, detector and their relative position have been set: the voltage and current inside X-ray tube was 150 kV and 66 μA respectively, was selected a small focal spot (7 μm) and an 40 μm thick aluminium filter has been placed at the output of source to cutoff low energies. The distance between the source and the object was 100 mm whilst the distance between source and detector was 900. These distances

imply a magnification value of 9 and equivalent pixel size of 5.55 µm. To perform the tomographic reconstruction, 1801 images were acquired every 0.2 degrees. The acquisition time was 2500 ms for each image.

5.2.2   X-ray Fluorescence Spectroscopy

Quantitative analysis to determine the composition of the various parts of the jewel was carried out using Bruker Artax 400 µXRF spectrometer located at the X-RAY laboratory of Biology, Ecology and Natural Science Department (DiBEST) of University of Calabria. Analysis was carried out at 50 kV, 700 µA, using the 0.2 mm collimator and with an acquisition time equal to 600 s. Quantitative analysis was carried out using pure element reference standard. Spectra were collected using the Artax Spectra 7® software.

5.2.3   Raman Spectroscopy

The Raman analysis was performed with a confocal Micro-Raman LABRAM by Jobin–Yvon Horiba scientific equipped with a long working distance objective 50 × and a Nd:YAG doubled laser source at 532 nm. A CCD detector was used cooled with a Peltier module 1024 × 256, dynamic range 16 bits and pixel dimensions of 27 µm. Spectral resolution was about 1 cm^{-1}.

5.3   Results and Discussion

The X-ray microtomography surveys allowed us to advance hypotheses on the jewel production method. The X-ray tomographic reconstruction reveal that the gold pendant is made by at least fourteen different pieces welded together. Some hidden parts in the artefact are impossible to be seen by a visual inspection. Already from the X-ray radiographic image in Fig. 5.3, it is easy to distinguish the various parts. Note that the red gemstone is nearly transparent to X-rays.

Each part of archaeological find has been better analysed by 3D rendering of the X-ray microtomographic reconstructions.

The external ring is a single wire coiled on itself to form a hollow tubular structure, as it is shown in Fig. 5.4.

Figure 5b shows the X-ray absorption intensity along the yellow line in transverse section reported in Fig. 5a. The graph shows a minimum on the centre and maxima on the edges of the wire. The minimum corresponds to the hole created by the wrapping of the gold wire. The diameter of the internal hole can be evaluated to be 0.4 mm.
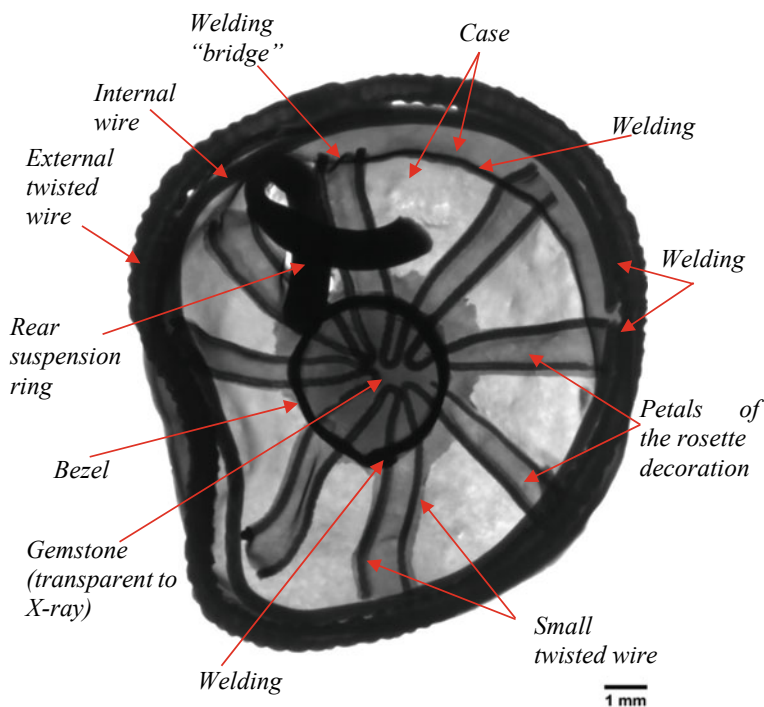
Fig. 5.3 X-ray radiography of the jewel in frontal projection. The arrows point to parts composing the earring

The same manufacturing technique was used to produce the wires placed on edges of the rosette petals. As a matter of fact, they present a hole along all their length as shown in Fig. 5.6. Moreover, the small wires welded on each petal are connected each other and welded together by a little "bridge" giving a greater stability to the whole structure. The intensity profile reported on the right of the lower panel of Fig. 5.6 was recovered along the yellow line in the virtual cut shown in false colours. The diameter of the hole is about 0.1 mm, whilst the diameter of twisted wire is about 0.4 mm.

The same manufacturing technique was used to make the solenoidal hollow wires welded on the rosette petals on the internal bottom of the case and on its external edge. They are produced with a single wire with a diameter of about 0.15–0.20 mm.

Lastly, the central bezel is made by a curved rectangular plate and welded to hold the red gemstone.

The XRF chemical investigation was performed to find out the composition of the metal as well as to follow any chemical difference in correspondence of the welding points.

Fourteen spectra in different positions on the artefact surface have been acquired, as it is shown in Fig. 5.7. Four spectra are recorded on the welding points (A1, A2,

External
twisted wire

Welding
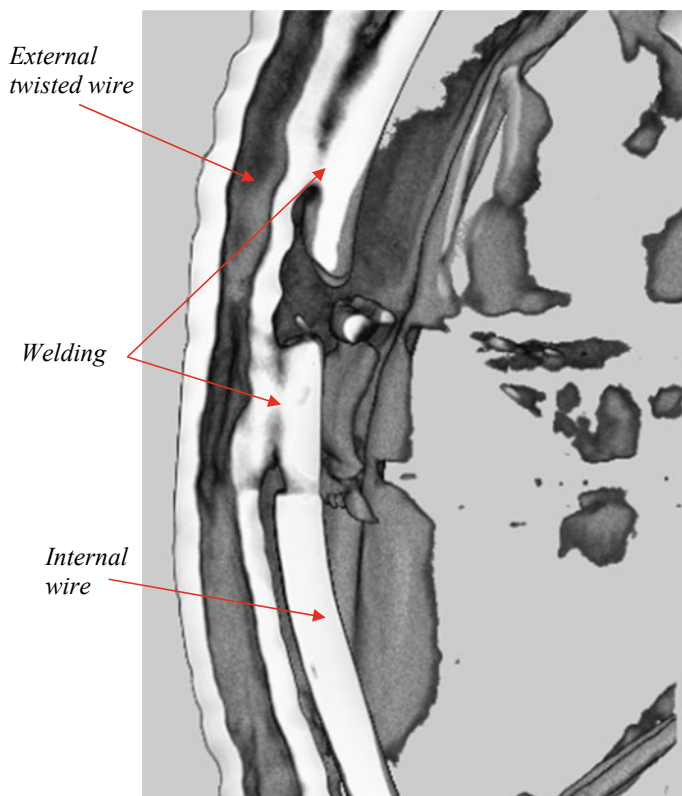
Internal
wire

Fig. 5.4 Virtual cross section acquired by using volume viewer function on Imagej software in which the external and the internal ring are visible as well as two welding points

A3 and A4 points) whilst the other ten (B1–B10 points) in other significative areas of the jewel.

The acquired spectra tell us that the jewel is made of a gold-rich Au–Ag–Cu alloy. The fluorescence results have also unveiled that the welding spots were somehow richer in silver even though the difference in concentration are very low and the percentage averages composition overlap in the error bar. Thus, if any, a very similar alloy was used for the welding.

The concentration value of Au, Ag and Cu were normalized to 100 and they are reported in Table 5.1.

Usually, in ancient jewellery, was used three different types of welding and soldering processes: solid-state diffusion bonding with copper salt, which is used in the granulation technique [14], brazing and autogenous or fusion welding [15]. The latter was used to solder the various pieces of the jewel under investigation, using a punctual heating source like a blowpipe [16].
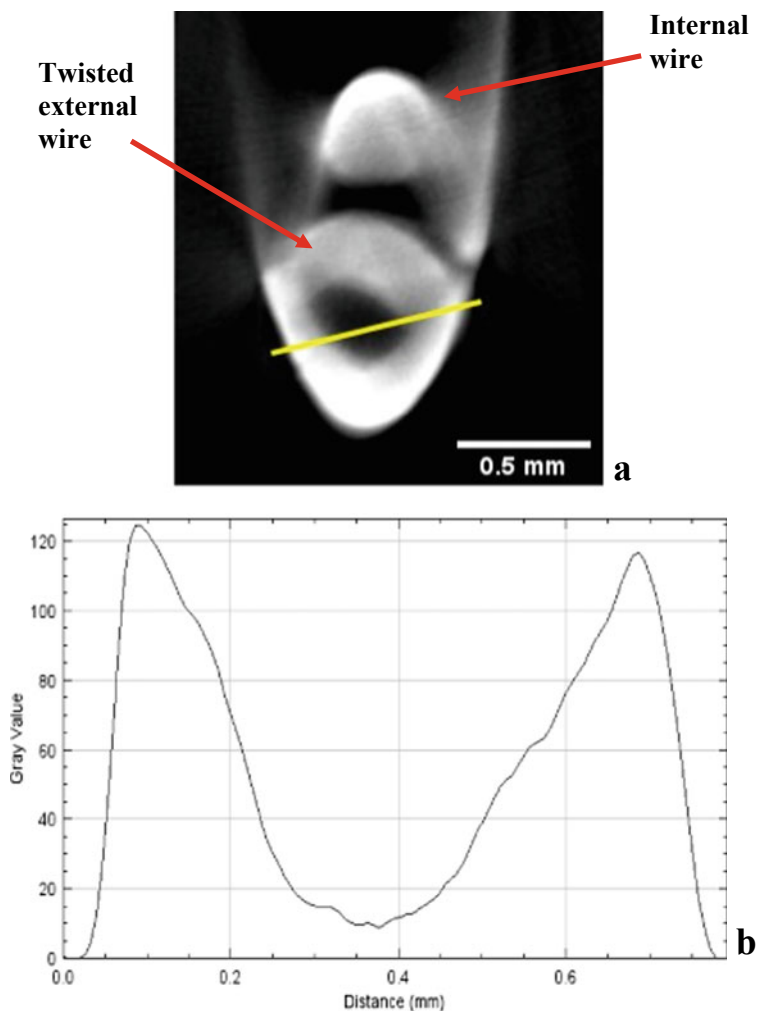
Fig. 5.5 **a** A particular of external wire shown on a single slice. The yellow line means the points at which is measured the intensity profile. **b** Histogram of greyscale's intensity

In Fig. 5.8, it is shown the representative Raman spectrum in the range between 300 and 1100 cm^{-1} collected on the red gemstone cast in a pendant.

Outside of such range (300 and 1100 cm^{-1}) there are non-detectable Raman features. As it can be seen in Fig. 5.8, the main bands fall at 355, 504, 555, 637, 856, 916 and 1048 cm^{-1}. In Table 5.2 is reported the attribution and the symmetry of the Raman modes of Fig. 5.8.

This pattern indicates that the gemstone is made by a mineral belonging to the family of the Garnets [17]. The general structural formula of the Garnets is $X_3Y_2(SiO_4)_3$, where it is possible to see the orthosilicate tetrahedral structure
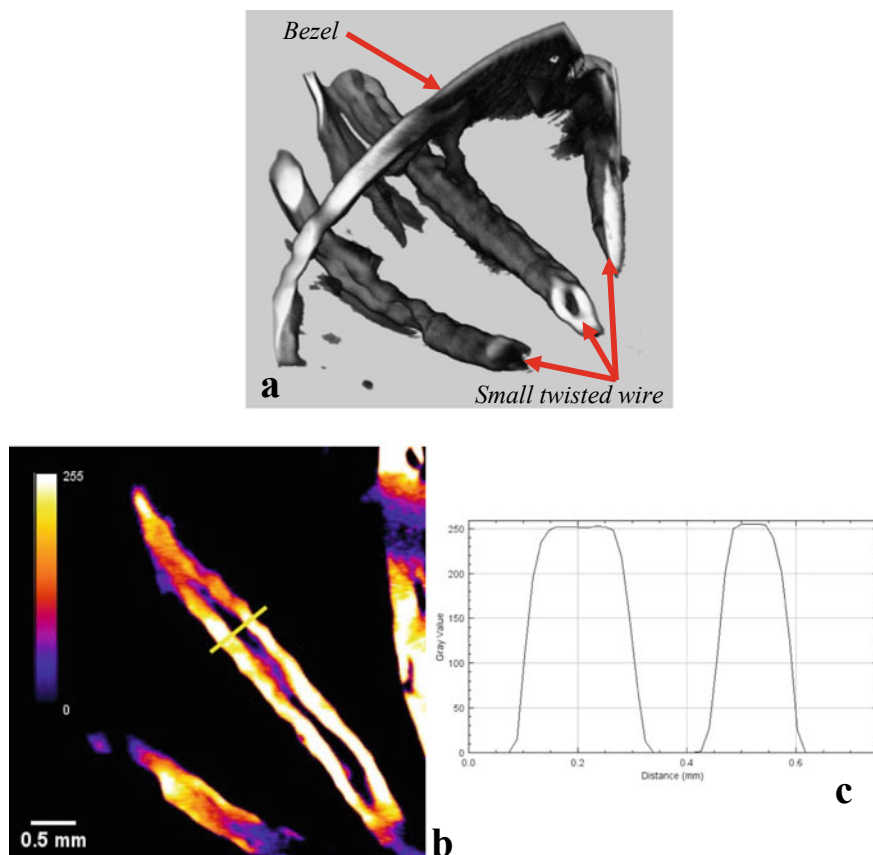
Fig. 5.6 Virtual cross section acquired by using volume viewer routine of the Imagej software in which is visible the tubular structure of the small twisted wire (**a**). In the lower panel, a closeup of small twisted wires is shown in false colors (**b**). The yellow line marks the line on which the intensity profile is extracted (**c**)

combined with bivalent and trivalent cations. In particular, the bivalent cations are Ca^{2+}, Mg^{2+}, Fe^{2+} and Mn^{2+} (indicated by the X) whilst the trivalent cations are Al^{3+}, Fe^{3+} and Cr^{3+} (indicated by the Y). Dependently from the cations involved in the structure, the garnets take different properties and different names. In particular, we have the isomorphic series denominated pyralspite when Y is aluminium (Al^{3+}): $Fe_3Al_2(SiO_4)_3$ (Almandine), $Mn_3Al_2(SiO_4)_3$ (Pyrope) and $Mg_3Al_2(SiO_4)_3$ (Spessartine). Indeed, if the X position is occupied by calcium cation (Ca^{2+}), the ugrandite isomorphic series is present: $Ca_3Fe_2(SiO_4)_3$ (Andratite), $Ca_3Al_2(SiO_4)_3$ (Grossular) and $Ca_3Cr_2(SiO_4)_3$ (Uvarotite).

On the basis of the attribution of the Raman bands, it is possible to state that the spectra of Fig. 5.8 indicated that the red gemstone in the pendant is a garnet made by a solid solution of Almandine ($Fe_3Al_2(SiO_4)_3$) and Pyrope ($Mn_3Al_2(SiO_4)_3$) [18].
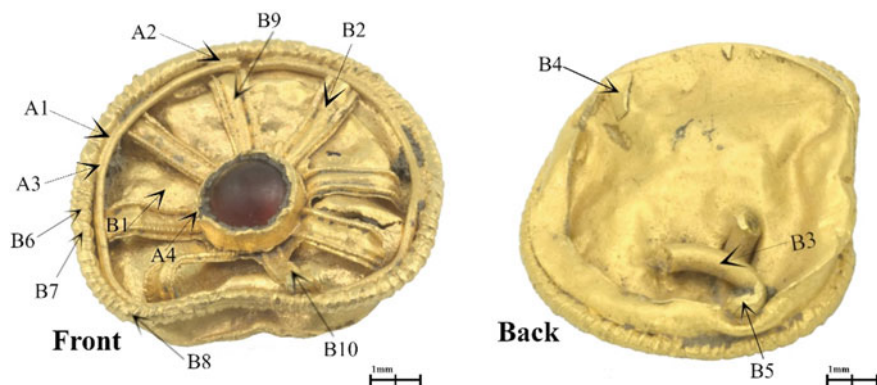
Fig. 5.7 XRF measuring points

Table 5.1 Concentration value of Au, Ag and Cu in percentage

	Au lα$_{1-2}$ (conc. %)	Ag kα$_{1-2}$ (conc. %)	Cu kα$_{1-2}$ (conc. %)
A1	93.64	5.57	0.79
A2	93.06	5.96	0.98
A3	93.48	5.67	0.85
A4	94.16	4.92	0.92
A	93.58 ± 0.55	5.53 ± 0.52	0.89 ± 0.10
B1	94.83	4.20	0.97
B2	94.43	5.00	0.56
B3	93.11	6.10	0.79
B4	93.45	5.66	0.89
B5	93.42	5.71	0.87
B6	93.26	5.91	0.82
B7	93.17	5.88	0.95
B8	93.39	5.66	0.95
B9	94.35	5.22	0.43
B10	93.2	5.98	0.82
B	93.66 ± 0.86	5.53 ± 0.95	0.81 ± 0.27

During the Hellenistic period were used widely the Garnet to give more value to goldsmith's production [19]. The provenance of these gemstone was usually India and other eastern lands [19, 20].
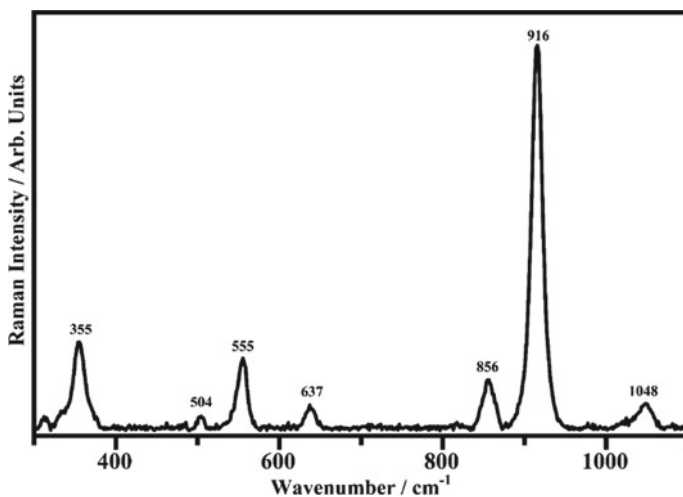
Fig. 5.8 Representative Raman spectrum in the range between 300 and 1100 cm^{-1} of red stone set in a pendant

Table 5.2 Attribution of the Raman bands of the representative spectra collected on the red stone set in a pendant and shown in Fig. 5.8

Wavenumber[a]/cm^{-1}	Raman mode and relative symmetry [14, 15]
355 (m)	Librational SiO$_4^{4-}$, F$_{2g}$ mode
504 (vw)	Si–O Bending, F$_{2g}$ mode
555 (m)	Si–O Bending, A$_1$ mode
637 (m)	Si–O Bending, F$_{2g}$ mode
856 (m)	Si–O Stretching symmetric, F$_{2g}$ mode
916 (vs)	Si–O Stretching symmetric, A$_1$ mode
1048 (m)	Si–O Stretching symmetric, F$_{2g}$ mode

[a] *on bracket the relative intensity of the bands: m = medium; vw = very weak; w = weak; s = strong; vs = very strong*

5.4 Conclusions

An ancient gold earring has been studied by complementary physical method-ologies through X-ray microtomography, XRF portable spectroscopy and Micro-Raman spectroscopy. These completely non-invasive and non-destructive methods methodologies have allowed to understand the constituent materials and the manu-facture technology of the find. The results allow the identifying and describing of manufacturing methods used by Hellenistic goldsmiths to create amazing jewellery.

X-ray microtomography has been used to investigate the internal morphology of the jewel that is made by about fourteen different pieces welded together, some of which are impossible to see at naked eye. The solenoidal hollow wires welded on the rosette petals on the internal bottom of the case and on its external edge are coiled on themselves to form the hollow tubular structure using the strip-twisting technique. The technique of strip-twisting, best described by Oddy [21, 22], was very common in the Hellenistic jewellery [23] and involves cutting a strip of metal foil and wrapping it round an existing wire which is then removed. This helix is then tightened and gently extended by hand. The wires welded on the rosette petals are connected each other and welded together by a little "bridge" to gives it more stability.

Through the XRF chemical investigation we can confirm that the jewel is made of a gold-rich Au–Ag–Cu alloy. Furthermore, the fluorescence result has unveiled that a very similar alloy was used for the welding. This allows us to guess that the welding process was carried out forging by rapid fusion of discrete parts in contact by autogenous welding method without filler different material [24]. As the chemical composition of the earring is very similar to some Hellenistic jewels manufactured in Greek colony of Taranto and preserved at Archaeological Museum of Taranto [25], the investigated earring was likely manufactured there.

Micro-Raman spectroscopy has been used to investigate the red gemstone set in the pendant. The representative Raman spectrum and the relative assignment of the Raman features lead us to identify the composition of the gemstone as a Garnet.

Through surveys we furnished important data for the attribution of the nature of the constituent materials, which in turn may be considered a valid support for an eventual restoration. The information obtained from archaeological and archaeometric studies contributes to the discussion of the knowledge and technological capabilities of the Hellenistic goldsmiths and the spread of jewellery in the Magna Graecia area.

A more in-depth study of the raw materials used, including alloys and precious stones, could give an indication on their places of origin. Trade in Mediterranean area in Hellenistic period information could be provided, opening new topics about socio-cultural and anthropological aspects of Magna Graecia population.

Future investigation will be directed to further on the provenience of the raw materials used for the Hellenistic gold jewel making.

References

1. Guzzo PG (1992) Introduzione all'artigianato della Puglia antica, dall'età coloniale all'età romana. In: Mazzei M (ed) Oreficerie. Edipuglia, Bari, pp 161–180
2. Taliano Grasso A (2020) Approdi, rotte e naufragi lungo la costa meridionale del Sinus Tarentinus. In: Spadea R, Lo Schiavo F, Lazzarini ML (eds) Tra Ionio e Tirreno: orizzonti d'archeologia. Omaggio a Elena Lattanzi, pp 795–808
3. Marino D, Taliano Grasso A, Medaglia S, Nicoletti G (2017) Rocche protostoriche e abitati brettii tra Sila e mare Jonio. In: Atti Convegno Internazionale Centri fortificati indigeni della Calabria dalla protostoria all'età ellenistica, Università Federico II, Napoli 2014. Napoli, pp 97–130
4. Pennestrì S (1983) Il ripostiglio di Cariati. AIIN 30:39–62
5. Guzzo PG (1993) Oreficerie dalla Magna Grecia. Ornamenti in oro e in argento dall'Italia meridionale tra l'VIII e il I secolo. Taranto, La Colomba
6. Lippolis E (2008) L'età classica ed ellenistica. In: Gandolfo L (ed) Pulcherrima Res. Preziosi ornamenti dal passato. Palermo, pp 143–191
7. Marshall FH (1911) Catalogue of the jewellery, Greek, Etruscan and Roman, in the Departments of Antiquities. British Museum, London
8. Schojer T (1984) Orecchini 129–137. In: De Juliis EM (ed) Gli ori di Taranto in età ellenistica, Catalogo della mostra (Milano-Taranto 1984–1986). Milano, pp 140–178
9. Guzzo PG (2014) Oreficerie dell'Italia antica. Rossano (CS)
10. Taliano Grasso A (2019) La ceramica argentata in Calabria. Orizz Rass di Archeol XX:27–46
11. Agostino RG et al (2016) Microtomographic studies as a tool in the identification of a new ceramic class: the metal-imitating pottery as grave goods among Brettians and Lucanians. Microchem J 126:138–148. https://doi.org/10.1016/j.microc.2015.12.007
12. Morigi MP, Casali F, Bettuzzi M, Brancaccio R, D'Errico V (2010) Application of X-ray computed tomography to cultural heritage diagnostics. Appl Phys A 100(3):653–661. https://doi.org/10.1007/s00339-010-5648-6
13. López-Prat M et al (2021) Architectural Terracruda sculptures of the Silk Roads: new conservation insights through a diagnostic approach based on non-destructive X-ray micro-computed tomography. Stud Conserv 1–13. https://doi.org/10.1080/00393630.2020.1862605
14. Nestler G, Formigli E (2010) Etruscan granulation: an ancient art of goldsmithing, Brynmorgen
15. Scrivano S et al (2013) Identification of soldering and welding processes in ancient gold jewellery by micro-XRF spectroscopy. X-Ray Spectrom 42(4):251–255. https://doi.org/10.1002/xrs.2482
16. Pacini A (2006) Appunti di bottega—Microsaldature nell'oreficeria antica, Don Chisci. San Quirico D'Orcia (SI)
17. Kolesov´ BAK, Geiger KA, Kolesov BA, Geiger CA (1998) O R I G I N A L P A P E R Raman spectra of silicate garnets. Phys Chem Miner 25:142–151
18. Culka A, Jehlička J (2019) A database of Raman spectra of precious gemstones and minerals used as cut gems obtained using portable sequentially shifted excitation Raman spectrometer. Raman Spectrosc 50(2):262–280
19. Spier J (1989) A group of Ptolemaic engraved garnets. J Walters Art Gall 47:21–38
20. Pappalardo L, Karydas AG, Kotzamani N, Pappalardo G, Romano FP, Zarkadas C (2005) Complementary use of PIXE-alpha and XRF portable systems for the non-destructive and in situ characterization of gemstones in museums. Nucl Instrum Methods Phys Res Sect B Beam Interact Mater Atoms 239(1–2):114–121. https://doi.org/10.1016/j.nimb.2005.06.184
21. Oddy A (1977) The production of gold wire in antiquity hand-making methods before the introduction of the draw-plate. Gold Bull 79–87
22. Oddy WA (2004) The manufacture of wire since the Bronze Age: a technological investigation using the microscope. Phys Methods Archaeom 257–267
23. Perea A, Gutiérrez-Neira PC, Climent-Font A (2018) Archaeometric investigation of a hellenistic golden funerary belt: a case study. Mediterr Archaeol Archaeom 18(3):1–16. https://doi.org/10.5281/zenodo.1461657

24. Karydas AG (2007) Application of a portable XRF spectrometer for the non-invasive analysis of museum metal artefacts. Ann Chim 97:419–432
25. Buccolieri A, Castellano A, Degl'innocenti E, Cesareo R, Casciaro R, Buccolieri G (2017) EDXRF analysis of gold jewelry from the Archaeological Museum of Taranto, Italy. https://doi.org/10.1002/xrs.2761

Chapter 6
Use of a GIS-Based Solution for the Design of Preventive Conservation Plans in Heritage Constructions

E. Sedano-Espejo , **C. Méndez-Moreno** , **L. J. Sánchez-Aparicio** ,
S. García-Morales , **J. R. Aira** , **E. Moreno** , **J. Pinilla-Melo** ,
D. Sanz-Arauz , **M. Palma-Crespo** , **and D. González-Aguilera**

Abstract This paper aims at improving part of the HeritageCare method for preventive conservation of historical constructions. This method was developed in 2019, resorting to the use of digital technologies for analyzing and managing the information required for generating a preventive conservation plan. More specifically, we have focused on the improvement of the service level 1 on which we propose the use of a geospatial database and the GIS technology for the management of information

E. Sedano-Espejo (✉) · C. Méndez-Moreno · L. J. Sánchez-Aparicio · S. García-Morales ·
J. R. Aira · E. Moreno · J. Pinilla-Melo · D. Sanz-Arauz · M. Palma-Crespo
Department of Construction and Technology in Architecture (DCTA), Higher Technical School of
Architecture of Madrid (ETSAM), Universidad Politécnica de Madrid, Madrid, Spain
e-mail: eneko.sedano.espejo@alumnos.upm.es

C. Méndez-Moreno
e-mail: carlos.mendez.moreno@alumnos.upm.es

L. J. Sánchez-Aparicio
e-mail: lj.sanchez@upm.es

S. García-Morales
e-mail: soledad.garcia@upm.es

J. R. Aira
e-mail: joseramon.aira@upm.es

E. Moreno
e-mail: esther.moreno@upm.es

J. Pinilla-Melo
e-mail: javier.pinilla@upm.es

D. Sanz-Arauz
e-mail: david.sanz.arauz@upm.es

M. Palma-Crespo
e-mail: m.palma@upm.es

L. J. Sánchez-Aparicio · D. González-Aguilera
Department of Cartographic and Land Engineering, Higher Polytechnic School of Ávila (USAL),
University of Salamanca, Ávila, Spain
e-mail: daguilera@usal.es

and automatic risk calculation. This geospatial database is managed by the open-source platform Quantum GIS and supported by several Python scripts for the risk analysis as well as for the QField app for capturing data infield. For its validation, a small Romanesque-Gothic Basilica is selected as the case study. This church is located in the north of Spain, in the village of Becerril del Carpio. This building has suffered severe conservation problems (soil settlements, moistures, and lack of maintenance of the assets), being restored recently. However, the lack of a proper preventive conservation plan is promoting the degradation of the church.

Keywords Preventive conservation · Geoinformatics · Geographic information systems · Pathology · Risks evaluation · Vulnerability

6.1 Introduction

The economic importance that activities related to cultural heritage can generate nowadays is threatened by the lack of resources invested in heritage conservation. The current economic situation must be added to all this, because of the convergence of a deep crisis from years ago and the health situation caused by Covid-19. This situation causes a large gap and imbalance between the funds allocated to projects and initiatives promoting the maintenance and conservation of the cultural heritage and the funding that would actually be needed [1]. This factor leads to a continuous search for new methods to deal with this issue. Within this context, preventive conservation has been placed as the most relevant one [2]. This method, born in the sixties, bases its performance in carrying out a set of periodic inspections on the building and a maintenance under the slogan: "prevention is better than cure" [3]. In accordance with Matulionis and Freitag [4], this method is able to save between 40 and 70% of the total maintenance costs by avoiding major interventions and promoting systematic inspections and monitoring tasks on which the digital technologies could play a relevant role [5].

Under the basis previously mentioned, this article aims at giving a step forward in the implementation of digital technologies by developing a geographical information system (GIS) tool able to manage the information required for developing preventive conservation plans.

After contextualizing the importance of the development of digital tools for preventive conservation, Sect. 6.2 will expose the main initiatives. Section 6.3 will show the architecture of the platform. Section 6.4 will be devoted to show the experimental results obtained after applying it to one study case. Finally, Sect. 6.5 summarizes the main conclusions that emerged after this study.

6.2 HeritageCare Approach

6.2.1 Current Methodologies

Nowadays, there are numerous research initiatives that have opted for this new conservation strategy as a necessary tool for the preservation of heritage that has only grown since its first appearances. These include programs in the European framework such as Horizon 2020 (https://ec.europa.eu/programmes/horizon2020/en/home), INTERREG-SUDOE (https://interreg-sudoe.eu/home) or JPI Cultural Heritage (https://www.heritage-researchhub.eu/) [6] as well as newly created programs such as Next Generation EU (https://ec.europa.eu/info/strategy/recovery-plan-europe_es) [7]. Initiatives that have allowed the foundation of entities focused on preventive conservation such as Monumentenwatch (1973) in the Netherlands [8], Monumentenwacht Vlaanderen (1991) in Flanders, Belgium [8], Denkmalwacht (1999) in Germany [8], Bygningsbevaring (2004) in Denmark [8] or Mamég (2006) in Hungary [8]. Several projects have also been developed in the field of preventive conservation such the Fondazione Cariplo-Cultural District (2005) in Lombardia, Italy [8], Müemlékör (2012–2014) in Hungary [8], Traditional Buildings Health Check Scheme (2013) in the UK [8], Pro-Monumenta (2014) in Slovakia [8] or HeritageCare (2016) in Portugal, Spain, and southern France [3].

6.2.2 The HeritageCare Project

The latest of these initiatives, the HeritageCare project, is focused on the development of a standardized methodology for preventive conservation purposes by using digital technologies such as Web-GIS or BIM models in order to overcome much of the existing constraints [3]. This methodology is based on a multi-level system of services for the systematic inspection and monitoring of buildings [9]. This system of services is organized in three levels [10]:

- *Service level 1 (SL-1 or StandardCARE)*: basic inspection level suitable for all types of buildings and whose main advantage is simplicity and speed. It is based on regular inspections carried out through a mobile or tablet app. These inspections are carried out on the basis of a team consisting of two technicians.
- *Service level 2 (SL-2 or PlusCARE)*: inspection level is more advanced than the previous one. It is based on the use of 360° technology, 3D points clouds, and a web-GIS platform. This virtual platform is based on GIS technology that allows to organize and consult all the data related to the preventive conservation plan, achieving a total connection between technicians and the owner.
- *Service level 3 (SL-3 or TotalCARE):* the most advanced level, suitable for unique buildings, focuses on the use of HBIM technology for the management of its preventive conservation.
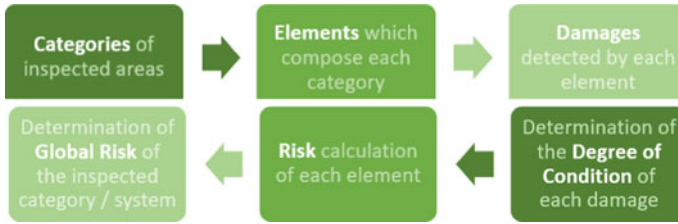
Fig. 6.1 Hierarchical workflow classification and process followed during the risk calculation

It is worth mentioning that service levels 2 and 3 are based on the use of a geospatial database. This question is not implemented in the service level 1.

Risk Analysis

One of the key factors when we deal with preventive conservation is the proper analysis and management of the risks [11]. Risk is the chance of an undesirable change occurring in the building (i.e., degradation of the assets). This value is directly related with the vulnerability of each element (constructive or not) and the different hazards. The main goal of the preventive conservation is to minimize the level of risks in each element, preserving the tangible and intangible values of the heritage site [12].

In the case of HeritageCare, the calculation of the risks is performed as follows (see Fig. 6.1).

Each element, in turn, can be affected by a series of damages or injuries that will be identified and the risk to which the element is subjected will be calculated.

The risk calculation adopted by HeritageCare starts with the damage identification. To this end, the construction systems of the building are inspected by categories. Nowadays, the HeritageCare methodology considers the following categories: (i) roof_covering, (ii) roof_supporting_structure, (iii) rain_water_system, (iv) building_envelope, (v) building_interior, (vi) ornamentation, (vii) technical_instalations_and_equipment, (viii) indoor_climate, (ix) prevention_and_safety, (x) accessibility_and_hygiene, and (xi) site. Each one of these categories is at the same time divided into elements (e.g., the roof supporting structure is divided into structural elements and materials, supports of structural elements, and others). Then, the damage is defined by the following fields: (i) a classification in accordance with the damage atlas of HeritageCare [3], (ii) its extension (from 0 to 100%), and (iii) its degree condition which varies from 0 (good long-term urgency) to 3 (bad short-term urgency). The value resulting from multiplying the second and third variables is weighted. The value of this weight is established by the technician in accordance with the characteristics of the site and her/his experience, varying from 0 to 100. Once all the damages presented in each element are defined completely the methodology demands the calculation of the risk of each element. To this end, the average of the weighted damages detected in the element is computed. Finally, the risk of the category is considered as the highest value obtained from all the elements.

The combination of all these results is an intuitive risk system and of rapid application.

6.3 Architecture of the Application

The software selected to develop this investigation work has been Quantum GIS (QGIS) (https://www.qgis.org/es/site/). It is based on an open-source platform which allows us to compile and manage geospatial databases as well as different types of information such as raster or vectorial layers. These blocks of information contain all data required to elaborate an evaluation of case study risks in order to establish accurate conservation and prevention measures guide. The following figure summarized the workflow proposed in the present publication (see Fig. 6.2).

6.3.1 Sources of Information Required for the Evaluation of Risks

For an adequate evaluation of risks, it has been defined a variety of data to ultimately develop and complete the preventive conservation plan. A classification into five groups has been established as follows:
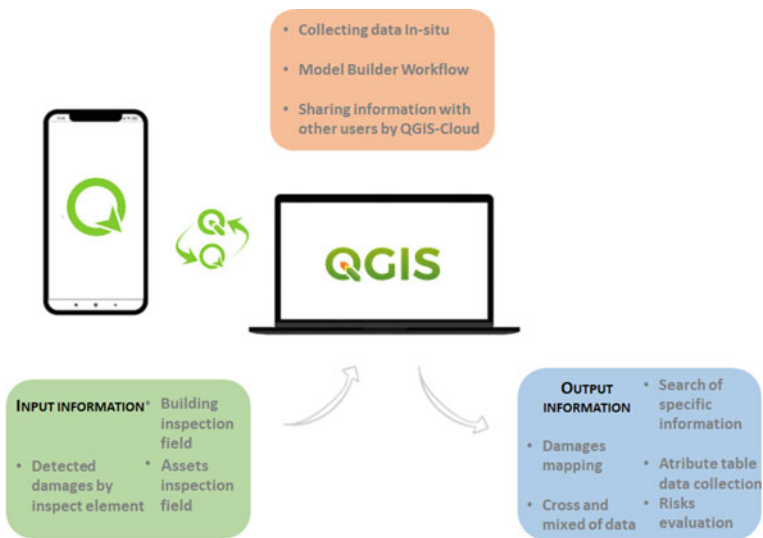
Fig. 6.2 Relation between the different types of information managed by the GIS platform for preventive conservation

- *Planimetry:* this category has the aim of being useful to mapping not only damages but also the inspected constructive systems through eight unique drawings within which are shown different floors, sections, and elevations.
- *Detected damages by inspected element:* through this layer, it is collected and digitized all information related to current damages noticed with the visual inspection of the building, including the images captured in-field. This layer allows us to introduce the type of damage (in accordance with the damage atlas of Heritage-Care), its extension (%), and the degree of risk that could vary from 0 (good) to 3 (bad). This information is required for the risk computation.
- *Building inspection field:* this field is devoted to map the different constructive systems as well as calculating its associated risks.
- *Assets inspection field:* Similar to the previous explained layer, this category analyzes the global risk of assets located inside the inspected building, following the same mathematical operations. It is distinguished between movable or fixed assets.
- *New symbology:* the aim of this group is to take information about output layers to show visual and intuitive final risk results once the evaluation is completed, exhibit over the existing cartography.

6.3.2 Platform's QGIS

Complements and updates offered by the GIS program have made possible an on-site collection and management of data through the QField app (https://qfield.org/) [13] (see Fig. 6.3). This multifunctional application gathers required shapefiles data within its pertinent attribute, allowing an online or offline mapping and edition. Furthermore, images and videos can be taken directly from the inspect element, with independence of being connected to any network.

Fig. 6.3 Graphical representation of the connection between the QGIS and QField projects

As it is described in the Sect. 6.2.1, collected data for the risk evaluation is stored in different shapefiles within the GIS system. Each of those information files contains the following fields, located in each shapefile of the different groups:

- *Building inspection field:* shapefiles located in this group are focused on identifying the categories and elements considered by the HeritageCare methodology (for more details see section risk analysis). At the same time, each of them are composed by the following attribute fields: (i)eElement, (ii) i, j ("i" is the shapefile and "j" the corresponding analyzed element among the ones which composed each building inspection category), (iii) importance_weighing_i, j, (iv) state_i, and (v) risk_i. All the previous fields are compound by means of real and integer numbers, except for the last one which is text.
- *Assets inspection field:* similar to the previous group, there is a unique shapefile named: 12_assets, which follows the same attribute field structure as previously.
- *Detected damages:* this shapefile maps the damages observed on the different constructive elements. To this end, it is followed the damage atlas proposed by HeritageCare [3]: (i) class, (ii) subclass, (iii) sub-subclass, (iv) element, (v) grade, (vi) state, (vii) extension, (viii) condition, (ix) date_of_inspection, (x) frequency_of_inspection, (xi) reparation_proposals, (xii) inspector, and (xiii) images (maximum 4). All the previous fields are compound by means of text, except for the date_of_inspection which is a date.

6.3.3 Automatic Risk Calculation

Once the different fields and shapefiles are defined, it is necessary to integrate the entire calculation methodology for risk assessment, which requires the development of an in-house script. This script was developed in Python language with the assistance of the QGIS graphical modeler named model builder. Model builder provides an interactive interface on which is possible to load, connect and run different algorithms (see Fig. 6.4). In our case, the workflow implemented for the risk analysis was the following one:

- *Input layers*: first of all, it is required to load the input parameters as vector layers. For the risk analysis, these layers are: (i) *building inspection field*, (ii) *assets inspection field*, and (iii) *detected damages by inspected element.*
- *Update field:* algorithm used in different phases of the workflow, applying the corresponding formula in each step to determine the degree of condition of each damage, make the sum of all the degrees for each element, determine the respective state situation of each field, determine their risk, and round off the final results.
- *Establish style for vector layer:* it has been possible to show the results of the risks in a visual and intuitive way, taking the previous calculations run with the prior command and substituting the colors of the cartography previously elaborated in each inspected layer.
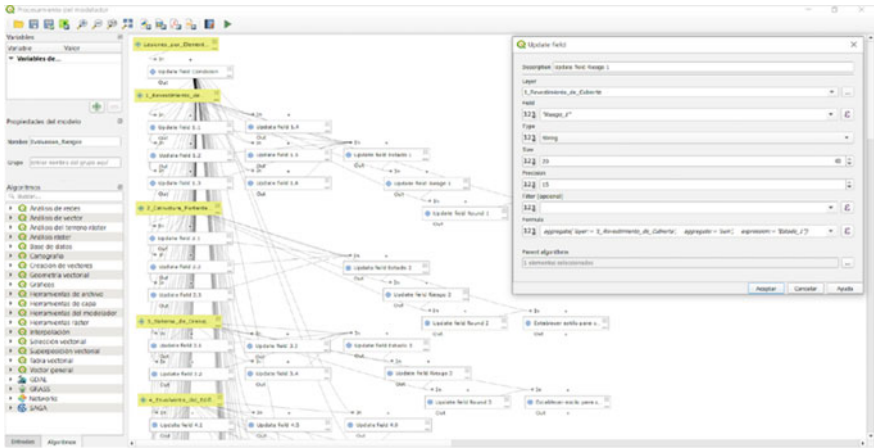
Fig. 6.4 Algorithms and operations from the risk evaluation workflow through the model builder complement

6.4 Experimental Results

6.4.1 The Romanesque-Gothic Church of San Pedro

The case study used for validating the proposed approach was the Romanesque-Gothic church of San Pedro. This building was built in the middle of the thirteenth century in the village of Becerril del Carpio in the region of Castilla y León (Spain) (see Fig. 6.5) [14]. The church is recognized as BIC (register of Cultural Heritage in Spain).

The building consists of a single nave whose dimensions are: length ≈ 2371 m, width ≈ 878 m, with double height and openings in the vertical walls that allow ventilation and light entry. The construction system of the walls consists of three

Fig. 6.5 General external view of San Pedro church

a)   b)

Fig. 6.6 Indoor images of the main name: **a** image of the conservation status before the restoration project; and **b** image of the current appearance

leaves, the exterior of sandstone masonry and between them a core of rubble masonry. The northeast wall is reinforced by four buttresses that constrict the pushing of the land that borders the northwest wall (see Fig. 6.6a). The nave is covered by a barrel vault and on reaching the east apse is covered by an octopartite ribbed vault from the late Gothic period. The tower is one of the characteristic elements of the church. It is built in sandstone masonry and on the east side combines sandstone masonry with brick (see Fig. 6.6b).

The main space is accessed through the entrance portico which is articulated by a barrel vault and then a cross vault supported by two columns with Gothic style capitals. Beside to the apse is the sacristy covered by a ribbed vault and at the west side of the church, under the tower, there is a space dedicated surely to the maintenance of the bells.

Furthermore, the basilica suffered from a settlement on its northern façade due to a modification in the properties of the soil on which it stands, which caused the main nave to undergo a great structural movement to adapt its shape to the new conditions. Its consequences were shown in the form of cracks and deformations along the tower, the annexed body, and even in the vaults themselves, which had to be reinforced in 2011.

However, the lack of a proper maintenance plan has promoted the presence of biological colonies along the façades, and the presence of moisture along the main nave among other damages that are compromising the heritage values of this church (see Fig. 6.5 and 6.6).

6.4.2   Preventive Conservation Plan for the Case Study

Previous to the data capturing and the analysis of risks of the building, it was necessary to load the default template for designing the preventive conservation plan. This template is a new QGIS project that includes the layers proposed

a) b)
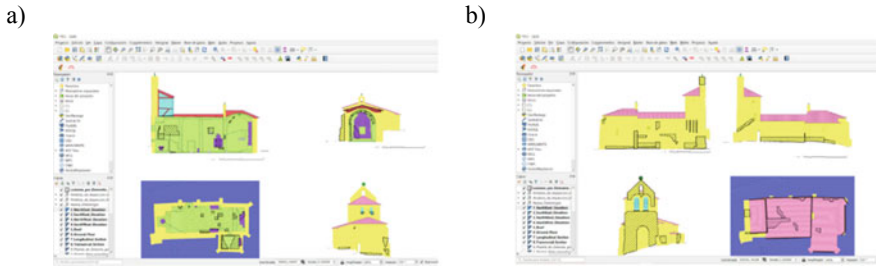
Fig. 6.7 Raster images introduced in the QGIS template: **a** 1_northeast_elevation, 3_northwest_elevation, 4_southwest_elevation, and 5_roof; **b** 2_southEast_elevation, 6_ground_floor, 7_longitudinal_section, and 8_transversal_section

in Sect. 6.3.1. This stage avoids the presence of errors during the computation of the risks. Then, the planimetry of the church was loaded (raster information) as follows (see Fig. 6.7): 1_northeast_elevation; 2_southeast_elevation; 3_northwest_elevation; 4_wouthwest_elevation; 5_roof; 6_ground_floor; 7_longitudinal_section; and 8_transversal_section.

In-Field Work Through the QField App

Once the project has been created and the shapefiles with their pertinent fields have been established, then it is transferred to the mobile device, allowing online or offline digitization. This process is carried out through the QField® application (see Fig. 6.8). Its efficient synchronization with the QGIS® platform is achieved through QField Sync®, a complement that allows to forward the information and data captured on the smartphone back to the project created on the computer.

The first step to establish a maintenance plan on the defined case study is to know the constructive systems and damages that are still present, which require periodic control and simple repairs, preventing the pathology from worsening. For this reason, as recently mentioned, thanks to the QField® mobile complement the pathological study of the building is carried out by mapping damages and collecting the necessary

Fig. 6.8 Capture of on-site data through the QField application

a)   b)
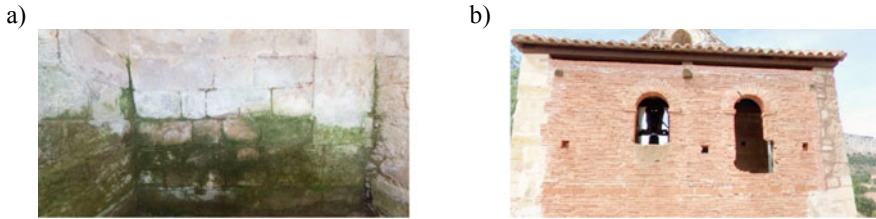
Fig. 6.9 Images captured during the in-field work: **a** biological colonization of an internal wall; and **b** loss of material on the bell tower windows

data. This information could be introduced within the QGIS project by activating the shapefile edition tool and creating the polygon shapefile that represents the damage or the construction system. Then, the user needs to introduce the required information in the different fields (see Fig. 6.8).

It is worth mentioning that the damage layer allows to introduce a maximum of 4 in-situ images. These images could be captured with the phone camera by following the approach described in Sedano-Espejo et al. [15] (see Fig. 6.9).

The whole process, digitization and data capturing, was performed in one-working day. Then, once the inspection has been done, changing to exploration mood is enough to save data collection into our portable device. Finally, this information is synchronized with the QGIS project of the computer, having all the data in the same location.

QGIS Model Builder Workflow Operations and Results

Once all the data was properly registered within the QGIS project it is time to compute the associated risks of the building [16]. To this end, it was executed with the Python script developed and shown in Sect. 6.3.2. This script allows to obtain the associated risks to each inspected area or system, showing it inside the program not only in a quantitative (area) but also in a qualitative way (see Fig. 6.10).

The risk evaluation carried out showed that the roof covering, the rainwater system, the building envelope, and the indoor climate present a high risk, so their intervention

a)   b)
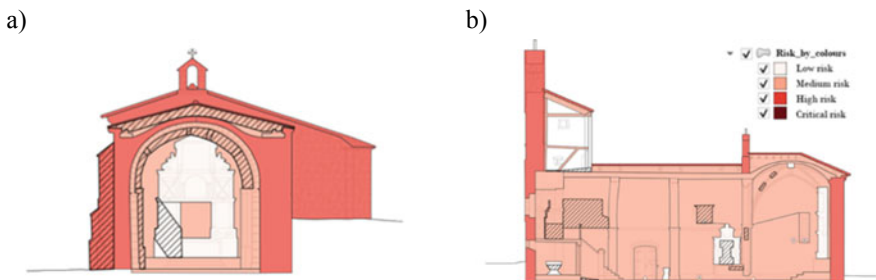
Fig. 6.10 Images (**a**) and (**b**) layers of visual risk classification of the different inspected areas; from inside sections of the church

must be immediate. On the other hand, the roof supporting structure, the building interior, the accessibility and hygiene, the ornamentation, the technical installations and equipment, and the prevention and safety, showed a medium and a low risk respectively, so their intervention can be realized on a long-term action.

Elaboration of the Preventive Conservation Plan

The final step performed in this work was the design of the preventive conservation plan of the church. This document, which is written in non-technical language, establishes some guidelines to follow for periodic maintenance [17]. This document is based on the information and calculations previously collected and elaborated, having the following structure (see Fig. 6.11): a brief description and situation of the case study treated; the risks shown by each scope of inspection are exposed; a set of 37 files are established, containing each damage detected in the building; and finally, a calendar with regular monitoring tasks and a Gantt diagram are created to make it easier to understand for the respective maintenance service [18].

Each of those 37 damages files are made up by the following data: name of the building of the case study, name of inspected area, final risk evaluation, file number, inspection date, final state condition, kind of damage (class, subclass, and sub-subclass), the name of the element analyze inside the inspected area, and an identifying code of each file (see Fig. 6.12). Furthermore, it is shown a planimetry with the location of the damages followed by possible consequences if the intervention is not realized, several maintenance tips, a recommendation of the inspection frequency, the intervention priority, the specialized worker request for the inspection, and finally some on-site images from the detected damage.

Fig. 6.11 PDF sheets from the preventive conservation plan: **a** brief description and location of the case study; **b** calendar with regular monitoring tasks and the Gantt diagram
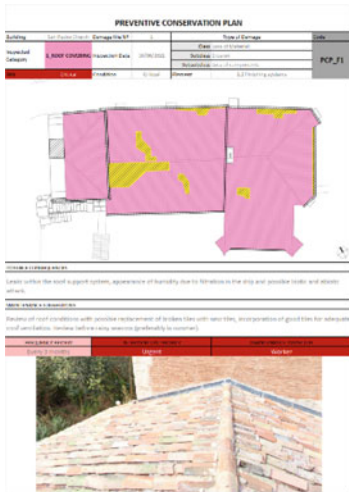
a)   b)

Fig. 6.12 PDF sheets with the damages observed during the inspection: **a** broken elements (ceramic tiles); and **b** deformation of the barrel vault

6.5   Conclusions

This article shows the development of a GIS application for management and design of the preventive conservation plans. To this end, it was used the open-source platform QGIS, the Python programming language as well as the android app QField. The workflow developed during this work allows to manage all the multisource information necessary to elaborate the risk analysis over a heritage building. This analysis is performed in an automatic way by using a Python language application (QGIS modeler).

The use of geospatial information (i.e., planimetries and shapefiles) proves to be very efficient as an entire visualization of risks damages, especially if it is combined with the mobile QField application. This app allows not only to register the required risk data but also to capture infield images from the inspected systems, elements and damages over the case study, reducing the time required to map the damages of the buildings.

This approach improves the service level 1 of the HeritageCare methodology by enhancing the productivity and the proper registration of information in a common geospatial database. In order to evaluate this improvement, it was decided to apply this approach to the Romanesque Church of San Pedro. The risk analysis carried out allowed us to design a preventive conservation plan, prioritizing the most urgent conservation activities as well as design easy-reading report for the owner of the Church.

Thanks to this work, it has been possible to recognize the geographic information systems and the visual geo-mapping efficiency in relation to the preventive conservation of heritage buildings. Moreover, the agility which offers the elaborated workflow provides a series of advantages to establish standardized maintenance guidelines to keep and preserve heritage architecture, from the ability to collect in-field images and damages information, to the promptness to obtain visual and numerical risk results.

Future works will be focused on developing and evaluating an interoperable geospatial database that allows to connect this GIS approach with the Web-GIS and BIM methodology proposed of the service levels 2 and 3.

References

1. HeritageCARE: monitoring and preventive conservation of historic and cultural heritage. Disponible online: http://heritagecare.eu/results/deliverables/. Last Accessed 27 Nov 2021 (2018)
2. IPCE (2013) Conservación preventiva: revisión de una disciplina. Revista Patrimonio Cultural de España nº7. Instituto del Patrimonio Cultural de España (IPCE), Ministerio de Educación Cultura y Deporte. Madrid
3. Masciotta MG, Morais MJ, Ramos LF, Oliveira DV, Sanchez-Aparicio LJ, González-Aguilera D (2019) A digital-based integrated methodology for the preventive conservation of cultural heritage: the experience of HeritageCare project. Int J Architectural Heritage 1–20
4. Matulionis RC Freitag JC (1991) Preventive maintenance of buildings
5. Sánchez-Aparicio LJ, Masciotta MG, García-Alvarez J, Ramos LF, Oliveira DV, Martín-Jiménez JA, González-Aguilera D, Monteiro P (2020) Web-GIS approach to preventive conservation of heritage buildings. Autom Constr 118:103304
6. Heritage Research Hub: JPI on cultural heritage. https://www.heritageresearch-hub.eu/homepage/joint-programming-initiative-on-cultural-heritage-homepage/. Last Accessed 12 Dec 2021
7. Comisión Europea: Plan de recuperación para Europa. Comisión Europea—European Commission. https://ec.europa.eu/info/strategy/recovery-plan-europe_es. Last Accessed 23 Dec 2021
8. Wu M, van Laar B (2021) The Monumentenwacht model for preventive conservation of built heritage: a case study of Monumentenwacht Vlaanderen in Belgium. Front Architectural Res 10(1):92–107
9. Mora R, Sánchez-Aparicio LJ, Maté-González MÁ, García-Álvarez J, Sanchez-Aparicio M, Gonzalez-Aguilera D (2021) An historical building information modelling approach for the preventive conservation of historical constructions: application to the historical library of Salamanca. Autom Constr 121:103449
10. HeritageCare: general methodology for the preventive conservation of cultural heritage buildings (2017)
11. ICCROM (2017) Guía de gestión de riesgos para el patrimonio museológico

12. Huerta Fernández S, López Manzanares G (1996) Informe sobre la estabilidad de la iglesia de Guimarei
13. Alonso D QField: QGIS para dispositivos móviles. MappingGIS. https://mappinggis.com/2019/04/qfield-qgis-para-dispositivos-moviles/. Last Accessed 28 Dec 2021
14. Sánchez-Aparicio LJ, Mora R, Conde B, Maté-González MÁ, Sánchez- Aparicio M, González-Aguilera D (2021) Integration of a wearable mobile mapping solution and advance numerical simulations for the structural analysis of historical constructions: a case of study in San Pedro Church (Palencia, Spain). Remote Sens 13(7):1252
15. Sedano Espejo E, Mackinlay P, Sanz Arauz D, Sanchez Aparicio M, Sanchez Aparicio LJ (2021) Use of geographical information system approaches for the diagnosis of San Isidoro ruins (Madrid, Spain). ISPRS
16. Ortiz P, Antunez V, Martín JM, Ortiz R, Vázquez MA, Galán E (2014) Approach to environmental risk analysis for the main monuments in a historical city. J Cult Herit 15(4):432–440
17. Do Norte DRDC (2020) Guía para las Buenas Prácticas en Conservación Preventiva
18. González MG, De Tapol B (2009) Medio siglo de Conservación Preventiva. Entrevista a Gaël de Guichen. Ge-conservacion 35–44

Chapter 7
Moisture Condition Evaluation in a Sixteenth Century Building Using Non-destructive Techniques

Letzai Ruiz-Valero , **Esteban Prieto-Vicioso** , **Virginia Flores-Sasso** , **and Gabriela Fernández-Flores**

Abstract The objective of this study is to analyze the surface moisture conditions in a sixteenth century building located in the colonial city of Santo Domingo, Dominican Republic, by non-destructive methods. Two techniques were used to accomplish the investigation: infrared thermography (IRT) and electrical resistance measuring (ERM). Additionally, a visual inspection was performed, and the thermo hygrometric conditions were registered. In visual inspection, it was observed that there is a significant deterioration in the walls, due to the presence of humidity, permitting the appearance of plants and the development of black crust. The results obtained with IRT have allowed us to detect humidity by capillarity, humidity by water infiltration due to the breakage of the downspouts or accumulation in the balcony and cornice area, in addition to growth of vegetation on the walls. While ERM results confirm the moisture found with the IRT, indicating that there are very humid areas, others sufficiently dry and intermediate areas. In conclusion, it can be said that the use of these two methods and visual inspection allows a precise and rapid detection of the humidity present in the construction elements of a historic building, thus contributing to its preservation.

Keywords Moisture · Infrared thermography · Electrical resistance measuring · Non-destructive techniques · Dominican Republic

L. Ruiz-Valero (✉) · V. Flores-Sasso · G. Fernández-Flores
Pontificia Universidad Católica Madre y Maestra (PUCMM), Santo Domingo, Dominican Republic
e-mail: letzairuiz@pucmm.edu.do

V. Flores-Sasso
e-mail: virginiaflores@pucmm.edu.do

G. Fernández-Flores
e-mail: ga.fernandez@ce.pucmm.edu.do

E. Prieto-Vicioso
Universidad Nacional Pedro Henríquez Ureña (UNPHU), Santo Domingo, Dominican Republic
e-mail: eprieto@unphu.edu.do

7.1   Introduction

Early detection of damage associated with moisture build-up in brickwork, brick or stone masonry, concrete and wood elements helps prevent irreversible harm and may supply relevant data for the rehabilitation and preservation of historic buildings. Moisture can cause different lesions in the building, some become harmful such as fungi that can cause health problems, or irreversible such as rot. Therefore, it is very important once the lesion is detected, to find out its origin to cure the root of the issue.

Some non-destructive techniques (NDT) allow for detection, characterization and evaluation of the moisture trapped in buildings, one of them is infrared thermography (IRT), which offers immediate results, in situ and without affecting the building; this allows us to detect areas with different temperatures due to the moisture present in porous materials that increases their conductivity and reduces the resistance, resulting in a thermal bridge [1].

The application of NDT as a diagnostic method in historic buildings is very frequent and has been used in various investigations. Rodríguez Liñan et al. [2] used IRT and ultrasound to evaluate the timber roof of the San Felipe Neri Oratory, in Cádiz, Spain, to identify various levels of degradation, density decay and damage that the building presented, with the aim of evaluating its state of conservation [2]. Likewise, Litti et al. [3] assessed the hygrothermal performance of brick masonry in a historical building in Antwerp (Belgium) using thermal images and ambient data to identify the changes in the surface due to humidity [3]. Kilic [4], also uses several non-destructive methods, including IRT, to evaluate the condition of a historical Ottoman structure, in Urla, Izmir, Turkey [4].

Pérez-Sánchez and Piedecausa-García [5] studied the constructive structure of historic domes of temples situated in the Province of Alicante (Spain) through thermal images [5]. Hoła et al. [6] selected the City Hall in Poland as a case study to analyze the dampness levels of masonry walls using the dielectric method [6]. Balík et al. [7] carried out a visual assessment of the Schebek Palace in the Czech Republic, also using the IRT and an electrical resistance meter to detect the humidity present in the construction elements [7]. Rocha et al. [8] apply IRT to detect capillary humidity that occurs in buildings [8].

Ruiz et al. [9] carried out an in-situ evaluation of the humidity conditions of the claddings of the Santa Bárbara church in Santo Domingo, Dominican Republic, by non-destructive techniques such as IRT and an electrical resistance meter [9]. Flores et al. [10] performed a visual inspection and applied IRT and electrical resistance measurements, and also measured the surface temperature of the brick vaults of the Royal Shipyard building located in Santo Domingo, Dominican Republic [10]. While Kavuru and Rosina [11] studied as a case study the British Residence in Hyderabad, Telangana, India, using used passive IRT to identify potential problems [11]. In addition, Gomes et al. [12] used as a sample the Delfim Moreira public school in Brazil to carried out a strategy approach for thermography assessment because of damp conditions on the claddings [12].

In the tropics, where ambient humidity levels are very high, humidity affects all construction materials, including those used to build historical buildings such as brick, stone, brick walls, wood and concrete. Therefore, the objective of this study is to analyze the surface moisture conditions in a sixteenth century building located in the colonial city of Santo Domingo, Dominican Republic, by non-destructive techniques: infrared thermography (IRT) and electrical resistance measurement (ERM) with humidity maps. To complete the analysis, the thermo hygrometric conditions of the building were registered.

7.2 Case Study

7.2.1 Building Description

The original building was built at the beginning of the sixteenth century (around 1530). It is located at 215 Arzobispo Meriño Street, 80 m from the Plaza de Armas, today, Parque Colón, and 150 m from the Cathedral of Santo Domingo, Primada de América. That area of the city is the oldest part known as the City of Ovando. The building site is 720 m^2 and is located on an east–west direction.

Its original use is unknown, but apparently it was a house and according to archaeological works the building also served to store valuables in the small rooms or vaults that are in the backyard. It is possible that the owner was a silversmith or was related to matters with silverware because in historical documents, it is mentioned that many silversmiths lived on that street and even the street was formerly called Plateros street.

The building is two stories, with a gallery, patio and backyard. The walls are built with mixed materials, some are stone and brick masonry, and others are rammed earth. The floors were originally brick, and today they are ceramic. It has a two-story gallery, with brick arches that join the two original bodies of the house. The mezzanine of the house was made of wood and currently has a light concrete slab. The original roof was gabled with wooden beams, mortar and brick. Currently, the roof is gabled with the same slope as the original roof, but it is made of lightweight concrete. In some mezzanines and ceilings of the house, old wooden beams are preserved.

On the south side of the house, there is a dividing well that rises to the second floor, being one of the only two wells of this type reported so far in the Colonial City. The façade is simple, with a cornice at the top and a baseboard at the bottom. It has nine doors and a continuous balcony with a metal railing on the second level, a product of the modifications made to the building at the end of the nineteenth century (Figs. 7.1 and 7.2).

Fig. 7.1 Main facade
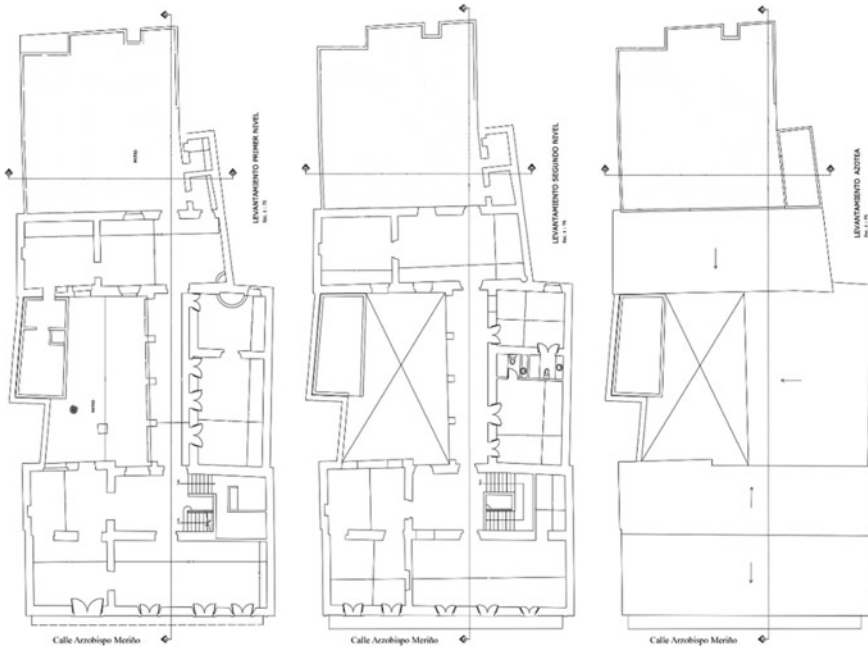
Fig. 7.2 Building floor plans

7.2.2 General Weather Specifications

Dominican Republic is located on the Caribbean, specifically in the northern latitude of the Tropic of Cancer, in a tropical climate zone, where the temperature remains

constant and generally humid almost all year round. Some annual cyclical changes occur in the tropics, but not as predictable as in the temperate zone [13].

The variation of the climate in the Dominican Republic is because of the geographic characteristics of the country that are affected directly from the mountainous terrain, resulting in two types of prevailing weather types: tropical jungle climate (Af) and tropical savanna climate (Aw). Regarding the low temperature, the yearly average is 21.0 °C and the high 30.4 °C. Meanwhile, 160 mm is the average for rainfall, 80% for relative humidity and 2.22 m/s for wind speed. On the other hand, 9 h is the average number of hours of sunshine per month during the year [14].

It is important to note that the building has been closed for several years, creating a microclimate since it has large trees that prevent the entry of much light, increasing the humidity levels in the building, therefore, it was also necessary to perform an analysis of the internal and external climatic conditions of the building.

7.3 Methodology

To perform the research, a number of tests in field were carried out, using two non-destructive techniques: Thermography (IRT) and electrical resistance measurement (ERM). Therefore, the thermo hygrometric conditions were registered. Visual inspection, thermal imaging and on-site measurements were carried out on July 17 and 18, 2019.

7.3.1 Visual Inspection

The condition of the construction systems of the building was visually examined to identify any signs of moisture damage. In the revision, the emphasis was on detecting possible water intrusions that could generate visible damage, as it can lead to deterioration of the surface.

7.3.2 Environmental Conditions

The parameters of outdoor and indoor ambient characteristics of the construction were carried out with an air quality monitor Tpi 1010ª (Table 7.1), which measures several variables and can be used on-site and supply the measures for monitoring and adjusting air treatment devices [15]. In addition, the Vantage Pro2 Weather Station Model 6152 wireless [16] located at the Cathedral of Santo Domingo, approximately 150 m away from the research building, was used to check the values of the environmental conditions.

Table 7.1 Tpi 1010ª equipment specifications [15]

Parameters	Range	Accuracy
CO_2	0–5000 pp	10 °C ~ 40 °C: ± 5% of rdg + 75 ppm < 10 °C, > 40 °C: ± 10% of rdg + 75 ppm
Air temperature	−20 °C to 60 °C	± 1 °C
Relative humidity	5–95%	± 1 °C
Dew point	−44 °C to 57 °C	Calculation ± 1 °C
Wet bulb	−16 °C to 57 °C	Calculation
CO	0–500 ppm	± 3 ppm or ± 5% of rdg whichever is higher
% Outside air	0–100%	Calculation

7.3.3 Infrared Thermography (IRT)

Infrared thermography, being a non-destructive method, offers certain unique capabilities for a variety of applications, within the preservation and safeguarding of historic monuments. [17], one of them being the detection of humidity that occurs in the different construction elements. There are currently two approaches to thermography inspections: active and passive. The passive method is based on measuring the difference in temperature of the object produced by standard conditions, while the active method measures the temperature differences of the object by taking into account outside stimulation [18]. In this investigation, the research is conducted on the passive thermography.

A thermal camera model T420 from FLIR systems was utilized to execute the thermal imaging. This equipment has a 240 × 320 pixels of IR resolution, FOL 18 mm objective, FOV of 25° × 19°/0.4 m, spatial resolution (IFOV) of 1.36 milliradians and spectral range of 7.5–13 microns. A thermal range of −20 °C to 120 °C was used for this investigation complying with the requisites of the UNE-EN 13,187: 1998 standard.

The procedure that has been followed is based on UNE-EN 13,187: 1998/ISO 6781: 1983 modified. "Thermal performance of buildings. Qualitative detection of thermal irregularities in building envelopes. Infrared method" [19]. The emissivity values of the construction materials (masonry: 0.93, bricks: 0.93, limestone: 0.95 and mortar: 0.92) [20] were considered, permitting to get a precise value of the temperature.

After taking the thermal images, the Flir Tool + program, version 6.4.18039.1003, was used to adjust some of the ambient parameters. In addition, in thermograms, dots or rectangles are positioned in several zones of the image to measure the temperature. The iron color palette was utilized in this research, where blue is the coldest temperature and yellow is the hottest temperature. In this way, we can identify the coldest point in the images.

7.3.4   Electrical Resistance Measuring (ERM)

Electrical resistance measuring (ERM) is a test that determines humidity by the measurement of the electrical resistance of the sample surface, which means that the tested resistance is influenced by the dielectric characteristic of the sample surface being evaluated, as well as by the potential effect of temperature [21]. Once the data is obtained, moisture mapping is carried out by specialized software.

The DELMHORST BD-2100 humidity meter was used in this investigation. The DELMHORST BD-2100 is a technique used for assessing and controlling the relative humidity level in surfaces. Measures moisture down to a depth of 19 mm. This equipment has three scales: # 1 Wood Scale, #2 Reference Scale 0–100 and #3 Gypsum Scale. For this investigation, Scale #2 was utilized [22]. The values obtained on this scale do not indicate the specific percentage of humidity, but are used as a relative indicator to approximate if the surface is "wet" or "dry" [23].

Specific areas in the building were selected to measure humidity with the DELMHORST BD-2100 and to be able to compare with thermograms. For data collection, a 50 × 50 cm grid was utilized, and each of these locations were monitored. Before the measurement, the equipment was graded. SurferV15 program was used to process the data [24]. With this software, an analysis of the information is carried out to generate the moisture charts of the selected surface. To elaborate the humidity maps, the blue color was used to show that the material is excessive humid (> 95), while the red color shows a sufficiently dry humidity condition (0–85) and the yellow color shows an intermediate position between the previous two (85–95) [22].

7.4   Results and Discussion

7.4.1   Visual Inspection

Moisture stains are observed on the façade on the first and second levels. Under the balcony, there is greenery and moss. In some areas, there is paint detachment, bulging in the plaster and some cracks. The upper cornice is broken in some places, and a black crust is observed. On the interior walls of the first and second levels, there are also large damp spots, bulging in the plaster, some cracks and paint peeling. In the main patio, dampness is observed by capillarity in the walls and columns. On the other hand, in some areas of the roof, humidity is observed due to the plugging of the downspouts, allowing water infiltration, the appearance of plants and the development of black crust (Fig. 7.3).

Fig. 7.3 Current building condition

7.4.2 Environmental Conditions

The average of the data measured in situ may be observed in Table 7.2, and Fig. 7.4 shows the indoor–outdoor air temperature and the relative humidity taken on July, 17 and 18, 2019. In this case, there is an average of 80% relative humidity, ambient temperatures are maintained in the range 25–34 °C during the day and night with few changes.

Table 7.2 Average environmental conditions for July 17, and 18, 2019

CO_2 (ppm)	Ambient temperature (°C)	Relative humidity (%)	Atmospheric pressure (hPA)	Dew point temperature (°C)	Wet bulb temperature (°C)	CO (ppm)	Wind speed per hour (m/s)
1053	31.54	80.2	1158	27.4	31.75	1	6.15
1125	30.86	79.6	1126	27.6	30.15	1	5.75
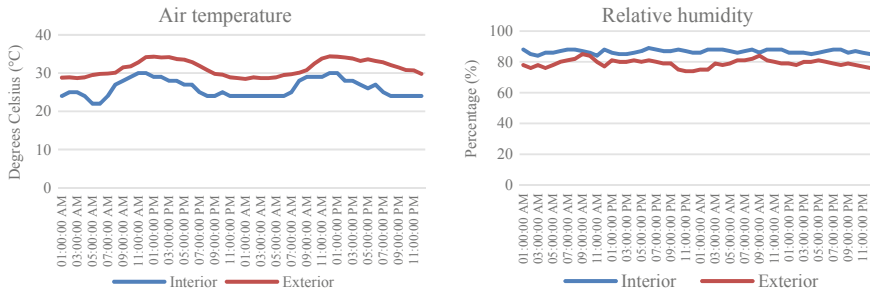
Fig. 7.4 Ambient temperature and relative humidity indoors–outdoors

7.4.3 Infrared Thermography (IRT)

Exterior Façade Thermograms of the exterior facade (Fig. 7.5a) humidity are observed just in the balcony area, permitting the appearance of plants and the presence of humidity in the wall. At the beginning of the wall, some specific humidity can be observed, due to the runoff of rainwater and humidity by capillarity. While, on the second level, there is a presence of humidity on the cornice and in a large part of the wall. This is probably since the water collection channel is not in good condition, allowing the infiltration of water toward the facade.

In the lower details of the thermal images (Fig. 7.5b), you can see the humidity in the balcony area. Where, the maximum surface temperatures were 33.2 °C, 34.3 °C and 34.4 °C, the minimum ones of 28.6 °C, 29.8 °C and 29.9 °C, while the average was 31.4 °C, 31.8 °C and 32.2 °C, respectively. While, in the upper details, the humidity of the cornice and part of the walls are observed. In this case, the maximum surface temperatures were 33.1 °C and 33.5 °C, the minimum 30.7 and 31.0 °C, while the average was 31.6, 31.7 and 32.0 °C.

Interior Façade In the thermal images of the first floor (Fig. 7.6), it can be observed that there is humidity inside just in the area of the mezzanine slab, due to the leaks that occur from the accumulated water on the balcony. The maximum surface temperatures were 29.2 °C, 30.1 °C and 30.3 °C, the minimum of 28.1 °C, 29.2 °C and 29.6 °C, while the average was 29.2 °C and 29.8 °C, respectively.

In the case of the second level thermograms, humidity is observed at the level of the mezzanine slab, due to the infiltration of water from the balcony toward the interior, creating humidity by capillarity in the walls at this level. It is also observed that there is dampness in the corners of the façade, most likely generated by the breakage of the rainwater downspouts. Likewise, some dampness is detected in the upper part of the interior façade, most likely due to the accumulation of water on the cornice or the breakage of the drains allowing the infiltration of water toward the wall. The detail shows that the maximum surface temperature is 31.8 °C, the minimum is 29.5 °C and the average is 30.6 °C.
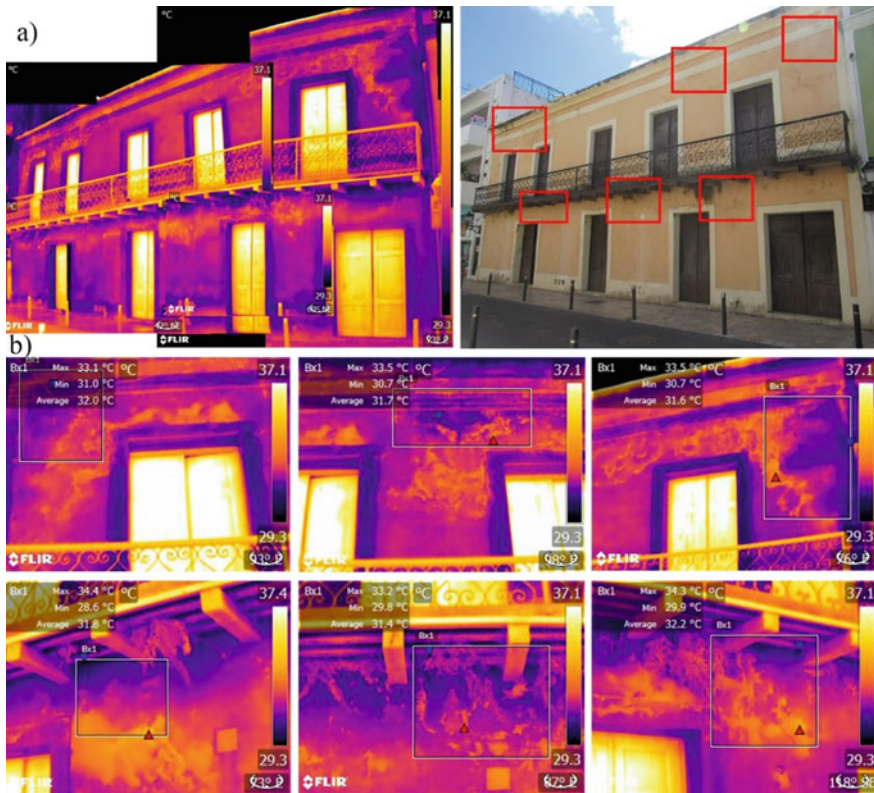
Fig. 7.5 Thermal images of the façade and details

Main Patio In the thermograms in Fig. 7.7, humidity can be observed throughout the cornice, as a result of the accumulation of water and the growth of vegetation in a large part of the walls; humidity from the roof to the ground, in the areas where the downspouts are located, due to their breakage, even allowing the presence of humidity in the mezzanine slab; dampness due to capillarity at the start of the columns and walls.

Corridor First and Second Levels In the thermograms of the first level corridor (Fig. 7.8a), it can be observed that, in the columns at the ends of the corridor, humidity produced by the breakage of the downspouts is present, generating humidity both in the arches and in the slab of mezzanine. In addition, dampness is also produced in the arches due to the infiltration of rainwater that falls on the second level, permeating toward the slab and descending to them. On the other hand, it can be seen that there is moisture by capillarity at the base of the columns and on the wall on the inside of the corridor. In the detail of the thermogram, the maximum surface temperature is measured, which is 28.1 °C, the minimum of 27.1 °C and the average of 27.7 °C.
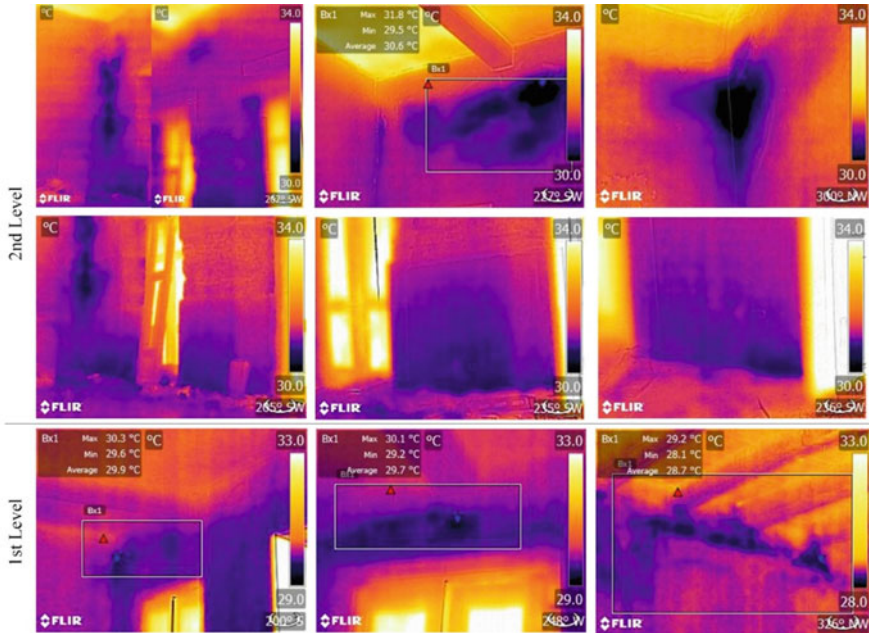
Fig. 7.6   Thermograms of the facade on the inside

In the case of the second level corridor (Fig. 7.8b), the thermograms show significant humidity from the roof to the mezzanine slab in the corner area, because of the breakage of the rainwater downpipe and the growth of the vegetation on the wall. Also, localized humidity is seen in the arch, it must be the product of water infiltration through the roof. On the other hand, at the start of the columns, there is dampness due to capillarity, due to the water that accumulates because of the rains and in the columns at the ends also due to water infiltrations due to the breakage of the downspouts. In the interior wall, there is a point humidity, this is due to the breakage of a bathroom water pipe that is inside that space. In this case, the maximum surface temperature was 29.5 °C, the minimum was 28.9 °C, and the average was 29.2 °C. On the roof, there is a hotter area than the others, this is probably due to the fact that just at that point there is greater solar incidence, while the rest of the roof is shaded by the trees present.

First Floor Walls In the thermograms, it can be observed that there is dampness by capillarity at the start of the wall in practically all the walls of the first level (Fig. 7.9). Where, the minimum surface temperatures are 27.4, 27.2 and 27.7 °C, the maximums are 28.8, 29.1 and 30.3 °C and the average temperatures are 28.4, 28.5 and 28.6 °C.
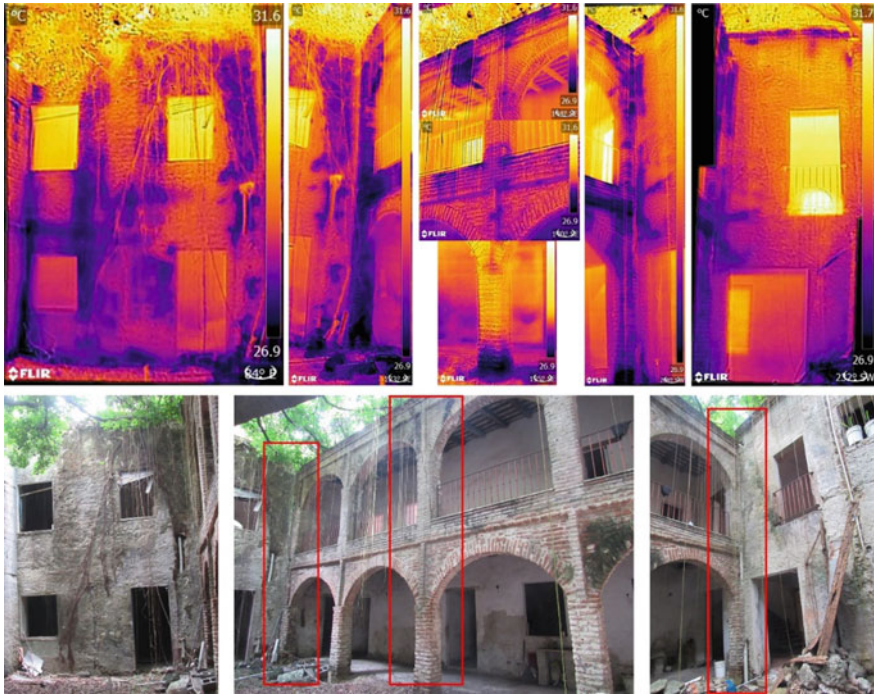
Fig. 7.7 Thermal imaging of the Main Patio

Fig. 7.8 a Thermal imaging of the corridor first level and **b** second level
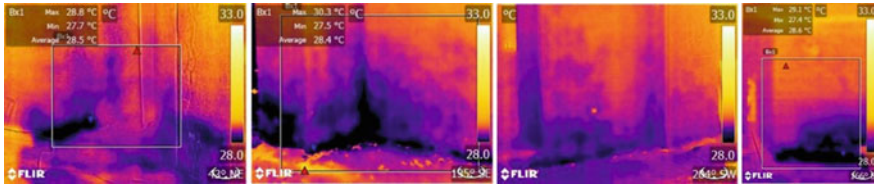
Fig. 7.9 Thermal images of start of the walls

7.4.4 Electrical Resistance Measuring (ERM)

Humidity maps show the extension of the humid and dry areas, where they are marked with several colors (the blue marked an extremely humid surface (> 95), while the red marked a sufficiently dry humidity condition (0–85), and the yellow marked an intermediate position between the two previous ones (85–95). Figure 7.10a illustrates a zone that is too humid (blue) just at the beginning of the column, produced by dampness due to capillarity, likewise, it is observed that the humidity decreases toward the top of the column, having an intermediate area (yellow) and then a sufficient dry humidity (red).

In Fig. 7.10b, a significant humidity is shown on the map at the meeting between the wall and the arcade of the second level corridor. An overly humid area (> 95) is observed running from the roof to the mezzanine slab, opening up more and more as you get closer to the slab. Areas with an intermediate position are also present (85–95) and other zones that are sufficient dry with humidity (0–85).

In the case of Fig. 7.10c, a small section of the exterior facade is observed just below the balcony, where there is a zone that is too humid (blue), followed by an
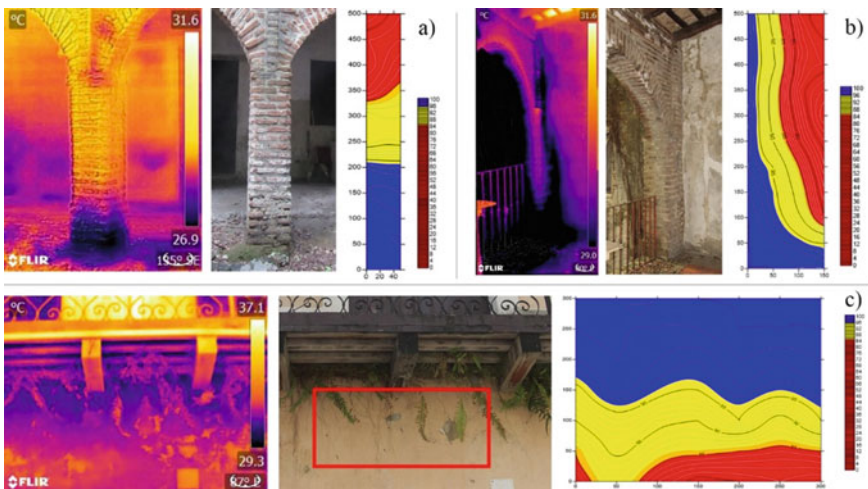
Fig. 7.10 a Column first level, b corner of corridor second level and c exterior façade details

intermediate zone (yellow) and finally a sufficiently dry humidity (red). The results of the humidity maps are confirmed with the thermal images (Fig. 7.10), which present a similar result, confirming the presence of humidity in the study areas.

7.5 Conclusions

In this study, two of non-destructive techniques have been applied: infrared thermography and electrical resistance measurement, to a sixteenth century building located in Santo Domingo, Dominican Republic. These non-destructive techniques used had the same objective, to verify the humidity contained in the construction elements. The IRT and ERM can be considered powerful and simple methods for the on-site supervision of buildings with heritage value, specifically for the detection of humidity.

In the visual inspection, it was observed that there is a significant deterioration in the walls of the façade and the main patio, especially due to the presence of humidity, permitting the appearance of plants and the development of black crust. The mezzanine slab in general is in good condition, with small exceptions, while the roofs are in good condition and do not present damp.

The results obtained with the IRT have allowed the detection of a series of humidity, which can be summarized as: humidity by capillarity, humidity by water infiltration due to the breakage of the downspouts or accumulation of water in the balcony and cornice area, in addition the growth of vegetation on the walls.

While the results of the ERM confirm the humidity found with the IRT, indicating that there are very humid areas, others sufficiently dry and intermediate areas between these two. In conclusion, it can be said that the use of these two methods combined with visual inspection allows a precise and rapid detection of the humidity present in the construction elements of a historic building, thus contributing to its preservation.

References

1. Grinzato E, Bison PG, Marinetti S (2002) Monitoring of ancient buildings by thermal method. J Cult Herit 3(1):21–29
2. Rodríguez Liñán C, Morales Conde MJ, Rubio de Hita P, Pérez Gálvez F (2011) Inspección mediante técnicas no destructivas de un edificio histórico: Oratorio San Felipe Neri (Cádiz). Informes de la Construcción 63(521):13–22
3. Litti G, Khoshdel S, Audenaert A, Braetb J (2015) Hygrothermal performance evaluation of traditional brick masonry in historic buildings. Energy Build 105:393–411
4. Kilic G (2015) Using advanced NDT for historic buildings: towards an integrated multidisciplinary health assessment strategy. J Cult Herit 16(4):526–535
5. Pérez-Sánchez JC, Piedecausa-García B (2016) Termografía infrarroja aplicada en cúpulas históricas: identificación y análisis de sistemas constructivos. Inf Constr 68(541):e129
6. Hoła A, Matkowski Z, Hoła J (2017) Analysis of the moisture content of masonry walls in historical buildings using the basement of a Medieval Town Hall as an example. Procedia Eng 172:363–368
7. Balík L, Kudrnáčová L, Pavlík Z, Černý R (2017) Application of infrared thermography in complex moisture inspection of the Schebek Palace. AIP Conf Proc 1866:040002
8. Rocha JHA, Santos CF, Póvoas YV (2018) Evaluation of the infrared thermography technique for capillarity moisture detection in buildings. Procedia Struct Integrity 11:107–113
9. Ruiz Valero L, Flores Sasso V, Prieto Vicioso E (2019) In situ assessment of superficial moisture condition in façades of historic building using non-destructive techniques. Case Stud Constr Mater 10:e00228
10. Flores Sasso V, Ruiz Valero L, Prieto Vicioso E (2020) Non-destructive techniques applied to historic building for measuring moisture content in brick vault. In: REHABEND 2020 Congress. Construction pathology, rehabilitation technology and heritage management. Granada, Spain, pp 778–789
11. Kavuru M, Rosina E (2021) IR thermography for the restoration of colonial architecture in India—case study of the British Residency in Hyderabad, Telangana. J Cult Heritage 48:24–28
12. Gomes Barbosa MT, Junio Rosse V, Gaudereto Laurindo N (2021) Thermography evaluation strategy proposal due moisture damage on building facades. J Build Eng 43
13. Gray WM, Ruprecht E, Phelps R (1975) Relative humidity in tropical weather systems. Mon Weather Rev J 103:685–690
14. Oficina Nacional de Meteorología (ONAMET). http://www.onamet.gov.do/m/. Last Accessed 17 July 2019
15. Tpi USA. https://www.testproductsintl.com/indoor-air-quality-iaq-2/indoor-air-quality-iaq-meters/1010a-indoor-air-quality-meter/. Last Accessed 8 Apr 2021
16. Davis Instruments. https://www.davisnet.com/solution/vantage-pro2/. Last Accessed 2 Apr 2021
17. Moropoulou A, Labropoulos KC, Delegou ET, Karoglou M, Bakolas A (2013) Non-destructive techniques as a tool for the protection of built cultural heritage. Constr Build Mater 48:1222–1239
18. Kylili A, Fokaides PA, Christou P, Kalogirou SA (2014) Infrared thermography (IRT) applications for building diagnostics: a review. Appl Energy 134:531–549
19. UNE-EN 13187:1998/ISO 6781:1983 modified. Thermal performance of buildings. Qualitative detection of thermal irregularities in building envelopes. Infrared method
20. OMEGA. https://www.omega.com/temperature/Z/pdf/z088-089.pdf. Last Accessed 6 Apr 2021
21. TRAMEX Meters (2017) Moisture detection and moisture mapping, innovation in moisture detection. Ireland

22. Delmhorst Instrument Co (1999) BD-2100 Owner's manual. Towaco, EEUU
23. Delmhorst Instrument Co. https://www.delmhorst.com/blog/bid/360520/what-is-a-moisture-meter-reference-scale-and-how-do-i-interpret-it. Last Accessed 27 Apr 2021
24. Golden Software. http://www.goldensoftware.com/products/surfer. Last Accessed 14 May 2021

Chapter 8
Spectroscopic Characterization of Sensitive Museum Plastic-Based Objects

Anna Klisińska-Kopacz , **Paulina Krupska-Wolas** ,
Michał Obarzanowski , **Anna Kłosowska-Klechowska** ,
and Julio del Hoyo Meléndez

Abstract Museum collections are constantly expanded to include plastic-based materials. Taking into account the dynamic development of polymer chemistry, presumably in the nearest years, the number of museum objects made of plastic continues to grow. Contrary to popular opinions, items made of plastic are not very durable, and they are easily susceptible to environmental conditions. The degradation process already starts when the object is created, but its speed and paths can be diverse. In the worst case, the degradation products of certain materials are harmful not only to them, but also to other objects stored in their surroundings. The presented work aims to improve a non-destructive method that allows for easy recognition of materials used in objects created from polymers in the collection of the National Museum in Krakow. Hyperspectral imaging (HSI) with SWIR spectral range of 1000–2500 nm and portable Raman spectroscopy were used to identify and characterize the polymers and additives composing the objects. Additionally, microfading testing (MFT) was carried out to investigate the reaction of plastic museum items to exposure to high intensity light in the visible range. Understanding the materials used to create the objects and new materials introduced as part of conservation treatments will allow to develop methods to minimize their physicochemical degradation. This will permit to make informed decisions regarding the care and display of these objects to ensure a safe exhibition and storage.

A. Klisińska-Kopacz (✉) · P. Krupska-Wolas · M. Obarzanowski · A. Kłosowska-Klechowska · J. del Hoyo Meléndez
National Museum in Krakow, al. 3 Maja 1, 30-062 Krakow, Poland
e-mail: aklisinska@mnk.pl

8.1 Introduction

In the twentieth century, to a greater extent objects containing synthetic polymer materials appeared in the collection of museums, libraries and archives [1–4]. Museum items generally are gathered for their purpose, form, rarity, source, cultural, historical or creative value, and rarely the nature of the material used has an influence on this process. Plastic-based objects are no exception and are collected for similar reasons.

About 1000 objects created using artificial polymer compounds are in the collection of the National Museum in Krakow. The oldest plastic-based objects come from the end of the nineteenth century. These are a variety of arts and crafts items such as parts of furniture, jewelry, headpieces of walking sticks and frames of eyeglasses. Most often, plastic was used to mimicry more expensive materials of natural origin such as turtle shell, amber, ivory, and coral. The artificial materials that appeared at the turn of the nineteenth and twentieth centuries include celluloid (1880), galalith (1904) and acetocellulose (1921). The oldest semi-synthetic plastics come from a natural polymer—cellulose for celluloid and acetocellulose, or milk casein for galalith.

Contrary to popular opinions, items made of plastic are not very durable and are easily susceptible to environmental conditions. As a result of the intrinsic unsteadiness of materials, sub-optimum preparation, and artistic rehearsals, a lot of artworks created with plastics tend to deteriorate at a disturbing speed. The degradation process already begins when the object is fabricated, but its speed and paths can be diverse. Low stability of the earliest plastics like cellulose nitrate and cellulose acetate is expected due to their poor design. The oldest man-made plastics found in museum collections are dated to the late nineteenth and early twentieth centuries. Initially, for a long period of time that could be even decades, the degradation processes may be almost imperceptible. However, usually after this slower process, there is a rapid transition to a much faster degradation path, which sometimes leads to complete total destruction of the objects. In the worst case, the degradation products of certain materials are harmful not only on them alone but equal to other objects stored in their surroundings.

The recognition of synthetic polymers present in museums is crucial for making informed decisions about their storage and to slow down the degradation process. The first step to create and develop guidelines for the guardianship and exhibit of polymer casts and plastic items in collections of historic objects is the chemical identification of materials included in their composition. Museums currently rely on appearance and odor as non-destructive simple tests used to make a preliminary identification of plastic-based materials. Initial recognition of the type of polymer present can be made based on color and transparency, however fillers and coloring materials can significantly change the look and surface of the plastic. The odor of chemical compounds is frequently used as a simple identification based on known smells given by certain gases associated with specific types of degradation. Unfortunately,

the description of smell is extremely subjective and to reach an agreement is usually complicated for the testers. For that reason, more sophisticated methods such as spectroscopic techniques to identify plastics in museum collections are required.

The most widely available technique used to identify polymers is attenuated total reflection (ATR) juxtaposition with Fourier Transform Infrared spectroscopy (FTIR). This method has allowed to examine the surface of plastic-based cultural heritage objects in a non-destructive way since the late 1990s. However, for the measurement, the sample is placed on an ATR crystal made of diamond or germanium, through which the infrared beam is reflected. Small objects can be measured directly without taking any samples. Recently, it was reported that portable FTIR spectroscopy systems for the identification of synthetic materials in museum pieces are highly promising [5–8]. In recent years, near-infrared reflectance spectroscopy as well as hyperspectral imaging (HSI) have been widely used for polymer identification, especially in the field of waste sorting. Spectral imaging is also used as a fast and inexpensive tool in the plastics recycling industry [9].

Also, Raman spectroscopy is used more and more often to identify polymers since it is a non-destructive and non-contact technique. For example, fast Raman spectroscopy has been effectively applied into an online recognition system of fragmented plastics in a recycling plant [10]. Raman spectroscopy for the reconnoitering of synthetic materials used in museum pieces has been discussed in the work of Klisińska-Kopacz et al. [11] and Reggio et al. [12].

This study had the objective of developing a quick and effective methodology for researching plastic objects from the museum collection, which would allow for quick grouping of the examined objects and then their easy, non-invasive analysis without interfering with the object and without the need to take samples. For this purpose, hyperspectral imaging (HSI) and Raman spectroscopy were employed in the current study.

8.2 Experimental

8.2.1 Samples

A group of plastic items of everyday use from the nineteenth century was selected for the study. These include a razor, a plastic box, umbrella handles, and a walking stick with a carved head. Additionally, a set of combs, pins, and clasps used to pin up hair, dated to 1910–1930 were chosen. Also, tortoiseshell fragments were used as reference material. All examined objects form part of the collection of the National Museum in Krakow. Table 8.1 presents a list of the examined objects along with their inventory numbers and dating. A general view of the artifacts is shown in Fig. 8.1.

Table 8.1 Description of the examined objects

No.	Object	Inventory number	Dating
1.	Razor	MNK IV-M-3499	1860–1940
2.	Plastic box	MNK IV-V-539/1	After 1860
3.	Walking stick with a carved head	MNK IV-MO-1068	After 1860
4.	Umbrella handle A	MNK IV-PN-778/1	After 1860
5.	Umbrella handle B	MNK IV-PN-778/2	After 1860
6.	Hair comb A	MNK IV-V-1457/1	1910–1930
7.	Hair comb B	MNK IV-V-1457/2	1910–1930
8.	Hair clip A	MNK IV-V-1462/1	1910–1930
9.	Hair clip B	MNK IV-V-1461/3	1910–1930
10.	Tortoiseshell A	MNK IV-PN-775/1	1867
11.	Tortoiseshell B	MNK IV-PN-775/2	1867
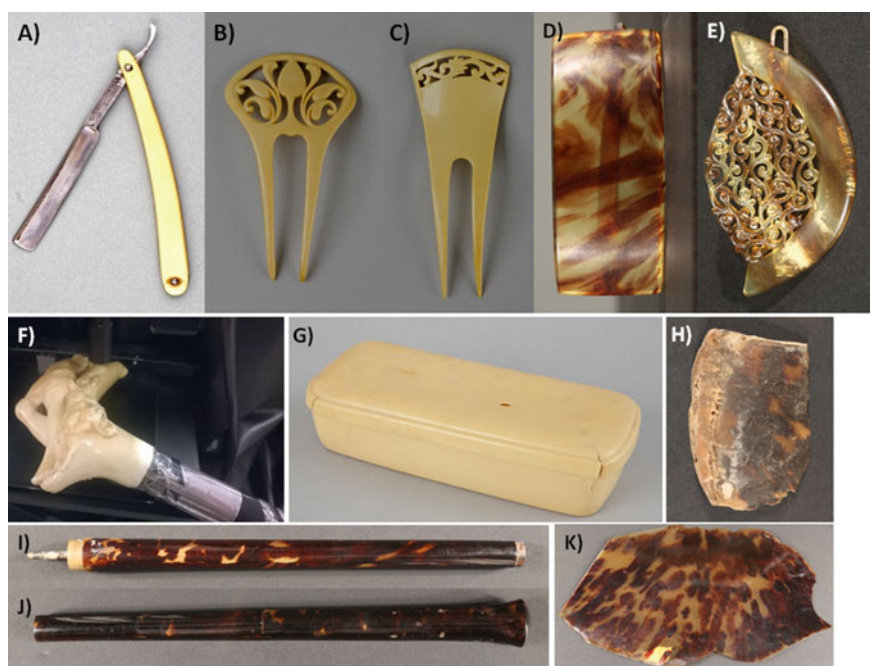
Fig. 8.1 Investigated objects: **a** Razor; **b** Hair comb A; **c** Hair comb B; **d** Hair clip A; **e** Hair clip B; **f** Walking stick with a carved head; **g** Plastic box; **h** Tortoiseshell A; **i** Umbrella handle A; **j** Umbrella handle B; **k** Tortoiseshell B

8.2.2 Methods

Before starting the research, all objects were photographed in visible light (VIS) to document their appearance and state of preservation and to select appropriate areas for measurements. Then, SWIR reflectance spectroscopy measurements were performed using a hyperspectral imaging system to group the analyzed objects based on their spectral signals. Next, the ability to identify chemical components present in the objects was assessed using Raman spectroscopy. Finally, microfading (MFT) tests identified the potential degradation effects experienced by museum lighting facilities.

SWIR reflectance spectroscopy A hyperspectral imaging camera was used working in the SWIR region (1000–2500 nm). 256 spectral bands were collected. The Specim detector exposure time was 11.0 ms. The scanning speed was set at 8 mm/s and a frame rate at 10 Hz. Halogen light sources positioned at an angle of 45° to the straight line perpendicular to the plane of the object were applied. Thanks to this configuration, it is possible to parse the spectral curve at chosen points and to evaluate the distribution of the reflectance at certain wavelengths. Individual notationed spectral curves were pre-corrected for dark stream. A white Spectralon standard was used for reflectance calibration (Labsphere, New Hampshire, USA). The above parameters were used to record both dark and white reference frames. The software ENVI 5.0 (Research System Inc., Colorado, USA) was applied for further analysis of the obtained spectral images.

Raman spectroscopy A handheld Raman system (DeltaNu, Wyoming, USA) was used to recognize and categorize the polymers and admixtures forming the items. This spectrometer works in the 200–2000 cm^{-1} spectral range applying a red line laser (785 nm). The maximum laser power is 120 mW, and the system allows you to set the laser power on three levels from maximum, through medium to low. The spectral resolution of the equipment is 8 cm^{-1}. Data acquisition was done with the NUSPEC software (DeltaNu). To obtain good quality spectra, alternative exposition times, laser power, and the quantity of accumulations, were tested to determine the best analytical conditions. Finally, an accumulation of 30 scans with the acquisition time from 5 to 30 s was used for the measurements.

Microfading testing (MFT) The MFT method was used to investigate the response of objects to irradiation with visible light. The MFT instrument used has been described in the literature [13]. Its design is inspired by an earlier product [14]. The components of the device are a high-power light source, an optical system with a geometry of 0°/45°, and the VIS reflection spectrometer. A HPLS 30-04 (LIFI) semiconductor plasma light source from Thorlabs (New Jersey, USA) was used as the light source. The tests were performed using only visible light to better simulate the lighting conditions in the museum. Currently, the objects displayed in galleries, by the museum lighting standards, are illuminated with light where the UV light component is removed. Optical fibers were used in the measuring system, which ensures non-contact measurement and detection. A Jaz spectrometer from Ocean

Optics (Florida, USA) was used. The diameter of the light spot was approximately 0.5 mm. The appraisal irradiance as measured in the spot was about 4.0 Mlx. The first visible light reflection spectrum was used as a reference. Successive data were assembled every 10 s, and the total test time was 600 s. The acquisition time was fixed on 100 ms. The average of 10 consecutive spectra was used. The SpectraSuite software (Ocean Optics, USA) was applied for data accumulation. In the case of plastic objects not only the type of the material influence their photosensitivity. In addition, the plasticizer concentration and chemical environment conditions such as oxygen concentration, humidity, and air pollutants have an effect on their stability. The CIE L * a * b* 1976 color space was used for the calculation of the spectrocolorimetric differences.

8.3   Results and Discussion

8.3.1   SWIR Reflectance Spectroscopy

Characteristic spectral bands in the VIS range differentiate the materials by their color and provide information about their chemical structure. Therefore, only the spectral signatures of the objects in the SWIR region are analyzed, as they are more efficient in classifying materials by type of polymer. Regions of Interest (ROI) were generated for each tested object, and the corresponding signatures were extracted and used as a spectral library. Representative reflectance spectral signatures of the analyzed objects in the range 1000–2500 nm are presented in Figs. 8.2, 8.3 and 8.4. They were obtained using the average of bands in the library of spectra. The *x* axis shows the wavelengths while the *y* axis shows the values of reflectance (dimensionless by definition).

The above results clearly show that each polymer has a characteristic spectral signature with absorption peaks located at characteristic wavelengths. In the SWIR region, absorbance of light by polymers through the overtones of normal vibration modes and combination bands concerning the distending of C–H and O–H bonds is observed. The recorded spectrum shows characteristic bands at approximately 1180 nm consistent to the second overtone of the C–H distending and approximately 1400 nm corresponding to a jugglery of C–H distending and C–H distortion. Two groups of materials can be clearly distinguished. As can be seen, the spectral characteristics obtained for the razor, box, and head of the walking stick (Fig. 8.2) are similar to that acquired for the hair combs and clips (Fig. 8.3). The spectral signatures show that samples of the same polymer, even at dissimilar steps of their life cycle, present similar characteristics. The obtained spectra show comparable tendencies that vary simply by their reflectance values. The umbrella handles as well as the tortoiseshell samples form a separate group of materials (Fig. 8.4).

This initial rapid screening of the objects was followed by the identification of their materials using Raman spectroscopy.
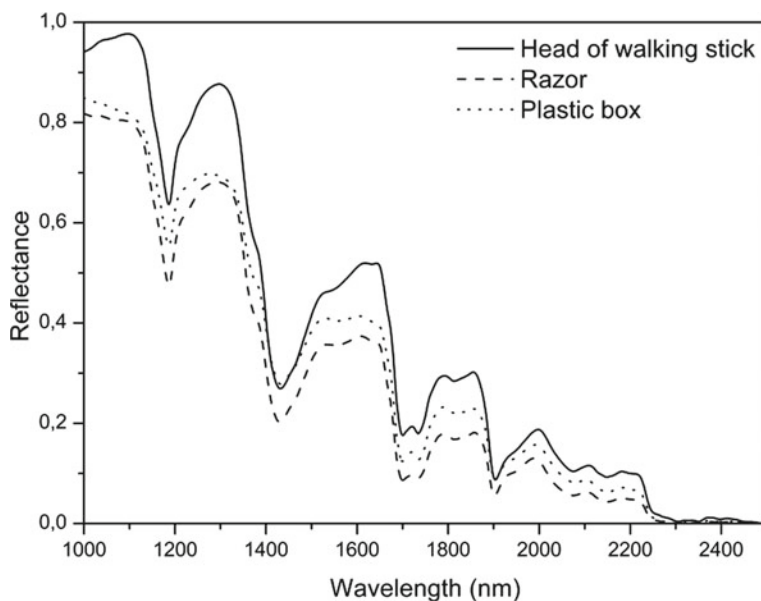
Fig. 8.2 SWIR spectra obtained for a head of walking stick, a razor and a plastic box
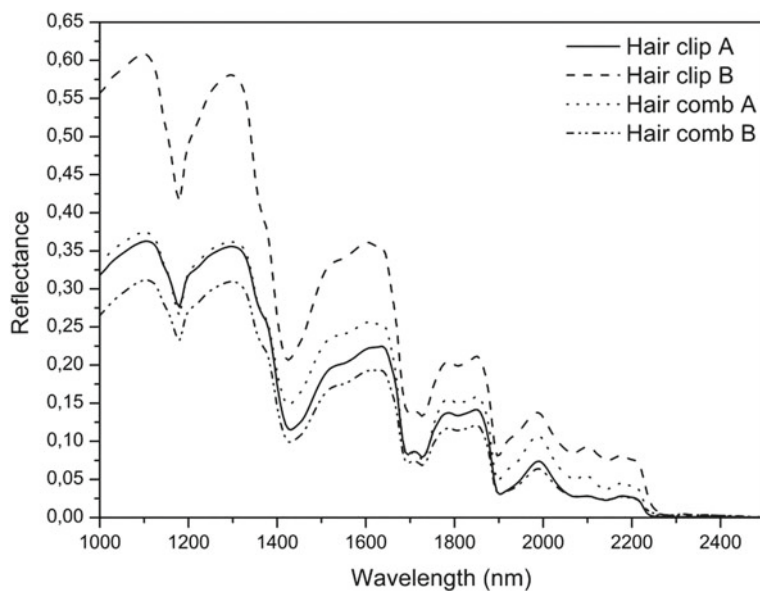
Fig. 8.3 SWIR spectra obtained for the hair clips and hair combs
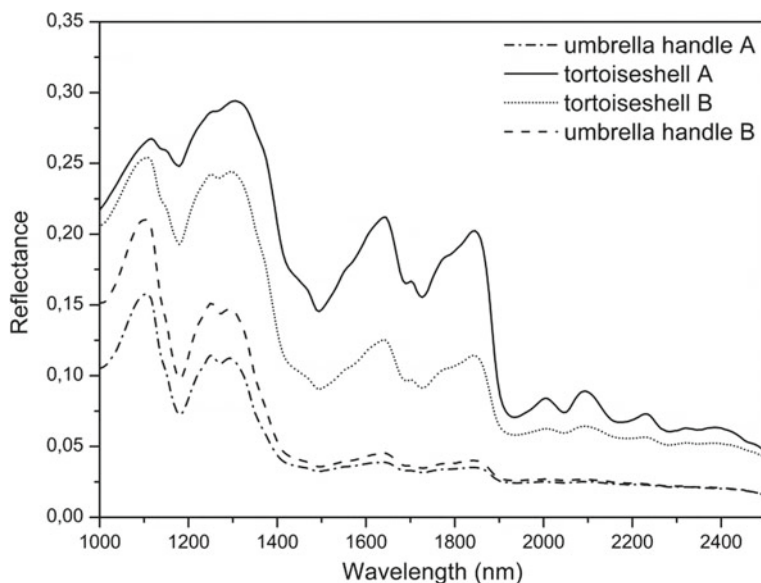
Fig. 8.4 SWIR spectra obtained for the umbrella handles and tortoiseshell samples

8.3.2 Raman Spectroscopy

Raman spectra obtained for the first group of objects are shown in Fig. 8.5. The results of Raman analysis of objects forming the second group are presented in Fig. 8.6.

In both cases, in the registered spectra, the bands characteristic for celluloid were observed. The strong peak at 1280 cm^{-1} was assigned to the vibration of nitrate group, v_sNO$_2$, while the band at 1650 cm^{-1} to the v_{as}NO$_2$ mode. The bands noted at 1375 cm^{-1} and 1120 cm^{-1} were assigned to cellulose ring mode and vCOC vibration, respectively [15]. The strong band at 650 cm^{-1} is typical for the bicyclocamphane compounds and indicated the presence of camphor. The peak at 1730 cm^{-1} was associated to the vC $=$ O mode, also characteristic of camphor [16].

Celluloid was produced from nitrocellulose, which was obtained by esterification of cellulose with nitric acid. Camphor was added to nitrocellulose as a plasticizer to obtain a moldable mass, celluloid.

The Raman spectra obtained for the second group of objects, containing umbrella handles and tortoiseshell pieces as reference, are presented in Fig. 8.7. The similarities in the spectra indicate that the umbrella handles were made of tortoiseshell. The Raman band observed at 645 cm^{-1} was related to the vC–S stretching vibration originating from cystine and cysteine fragments. The band at 856 cm^{-1} was assigned to tyrosine side-chains involving C–CH aromatic deformation. The band found at 1004 cm^{-1} was attributed to C–C stretching vibrations of aromatic rings in the phenylalanine side chain. The intensive band observed at 1240 cm^{-1} corresponds to vC–N amide III deformation. After comparing the obtained results to literature
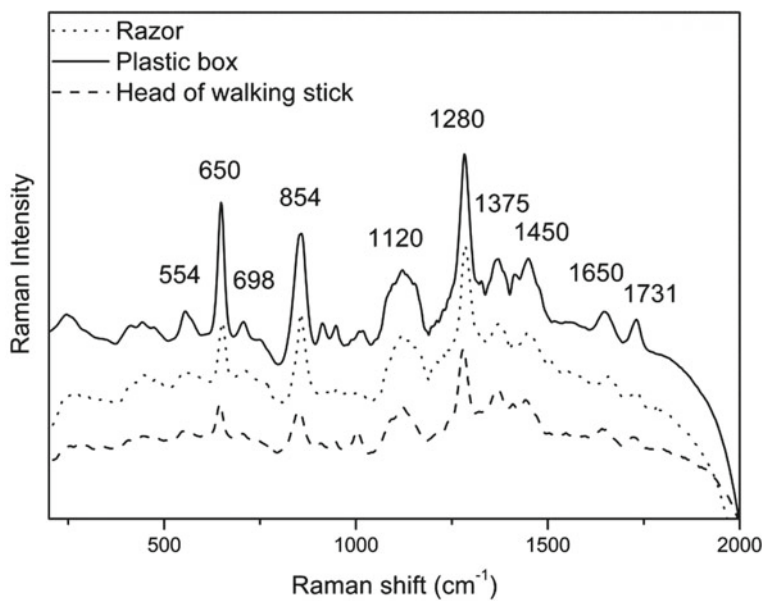
Fig. 8.5 Raman spectra obtained for the head of a walking stick, razor, and plastic box
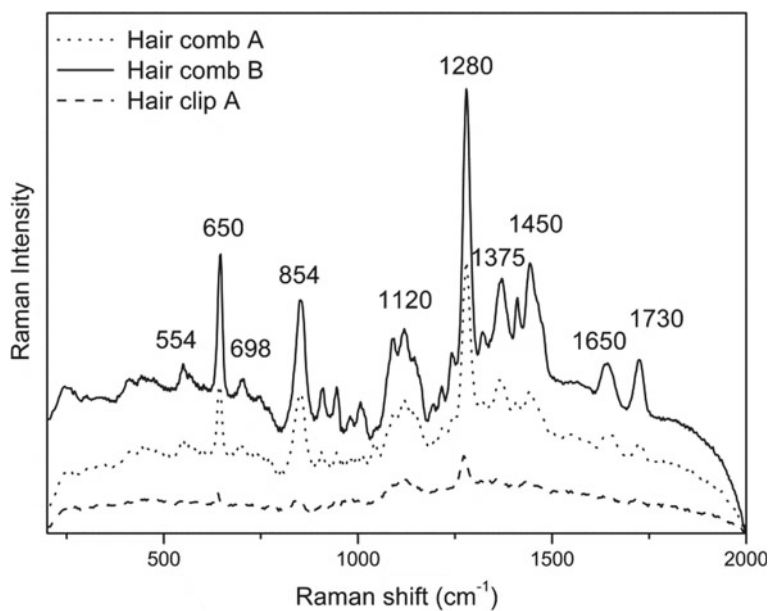
Fig. 8.6 Raman spectra obtained for two hair combs and a hair clip
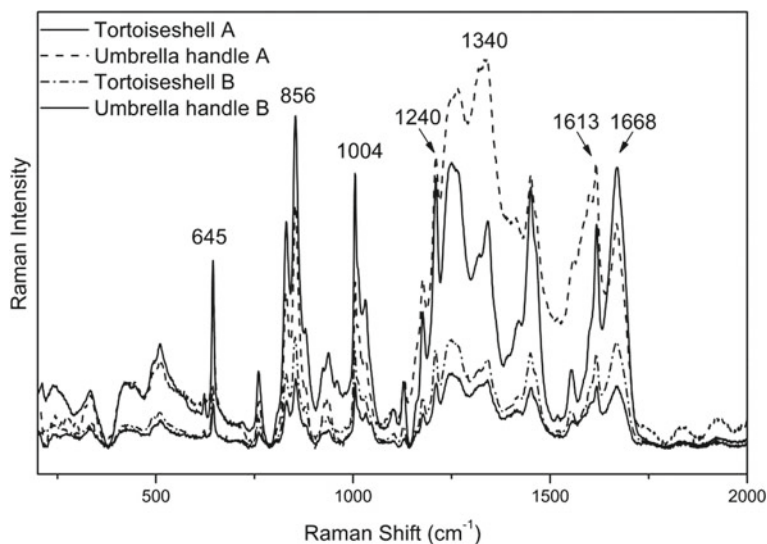
Fig. 8.7 Raman spectra for the umbrella handles and tortoiseshell samples

data, in the case of tortoiseshell, it was observed that the band at 1240 cm^{-1} has a stronger intensity than that observed for bovine keratin, which is consistent with the β-sheet preference of the reptilian keratinization process [17]. In the amide III bands region, the broad band observed at 1340 cm^{-1} was assigned to the methylene band (CH$_2$) deformation, while the sharp band at 1450 cm^{-1} was associated to methylene (CH$_2$) deformation bands (scissoring). Two strong bands centered at 1613 cm^{-1} and 1668 cm^{-1} were related to νC–C and β-sheet amide I vibrational modes, respectively.

8.3.3 Microfading Testing (MFT)

A survey was conducted on the stability to high intensity light irradiation of 4 representative objects: the plastic box, razor, and hair combs. The aim was to make a preliminary assessment of the response of these objects to high intensity light with the aim of identifying any potential risks associated with their degradation. The results are presented graphically in the form of microfading curves that show the variation of color (Delta E 1976) with respect to time in seconds. The color changes were correlated to those obtained for BW category 1–3 using identical experimental circumstances. The results are presented in Table 8.2. All investigated objects made of celluloid showed very high light sensitivity remaining within the BW1–BW2 range. Figure 8.8 shows examples of microfading curves obtained for the two hair combs.

Table 8.2 Objects examined with MFT

Object	Calculated color changes (ΔE76)	BW range
Razor	3.0–3.5	1–2
Plastic box—exterior part	2.0	2
Plastic box—interior part	1.0	1
Hair comb A	0.9	1
Hair comb B	2.0	2
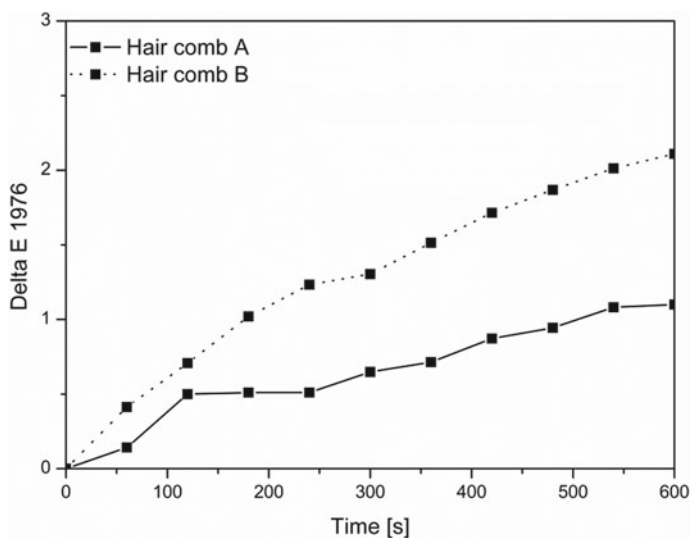
Fig. 8.8 Microfading curves obtained after testing two hair combs

8.4   Conclusions

The results obtained as part of this research indicated that in most cases in situ analysis with Raman and SWIR spectroscopy can be efficiently used to recognize the major components of plastic-based cultural heritage objects with proper quality spectra obtained a part of the shape and color of the object.

A methodology based on Raman spectroscopy preceded by SWIR spectroscopy used to screen and group the objects provided satisfactory results. An advantage of this type of examination is its rapid character and that it requires no sampling.

Chemical material recognition is the primary stage in the development and implementation of suggestions for the attention and exhibit of polymer objects and plastic items in museum collections. The MFT results are regarded promising as the method allows to assess the degree of degradation of objects based on the specific color modifications resulting from their natural aging processes.

References

1. Shashoua Y (2008) Conservation of plastics: materials science, degradation and preservation. Butterworth-Heinemann, Oxford
2. Keneghan B, van Oosten T, Lagana A, Wagenaar M, Barabant G, Balcar N, Bluzat H, Bollard C, Fayen J, Kuperholc S (2012) In what conditions are my artefacts? Case studies. In: Lavedrine B, Fournier A, Martin G (eds) Preservation of plastic artefacts in museum collections. Comité Des Travaux Hisoriques Et Scientifiques, Paris, pp 109–137
3. de Sá SF, Da Cruz SM, Callapez ME, Carvalho V (2020) Plastics that made history—the contribution of conservation science for the history of the Portuguese plastics industry. Conservar Património 35:85–100
4. Lazzari M, Reggio D (2021) What fate for plastics in artworks? An overview of their identification and degradative behaviour. Polymers 13(6):883–904
5. Doménech-Carbó MT, Doménech-Carbó A, Gimeno-Adelanto JV, Bosch-Reig F (2001) Identification of synthetic resins used in works of art by Fourier transform infrared spectroscopy. Appl Spectrosc 55(12):1590–1602
6. Pereira A, Candeias A, Cardoso A, Rodrigues D, Vandenabeele P, Caldeira AT (2016) Non-invasive methodology for the identification of plastic pieces in museum environment—a novel approach. Microchem J 124:846–855
7. Saviello D, Toniolo L, Goidanich S, Casadio F (2016) Non-invasive identification of plastic materials in museum collections with portable FTIR reflectance spectroscopy: reference database and practical applications. Microchem J 124:868–877
8. Angelin EM, de Sá SF, Soares I, Callapez ME, Ferreira JL, Melo MJ, Bacci M, Picollo M (2021) Application of infrared reflectance spectroscopy on plastics in cultural heritage collections: a comparative assessment of two portable mid-Fourier transform infrared reflection devices. Appl Spectrosc 75(7):818–833
9. Moroni M, Mei A (2020) Characterization and separation of traditional and bio-plastics by hyperspectral devices. Appl Sci 10:2800–2819
10. Kawazumi H, Tsuchida A, Yoshida T, Tsuchida Y (2014) High-performance recycling system for waste plastics using Raman identification. In: Dincer I, Midilli A, Kucuk H (eds) Progress in sustainable energy technologies, vol II. Springer, Cham, pp 519–529
11. Klisińska-Kopacz A, Łydżba-Kopczyńska B, Czarnecka M, Koźlecki T, del Hoyo Mélendez J, Mendys A, Kłosowska-Klechowska A, Obarzanowski M, Frączek P (2019) Raman spectroscopy as a powerful technique for the identification of polymers used in cast sculptures from museum collections. J Raman Spectrosc 50:213–221
12. Reggio D, Saviello D, Lazzari M, Iacopino D (2020) Characterization of contemporary and historical acrylonitrile butadiene styrene (ABS)—based objects: pilot study for handheld Raman analysis in collections. Spectrochimica Acta Part A Mol Biomol Spectrosc 242:118733
13. Łojewski T, Thomas J, Gołąb R, Kawałko J, Łojewska J (2011) Note: light ageing with simultaneous colorimetry via fibre optics reflection spectrometry. Rev Sci Instrum 82(7):76102–76106
14. Whitmore P, Bailie C, Connors SA (2000) Micro-fading tests to predict the result of exhibition: progress and prospects. Stud Conserv 45:200–205
15. Paris C, Coupry C (2005) Fourier transform Raman spectroscopic study of the first cellulose-based artificial materials in heritage. J Raman Spectrosc 36:77–82
16. Dafera DJ, Tarantilis PA, Polissiou MG (2002) Characterization of essential oils from Lamiaceae species by Fourier transform Raman spectroscopy. J Agric Food Chem 50:5503–5507
17. Edwards HGM, Hunt DE, Sibley MG (1998) FT-Raman spectroscopic study of keratotic materials: horn, hoof and tortoiseshell. Spectrochimica Acta Part A 54:745–757

Chapter 9
How Trustworthy Is an Adhesive? The Suitability of Adhesives for Use in Conservation of Fine Art

Bastien Vassort, Vendula Prázná, Anna Nguyen, Bhavana Kapalli, Noah Whitney, Ruben Mevius, Veronique Hehl, Dunya Handor, Nikita Shah, Kate Seymour ⓘ**, and Giuditta Perversi** ⓘ

Abstract Adhesives used for treatments in the conservation of fine art are often proprietary and subject to change in formulation without notification by manufacturers. Following the market discontinuation of a number of commonly used vinylic and acrylic dispersion adhesives, substitutes are often integrated into working practice without full knowledge of any shift in formulae. Deceptively similar substitutes can result in very different working properties and aging characteristics, eroding trust and confidence in the working practice and rising ethical concerns on adverse consequences for the artwork. This study provides the result of a long-term aging study on 21 common adhesives applied to glass slides and brushed out on opacity charts. Empirical evidence on the properties is provided and correlated with attenuated total reflectance-Fourier-transform infrared (ATR-FTIR) spectroscopy analysis. The thorough comparison across a decade of aging allows for a compelling performance estimate and can offer guidance for long-term application process and new formulation efforts.

Keywords Adhesives · Acrylics · Vinylics · Aging · Stability

K. Seymour
Stichting Restauratie Atelier Limburg (SRAL), 6221 KX Maastricht, Netherlands
e-mail: k.seymour@sral.nl

B. Vassort · V. Prázná · A. Nguyen · B. Kapalli · N. Whitney · R. Mevius · V. Hehl · D. Handor · G. Perversi (✉)
Maastricht Science Programme, Maastricht University, 6229 EN Maastricht, Netherlands
e-mail: g.perversi@maastrichtuniversity.nl

N. Shah
University of Amsterdam, 1012 WX Amsterdam, Netherlands

9.1 Introduction

9.1.1 Adhesives in Conservation of Fine Art

Polymers are the building blocks used by artists to create artworks—they bind pigments, adhere components, and coat surfaces. Polymer adhesives are used by conservators for a wide range of treatments in conservation. They are used for consolidating loose paint, re-gluing broken pieces, and replacing damaged or degraded coatings [1]. However, adhesives used for treatments in the conservation of fine art are often proprietary and subject to change in formulation without notification by manufacturers. Conservators also use adhesives readily available and accessible, purchased at home improvement stores or distributed by well-established suppliers of conservation materials.

Over the last decade, several commonly used vinylic and acrylic dispersion adhesives used by conservators have been discontinued by manufacturers.[1] Substitutes are often integrated into working practice without full knowledge of any shift in formulae. Even substitutes with similar identifiers, however, can result in very different working properties and aging characteristics. Conservators have noted subtle changes in pH, tackiness, color, film-forming temperature, Tg, embrittlement, and more in some of these replacements [2]. Trust in an adhesive's working properties provides surety and confidence in application. Furthermore, changes in behavior over time are ethically undesirable as these may lead to adverse consequences for the artwork.

This paper highlights an empirical study undertaken over 10 years at SRAL to study and evaluate a set of commonly used vinylic and acrylic adhesives by observing changes in color and film characteristics of brushouts and of molecular structure through sample analysis using Fourier-transform infra-red spectroscopy using an attenuated total reflectance mode (FTIR-ATR). The analysis was performed with the aim help conservators in selecting polymers for use as an adhesive, binder or coating, and provide qualitative confirmation of performance in comparison to established best practices of the field.

Vinylic Adhesives Vinyl acetate-based polymers are commonly polyvinyl acetates (PVAc), but several modifications can be available based on hydrolysis level (polyvinyl alcohols, PVAl or PVOH) or on copolymerization procedures (e.g., copolymers of vinyl acetate and ethylene, VAE). All are available in emulsion form and in different molecular weights varying from high to low. All vinyl polymers result in a long, branched chain of linked monomers, exemplified in Fig. 9.1. Vinyl acetate-based polymers are extremely versatile and form strong, flexible, adherent films that offer excellent adhesion to common substrates, such as wood, textile, or paper; they are also used commercially in construction products, carpet backing, paper and paperboard coatings, and engineered fabrics. PVAc is low cost to produce and is therefore readily available.

---

[1] The following adhesives studied in this project have been discontinued: Mowilith DMC2, Bison Woodglue superfast; Plextol D540; and Plextol D360.

Fig. 9.1 Example of repeating unit of a poly-vinyl acetate (PVAc)
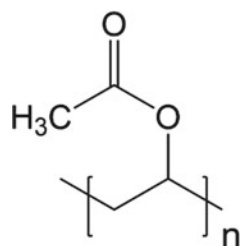
PVAcs are a polymers with good aging characteristics, but in some cases, its water sensitivity can be a problem. This is typically taken care of by formulating it with plasticizers to increase its reliability and stability. Additives may be included in the formulation of all forms of PVA adhesives in order to prolong shelf-life and inhibit foaming when brushing out. Cellulosic stabilizers may also be added, especially to the low viscosity variants [3].

Acrylic Adhesives Acrylic is a generic term denoting derivatives of acrylic and methacrylic acid. Acrylic resin emulsions are usually prepared by polymerization of various kinds of acrylic monomers in water, usually in the presence of an emulsifier or a dispersing agent. The starting product is acrylic acid ($CH_2 = CHCOOH$) and methacrylic acid ($CH_2 = C[CH_3]COOH$). The resulting resin can be engineered to have a desired functional group (–R). R may be a methyl (CH_3) or ethyl (CH_2CH_3) group or a longer carbon chain, such as butyl ($CH_2CH_2CH_2CH_3$). Co-polymerization with a mixture of different starting points is also possible (Fig. 9.2) [3].

The viscosity of aqueous dispersions can be modified by the presence of the functional group. The rheology of the emulsion can be further regulated with the presence of a cellulosic thickener or an acrylic emulsifier. Surfactant additives are often included to commercial formulations to improve shelf-life, to prevent foaming and to maintain suspension. Studies of acrylic paints have shown that surfactants migrate out of dried films. Acrylic resins have good UV stability and show little cross-linking as they are resistance to oxidative degradations [4].

Vinylic and acrylic formulations Vinyl acrylic is a copolymer of vinyl acetate and an acrylate monomer, most commonly butyl acrylate. Vinyl acrylics are both very flexible and water resistant, and their economical price means they are used extensively in interior architectural paints. Other applications of this copolymer include

Fig. 9.2 Example of repeating unit of an acrylic resin, with the possibility of co-polymerization with R ≠ R'
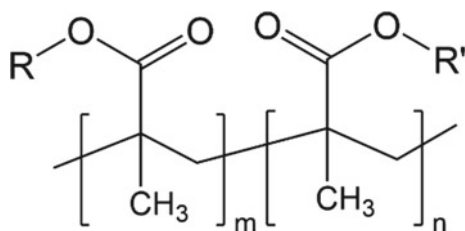
Table 9.1 List of Vinyl adhesives

Brand name (code)	Known chemical details	Brushout	Glass slide
BEVA D-8 (E1) [9]	Ethylene vinyl acetate	D, L	D, L, TRH
Evacon R (E2) [10]	Ethylene vinyl acetate (Copolymer)	D, L	D, L, TRH
Mowilith DMC2 old (M1) [11]	Vinyl acetate	D, L	D, L, TRH
Mowilith DMC2 new (M2) [11]	Vinyl acetate	D, L	D, L, TRH
Bison Woodglue—superstrong (B1) [12]	Vinyl acetate	D, L	D, L, TRH
Bison Woodglue—water resistant (B2) [13]	Vinyl acetate	D, L	D, L, TRH
Bison Woodglue—superfast (B3) [14]	Vinyl acetate	D, L	D, L, TRH
Pattex Woodglue—express (P1) [15]	Vinyl acetate	D, L	D, L, TRH
Pattex Woodglue—classic (P2) [16]	Vinyl acetate	D, L	D, L, TRH
Frencken Noval Col D2S—Woodglue fast New (F1) [17]	Vinyl acetate	D, L	D, L, TRH
Frencken Noval Col—PVAc Woodglue fast old (F2) [17]	Vinyl acetate	D, L	D, L, TRH

The assigned code is indicated in parentheses beside the brand name. A note detailed the presence of dark aging (D), light aging (L), and temperature + relative humidity (TRH) conditions

pigment dispersions, sealing, and paper saturation, and it can also be applied to engineered, non-woven fabrics [3].

Typical brand names used in the conservation field and commercial products with well-established performance stability are included in Tables 9.1 and 9.2.

9.2 Materials and Methods

9.2.1 Sample Preparation and Aging Conditions

Common vinylic and acrylic emulsion adhesives found in the SRAL conservation studio were applied to two substrates: brushouts of each adhesive were coated onto laminated, opacity drawdown cards (PA-2854, BYK-Gardner), and drops of each adhesive were applied to glass microscope slides (Fig. 9.3). The majority of these adhesives were aqueous dispersions, although some solvent-based acrylics formulations were studied.

Table 9.2 List of acrylic adhesives

Brand name (code)	Known chemical details	Brushout	Glass slide
Paraloid B72 (B72) (solvent) [18]	Ethyl-methacrylate	D, L	D, L, TRH
Plextol B500 (B500) [19]	Butyl acrylate/methyl methacrylate	D, L	D, L, TRH
Lascaux medium for consolidation (LMC) [20]	Acrylic dispersion	D, L	D, L, TRH
Plextol [Dispersion] K360 (K360) [21]	Acrylic dispersion	D, L	D, L
Plexigum PQ611 (PQ611) (solvent) [22]	Iso-butyl methacrylate	D, L	D, L, TRH
Plexigum PQ610 (PQ610) (solvent) [23]	Butyl/C5-C10 methacrylates	D, L	D, L, TRH
Plexigum P28 (P28) (solvent) [23]	Iso-butyl methacrylate	D, L	D, L, TRH
Plextol D540 (D540) [24]	Methacrylic ester/Acrylic ester	D, L	D, L, TRH
Lascaux Acrykleber 360 HV (HV360) [25]	Butyl acrylate/methyl methacrylate + acrylic butylester	D	D, TRH
Lascaux Acrykleber 498 HV (HV498) [26]	Butyl acrylate + methacrylic acid	D	D, TRH
Plextol D360 (D360) [27]	Methacrylic ester/Acrylic ester	D, L	D, L, TRH

The assigned code is indicated in parentheses beside the brand name. A note detailed the presence of dark aging (D), light aging (L), and temperature + relative humidity (TRH) conditions

Fig. 9.3 Adhesive sample brushouts on laminated, opacity cards and drop applications on glass slides before aging (2011). *Photo* Kate Seymour

Three glass-based sets were arranged for each adhesive: a reference to be kept in dark conditions (Set 1); a set exposed constantly for 1320 h to light with a high UV content in a light aging chamber (Set 2); a set placed in a Climacell chamber, provided by St. Luc Academy in Liege, exposed to elevated relative humidity (85%) and temperature (65 °C) for 720 h (Set 3). Sets 2 and 3 were placed in dark storage at room temperature after the initial artificial aging. Two additional sets were added for brushout applications: the reference set was kept in the dark from conception, while a second set was exposed to light for an initial period of 3 months and then moved to dark storage. Each adhesive was given a code, with additional labels to track aging conditions (Tables 9.1 and 9.2).

The light aging was optimized to expose the samples to high levels of light containing UV energy for a number of years.[2] The light aging chamber uses Philips fluorescent tubes (daylight TL 96.5) that provide an output of 9000 lx (including UV). The lights are kept on continuously 24/7 for 55 days, equivalent to 18 accumulative light years under museum lighting conditions. Previous studies have provided information about the stability of these polymers to photooxidation and allowed to optimize this timing for a proper photodegradation study [5, 6].

The temperature and relative humidity conditions (TRH) were designed to delay the curing process while in progress by maintaining high levels of moisture (85% humidity, 65 °C, 720 h). In addition, these conditions simulated different environmental situations in different global climatic regions, thus providing further relevant information for conservators [7].

In total, brushouts and sample slides of 21 adhesives were included in the study. A comprehensive list of samples, and their relative data available upon aging, is provided in Tables 9.1 and 9.2.

The follow-up study was executed in June 2021, after a decade of dark storage for all samples. The dark storage conditions simulate the state as an adhesive inserted between two adherends, which replicates the state of an adhesive used to repair fractured or split wood, ceramics, glass, paper or textile. The same polymers are often used as coatings, varnishes, or sealants in the treatment of art objects such as paintings, glass, ceramics, or metals [8].

9.2.2   Experimental Methods and Data Collection

Attenuated total reflectance-Fourier-transform infrared (ATR-FTIR) spectroscopy analysis of all samples was carried out after application in 2011 by posmaster students from the University of Amsterdam (UvA) at the Academy of St. Luc, Liege. The

---

[2] Total light doses per day = $8000 \times 24 \times 1 = 192.000$ lx hrs. A painting or mixed media under 'normal' museum lighting is exposed to 200 lx. Considering 1 day = 8 h of exposure, the total lux hours per day is around 1600. So, 1 day in the accelerated light chamber equals = 120 days of input from museum lighting. 2 days in the box = 240 days of natural aging. (Thomson, Garry. "Annual Exposure to Light within Museums." Studies in Conservation, vol 12, no 1, 1967, pp 26–36, https://doi.org/10.2307/1505437. Accessed 15 Apr 2022.).

experiment was executed under supervision of Nico Broers on a Thermo Nicolet 380 FTIR spectrometer coupled with a smart orbit diamond ATR detector and processed with a built-in Thermofisher OMINCTM Speca software. The protocol followed standard operating practice: background scans (32) were implemented to eliminate interference from air. The samples were recovered dry from the glass microscope slides, removing small sections of each adhesive with a clean scalpel, and placing them on the diamond cell using sterilized tweezers. Each sample was analyzed with 32 scans accumulated scans in the 400–4000 cm^{-1} range, with a 2 cm^{-1} steps. Data was saved with and without labeling the peaks, in.spa format.

This sequence was repeated in 2021 by Bachelor students from the University of Maastricht's Science Programme. Infrared spectra of were collected with a Shimadzu IRAffinity-1 FTIR Spectrometer equipped with Shimadzu MIRacle 10 diamond/ZnSe prism with high-pressure clamp single reflection ATR accessory. All spectra were collected at 4 cm^{-1} steps in the range of 400–4000 cm^{-1}, with accumulation over 64 scans and background subtraction with consistent acquisition. Samples were delicately scraped off the application surface (glass or brushout) with a sterile scalpel, and placed on the FTIR cell with a clean spatula. In order to improve data preservation, the 2021 data were saved in ASCII format. The 2011 data were also converted from the original spectrographic format into ASCII format using the Spectragryph software [28].

It is noteworthy that the equipment with ATR setups allows for highly reproducible and consistent measurements of solid samples with no further pre-treatment. The pressure cell reduces variability in the sample mount by compressing the material, and create a layer of reproducible thickness for the IR light transmission. By keeping the sampling technique, the backgrounding, and the acquisition methods consistent, the spectral outcome was reproducible and reliable. No internal standard was added to the data, which are presented with no further modification for qualitative analysis in the next section.

9.3 Results

9.3.1 FT-IR Spectra

Infrared spectroscopy is commonly used as an analytical tool in chemistry for its capability of showing absorption process of radiation between 2.5 and 25 µm (equivalent to 400–4000 cm^{-1}) from gas, liquid, and solid compounds. Especially when using organic matrices, the frequencies used to fall in a range capable of activating stretching and bending motions of the chemical bonds present. Different molecules would show band of absorption in different positions, showing bands at specific frequencies. Even though some shift can be ascribed to inherent chemical differences even in similar matrices, specific kinds of bonds (e.g. C–H, C–C, C–O, C = O, N–C, N–H, etc.) are consistently found in narrow regions of the infrared
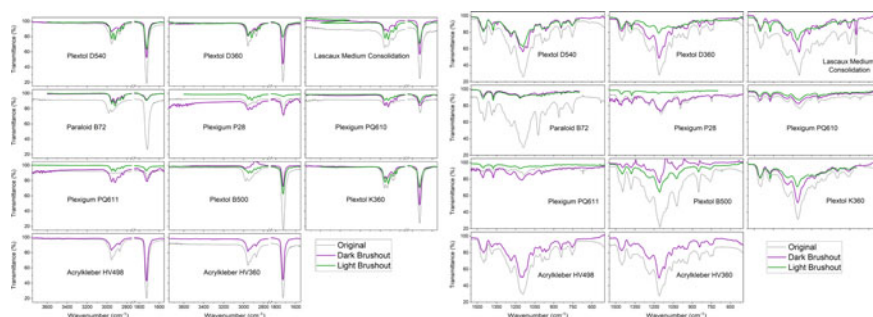
Fig. 9.4 Acrylic adhesive samples, IR spectra of brushout substrates (light and dark aging compared to original). For clarity, the graphs are split in functional group region (**a**) and fingerprint region (**b**)

vibrational frequencies. As such, even when presented with different molecules, a FT-IR spectra can give unique insights in the chemical features of a material, and any changes that might occur overtime. Given the nature of the chemical vibrations, it is usual practice to separate the analysis of an IR spectra in *fingerprint region* (400–1500 cm^{-1}, showing a great number of bands and usually analyzed as a whole to get a glimpse of the skeleton of a molecule), and *functional group region* (1500–4000 cm^{-1}, containing the most unique and strongest absorption frequencies associated with distinct chemical features) [29].

In accordance to the above concepts, the spectra acquired on the adhesive samples are subdivided in functional and fingerprint regions. The functional group spectra are available in Figs. 4a and 9.5a for the acrylic adhesives and Figs. 6a and 9.7a for vinyl adhesives. The fingerprint spectra are available in Figs. 4b and 9.5b for acrylic adhesives and 6B and 7B for vinyl adhesives. A further grouping was provided depending on the substrate, allowing a correlation of brushout-applied samples (original, dark- and light-aged, Figs. 9.4 and 9.6) and glass-applied samples (original, dark-and light-aged, and temperature + relative humidity aging, Figs. 9.5 and 9.7).

Overall, acrylic and vinyl adhesives have several recurring features, which is unsurprising given some chemical similarities in the nature of the molecules previously discussed. A summary of all approximate position of IR bands for the samples in their original form (before aging) is provided in Table 9.3, associated with an approximate chemical assignation of the vibrations [30–34]. A precise assignation would require a spectra-by-spectra analysis, complemented with additional analytical techniques to reconstruct a chemical structure with full confidence. However, this task is beyond the scope of this work, and trying to discern the details of proprietary commercial formulation would not add to the analysis. The broader approach to the bond vibration identification in Table 9.3 provides the overall chemical picture consistent with the hypotheses from the available technical datasheet of the commercial adhesive under investigation.
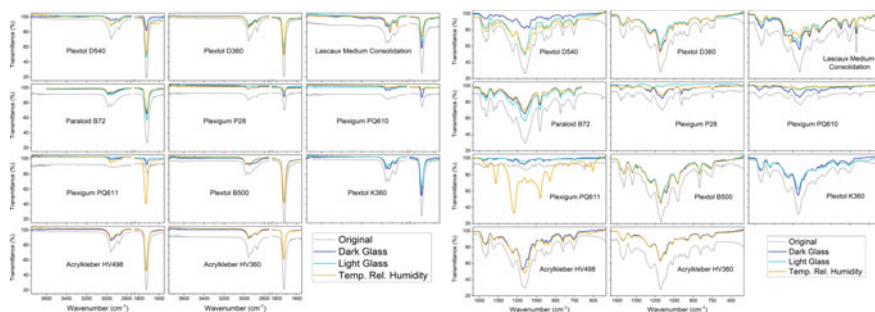
Fig. 9.5 Acrylic adhesive samples, IR spectra of glass substrates (light and dark aging compared to original, plus temperature + relative humidity aging conditions when available). For clarity, the graphs are split in functional group region (**a**) and fingerprint region (**b**)
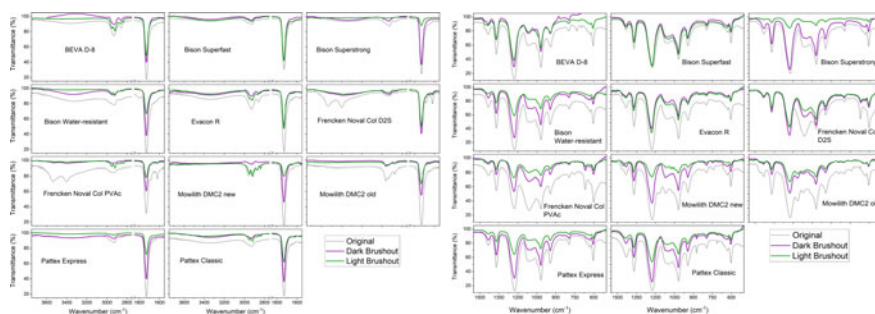
Fig. 9.6 Vinyl adhesive samples, IR spectra of brushout substrates (light and dark aging compared to original). For clarity, the graphs are split in functional group region (**a**) and fingerprint region (**b**)
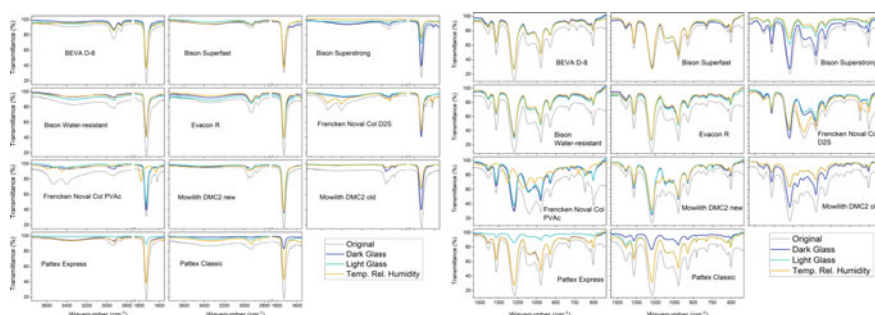
Fig. 9.7 Vinyl adhesive samples, IR spectra of glass substrates (light and dark aging compared to original, plus temperature + relative humidity aging conditions when available). For clarity, the graphs are split in functional group region (**a**) and fingerprint region (**b**)

Table 9.3 List of most prominent IR bands in acrylic and vinyl adhesive spectra, as observed in the original spectra collected in 2011

Acrylic IR bands (cm^{-1})	Chemical signature	Vinyl IR bands (cm^{-1})	Chemical signature
3535 *	N–H [primary amine]	3040–2845	C–H (stretch)
3400 *	N–H [primary amine]	1722	C $=$ O [ester, saturated]
3336 *	– OH [water]	1446	– CH_2– (scissoring)
2969–2835	C-H (stretch)	1377	CH_3 (rocking)
1801 *	N–H [primary amine]	1236	– CH_2– (rocking)
1728	C $=$ O [ester, saturated]	1145	C–CO–O, C–O–C
1618 *	C $=$ C	1060	– O–C–C (stretch)
1433	– CH_2– (scissoring)	1024	-C–O–C (stretch)
1369	CH_3 (rocking)	989	CH, CH_2, CH_3 vibrations region
1218	– CH_2– (rocking)	958	
1174 *	C–N	937	
1110	– C–N, C–CO–O, C–O–C	852	
1018	– C–N, –O–C–C, –C–O–C	755	
945	C $=$ C, C–H (out of plane)	698	
869	CH, CH_2, CH_3 vibrations region		
848 *			
787 *			
736			
669 *			
601			

The positions are roughly approximated from the multiple overlapping of the same band from different spectra. Bands labeled with a * do not appear in all the spectra. A suggested assignation of the signals to specific functional groups and bond vibrations is provided

9.4   Discussion

Results for some adhesives, still in production and with continual use in the conservation sector, are consistent with those reported in literature. [5, 6] On the other hand, results for some of the substitutes illustrate that these do not hold up to the same aging characteristics as the original formulae.

A comprehensive outline of the spectroscopic and physical evidence for all adhesives, in all conditions, is provided in the following detailed list. A schematic highlight of all considerations is tabulated in concise format in Table 9.4. It is worth noting that the considerations are purposefully qualitative and not quantitative, in keeping with the level of chemical uncertainty surrounding the exact composition of the adhesives.

Table 9.4 Summary table of the observed variability of the sample, based on FT-IR signal features

Adhesive code	No change	Modest dampening	Marked dampening	Extreme changes	Physical
E1		D, L, TRH			**bL**
E2		D, L, TRH			bL
M1 ⊗		gD, gL, TRH	bD, bL		**All, bL**
M2 ⊗		gD	bD, L, TRH		**bL**
B1		D	L, TRH		bL
B2		D, bL, TRH	gL		**bL**
B3 ⊗	D, L, TRH				L
P1		D, TRH	bL	gL	L
P2		bD, TRH	L, gD		L
F1		L*, D*, TRH			**L**
F2		gD*, gL*	bL*, bD*, TRH*		bL, bD
B72		gD, gL, TRH	bD, bL		**L**
B500		gD, gL, TRH	bD, bL		All
LMC		D, L	TRH		Harden
K360		gD, gL	bD, bL		**L**, bD
PQ611		bD	bL	gD, gL, TRH	Harden
PQ610		D, bL		gD, gL, TRH	Harden
P28	bD	gD, TRH		L	/
D540 ⊗		bD, L, TRH	gD		**All**
HV360		D, TRH			**All**
HV498		D, TRH			**All**
D360 ⊗		D, gL, TRH		bL	/

For every adhesive code, the various sample are marked as dark (D), light (L), and temperature + relative Humidity (TRH) aged; if there is a specific substrate that is subjected to a specific effect, an additional label is provided for "Brushout" (b) or "Glass" (g). One additional column (physical) contains labels for any sample that shows color changes upon aging, and bolded labels highlight samples affected by scaling; additional effects (e.g. hardening) are "?>

Summary of outcome for vinyl adhesives

- BEVA D-8: consistent IR spectra both in dark and light. Age-related drop in intensity and definition of the transmission signal in brushout and glass samples alike. The light-aged brushout sample shows yellowing and scaling.
- Evacon R: consistent IR spectra both in dark and light. Age-related drop in intensity and definition of the transmission signal in brushout and glass samples alike. The light-aged brushout sample show some yellowing.

- Mowilith DMC2 (old): marked loss of signal intensity and associated loss of peak resolution with aging, for both dark and light samples. All samples tend to yellow with aging, light exposure also causes scaling of the brushout.
- Mowilith DMC2 (new): glass samples have consistent IR spectra for all aging, with only loss of intensity. The signal breakdown is much more pronounced in the brushout samples, where light-aging causes loss of a significant proportion of the IR signal, especially on all the peaks associated with the characteristics C–O bonds. The light-aged brushout samples are also affected by yellowing and scaling.
- Bison Woodglue—Superstrong: all the dark-aged samples have an excellent behavior, with very modest loss of IR signal with aging and no macroscopic issue. On the other hand, the signal loss for light- and TRH-aging is very marked and correlates with the yellowing and whitening of brushout samples with light.
- Bison Woodglue—Water resistant: consistent IR spectra both in dark and light. Age-related drop in intensity and definition of the transmission signal. The signal drop is more marked with the light-aged brushout sample, which is also extremely yellowed and scaled. In general, the color changes are a consistent issue with this sample set.
- Bison Woodglue—Superfast: excellent consistency of the IR spectra among all specimens, with very little change even in signal intensity. However, light-aged samples tend to yellow and whiten with aging. Based on the functional group feature, the dark-aged samples have a tendency to adsorb some water. This adhesive is discontinued.
- Pattex Woodglue—express: the dark-aged samples and the TRH sample have consistent IR spectra upon aging, with mild signal loss comparable to other samples. The light-aged samples, however, are extremely affected and lose almost all the features in IR, which is also reflected on a substantial yellowing and whitening.
- Pattex Woodglue—classic: consistent IR spectra for almost all, with age-related drop in intensity of the transmission signal. The dark-aged sample on glass, however, experience extreme loss of signal intensity in IR. Despite their good quality IR, the light-aged samples show a substantial yellowing and whitening on a macroscopic scale.
- Frencken Noval Col D2S—Woodglue fast (new): this glue shows a functional group feature consistent with the presence of a primary amine group. This feature is loss in all but the TRH-aged sample. The rest of the IR spectral feature are consistent along the tested condition, with age-related drop in intensity of the transmission signal. Light-aging, however, causes changes in color on the sample, and induces scaling.
- Frencken Noval Col PVAc—Woodglue fast (old): this glue shows a functional group feature consistent with the presence of a primary amine group. This feature is partially retained only in the TRH-aged sample, and faintly visible in the light-aged glass sample. There is a general age-related drop in intensity of the signal across all samples, but it is more marked on the brushout species, which are also macroscopically affected by yellowing-whitening. The TRH sample is extremely

modified by age, with a general shift of signal toward higher wavenumbers and possible loss of functional groups.

Summary of outcome for acrylic adhesives

- Paraloid B72: overall severely affected by aging, with extreme dampening of the IR signal with fundamental changes in the fingerprint region. This effect is particularly pronounced in the brushout samples, and slightly more contained in the glass samples. The changes are also reflected in the macroscopic behavior, with shifts in color of all samples (whitening on dark-aged, yellowing in light aged) and a tendency to scaling upon exposure to light.
- Plextol B500: roughly consistent IR spectra for the various samples, with a general better behavior and reduced dampening of the signal for the glass-applied samples. However, all samples are whiten or yellow with aging.
- Lascaux Medium for Consolidation: consistent IR spectra for the various samples, with dampening of the signal upon aging. The functional group region remains roughly consistent, but there are some changes in the fingerprint area that are particularly evident in the brushouts and in the TRH aging. Macroscopically, the samples undergo extreme hardening, they cannot be mechanically removed from the surface of application without damages.
- Plextol [Dispersion] K360: consistent IR spectra for the various samples, with dampening of the signal upon aging. The light-aged brushouts are the most affected by changes in the fingerprint region. Light-aged samples have a tendency toward yellowing and scaling, the dark-aged brushout samples appear not to dry uniformly.
- Plexigum PQ611: general lack pronounced FT-IR features, likely correlated to a lower degree of cross-linking and crystallinity of the sample. Upon aging, the signal fades further, especially with light exposure. TRH treatment severely changes the chemical arrangement, with sharp increase of signal in the functional group region and general modification of the fingerprint region. Macroscopically, the samples undergo extreme hardening, they cannot be mechanically removed from the surface of application without damages.
- Plexigum PQ610: general lack pronounced FT-IR features, likely correlated to a lower degree of cross-linking and crystallinity of the sample. Upon aging, the signal fades further, with flattening to background noise in TRH conditions aging. Macroscopically, the samples undergo extreme hardening, they cannot be mechanically removed from the surface of application without damages.
- Plexigum P28: This sample is particularly consistent upon dark aging, especially when applied as a brushout, where the FT-IR features are fundamentally maintained. It is also resistant to TRH degradations. However, it seems to be severely affected by light-aging, which causes the disappearance of all signals.
- Plextol D540: the IR features remain roughly consistent with every type of aging, with age-related drop in intensity of the transmission signal. The effect is more marked in dark-aged samples. However, all the samples of this glue displayed an extreme tendency to scaling off the surfaces.

- Lascaux Acrykleber 360HV: consistent IR spectra for all aging conditions, with age-related drop in intensity of the transmission signal. Upon aging, the samples assumed a yellow-whiteish color and showed tendency toward scaling. This sample has not been tested for light-aging.
- Lascaux Acrykleber 498HV: consistent IR spectra for all aging conditions, with age-related drop in intensity of the transmission signal. Upon aging, the samples assumed a yellow-whiteish color and showed tendency toward scaling (more modest than 360HV samples). This sample has not been tested for light-aging.
- Plextol D360: consistent IR spectra for all aging conditions, with age-related drop in intensity of the transmission signal. The light-aging of the brushout sample results in a much more severe loss of IR features in comparison to all other conditions, and it should be considered as a potentially delicate point.

Overall, the body of evidence reconstructed in the course of ten years allows to pinpoint the critical aspect of light-aging, which is unsurprisingly one of the most delicate conditions to uphold. Even adhesives that do not display overwhelming chemical changes in FT-IR signal are often affected by macroscopical deterioration of appearance and adherence. In some occasions, especially for vinyl-based adhesives, the deterioration can be subsided by manipulating the quantity of the adhesive when possible: by testing a globular deposition on glass substrate against a layer deposition on laminated paper, the analysis can pinpoint which of the materials is more suitable for lining applications as opposed to structural correction of bulky objects.

Combined with the performance outcome upon light- or dark-aging conditions, the analysis can be used to optimize the fine-art conservation practice, but also to create a more evidence-based experimental protocol for new projects.

9.5   Conclusions

The long-term experiment highlighted in this study proves how straightforward tools like FT-IR analysis can provide valuable insights on chemical changes of commonly used adhesive formulations, even when the detailed composition of the materials is unknown. When combined with additional physical evidences that are easily observable, like color shifts and scaling, a clear picture on aging effects on acrylics and vinylic adhesives in the conservation field arises. Results prove interesting and indicate that some of the adhesives formulated for conservation purposes are less stable than commercially produced materials for the home improvement market. On the other hand, other well-established adhesives specifically formulated for the conservation market performed well.

Based on the summary of the observations, while all samples have been naturally aging for 10 years, the samples with artificial light aging (equivalent to 18 years of museum lighting conditions) are in general more affected by the process. Additionally, elevated moisture conditions during curing may result in dramatic chemical changes in a minority of adhesives; as such, for conservation efforts of samples in

delicate environmental condition, educated decisions should be made on the base of the available evidence to avoid the outstanding cases of chemical degradation. Overall, all brushouts analyzed in 2021 show some chemical aging in their FT-IT profiles. Additionally, vinylic adhesives are proven to be more severely influenced by high-temperature and relative humidity condition or light-aging conditions, in comparison to a good number of acrylic adhesives. The different application modes produced, as expected, different results, with the thicker applied coatings on the glass slides showing less chemical change than the thinly applied brushout coatings. However, yellowing of these samples was consistent across brushouts and glass slides for the same adhesive.

Interestingly, some of the more well established and examined adhesives used in the conservation field, such as Paraloid B72 (acrylic), Lascaux Medium for Consolidation (acrylic), and BEVA D8 (vinylic), showed more variance between the different aging conditions than the commercial materials, such as Bison Superfast (vinylic) and Patex Classic (vinylic). Some adhesives performed well with considerably less shift in the spectral output between the different aging conditions. These include Lascaux Acrylkleber HV498 (acrylic), Plextol B500 (acrylic), and Dispersion K360 (acrylic). The experiment has shown that commercially produced materials often rejected for lack of knowledge of components and testing, for example, Bison Superfast (vinylic) or Patex Classic (vinylic), could be included within the conservator's toolbox. It is unfortunate that some of the more stable formulations have been discontinued and are no longer available to the conservator.

While it would be possible to perform additional analyses to gather further physical behavior insight on the samples (e.g. mechanical testing and a quantitative assessment of the adherence), the results presented are conclusive enough to act as guidance for fine-art conservators, who are rarely provided with in-depth insight on long timeframe as the one that this study present. The highlight summarized could be used as guidance to design a more evidence-informed intervention for long-term projects. Additionally, any exploration for new formulations that are particularly geared toward the restoration and conservation field should take into account any study provided on the topic, so that new materials with better performances could potentially be distributed in the future.

References

1. Wilks H (1992) Science for conservators, vol 3. The Conservation unit of the museums and galleries commission, London. https://doi.org/10.4324/9780203886588
2. Down JL (2016) The effect of modifiers on the stability of a vinyl acetate/ethylene copolymer dispersion. Stud Conserv 61(1):26–45
3. Horie CV (2010) Materials for conservation. ISBN: 9780750669054
4. Ormsby B, Kampasakali E (2013) Surfactants and acrylic dispersion paints: evaluating changes induced by wet surface cleaning treatments. In: New insights into the cleaning of paintings: proceedings from the cleaning 2010 international conference. Universidad Politecnica de Valencia and Museum Conservation Institute, Smithsonian Institution

5. Down JL, MacDonald MA, Tétreault J, Scott Williams R (1996) Adhesive testing at the Canadian Conservation Institute-an evaluation of selected poly(vinyl acetate) and acrylic adhesives. Stud Conserv 41(1):19–44. https://doi.org/10.1179/sic.1996.41.1.19

6. Down JL (2015) The evaluation of selected poly(vinyl acetate) and acrylic adhesives: a final research update. Stud Conserv 60(1):33–54. https://doi.org/10.1179/2047058414Y.0000000129

7. Poulis JA, Seymour K, Mosleh Y (2022) The creep performance of bio-based and synthetic lining adhesives at different environmental conditions. Int J Adhes Adhes (In publication)

8. Bria Jr CF (1986) The history of the use of synthetic consolidants and lining adhesives. Newsletter (Western Association for Art Conservation) 8.1:7–11

9. BEVA® D-8 Dispersion, product 87023 by Kremer Pigmente. https://www.kremer-pigmente.com/elements/resources/products/files/87023e.pdf

10. Evacon R conservation, by CXD international. https://www.cxdinternational.com/equipment-tools/adhesives-pastes-consolidants/cxd-evacon-r-conservation-adhesive-25kg-suevar0005

11. Mowilith glues by Clariant GmbH, Germany. http://cameo.mfa.org/wiki/Mowilith_DM

12. Product 1337100 by Bison. https://www.bison.nl/content/dam/boltonadhesives/products/import/48/nl/1337100/50.pdf

13. Product 1339050 by Bison. https://www.bison.nl/content/dam/boltonadhesives/products/import/48/nl/1339050/50.pdf

14. Product 1338711 by Bison. https://www.bison.nl/content/dam/boltonadhesives/products/import/48/nl/1338711/50.pdf

15. Product 1419263 by Pattex. https://dm.henkel-dam.com/is/content/henkel/nl-pattex-tds-1419263-pattex-houtlijm-express-flacon-250-grammes

16. Product 1419248 by Pattex. https://dm.henkel-dam.com/is/content/henkel/nl-pattex-tds-1419248-pattex-houtlijm-classic-flacon-750-grammes

17. Product by Frencken. https://www.frencken1901.nl/wp-content/uploads/2019/04/frencken-pds-nl-novacol-d4-1k.pdf

18. Product 67400 by Kremer Pigmente. https://www.kremer-pigmente.com/elements/resources/products/files/67400e.pdf

19. Product 2556500 by Deffner Johann. https://deffner-johann.de/pub/media/datasheets/2556500/DE/2556500_PLEXTOL_B-500_DJ_DE_SDB.pdf

20. Hedlund HP, Johansson M (2005) Prototypes of Lascaux's medium for consolidation. Restauro 6(2005):432–439

21. Product by Deffner Johann. https://deffner-johann.de/de/dispersion-k-360-nachfolgeprodukt-von-plextol-d-360-1-l.html

22. Product 67380e by Kremer Pigmente. https://www.kremer-pigmente.com/elements/resources/products/files/67380e.pdf

23. Samet W (1998) Painting conservation catalog, v. 1: varnishes and surface coatings

24. Product 76202e by Kremer Pigmente. https://www.kremer-pigmente.com/elements/resources/products/files/76202e.pdf

25. http://cameo.mfa.org/wiki/Lascaux_Acrylic_Adhesive_360_HV

26. Product 81002e by Kremer Pigmente. https://www.kremer-pigmente.com/elements/resources/products/files/81002e.pdf

27. https://coatings.specialchem.com/product/r-synthomer-plextol-d-360

28. Menges F 2017 Spectragryph—optical spectroscopy software. Spectroscopy Ninja, Oberstdorf, Germany. https://wwweffemm2.de/spectragryph/index.html

29. Derrick MR, Stulik D, Landry JM (1999) Infrared spectroscopy in conservation science. In: Scientific tools for conservation. Getty Conservation Institute, Los Angeles, CA. http://hdl.handle.net/10020/gci_pubs/infrared_spectroscopy

30. Learner T, Gallery T (1998) The use of a diamond cell for the FTIR characterisation of paints and varnishes available to twentieth century artists. In: Postprints: IRUG2 meeting, pp 7–20

31. Loginova EV, Mikheev IV, Volkov DS, Proskurnin MA (2016) Quantification of copolymer composition (methyl acrylate and itaconic acid) in polyacrylonitrile carbon-fiber precursors by FTIR-spectroscopy. Anal Methods 8(2):371–380

32. Ramírez-Hernández A, Aguilar-Flores C, Aparicio-Saguilán A (2019) Fingerprint analysis of FTIR spectra of polymers containing vinyl acetate. Dyna 86(209):198–205
33. Alia C, Jofre-Reche JA, Suarez JC, Arenas JM, Martín-Martinez JM (2018) Characterization of the chemical structure of vinyl ester resin in a climate chamber under different conditions of degradation. Polym Degrad Stab 153:88–99
34. Nikolic G, Zlatkovic S, Cakic M, Cakic S, Lacnjevac C, Rajic Z (2010) Fast fourier transform IR characterization of epoxy GY systems crosslinked with aliphatic and cycloaliphatic EH polyamine adducts

Chapter 10
Restoration and Research of Ilya Repin's Painting "Ivan the Terrible and His Son Ivan on November 16, 1581" in State Tretyakov Gallery

Yulia Dyakonova and Kirill Shumikhin

Abstract This paper describes the research of iconic painting by Ilya Repin "Ivan the Terrible and his son Ivan on November 16, 1581" from the collection of State Tretyakov gallery, damaged in a vandal attack on May 25th, 2018. The painting had a complicated story since its creation including the fact that in 1913 it was cut by a vandal's knife. Extended technical study took place right after the accident and aimed at the evaluation of the painting condition and artistic materials. Significant part of this research is dedicated to the issue of paint layer flaking and it's reasons. This problem was observed and remained a topic for the regular conservation procedures since 1913. This research was carried out by museum laboratory and included the use of panoramic X-ray scanning, UV-Vis-IR photography, polarized light microscopy, micro-XRF, and FTIR and Raman spectroscopy. Second part of the paper touches upon a number of studies, which were held in support of the conservation process. These include a study of conservation materials used by previous generations of conservators, evaluation of various methods for the removal of lining glue, and tests of selected number of modern consolidation materials. It was performed in collaboration with Moscow Institute of Physics and Technology, Federal Research Center for Chemical Physics and Federal Research Centre "Fundamentals of Biotechnology" of the Russian Academy of Sciences. This lecture illustrates a sequence of methods and the achieved results of the work that took place over the span of 3 years together with and in the purpose of restoration.

Keywords Technical studies in museum · Artistic materials · Vandal attack · State Tretyakov Gallery · Painting condition examination

Y. Dyakonova · K. Shumikhin (✉)
Advanced Research Department, State Tretyakov Gallery, 10 Lavrushinsky lane, Moscow 119017, Russia
e-mail: shumikhinkv@gmail.com

Y. Dyakonova
e-mail: yulia.dyakonova@gmail.com

10.1   Historical Background and the Events of 2018

10.1.1   History of the Painting

One of the most famous and outstanding paintings by Ilya Repin "Ivan the Terrible and his son Ivan on November 16th, 1581" from the collection of Tretyakov gallery was attacked by vandal on May the 25th, 2018. In the last hours before the gallery closed, one of the visitors unexpectedly grabbed a metal fence post and hit the picture three times. Central part of the image depicting Prince Ivan was damaged. This broke the protective glass and tore canvas in three places. The paint layer in this area suffered severe damage (Fig. 10.1).

Picture was painted by Repin in 1885 and at the time caused conflicting opinions of critics and visitors alike, starting from its first display at the 13th exhibition of the Society for Travelling Art Exhibitions. The painting depicts one of the most tragic episodes of Russian history-ruler's killing of his son in fit of uncontrollable anger. It touches upon the problems of power, violence, dark spots of the history, and the evaluation of its key figures. The painting attracted and frightened visitors and inevitably made a strong impression on the audience. It was even banned from the display for several months by censors. When the ban was lifted, for a long time it was forbidden to photograph the painting and distribute pictures [1].

The tragic coincidence with the events of 2018 is that almost a hundred years ago, the painting had already been attacked. In 1913, a visitor stabbed the painting with a knife. He made three vertical cuts on the images of the faces of Ivan the Terrible and the Prince. Fortunately, the knife was stopped by the stretcher bar, otherwise,

Fig. 10.1   Ilya Repin. "Ivan the Terrible and his son Ivan the 16th of November 1581". 1885. Oil on canvas. 199.5 × 254
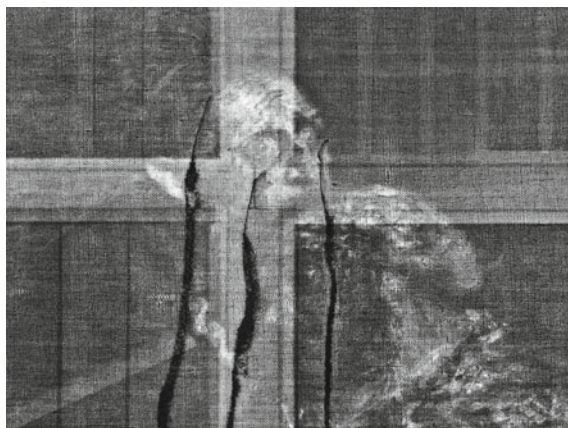
Fig. 10.2 Traces of knife cuts, left from the attack in 1913. XR image

the damage could have been more extreme. Traces left by the knife cuts may still be observed using x-ray imaging as seen on Fig. 10.2.

In 1913, the painting was restored by Dmitry Bogoslovsky, a prominent expert who worked for the Russian Museum in Saint-Petersburg, the Hermitage and other museums, and his colleague Ivan Vasiliev. The restoration was done in a month and a half. The progress of the restoration was covered in the press in 1913. «The canvas was removed from the stretcher and stretched on large sheets of paper on the floor… The stitches of the cuts will then be covered with a special mixture, on top of which the author himself will overpaint the damaged places» [2]. «…The painting was lined to a new canvas and stretched on a specially ordered frame with shields… The whole process of lining went very favorably. Now it will take a few days for canvas to dry, and then Repin will apply fresh paint» [3]. «The restoration can be considered a success…There were only gaps where the paint had fallen off from the force of the blow. Repin specially came from Kuokkala, Finland to restore the picture» [4]. Instead of restoring the lost pieces the artist completely re-painted the head of the Tsar. Difference between the re-painted part and the rest of the picture was obvious. After the artist had left the gallery Igor Grabar, head of Tretyakov gallery at that time, who was also a restorer, removed the new parts Repin had painted and instead toned the damaged areas with watercolor, then covering them with varnish. A few months later, Repin visited the Tretyakov gallery again, but did not notice the changes made by Grabar [5].

In the difficult post-war year of 1922, the painting condition suffered strongly again in as much the heating system of the gallery was out of service while autumn rains occurred. It was reported to have caused a spike in humidity in the halls of the gallery. The painting at the time was displayed in a frame under glass and the back side was closed with a wooden shield.

From the mid-1920s to the present day, the painting displayed local paint flaking in certain areas, so regular observations on the condition of the painting have been

conducted [6]. In 1920's, around a dozen spots were documented to have displayed paint flaking. In 1939 that number was already around 730 [7]. The issue of paint and ground layer bind became a "chronic disease" for the painting and the flaking of the paint layer could be observed till before the attack of 2018. Its mechanism and reasons are discussed in this paper.

10.1.2 Condition of the Painting After the Attack in 2018

During the attack in 2018, picture withstood heavy damage. Original and lining canvases were broken in three places: the upper tear in the image of the Prince's clothes over the hand of Ivan the Terrible—13.5 × 5 cm; the branched tear in the image of the Prince's clothes under the hand of Ivan the Terrible—24 × 8 cm long; and the tear in the image of the Prince's clothes on the thigh—11 × 5 cm long. Wooden shield mounted behind the painting prevented much of the damage and softened the impact, results of which may be seen on Fig. 10.3. There are numerous scratches on the paint layer from the broken glass. Peeling and flaking are observed on the paint layer. The image is covered with different craquelure patterns: hard and drying craquelure, signs of matter protruding to the surface are seen (salts of fatty acids). A similar type of craquelure is also observed in other works of Repin and appears to be common to many paintings of other painters of the late nineteenth century.

Fig. 10.3 Impact marks of damages made by the metal fence post

Example of the paint flaking which was mentioned before may be seen in Fig. 10.4. According to the photographs made during previous preventive conservation and the results of micro-photography taken in 2018, the flaking is localized along the perimeter of the image, in areas with smooth relief on the background—where the artist assumingly worked in many layers, but with a more liquid consistency of paints.

10.2 The Pre-restoration Research

10.2.1 Goals and Approaches

Considering a complicated history of the painting aim of the research was to provide necessary support for the restoration and conservation program. Following goals were set:

- Detailed investigation of canvas, ground, paint layer, and varnish contents and properties in comparison with the artistic materials and their condition in the other works by Repin;
- Detection and analysis of the factors that might have caused the "chronic" disease of the picture associated with the paint layer flaking so that to predict their possible influence on the restoration process;
- Archival search of documents related to previous restorations and condition reports;
- Cross analysis of obtained data.

In a fortunate turn of events during this work, preparations for the Repin exhibition were under way which allowed us to obtain additional data for comparison from eight other pieces by Repin dated around the same time period as "Ivan the Terrible and his son Ivan the 16th of November 1581".

Following methods were used for the examination:

- Photography of the painting;
- Micro and macro photography of the painting layer;
- Reflected UV and IR photography;
- Full surface X-ray scan (87 scans total) with panoramic picture stitching;
- Microscopy examination.

In order to study the canvas, ground, and paint layer contents following methods were used:

- XRF of the painting surface using Artax by Bruker. A total of 70 spots were analyzed. Measurement conditions—voltage of 50 kV and measurement time of 60 s. Measurements were conducted in air atmosphere.
- ATR-FTIR analysis using Lumos by Bruker. Measurement conditions—resolution of 4 cm^{-1}, 100 total scans, and measurement time of ~ 2 min.
- Raman spectroscopy of ground and paint layer samples using Nicolet iS50 FTIR spectrometer with Raman module by Thermo Scientific. Measurement conditions—voltage of 0.15 mV, resolution of 8 cm^{-1}, 100 total scans, and measurement time of ~ 2 min.
- Polarized light microscopy using Olympus BX43 with total magnification 400x, equipped with polarization plates and lambda plate.

10.2.2   Examination Results

Canvas Original canvas is a two-thread plain weave canvas with thread density of 7 × 7 threads per cm^2. Many open areas show signs of stiffness and are in fact covered with lining glue used in 1913. Examination of separate fibers using polarized light microscopy using modified Herzog method showed that original canvas is comprised of a mixture of flax and jute, where the former is the primary component. Lining canvas was found to be a plain weave canvas with thread density of 15 × 15 threads per cm^2. Its content was revealed to be the same as original canvas.

Lining glue contents were examined using ATR-FTIR. A mix of animal glue with carbohydrate was found—latter was potentially present in a form of honey. It was further confirmed during the relining process when a strong sweet odor was noted. Lining glue, according to conservation documents, is present in the form of isinglass—a type of glue prevalent in Russian conservation history.

Ground Preliminary microscopy examination showed that artist used a commercially primed canvas with white presumably oil-based ground. The layer is very dense and strong and shows little damage even in the areas of rupture. Some areas where ground layer may be observed showed an irregularity in the color tone as may be seen in Fig. 10.5. This layer is lying directly on top of the ground and in some cases seeps into it. Content and purpose of said layer are not completely understood. Due to its

Fig. 10.5 Imprimatura layer found in areas with naked ground
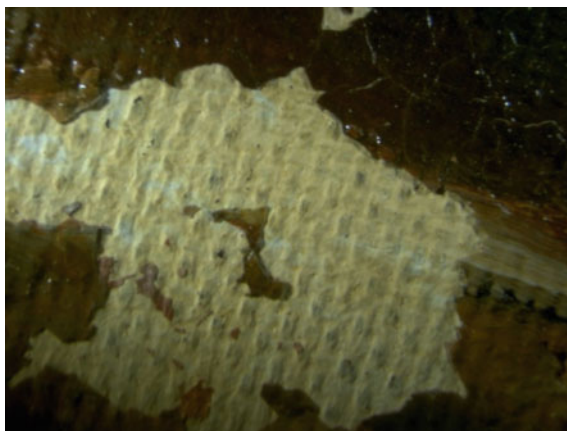
irregularity and color, we believe it serves as imprimatura to tone the underlying ground in compliance with the coloristic theme of the scene.

Cross analysis using XRF, ATR-FTIR, and raman spectroscopy helped establish the content of the ground. It comprises of oil, lead white pigment, and calcite. Presence of fatty acid salts was also observed on IR-spectra which can be attributed to the presence of lead white pigment. Analysis of separate imprimatura particle was near impossible so two particles of ground were compared-with and without imprimatura. Besides the usual ground components-oil, kaolinite filler, and iron presence were discovered which lead us to believe that an earth-based pigment was used for the toning.

With the purpose of comparison, eight other paintings of Repin created during the same time period were examined. It was established that he primarily used white-colored factory-made oil-based grounds including the same components—oil, lead white pigment, and calcite. In some cases, presence of zinc white and kaolinite was observed.

Paint layer Pigment composition was examined using noninvasive method of XRF. Results are presented in Table 10.1. Comparison to other Repin paintings helped establish that materials encountered in this painting not only were abundantly used in the time period of painting's creation but also were favored by author and observed in many of his other works.

Additionally, a number of paint layer samples were taken in order to investigate binding material and additives. Oil was found to be the primary binding media, in many cases presence of fatty acid salts was observed. We believe lead and zinc pigments, in particular lead white and zinc white, are the cause of that. Their presence may also be observed with the naked eye on the surface of the painting—a web of dry craquelure with white material protruding to the surface as can be seen on Fig. 10.6. Results of the comparison show that Repin used a stable list of materials which he was used to and understood their characteristics.

Table 10.1 Artistic materials were discovered in the painting using XRF, ATR-FTIR, and Raman-spectroscopy methods

Color	Content
White	Oil, lead white, zinc white, barium sulfate
Blue	Oil, blue cobalt, Prussian blue
Red	Oil, resin, cinnabar, red ochre, red organic pigment
Yellow	Oil, zinc yellow
Brown	Oil, brown ochre with manganese traces
Green	Oil, green chrome pigment, green copper pigment
Black	Oil, black iron pigment
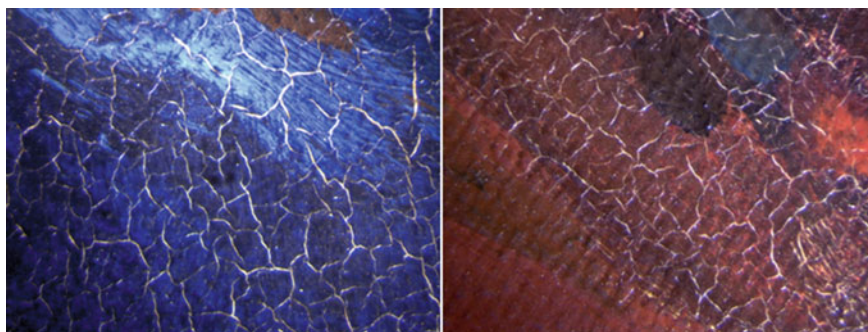
Fig. 10.6 Dry craquelure with white material protrusions

Other than that the surface of the painting is speckled with aforementioned paint layer losses. Microscopy examination conducted during the research revealed numerous paint layer losses most of which are attributed not to the damage from the assault but to the "chronic disease" of the painting.

10.2.3 Discussion and Theories on Weak Adhesion Between Ground and Paint Layers

Results of the research confirm an established opinion that Repin showed great care and thoroughness in his choice of artistic materials. Despite the frequent reproaches of contemporaries in the decline of the craft encountered in the literature, the artistic practice of the late nineteenth century had all the opportunities and extensive experience in creating stable combination of all its components. In this sense, the craft of the painting, the selection of used artistic materials (the type of the canvas, the type of ground, the binding materials of the ground, the pigments) does not show any deviations from the standards of practice attributed to that time. It goes to show that a matter of artist's technique cannot be considered a reason for the problem at hand.

A number of different factors could be attributed to the development of paint layer flaking. One of them is the difference in density of original and lining canvases which could lead to different strain vectors impacting the paint layers. Dense thick layer of animal glue used both for lining of the lining canvas and the sizing of the original canvas also plays a part in that. Another factor is related to the fatty acid salts formation, which was discovered in ground and paint layers. We discovered that in the case of "Ivan the Terrible" fatty acid salts manifest in form of the dry craquelure formation with white mass protrusions and in deposits in paint and ground layers. Many articles report a risk behind that which ultimately may result in catastrophic damages to the adhesion between ground and paint layers [8, 9]. Next, starting at the beginning of the twentieth century a number of books on painting technique reported oil ground to be a doubtful choice due to accidents of paint layer peeling off the ground over time, so the oil ground choice in combination with oil painting technique could have played a part [10–13]. In this case, however, it was also observed that a choice of oil ground persisted in Repin's art and every selected picture demonstrated a stable and satisfactory condition with no paint flaking.

Aforementioned spike of humidity in gallery halls can be considered to have had a substantial impact on the flaking issue. It was reported that in 1922 during the reinstallation of the painting the glass was removed and some powder on the surface was discovered [6]. The paint layer in that area immediately showed signs of flaking. Soon after these events, first cases of paint layer flaking were reported.

Having put those events and details in perspective we believe it was a sum of several various details, which combined into such an issue, rather than a single reason. It was thanks to the complex approach to studying the painting that we were able to uncover those details. One piece of information compliments another—so the detailed examination of documents helped us analyze results of thorough technical study and meticulous study of the picture under the microscope shown actual proof to the theories we had. Actual trigger that set off the development of those factors in our understanding was the humidity spike in 1922.

Understanding the issue of paint layer flaking was very important for the conservation program. It allowed us better judgment on how it could influence or be influenced by different conservation procedures.

10.3   Further Conservation Procedures and Additional Applied Investigations

Work on this paper began two years ago and presentation was postponed due to COVID regulations. During that time conservation program made a significant step forward. Many conservation steps were made and additional applied research conducted. Considering that, we find it important to describe selected significant stages of this process—they will be described in no particular order.

10.3.1 Relining and Sizing Layer Removal

During the conservation process, one of the major points was the removal of lining canvas which was applied almost a hundred years ago. It was then that the presence of a thick brittle layer of lining glue between the original and lining canvases was discovered. That inevitably posed a danger to the picture. Lining process was a widely accepted practice back in 1913, but its consequences can now be observed. The glue layer was very hard and, attached to the canvas, severely limited the natural fluctuations of the fabric. Not only that but due to its thickness and content which was found to be animal glue (presumably isinglass) and honey, it also added two other possible issues—a significant weight on the canvas and risk of biological damage due to the mixture of glue and honey.

Considering intricate state of the paint layer, approach toward the glue removal required non-standard solutions. Isinglass is known for its sensitivity to moisture which can lead to consecutive compression of the canvas and damage the painting layer. This severely limited available options to those which excluded any presence of water. Not only that but since the glue already seeped into the canvas it became a part of the painting, so its complete removal was not an option as it could potentially damage the adhesion between layers. Conservation department of Tretyakov gallery began the search for an appropriate solution, whereas new project also took place—investigation into the use of laser for glue layer removal. Special models of canvas with animal glue sizing were used in order to evaluate the possibility of pulse laser application for the removal of the sizing without damaging the threads of the canvas. Investigation was conducted by Federal Research Center for Chemical Physics of the Russian Academy of Sciences. Figure 10.7 presents results of a canvas surface treated with pulse laser. Results showed that it is effective in the removal of sizing layer; however, a level of its impact and control was still a matter of further investigation.

Fig. 10.7 Sized canvas treated by pulse laser
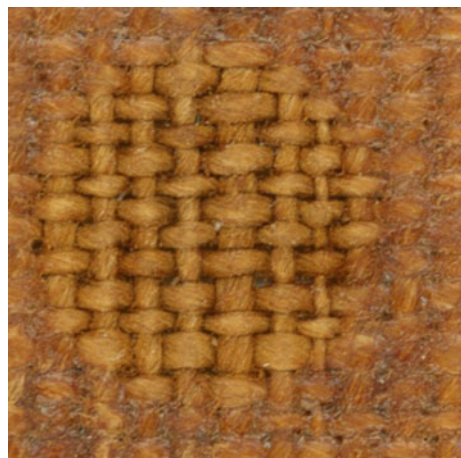
10.3.2   Selection of Paint Layer Consolidation Materials and Applied Research for Comparison

Another in-depth study was conducted on a number of consolidation materials with the goal of examining and comparing their properties. Tests included both historical materials and modern adhesives. Investigation was conducted by two institutions independently of each other-Moscow Institute of Physics and Technology and State Research Institute for Restoration in Russia.

Aim of the study was comparison in direct application and material behavior over time. Conservation adhesives were also required to display inert behavior. It was due to many different restoration materials which were used throughout the last hundred years and can be encountered on the surface of the painting. This research would allow us better ground for prediction of long-term consequences. Test models were subjected to natural aging process with control points at 6 days, 30 days, and 44 days. For comparison purposes, a different set of same models were subjected to artificial aging-samples were held in a weather chamber under conditions of 60 °C and ~ 95% relative humidity for 12 days. Changes of chemical composition, optical properties, fragility of the layer, tendency toward cracking, and adhesive properties were evaluated. As a result, it was found that in every test, synthetic adhesives proved to be superior to regular organic adhesives common to conservation procedures in different areas. This research provided crucial data that was used as a fundament in choice of adhesives for paint layer consolidation. Based on the results, Paraloid B-72 and Plexisol P550-40 showed significantly superior qualities not only in the direct apply but also in long-term effects and changes in their qualities and stability.

Additionally, a detailed research on the same objects for the estimation of susceptibility of adhesives to different biological damage was held by Federal Research Centre "Fundamentals of Biotechnology" of the Russian Academy of Sciences. It demonstrated how susceptible traditional materials were to biological damage. Modern synthetic adhesives the tests on the contrary showed high resistance of the test models to bacteria and fungi which may be encountered in the strict conditions of exposition halls.

10.3.3   Varnish Layer Examination and Thinning Procedures

One of the main parts of the work before considering restoration approaches included study of the archives and previous restoration protocols for the painting. It was important to understand how previous generations of conservators worked and which exact procedures took place. Information on used materials was crucial in planning further restoration operations as it would help predict behavior of the painting surface in different areas.

This helped uncover that for the last hundred years conservators mostly stuck to adding new layers of adhesives and varnish without significantly touching upon

the layers added by previous conservators. This piece of information proved crucial for the restoration of the picture. Specialists of conservation department of State Tretyakov gallery believed that this approach could potentially lead to more harm than good as it would result in an extremely thick layer of varnish which adds extra weight and tension on the picture and only further aggravates the issue of ground–paint layer adhesion.

For the purpose of studying the varnish layers, several samples were taken for preparation of cross section. As a medium for cross sections, Technovit 2000 LC resin was used. Prepared cross sections were examined using light microscope with reflected light equipped with UV filter which helped discern varnish layers and the borders between them.

Captured photographs of the cross-section samples proved the aforementioned documents which spoke about the many varnish layers and the conservation strategy employed by conservators before. In Fig. 10.8, we can clearly see three varnish layers differing in their thickness. In between the second and third, one a thin layer with blue pigment particles is observed. Specialists of conservation department were able to recover the materials used in previous conservation treatments of the painting. Among those was a stick of wax-resin mastic which was described in documents as an adhesive material used for local paint layer consolidation. Its optical properties when viewed under the polarized light microscope are identical to the layer observed in this cross-section.

Another prepared cross-section sample is presented in Fig. 10.9. It gave us a unique glance into the structure of the painting with all the numerous layers of previous conservation treatment materials. On the image, we can clearly see how on top of the damaged paint layer an assumingly delaminated paint layer particle is placed and incased in the resinous layer. Layers above present, as we consider, overpaint which was delivered later on. Finally, the varnish layers on top actually show presence of two different layers, which were observed under higher magnification.
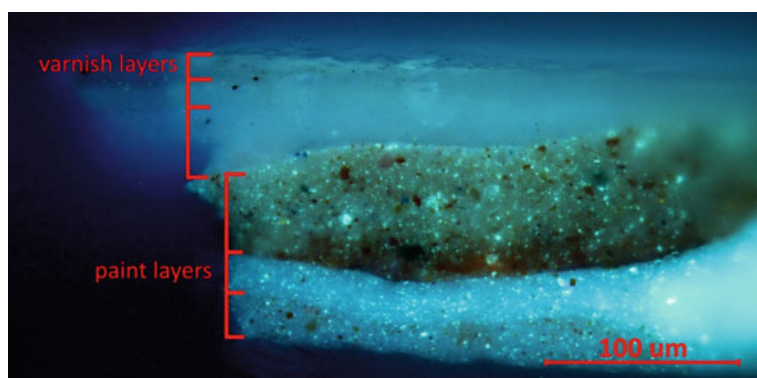
Fig. 10.8 Cross-section sample of varnish with paint layers
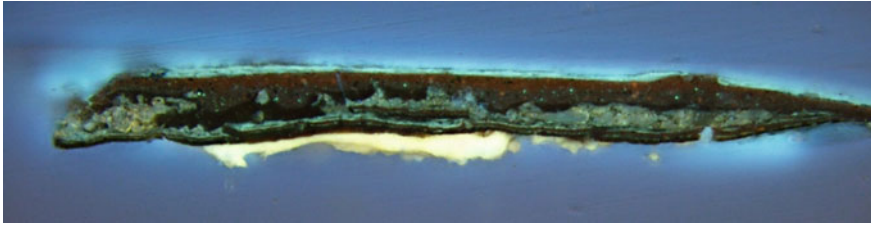
Fig. 10.9 Cross-section sample of varnish with paint layers and sings of previous restoration

Thickness of varnish layers based on several cross-sections was found to vary highly depending on the surface of the paint layer. It ranges from 2 to 20 microns for individual layers. In some cross-section samples, total thickness of several varnish layers goes up to 44–50 μm.

Soon after this study, it was decided to conduct varnish layer thinning. Not only did it ease the strain on the painting but it also significantly restored the color of the painting.

10.4   Conclusions

In the span of these four years, a difficult and thorough work took place in order to restore the painting back to its original state. Conservation program was shaped by the staff of the gallery and included consultation with leading specialists from both Russia and Europe. Each successive step in restoration and research was taken with "do no harm" mindset. Tasks were performed by specialists not only from different departments of State Tretyakov gallery but also other institutions. We believe paint layer flaking is connected to various reasons-from combination of materials to their behavior-and was set in motion by the humidity spike in 1922.

It is our hope for our colleagues to prepare more detailed papers on the other parts of this project-specifically concerning restoration process, as it would present an invaluable experience of complex projects conducted on museum grounds.

References

1. Churak G (2019) Ivan the Terrible and his son Ivan the 16th of November 1581. Tretyakov Gallery, Moscow, p 50
2. Peterburg sheet 13th February 1913
3. Evening Time 15th February 1913
4. Russian Word 20th February 1913
5. Grabar I (1963) Repin. USSR Academy of Sciences Publishing, Moscow, p 271
6. Typescript of State commission session on issue of condition report and conservation of "Ivan the Terrible and his son Ivan" by Repin, "Boyarynya Morozova" by Surikov, "Bogatyrs"

by Vasnetsov, "Over Eternal Quiet" by Levitan 1982 (USSR Academy of arts, Unpublished typescript) p 3

7. Kudryavtsev E (2002) Painting restoration techniques. V.Shevchuk Publishing, Moscow, pp 41–42
8. Shimazu Y, Keune K, Boon J, Townsend JH, Berg K-J (2008) In: Bridgland J (ed) 15th Triennial conferences New Delhi: 22–26 September 2008: preprints, vol 2. Allied Publishers Pvt. Ltd., New Dehli, pp 626–632
9. Keune K (2005) Binding medium, pigments and metal soaps characterized and localized in paint cross-sections. AMOLF, Amsterdam, pp 114–115
10. Rerberg F (1932) Painter about paints. Fine Arts Publishing, Moscow-Leningrad, p 135
11. Kiplik D (1947) Painting technique. Art Publishing, Moscow-Leningrad, pp 185–187
12. Doerner M (1984) The materials of the artist and their use in painting, with notes on the techniques of the old masters. Harcourt Brace Jovanovich, San Diego, p 28
13. Hill Stoner J, Rushfield R (2012) Conservation of easel paintings. Routledge, London-New York, pp 176–182

Chapter 11
Mapping Cadmium-Based Pigments Using Multispectral Imaging Techniques. A Case Study on Mrs. Ševa Ristić by Petar Dobrović

Marina Djuric, Zoran Velikic, and Vanja Jovanovic

Abstract A project of opening the legacy of a famous Serbian painter Petar Dobrović (1890–1942) consisted of a scientific research related to the collection of his paintings, where pigments were analysed using non-destructive imaging techniques. Petar Dobrović was a versatile person, who was engaged in politics, as well as a chronicler of his time, and a proponent of Serbian colourists. His painting is characterized by the intensiveness of colour and strong, impulsive drawing. The painter used a very complex mixture of pigments which resulted, along with the contribution of binder filtering, in a much colourful photograph of UV induced fluorescence that suggests using different yellow pigments; however, the application of green light induced fluorescence in NIR, thus clearly indicating the presence of cadmium pigments in yellow and other paints, and each brush stroke as well. In this paper, we present an application of multispectral imaging techniques complemented with reflectance and fluorescence spectroscopy in order to separate and map cadmium pigments in paints on the painting "Mrs. Ševa Ristić" by P. Dobrović. Multispectral images include reflectance and fluorescence images in a visible and infrared region with filters on 720 nm, 850 nm, and 940 nm. The fluorescence was induced with UV (365 nm LED), blue laser (405 nm), and green (520 nm LED) light. Reflectance (FORS) and fluorescence spectra performed in the selected points in the painting and in several samples of commercial cadmium oil paints verify the presence of cadmium pigments. This application mainly confirms the effectiveness and usefulness of special multispectral fluorescence imaging in NIR domain for locating and mapping cadmium pigments in paints presented in many researches. The excitation with visible green light minimized the contribution of other colours and binders on fluorescence and distinguished different cadmium based pigments.

Keywords Cadmium · Fluorescence · Multispectral

M. Djuric (✉) · V. Jovanovic
ArtLab, Bulevar Kralja Aleksandra 391, Belgrade, Serbia
e-mail: marina@ipb.ac.rs

Z. Velikic
Institute of Physics, Pregrevica 118, Belgrade, Serbia

11.1 Introduction

Petar Dobrović was a Serbian painter, political figure, and art critic. He is almost exclusively noted for his landscapes and portraits. His formative years as a painter are marked with impressionist and cubist influences. In 1937, Dobrović became one of the founders of the Academy of Fine Arts of Belgrade, thus imposing himself as a reference figure of the Yugoslavian painting until his death in 1942. The most notable examples of his rich artistic production are a series of portraits dedicated to artists and intellectuals, like the portrait of Mrs. Ševa Ristić, the wife of a prominent leader of the Surrealist movement in Belgrade, as well as a series of landscapes endowed with ecstatic colour sensitivity.

In the frame of the project related to opening the legacy of Petar Dobrović, along with the scientific research, the painting "Mrs. Ševa Ristić" (1930), rich in different yellow colours, was selected for the analyses of cadmium-based pigments (Fig. 11.2).

The aim of this research is to explore the possibility of using affordable and inexpensive tools that can achieve high-resolution images of fluorescence, important for diagnostics and conservation purposes. Fluorescence, as an analytical tool, especially for cadmium-based pigments, is subject of a number of researches. It could differentiate between materials with similar optical properties yet different chemical compositions. Many factors affecting fluorescence properties were described in researches: crystalline composition, alteration process, different production processes, and manufacturers; thus, it is difficult to establish fluorescence as a unique diagnostic method, especially when broadband UV excitation is used [1].

Low intensity of fluorescence emission [2] requires very sensitive cameras. High-sensitive cameras usually provide low resolution of images, which is the main disadvantage of the existing techniques. However, fluorescence is a unique "imprint" of the material, and visually easy to read, and therefore still attractive as an analytical tool.

11.2 Materials and Methods

11.2.1 Material

Materials chosen for this research are cadmium-based pigments on the painting "Mrs. Ševa Ristić"due to their remarkable, specific fluorescence and fluorescence in NIR domain.

Research material for comparative purposes includes samples of commercial paints and their mixture with Zn white. The commercial paints are cadmium yellow (0012) and cadmium red (0018) in linseed oil produced by Umton.

The fluorescence of Cd–based pigment is characterized by band edge emission in visible region, as well as emission in red to near-infrared associated with trap state due to impurity and crystal defect [1]. The value described in literature for band

gap energies ranges from 2.63 eV (472 nm) for Zn-rich yellow pigment to 2.32 eV (534 nm) for cubic CdS, and between 680–760 and 880–1000 nm, respectively, assigned to deep level emission [3].

11.2.2   Methods

Imaging techniques applied on the painting and commercial samples include recording reflectance images and fluorescence images in visible (VIS) and near-infrared region (NIR). Images in visible region were recorded with Nikon D7000 camera; images in NIR region were recorded with IR converted Samsung S1050 camera. Light source for reflectance images of the painting and commercial samples was the halogen lamp 400 W HQHR7SJ118003.

Fluorescence was induced with two excitation sources: homemade UV light source (2pcs of 5 W Ultra Violet LG3535 LED 365 nm 60°) and homemade green light source (nine green LED 3 W 520 nm), whose characteristics are depicted in Fig. 11.1. Fluorescence induced with green light (VIF) was recorded using long-pass filters IR720, IR850, and IR1000. Filter characteristics are presented in Fig. 11.1.

LED light source was selected because of its monochromatic, very intensive light. Long-pass filters transmit a large amount of light and it is possible to record low intensive fluorescence in NIR domain with high resolution. Two sources of excitation were used in order to compare the induced emission and influence of surrounding fluorescent binder.

All images were recorded under the same conditions: light sources were at 45° from the normal, approximately 2 m from the painting; camera was set at approximately 1 m from the painting. Fluorescence images were recorded in a dark room with a negligible amount of stray light. Calibration of Samsung camera was performed using luminance standard LS-6 Spectra (60 cd/m^2, $T = 2856$ K). Comparing the
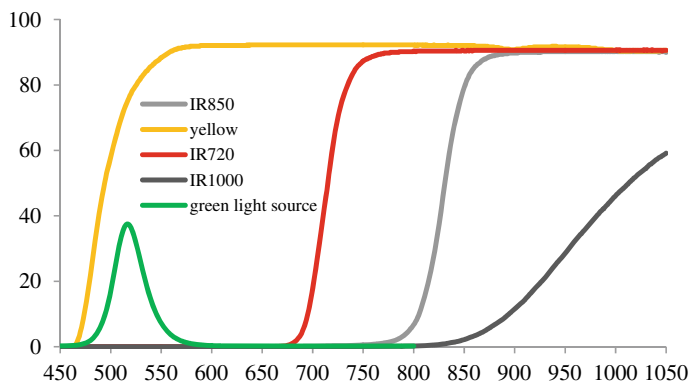
Fig. 11.1 Spectra of transparency of using filters and green light source

Fig. 11.2 "Mrs. Ševa
Ristić", VIS
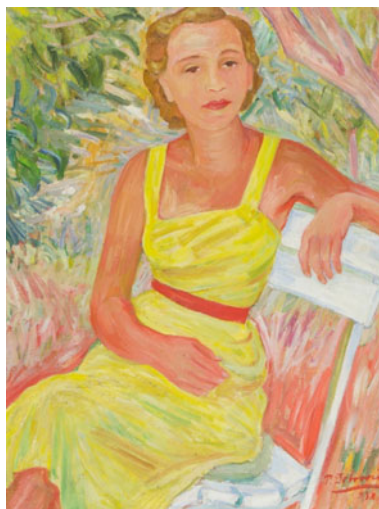
intensity of recorded photographs of luminance standard with the spectra of black
body (Table 11.1), concerning different filters, and the calculation of correction factor,
was executed and presented in Table 11.2.

Reflectance and fluorescence spectroscopy were performed as complement analyses. The spectra were recorded in selected points in the painting and samples of
commercial paints with Avantes Avaspec 2048-USB2-VA spectrometer range 350–
1100 nm, resolution 8 nm, calibrated with standard lamp Wi41/G OSRAM and with
a yellow filter. For the excitation source, blue laser 405 nm, 5.6 mW spot 1 mm, was
utilized.

Table 11.1 Spectra of black body at 2856 K

$\Delta\lambda$ (nm)	Integral area (arbitrary unit)	ratio (B)
720–1050	5230.747	1.000
850–1050	3371.908	1.551
950–1050	1724.753	3.033

Table 11.2 Calculation of correction factor

Filters	Intensity (arbitrary unit)	Ratio (A)	Correction factor ($C = A/B$)
IR720	220	1.00	1.000
IR850	106	2.08	1.338
IR1000	15	14.67	4.836

11.3 Result and Discussion

Visual examination of the painting (Fig. 11.2) confirms the use of different yellow pigments in paints. The yellow paints are vibrant with no evidence of fading, discoloration, or other manifestation of alteration phenomena and degradation process [4].

The image of UV induced fluorescence (UVF) of the painting "Mrs. Ševa Ristić" in VIS (UVF → VIS) was so colourful and it indicated the use of more than two yellow and red pigments, making each brush stroke visible as well (Fig. 11.3). Orange fluorescence of yellow pigments suggested the presence of cadmium-based pigment in some yellow paints, although Kubelka–Munk correction was not performed [5]. It was described and discussed in the analysis of the painting "Self portrait " by Igor Vasiljev [6], dating from the similar time period.

The image of fluorescence in NIR was performed in order to confirm the presence of Cd-based pigment in some yellow paints, knowing that only few pigments have these characteristics [7].

Photographs of a detail from the painting recorded using different imaging techniques are present in Fig. 11.4. It should be noticed that the painter used at least two different yellow pigments regarding the emission in NIR domain: one based on the cadmium pigment, and the other without cadmium pigment. Besides that, comparing the images recorded in NIR domain induced with different light sources, we could distinguish different layers of paint. The image in Fig. 11.4d illustrates the emission from deeper layers of paints. Furthermore, discreet emission from the area containing red pigment was noted, suggesting that green light excitation is more effective concerning the Cd-based red pigment. Since both images in NIR are recorded using the IR850 filter, the contribution of emission from paints containing

Fig. 11.3 "Mrs. Ševa Ristić", UVF → VIS
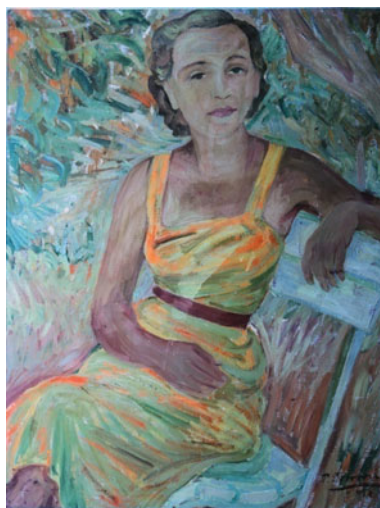
Cd red pigment could explain the larger emission area in Fig. 11.4d. White pigments, binders, and most of the painting's pigments have emission under 700 nm.

Images of green light induced fluorescence recorded with three different filters (Fig. 11.5) are produced with the correction factor applied. Images in Fig. 11.5b, c are modified: brightness is increased 2 and 4 times, respectively, in order to improve detail visibility. Changes of emission intensity of yellow and red pigments related to the filters used are obvious. Emission intensity of yellow pigments decreases more rapidly than of red pigments, and emission from red pigments becomes more intensive than yellow, as we can observe in Fig. 11.5c. Concerning the fact that fluorescence of red pigments is noted only in NIR domain, it also suggests Cd–based red pigment. The areas of different concentrations of cadmium can be noted on the presented images because mixing with other colours weakens the fluorescence intensity of cadmium pigment. Image recorded with the IR720 filter (Fig. 11.5a) show fluorescence from white pigment (probably Zn white) as well as cadmium based pigments. Emission from white pigment significantly decreases at longer wavelength, while in images recorded with IR850 and IR1000 filters it cannot be observed. In these images, only fluorescence from cadmium-based pigments is present.

Fig. 11.4 Detail from the painting in different techniques **a** VIS, **b** UVF → VIS, **c** UVF → NIR, and **d** VIF → NIR
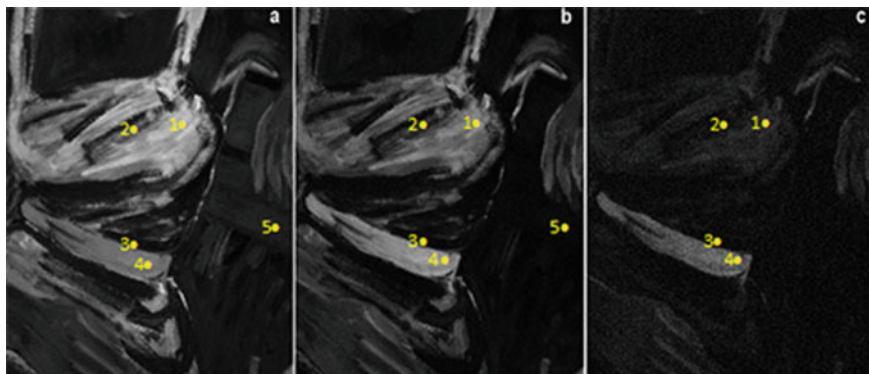
Fig. 11.5 Green light induced fluorescence with different filters **a** IR720, **b** IR850, and **c** IR1000

Spectroscopic analyses in selected points are marked in Fig. 11.5. These were performed in order to complete the previous research and are presented in Fig. 11.6.

Acquired spectra also confirmed the presence of different yellow pigments. The higher intensity is detected for the spectra of yellow paint at the point 1 with the emission peak at 750 nm; in images UVF → VIS (Fig. 11.4b) this is recorded as orange fluorescence. The shape of these spectra (wide in the range from 620 to 850 nm) explains the orange colour of emission in the visible region. On these spectra, we can also view that the value of NBE [3] is 510 nm, thus the approximate value of inflection point was obtained from the first derivate of reflectance curve at 492 nm. This characteristic corresponds to hex-CdS by Aldrich described in the research of Rosi et al. [3]. Much better match of characteristics was with the sample of historical pigments marked as 7914 in the same article with an inflection point at 510 and the calculated band gap 490 nm.
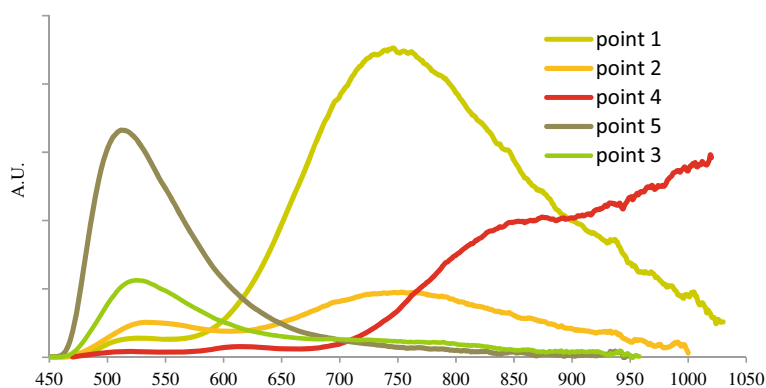
Fig. 11.6 Spectra of fluorescence in selected points marked in Fig. 11.5

Spectrum at point 2 (Fig. 11.5) has the similar shape as spectrum at point 1, though it has less intensity. The NBE value shifts to 525 nm. Both suggest the mixture of Cd-based pigments with white pigment: the influence of Zn white in mixture significantly decreases the intensity of fluorescence.

Spectrum recorded at point 3 did not peak in NIR, which can is depicted in the recorded image in NIR (Fig. 11.5c, d), confirming the presence of yellow pigments without cadmium.

Spectrum at point 4 has two peaks at wavelength 850 nm and over 1050 nm, which corresponds well with the image in Fig. 11.5c, indicating Cd-based red pigment. Spectrum of white paint at point 5 confirms fluorescence (visible in Fig. 11.5a) recorded with the IR720 filter.

Part of the recorded spectra is presented in Fig. 11.7 in order to identify NBE peaks of the observed pigments. The NBE peak position at 510 nm for spectrum recorded in point 1 is consistent with data from literature for hexagonal CdS pigments [3]. Likewise, peaks positions of spectra at points 2 and 3 are shifted to longer wavelengths, thus illustrating the influence of white pigment in mixture and binder. The comparison of the recorded spectra and images of fluorescence confirms the calculated correction factor presented in Table 11.2. In tables below, one can observe the ratio of emission intensity for red and yellow pigments calculated from photographs in Fig. 11.5 (Table 11.3), as well as the ratio of emission intensity for red and yellow pigments calculated from spectra in the selected points (Table 11.4).
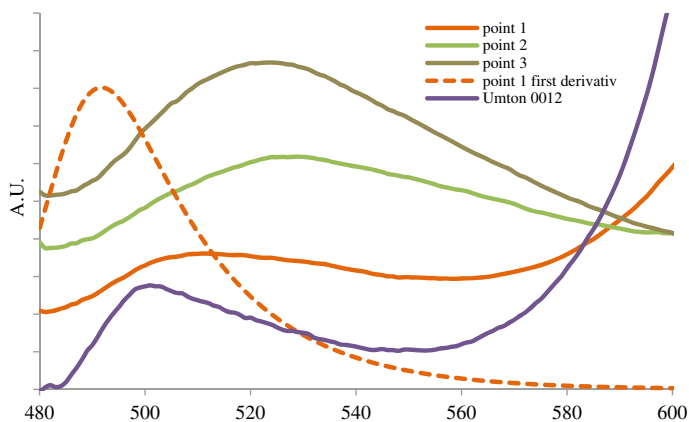
Fig. 11.7 Spectra of fluorescence in the selected points marked in Fig. 11.5

Table 11.3 Emission intensity for images in Fig. 11.5

Filters	Yellow (point 1)	Red (point 4)	Ratio red/yellow
IR720	100.00	67.03	0.67
IR850	47.03	57.30	1.22
IR950	9.73	25.51	2.62

Table 11.4 Integral area from spectra in Fig. 11.6

Integral area	Yellow (point 1)	Red (point 4)	Ratio red/yellow
720–1040	100.00	69.49	0.69
850–1040	35.26	49.67	1.41
950–1040	9.18	23.43	2.55

We can observe that the presented calculation illustrates a very good agreement between recorded images and spectra in spite of using different excitation sources, suggesting that the images of fluorescence in NIR region could provide objective information of fluorescence intensity of cadmium-based pigments.

Identical techniques were applied on commercial samples of Cd yellow, Cd red, Zn white, and their mixtures. The recorded images (Fig. 11.8) confirm an intensive fluorescence in NIR as a main characteristic of cadmium pigments.

In the presented images, we can note that the sample of commercial yellow paints does not fluorescence in VIS, and the intensity of fluorescence of yellow and red paints is more different compared to pigments from the painting. The emission of red paint is more intensive than of yellow paint regardless used filters. The fluorescence of white paint was recorded only with the IR720 filter and Zn white in the mixture with Cd paint (50%-50%), which decreased the emission intensity of Cd paints [8]. The recorded images also indicate that green light excitation is more efficient, especially for red and white paints.

The spectra of blue laser induced fluorescence of samples are presented in Fig. 11.9: two peaks positions at 730 nm and 1022 nm (belonging to the emission from trap state) for yellow and one peak position at 850 nm for red paint were
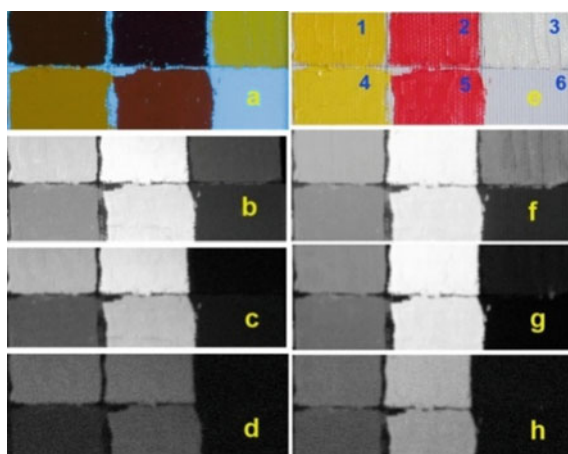
Fig. 11.8 Samples of commercial paints: **a** UVF → VIS, **b** UVF, **c** UVF → NIR, (IR850), **d** UVF → NIR (IR1000), **e** VIS: 1. Umton 0012, 2. Umton 0018, 3. Umton 0003, 4. yellow/white, 5. red/white, 6. Ground, **f** VIF → NIR (IR720), **g** VIF → NIR (IR850), and **h** VIF → NIR (IR1000)
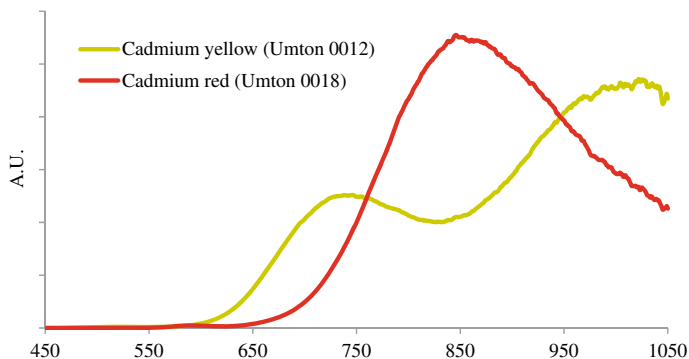
Fig. 11.9 Spectra of fluorescence of commercial samples

noticed. Even though the emission profiles of the pigments from the painting are rather different with respect to the commercial ones, fluorescence in NIR confirms the presence of cadmium in the observed pigments from the painting. We assume that different emission profiles are the consequence of different manufacturer and structure. The peak position of NBE emission for yellow sample at 500 nm (Fig. 11.7) explains less efficiency of green light excitation for yellow than for red samples.

11.4 Conclusion

Comparing the spectra of fluorescence of commercial samples and spectra of paints from the painting, we confirm the presence of cadmium in paints, regardless different emission profiles. Both spectra characterized the peak position in NIR domain, typical for Cd-based pigments. Furthermore, the shape of emission spectra of pigments from the painting confirms the recorded orange fluorescence (Fig. 11.2). It is very similar to the recorded fluorescence of yellow pigments from the painting by Vasiljev [6]. Although orange fluorescence of cadmium-based yellow pigment is described in literature as a characteristic of altered pigment [4], it is not always the case. Hexagonal Cd in powder or Cd pigments by Sigma Aldrich exhibit orange fluorescence, too.

The spectrum at point 2 confirms the influence of concentration of cadmium in paint, and in the case of the mixture with white, it illustrates less intensity although it preserves the position of maximum. Spectrum of yellow paint at point 3, with fluorescence in green, indicates the absence of cadmium. The spectrum of red paint is rather different in shape than the one acquired from the commercial sample, though it can be compared to the characteristic of the historical sample of red pigment named 508 and described in the article [9].

Comparing emission intensity from spectra and recorded images calibration of the recorded images was performed. As a conclusion, images of fluorescence could be used as a diagnostic tool for separating cadmium-based pigments in the painting.

For the excitation source, it is better to use green LED light in order to excite both yellow and red cadmium pigments. The use of longer (green) excitation wavelength penetrates more deeply into the painting and excites fluorescence from the intact cadmium yellow [4], which is applicable for varnished paintings as well, due to NIR. Excitation source is important for yellow paint (not red) since it could be used for separating different yellow paints; however, not every Cd-based yellow pigment could be identified [10]. In addition, the image could be recorded using the IR850 filter, obtaining only emission from the observed pigments, without any influence of surrounding fluorescent binder (most of the used pigments for the painting and binder have fluorescence in the visible region).

In spite of different behaviour of different types of cadmium-based pigments, separating and mapping these pigments in the painting could be performed using affordable, simple techniques of recording the image of fluorescence, an easy-to-use diagnostic tool, especially for conservators. It is a very sensitive method, even for small concentration of cadmium.

References

1. Thoury M, Delaney JK, de la Rie R, Palmer M, Morales K, Krueger J (2011) Near-Infrared luminescence of cadmium pigments: in situ identification and mapping in paintings. Appl Spectrosc 65(8) 939–51
2. Pelagotti A, Pezzati L, Bevilacqua N, Vascotto V, Reillon V, Daffara C (2005) In: 8th International conference on non-destructive testing and microanalysis for the diagnostics and conservation of the cultural and environmental heritage (Lecce) A study of UV fluorescence emission of painting materials
3. Rosi F, Grazia C, Gabrieli F, Romani A, Paolantoni M, Vivani R, Brunetti BG, Colomban P, Miliani C (2015) UV–Vis-NIR and micro Raman spectroscopies for the non destructive identification of Cd1– xZnxS solid solutions in cadmium yellow pigments. Microchem J 124:856–867
4. Mass J, Uffelman E, Buckley B, Grimstad I, Vila A, Daleney J, Wadum J, Andrews V, Burns L, Florescu S, Hull A (2016) In: Nevin A, Doherty T (eds) The Noninvasive analysis of painted surfaces. Smithsonian Institution Scholarly Press, Washington, D.C, pp 53–64
5. Clementi C, Miliani C, Verri G, Sotiropoulou S, Romani A, Brunetti BG, Sgamellotti A (2009) Application of the Kubelka-Munk correction for self-absorption of fluorescence emission in carmine lake paint layers. Appl Spectrosc 63(12):1323–1330
6. Djuric M et al (2018) IOP Conf Ser Mater Sci Eng 364:012065
7. de la Rie R, Fluorescence of paint and varnish layers, parts I, II, III. Stud Cons 27
8. Romani A, Clementi C, Miliani C, Favaro G (2010) Fluorescence spectroscopy: a powerful technique for the noninvasive characterization of artwork. Acc Chemal Res 43(6):837–846

9. Grazia C, Rosi F, Gabrieli F, Romani A, Paolantoni M, Vivani R, Brunetti BG, Colomban P, Miliani C (2015) UV-Vis-NIR and microRaman spectroscopies for investigating the composition of ternary $CdS1-xSex$ solid solutions employed as artists' pigments. Microchem J 125:279–289
10. Daveri A, Vagnini M, Nucera F, Azzarelli M, Romani A, Clementi C (2016) Visible-induced luminescence imaging: a user-friendlymethod based on a system of interchangeable and tunable LED light sources. Microchem J 125:130–141

Chapter 12
An investigation into the Decontamination of Biocide Polluted Museum Collections Using the Temperature and Humidity Controlled ICM Method

Boaz Paz and **Nikolaus Wilke**

Abstract Museum staff, conservators, restorers, curators, registrars and art handlers are often exposed to the harmful effects of biocides. These have been used in the past to protect and preserve art and cultural property from pests and microbial infestation. While the biocidal effect of inorganic salts, which often consist of arsenic and mercury compounds was known very early on, organic tar distillates such as paradichlorobenzene, carbolineum, creosote and naphthalene were increasingly used from the nineteenth century onwards. With the rapid development of organic synthesis chemistry in the twentieth century, these substances were replaced by highly effective pesticides and fungicides. Most frequently, low-volatile and lipophilic organic compounds such as chlorinated organic compounds (lindane, DDT and PCP), pyrethroids (permethrin, cyfluthrin and deltamethrin) or organophosphate pesticides (dichlorvos, chlorpyrifos, etc.) were used. Today we know that textile artefacts (costumes, uniforms, carpets and tapestries), wooden objects, herbaria, libraries, archives and historic wall decorations made of fabric, paper and leather were also widely treated with toxic inorganic and organic substances. Museums around the world are facing a problem that affects countless collection items, mainly in storage facilities. Given the requirements to minimise the use and handling of toxic substances and the obligations of employers regarding safe working environments for their employees, but also for visitors, the museum sector worldwide needs adequate decontamination solutions. This paper presents the results of a systematic study on the reduction of biocide contamination in wooden objects treated with the humidity and temperature controlled Integrated Contamination Management (ICM) method.

B. Paz (✉)
Paz Laboratories for Archaeometry, Planiger Straße 34, House 18/19, 55543 Bad Kreuznach, Germany
e-mail: info@paz-lab.de

N. Wilke
International Business Development Director ICM, Brussels, London, Berlin, Germany

12.1   Introduction

The detoxification of art and cultural assets poses a tremendous challenge to the museum world. In addition to the large number of collection objects and the variety of material types, the question arises of possible long-term effects associated with the degeneration of material-immanent substances and the alteration of characteristic material properties.

The treatment of objects, some of which are unique and irreplaceable cultural assets, is like open-heart surgery for the restorer, scientist and collector.

For preventive protection against pest infestation, insect damage and mould, a large part of the museum's collection of organic materials was treated with various chemical substances until the 1990s.

Among them were numerous chemical substances that are banned today because of their toxicity. While the biocidal effect of arsenic- and mercury-containing substances such as arsenic (arsenic(III) oxide) and sublimate (mercury(II) chloride) was known very early on, inorganic metal salts such as copper vitriol (copper sulphate), zinc chloride and organic tar distillates such as paradichlorobenzene (globol), carbolineum, creosote and naphthalene were increasingly used from the nineteenth century onwards, especially as wood preservatives. With the rapid development of organic synthesis chemistry in the twentieth century, highly effective pesticides were developed. Highly effective pesticidal and fungicidal substances from the group of phosphoric acid esters (tetraethyl pyrophosphate (TEPP), parathion (E 605), dichlorvos and chlorpyrifos) and organochlorines (polychlorinated naphthalene's (PCN), γ-hexachlorocyclohexane (lindane), dichlorodiphenyltrichloroethane (DDT) and pentachlorophenol (PCP)) were artificially produced. Due to the risk to humans and the environment, these substances have increasingly been replaced by synthetic pyrethroids (permethrin, deltamethrin and cyfluthrin), which are structurally derived from pyrethrins (naturally occurring in chrysanthemums).

Due to the initially inadequate documentation on the use of biocidal agents on museum collections, many objects were often treated several times and with different agents; gaseous as well as liquid and solid substances were used.

While it was initially assumed that mainly ethnological and natural history collections were affected by the biocide problem, it is now known that textile cultural goods (costumes, uniforms, carpets and tapestries), herbaria, archives, libraries as well as objects made of paper and leather materials (especially wall decorations) were also treated with toxic and material-damaging inorganic and organic substances.

The migration of pollutants from the contaminated objects (primary sources) leads to a continuous contamination and accumulation of the biocidal agents in the room air and dust (secondary sources). The emitted pollutants are adsorbed by the surfaces

of other collection objects as well as from the large surfaces (walls and floors) of the collection and storage rooms (contamination of the room shell) [1, 2].

What was once intended to ensure the preservation of valuable cultural assets for future generations now presents itself as a serious health hazard for those who handle contaminated collection items in the course of their work or who spend long periods of time in contaminated collection areas. The dangers posed by biocidal agents prevent restoration work and thus the long-term preservation of the collection.

In addition, the previously introduced substances lead to material damage of the cultural goods, which becomes visible in the form of crystalline efflorescence, of colour loss, oiling, efflorescence and fibre breakage in the case of textiles and unpleasant odours.

12.2 State of Research to Date

Due to the hazardous health and material-damaging effects of the substances used, numerous efforts are being made to develop suitable decontamination methods.

These can be divided into mechanical, thermal, extractive and microbiological methods. These are implemented by means of different technical processes.

Due to the high requirements resulting from conservation and restoration science aspects, the main limitation of most decontamination methods is the low depth effect and often only superficial removal of toxic and health-endangering pollutants.

There is an urgent demand from museums worldwide for a decontamination method that meets the following requirements:

(a) Material-friendly
(b) No use of chemical solvents
(c) Low mechanical stress
(d) Feasible under moderate physical conditions (under normal pressure and stable climatic conditions)
(e) Removal of pollutants as completely as possible
(f) Applicable to polychrome surfaces and sensitive multicomponent systems.

So far, only so-called extractive processes have been suitable for the sustainable and deep-effective removal of organic pollutants from contaminated museum objects. High removal rates from wooden, textile and paper objects could be achieved by extracting pollutants using liquid and supercritical carbon dioxide.

Due to the very high pressures (> 50 bar) required to liquefy the carbon dioxide on the one hand and the risk of object destruction when dry ice is formed (when the pressure inside the object decreases) on the other hand, routine application on museum objects can be ruled out for the time being. In addition, the depletion rate with the extractive method depends to a large extent on the size, geometry and material density of the object in question [3–5].

All previous extractive and solvent-based processes are based on the selective removal of non-polar, lipophilic, organic compounds or polar and inorganic metal salts.

Furthermore, the question arises about the material-damaging effect on the microstructure level and the associated long-term damage, which is due to the withdrawal of moisture and the degradation of natural material-immanent substances during the decontamination process.

12.3 Humidity-Regulated Warm Air Technology (ICM® Method)

Using the ICM® method, systematic decontamination tests were carried out for various classes of substances and material types. Both demonstrably contaminated objects from museum collections and prepared specimens were used for this purpose.

The ICM® method is classically used to control insect pests in museum collections, treating affected artefacts at temperatures and humidity levels of 48–55 °C and an average 45–60% RH, depending on the object humidity.

With the help of a technical modification of the method, which has been used for several decades, the possibility and limits of removing toxic and carcinogenic organic compounds (DDT, PCP, lindane and permethrin) as well as salt-like, inorganic pollutant compounds (arsenic and mercury) from art and cultural objects of different materiality were examined. In addition, various filter materials for the removal of biocidal agents were tested.

Based on the pollutant documentation and analyses as well as the corresponding decontamination tests, the process control can be modified according to the material and object.

The investigations also serve to optimise the process control, taking into account the results obtained for specific parameters.

12.4 Decontamination Procedure

12.4.1 Principle of Thermal Processes

By adding heat, the vapour pressure of organic and inorganic compounds is increased. In this way, even medium-volatile and low-volatile pollutants can be mobilised and transferred into the gas phase.

The change in the distribution coefficient of the pollutants in the solid leads to diffusion processes that result in the migration of pollutants from deeper layers to the surface.

The concentration gradient created by adding heat (energy) and the associated depletion of the pollutants depend on the type of material and the combination of pollutants present in each case. In particular, the type of application (sprayed, painted, soaked, etc.) determines the result of the depletion rates.

The capillary forces acting in porous materials and natural "defects" in the material structure (cracks, etc.) can lead to deviations in the diffusion process. This is associated with an undirected migration into the interior of the material or a distribution over the entire material.

The object of research is the depletion rate that can be achieved for certain substances in a routinely applicable process. The aim is to clarify which process steps and under which conditions the migration of the substances to the surface can be optimised.

12.4.2 ICM® process

In a climate chamber, a controlled supply of humidity-regulated warm air takes place. This procedure is routinely used for pest control. During a heat treatment at 55 °C for about one day, all insects in all stages (egg, larva and beetle) are permanently dehydrated and the protein molecules destroyed. During the treatment, the relative humidity is constantly controlled in relation to the temperature, i.e. when the room temperature slowly rises during the heating phase, the relative humidity is increased, when the temperature falls during the cooling phase, the humidity is lowered.

In this way, the wood humidity of the object always remains constant at the respective temperature. Tensions in the object itself can thus not arise; veneers, set or gilded surfaces do not change.

A prototype of the Espec LHL-114 climatic test chamber from ThermoTEC (Weilburg) was used for the research project. Various tests for thermal decontamination were carried out in it on selected objects and test materials (see Fig. 12.1).

The climatic test chamber has a usable volume of 105 l and operates within a temperature range of + 5 °C to + 85 °C. The humidity range is 40–95% RH.

For the special application of thermal decontamination, the climatic test chamber was additionally equipped with an adjustable external air circulation system. The recirculation system allows the air to circulate at a speed of approx. 0.5 m/s. A filter box has also been integrated into the recirculation system (see Fig. 12.2).

Depending on the application, various filter materials such as an activated carbon filter can be inserted into the filter box (see Fig. 12.3), which filters the released biocides out of the air.

Fig. 12.1 Espec LHL-114
climatic test chamber

Fig. 12.2 Recirculation
system with filter box and
adjustable ventilation motor

12.5 Experimentation

12.5.1 Tested Materials

Between the 1960s and 1990s, the product mixtures Xylamon, Hylotox 59 and Impra
Hgf were the most commonly used wood preservatives in Germany. They contained
a mixture of insecticidal and fungicidal organochlorines, such as DDT and lindane
(Hylotox 59), pentachlorophenol and lindane (Xylamon and Impra Hgf).

Fig. 12.3 Activated carbon filter (Camfil) is inserted into the filter box
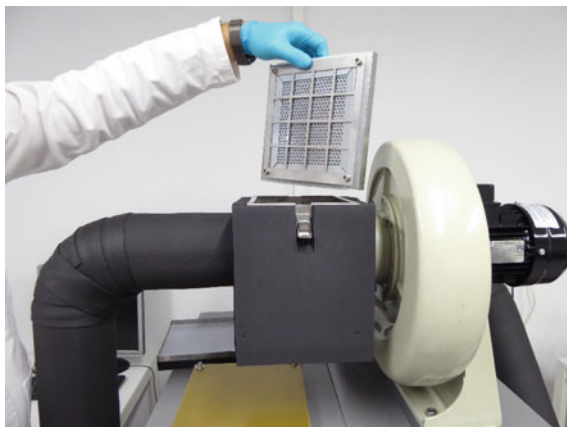
For the decontamination of wooden objects treated with DDT, lindane and, various test series were carried out using the ICM® process.

For this purpose, test specimens from different types of wood were prepared with biocidal agents. The preparation was carried out by brushing or soaking the sample baskets. After exposure and drying of the added substances, qualitative and quantitative pollutant analyses were carried out using portable X-ray fluorescence analysis (on the surface of the objects) and gas chromatography-mass spectrometry (GD-MS) to determine the actual condition.

Thermal decontamination in the climatic chamber was carried out on both prepared test specimens and treated waste wood. After the decontamination tests had been carried out, test specimens and waste wood were examined qualitatively and quantitatively for the contaminant content.

The depletion rates of the pollutants were determined by comparing the pre- and post-analyses. The migration behaviour to the surface or into the interior of the material could be characterised by the method evaluation.

Preparation of the test specimens. Test specimens (size: $2.5 \times 2.5 \times 2.5$ cm; volume: 6.25 cm3) were produced from various types of wood (birch, Douglas fir, oak, spruce, pine and larch) (see Fig. 12.4).

The wood samples were coated or soaked with various product mixtures (Hylotox 59 (3.5% DDT / 0.5% lindane); Impra Hgf (PCP/lindane) and individual substances dissolved in acetone (5% DDT in acetone and 1% lindane in acetone) (see Fig. 12.5).

Experiment I: Coating the wood samples with biocidal agents. In each case, three test specimens (cubes) of one wood species were coated with a product mixture/active substance. The treatment time of each test specimen was set to 24, 48 and 72 h, respectively. The temperature and humidity conditions were set to 55 °C and 55% relative humidity according to the ICM® method.

The following Table 12.1 shows the preparation of the respective wood species with certain biocidal active substances:

Fig. 12.4 Documentation of the test specimens.
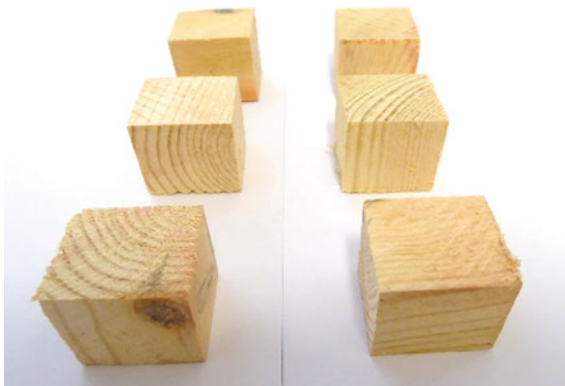
Fig. 12.5 Coating the wood test specimens with biocidal agents
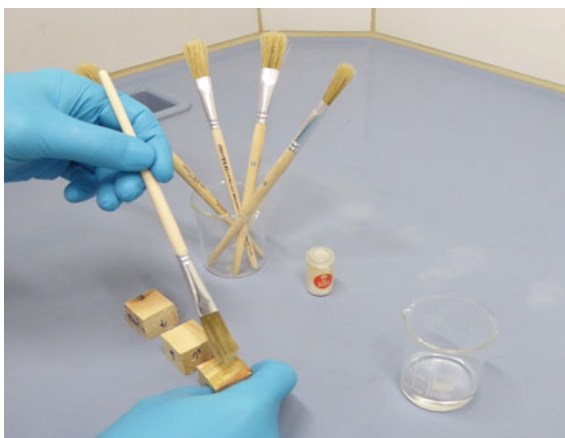
Table 12.1 Preparation of the individual wood species with biocidal agents

Wood type/Active substance	DDT	Lindane	DDT and lindane (Hylotox 59)	PCP and lindane (Impra Hgf)
Douglas fir	x	x		x
Oak	x	x	x	x
Pine	x	x	x	x
Birch			x	x
Spruce			x	x
Larch				x

Experiment II: Impregnation of the wood test specimens with the wood preservative Impra Hgf. In the second experiment, an untreated wooden cube of six wood species (Douglas fir, oak, pine, birch, spruce and larch) was completely soaked in the wood preservative Impra Hgf (active ingredients PCP and lindane) for 15 min and dried for three weeks. Subsequently, the six cubes were decontaminated for 24 h in the climate test cabinet.

Experiment III: Thermal decontamination of treated waste wood samples. In the fifth experiment, various treated waste wood samples (wall panelling, drawer, chair leg and wooden model) were treated for 24 h in the climate test cabinet (temperature: 55 °C, relative humidity: 55%).

12.5.2 Analytical methods used to determine depletion rates

Surface analysis with portable X-ray fluorescence analysis (p-XRF). By using non-destructive, mobile instrumental analysis methods, qualitative indications of objects contaminated with biocides can be found quickly and cost-effectively.

In the course of the experiments conducted, a qualitative determination of the chlorine content was carried out using the portable X-ray fluorescence analysis (p-XRF) method. The detection of chlorine provides significant evidence for the presence of chlorine-substituted organic compounds such as DDT, lindane, PCP and permethrin.

By carrying out non-destructive measurements before and after the decontamination tests, the chlorine content on the surface of the wood samples is determined, as the element chlorine can only be detected in wood at a depth of three micrometres using p-XRF.

An X-ray fluorescence analyser from Analyticon (type: NITON XL3t GOLDD+) was used for the pollutant measurements. The device has a 50 kV silver tube with silver anode and a built-in CCD camera with which the individual measuring points on the object are documented photographically. The measuring window of the analyser has a diameter of eight or three millimetres.

Wood matrix analysis with gas chromatography (GC/ECD). To quantitatively determine the depletion rates of the biocidal active substances, a material sample was taken from the wooden cubes and analysed using gas chromatography (GC).

For this purpose, the biocidal active substances are completely dissolved out of the samples by means of Soxhlet extraction, evaporated in the gas chromatograph and passed over a chromatographic column by means of a carrier gas flow (e.g. helium, nitrogen or hydrogen), where separation into the individual components takes place.

The results of the quantitative analyses reflect the content of organochlorines found in the entire test specimen, i.e. also in the deeper layers.

By comparing the results from the analysis by X-ray fluorescence analysis and gas chromatography, the mobilisation of the chemical substances to the surface or in the opposite direction, namely into the interior of the sample body, can be followed.

12.6 Results

12.6.1 Experiment I: Determination of the Depletion Rates

DDT. For the quantitative laboratory results by GC, the depletion rates for DDT in Douglas fir range between 13 and 49 % (see Fig. 12.6). The highest depletion rate was already reached after 48 hours.

In comparison, the surface measurements using p-XRF show depletion rates for the chlorine contents between 28 and 79 % (see Fig. 12.6). This result shows that the depletion of DDT on the surface of the object is very high. After 72 hours, more than 75 % of the chlorine content had been removed from the surface.

As the results for DDT on oak show, according to the laboratory results, depletion could only be achieved after 48 hours (see Fig. 12.7). The maximum depletion rate is 53% after 72 h.

After 24 h, a very high chlorine depletion rate (98%) was determined on the surface of the oak cube using p-XRF. After a further 24 h, DDT and thus the chlorine values were apparently transported from deeper layers of the wood to the surface, so that a depletion rate of only 67% of the chlorine content could be determined and after a total of 72 h a depletion rate of 73%.

The depletion rates (according to the laboratory results) for DDT in pine range from 22 to 63%, with the highest depletion rate already reached after 48 h (see Fig. 12.8). On the surface, a depletion of the chlorine content of 29% was observed after 24 h, 50% after 48 h and 56% after 72 h.
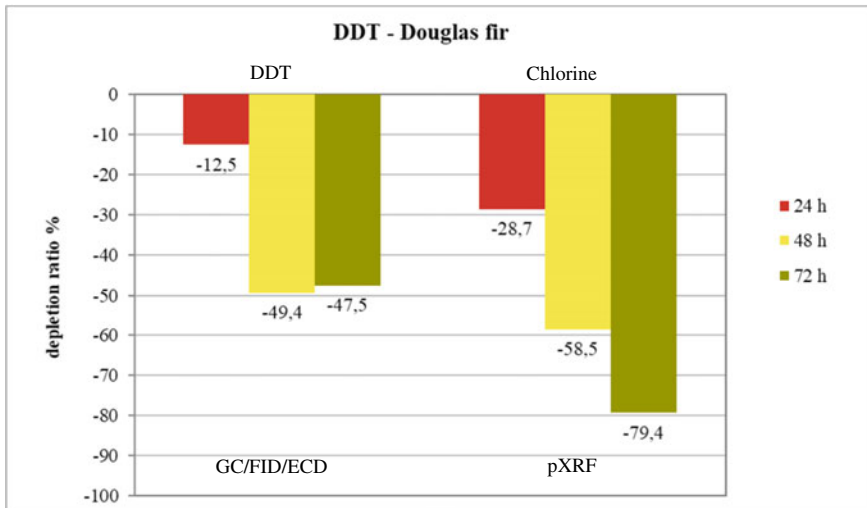
Fig. 12.6 Comparison of the depletion rates (laboratory results and p-XRF measurements) of DDT using the example of the wood species Douglas fir
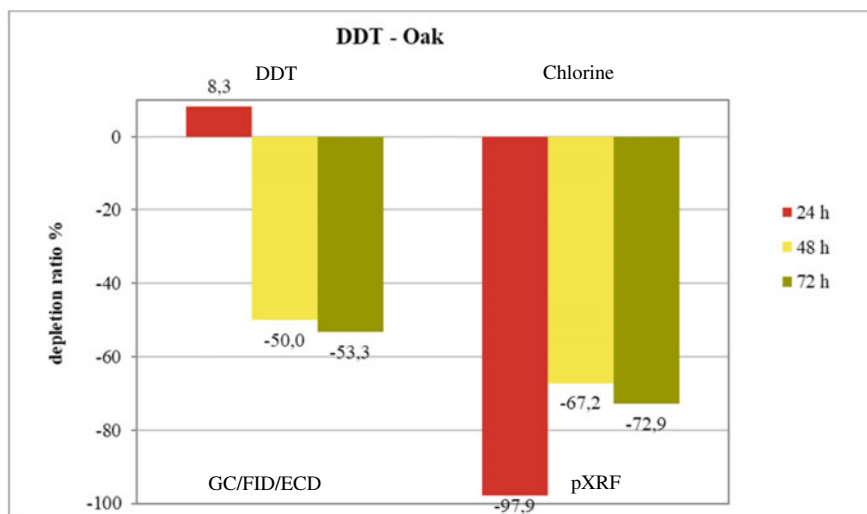
Fig. 12.7   Comparison of the depletion rates (laboratory results and p-XRF measurements) of DDT using the example of the wood species oak
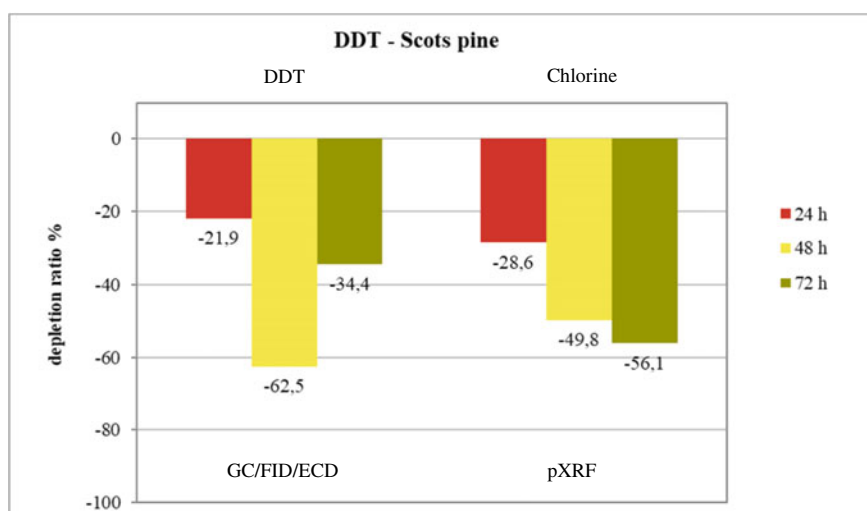
Fig. 12.8   Comparison of the depletion rates (laboratory results and p-XRF measurements) of DDT using the example of the wood species pine

Lindane. The biocidal active ingredient lindane can be depleted from the wood species Douglas fir by means of thermal decontamination very effectively. As the results in Figure 12.9 show, depletion rates of more than 90% were achieved both on the material samples and on the surface after 24 h and 48 h, respectively.
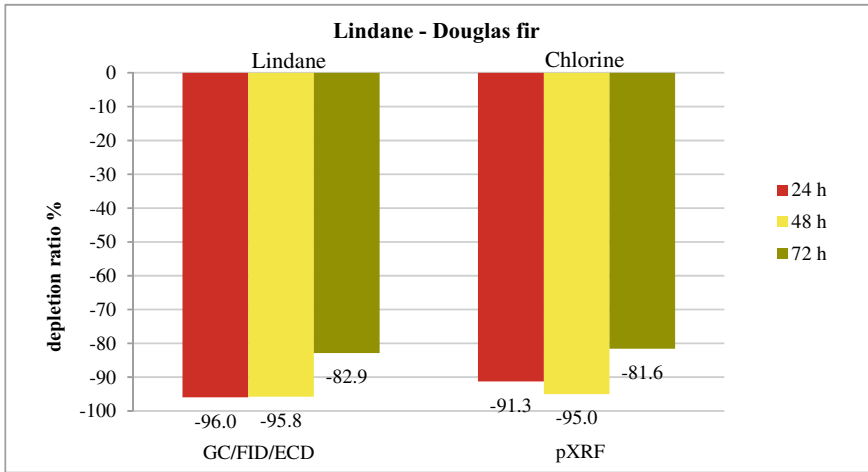
Fig. 12.9 Comparison of the depletion rates (laboratory results and p-XRF measurements) of lindane using the example of the wood species Douglas fir

Very good depletion rates for lindane were also detected in the test specimens made of oak. The highest depletion rates for the material samples as well as on the surface were found after 48 hours (see Fig. 12.10).
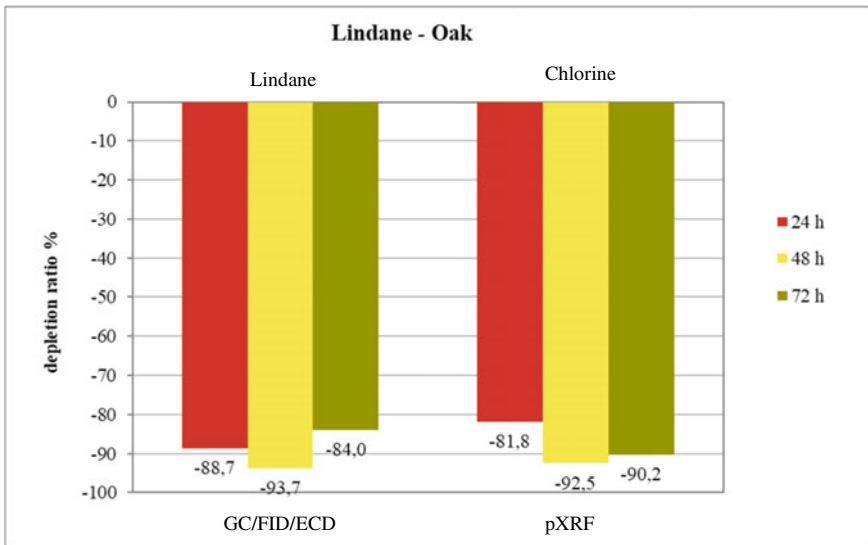
Fig. 12.10 Comparison of the depletion rates (laboratory results and p-XRF measurements) of lindane using the example of the wood species oak
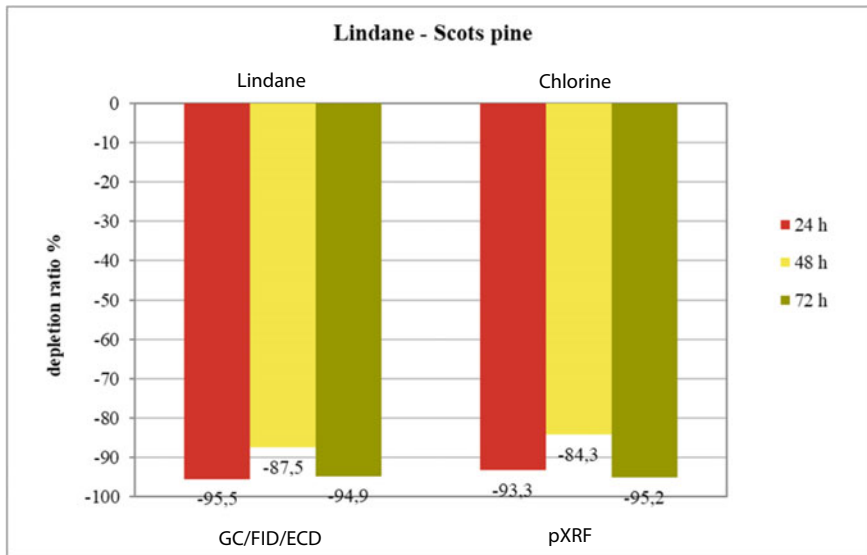
Fig. 12.11 Comparison of depletion rates (laboratory results and p-XRF measurements) of lindane using the example of the wood species pine

The depletion rates for the laboratory results and surface measurements by p-XRF can very well be compared to the pine wood cubes treated with lindane. For both investigations, depletion rates of more than 90% could already be determined after 24 h (see Fig. 12.11).

Hylotox 59. Hylotox 59 is a wood preservative used in the former GDR until 1989; it contained DDT (3.5%) and lindane (0.5%). The tests with Hylotox 59 were carried out on the test wood cubes of birch, oak, spruce and pine. The depletion rates for the wood preservative Hylotox 59 are very high on the birch wood cubes. Both the surface measurements by p-XRF and the taking of the material samples and subsequent analysis by GC/FID/ECD yielded depletion rates between 77 and 98% (see Fig. 12.12).

The depletion rates for Hylotox 59 on the oak wood cubes are high for lindane (see Fig. 12.13).

It is striking that both DDT and lindane were already very well depleted after 24 h. A decrease in the chlorine content of more than 70% was observed on the surface of the object. With the help of thermal decontamination, the wood preservative Hylotox 59 can be very well depleted on the spruce wood cubes (see Fig. 12.14).

For the wood species pine, the depletion rates for Hylotox 59 related to the active substance DDT are good at 76% after 24 hours (see Fig. 12.15). After 48 and 72 h, no better results could be achieved for the depletion rates of DDT. Lindane could be depleted very well with more than 90%. Very good results for the depletion of the chlorine content could also be determined at the surface.

Fig. 12.12 Comparison of depletion rates (laboratory results and p-XRF measurements)
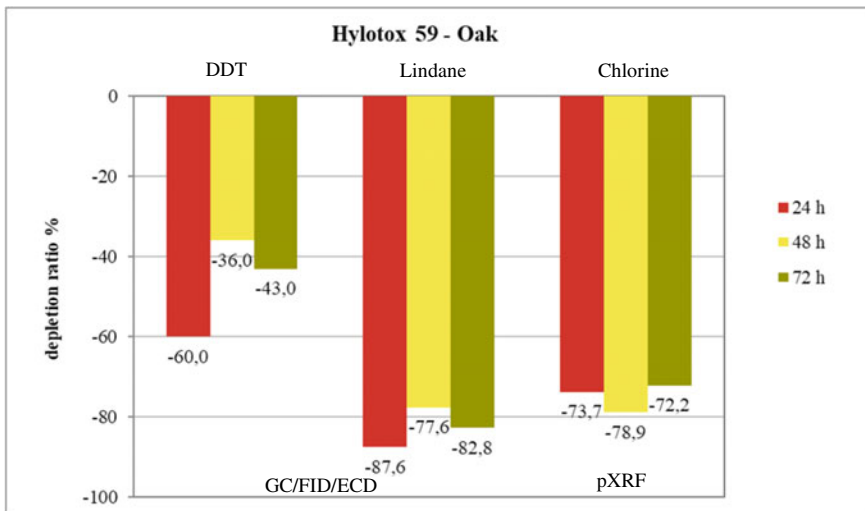
Fig. 12.13 Comparison of the depletion rates (laboratory results and p-XRF measurements) of Hylotox 59 using the example of the wood species oak.

Impra Hgf. The tests with Impra Hgf were carried out on the test wood cubes made of birch, Douglas fir, oak, spruce, pine and larch. With the help of thermal decontamination, the wood preservative Impra Hgf can be well depleted on the birch wood cubes. With regard to the two active substances PCP and lindane, lindane
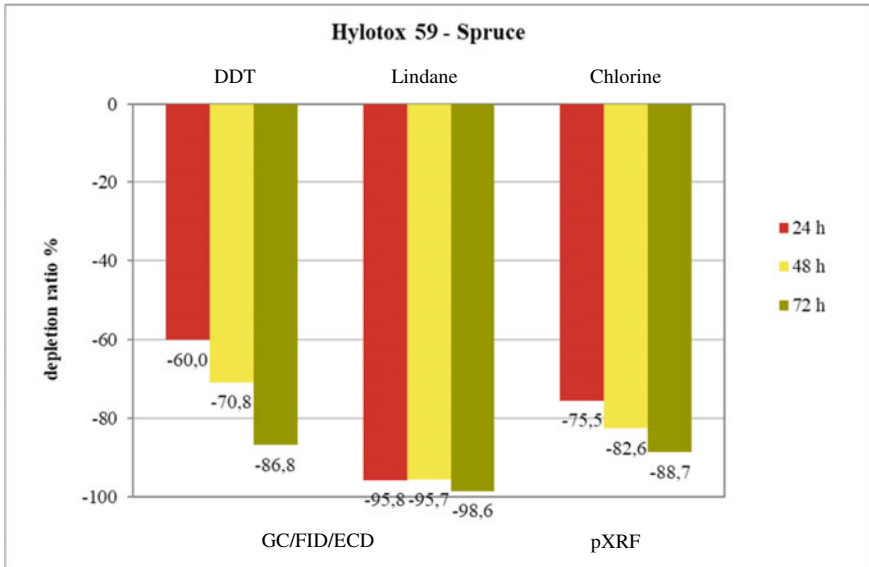
Fig. 12.14 Comparison of the depletion rates (laboratory results and p-XRF measurements) of Hylotox 59 using the example of the wood species spruce
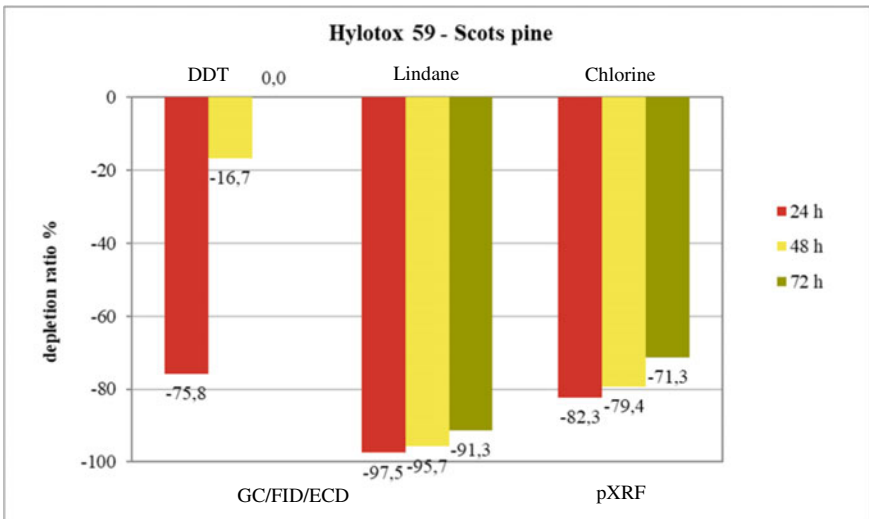
Fig. 12.15 Comparison of the depletion rates (laboratory results and p-XRF measurements) of Hylotox 59 using the example of the wood species pine
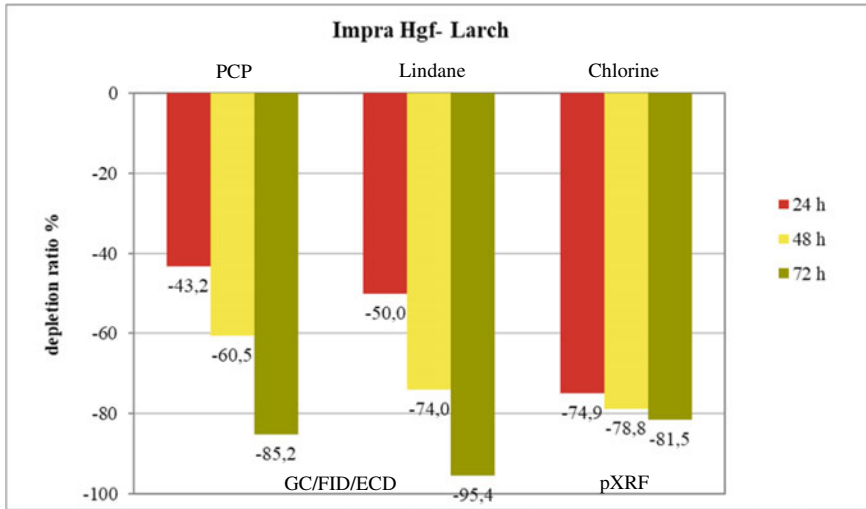
Fig. 12.16 Comparison of the depletion rates (laboratory results and p-XRF measurements) of Impra Hgf using the example of the wood species larch

can be better depleted. The highest depletion rates were obtained after 72 h. For the wood species Douglas fir, the depletion rates for Impra Hgf are comparable to those of the wood species birch, with the highest depletion rates being reached after 48 and 72 h, respectively. For the wood species oak, good depletion rates for the wood preservative Impra Hgf could also be determined. It is striking that both the material samples and the surface measurements showed an accumulation of the active substances after 48 hours, presumably from deeper wood layers. For the wood species spruce, comparable results to Douglas fir were found for Impra Hgf. The highest depletion rates were achieved after 72 h in the climatic test chamber. For the wood species spruce, comparable results to Douglas fir were found for Impra Hgf. The highest depletion rates were achieved after 72 h in the climatic test chamber. With the help of thermal decontamination, the wood preservative Impra Hgf can be depleted very well on the pine wood cubes. The best results were achieved after 48 h.

In comparison with the other wood species, the lowest depletion rate for PCP was determined for Impra Hgf in larch (see Fig. 12.16). In general, the highest depletion was determined after 72 h of thermal decontamination.

12.6.2 Experiment II: Determination of the Depletion Rates

In the second experiment, a wooden cube of the six wood species (Douglas fir, oak, pine, birch, spruce and larch) was impregnated with the wood preservative Impra Hgf and decontaminated for 24 h in a climate test cabinet at a temperature of 55 °C and a relative humidity of 55%.
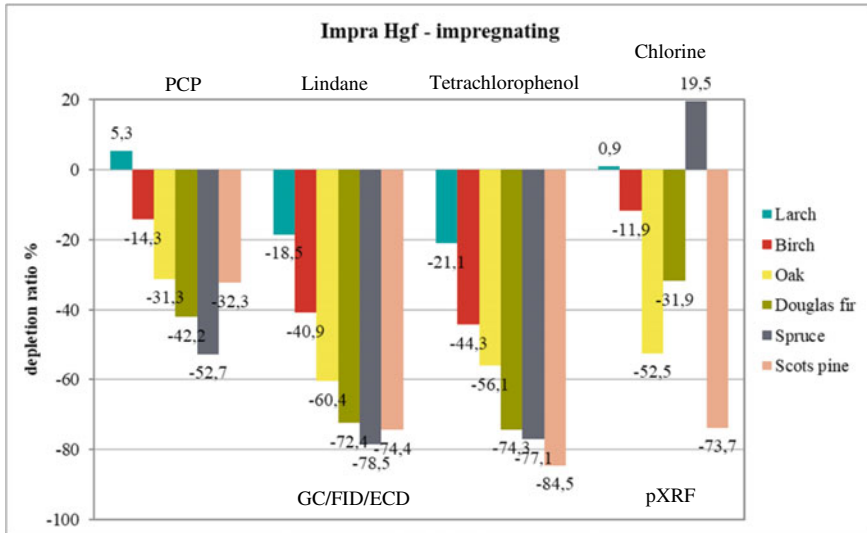
Fig. 12.17 Comparison of the depletion rates (laboratory results and p-XRF measurements) for the wood samples impregnated with Impra Hgf

The results for the depletion rates of the individual wood species are shown in Fig. 12.17.

According to the laboratory results, very good depletion rates could be determined for the substances lindane and tetrachlorophenol for the wood species Douglas fir, spruce and pine.

Good average depletion rates for these substances could also be determined for the wood species birch and oak. For the wood species larch, the depletion rates for the substances mentioned are low.

The surface measurements using p-XRF showed the best depletion rate for the wood species pine, followed by oak and Douglas fir. In contrast, a low depletion rate was found for the wood species birch. In the case of wood cubes made of larch and spruce, even a superficial enrichment of the measured values for chlorine was detected after the 24 h decontamination. These are wood species with a very high natural salt content. By means of p-XRF, inorganic chloride cannot be distinguished from organically bound chlorine.

12.6.3   Experiment V: Determination of the Depletion Rates

The results of the decontamination of the waste wood samples are shown in Fig. 12.18.

The best depletion rates on the waste wood samples were found for lindane. PCP was sufficiently well depleted during the 24-h decontamination test. The depletion rates for tetrachlorophenol and DDT were between 19 and 40%.
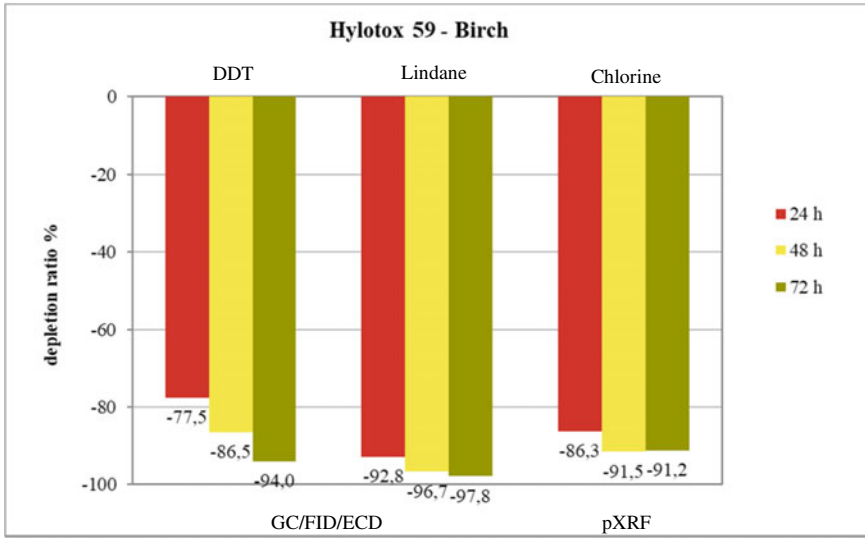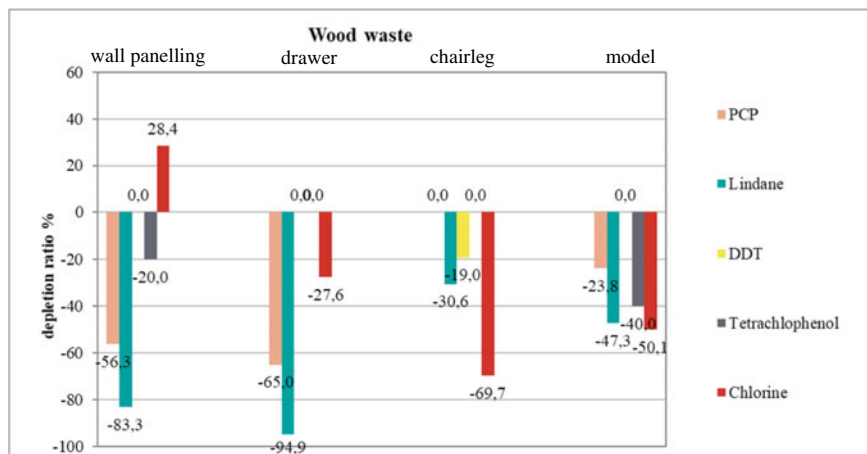
Fig. 12.18 Comparison of depletion rates (laboratory results and p-XRF measurements) for the waste wood samples

With regard to the surface measurements by means of p-XRF, depletion rates of 28–70% could be detected for the chlorine contents of the waste wood samples (except for the wall cladding). In the case of the wall cladding, an enrichment of the chlorine content on the surface could be determined by means of p-XRF. This can be attributed to the fact that the wood preservative application on the wall cladding was inhomogeneous.

12.7 Summary

In the course of the various trials, it was possible to show the extent to which the various biocidal active substances can be deposited in the different types of wood.

During the first test, six different types of wood (birch, Douglas fir, oak, spruce, pine and larch) were coated with different biocidal substances. Subsequently, the test wood samples were decontaminated at a temperature of 55 °C and a relative humidity of 55% for 24, 48 or 72 h in the climate test chamber.

The best decontamination results were found for lindane or wood preservatives containing lindane. Active substances containing DDT or PCP were also relatively well decontaminated.

With regard to the impregnation of the test cubes with the wood preservative Impra Hgf (test II), good to very good depletion rates were found for the substances lindane and tetrachlorophenol for the wood species douglaise, spruce and pine. For the wood species birch and oak, the active substances were only moderately depleted. In contrast, extremely low depletion rates were determined for the wood species larch.

Table 12.2 Documentation of the results of the second decontamination test with regard to the different types of wood

	Impra Hgf			
	PCP	Lindane	Tetrachlorophenol	Chlorine
Birch	+	+	+	+
Douglas fir	+	++	++	+
Oak	+	++	++	++
Spruce	++	++	+++	−
Scots pine	+	+++	+++	+++
Larch	−	+	+	−

+ represents a depletion rate < 50%, ++ a depletion rate < 75%, +++ a depletion rate > 75% and—represents enrichment

With regard to the surface measurements using p-XRF, the best depletion rate was found for the wood species pine. In contrast, a very low depletion rate was found for the wood species birch. For the wood cubes made of larch and spruce, which have a high natural salt load, a surface enrichment of the measured values for chlorine was even detected after the 24-h decontamination. A summary of the effectiveness of the second decontamination test on the different types of wood is shown in Table 12.2.

References

1. Gebefügi I (1989) Chemical exposure in enclosed environments. Toxicol Environ Chem 20–21(1):121–127
2. Bruckmann P, Kersten W, Hagedorn B, Ball M, Päpke O, Funcke W, Theisen J (1989) Immissionsmessungen halogenierter organischer Verbindungen in Hamburg. VDI-Berichte 745:209–221
3. Wörle M et al (2020) Decontamination of biocide treated museum objects of the swiss national museum's collection by liquid CO_2 technology. Stud Conserv 65(2):77–85
4. Unger A, Weidner AG, Tello H, Mankiewicz J (2011) Neues zur Dekontamination von beweglichem Kunst- und Kulturgut mit flüssigem Kohlendioxid. Beiträge zur Erhaltung von Kunst- und Kulturgut 2:85–96
5. Tello H, Unger A, Gockel F, Jelen E (2005) Decontamination of ethnological objects with supercritical carbon dioxide. In: ICOM Committee for Conservation, 14th Triennial Meeting The Hague 12–16 Sept 2005, vol 1, pp 110–119

Chapter 13
Structural and Diagnostic Investigations on Materials and Plasters of the Biblioteca Umanistica of the University of Florence

Chiara Gallo , **Luciano D'Agostino, Nicolino Messuti, Carmine Napoli, Marco Quarta, Daniela Valentini, and Eduardo Caliano**

Abstract In the last decades, the study of historical maintenance interventions performed on cultural heritage items has taken on a progressive development. These interventions are related to the restoration of structures and esthetical operations performed over time, sometimes without taking attention on the properties of pre-existing materials used. The main critical element related to these type of interventions is characterized by the alteration of functionalities and esthetic conception of the original monuments, due to the application of structural materials and colored-finishing surface layers selected according to esthetical trends and criteria of succeeding years. In the present paper, structural investigations on materials, and characterization of colored plasters of the historical Biblioteca Umanistica of the University of Florence, are reported. Above all, a specific diagnostic plan was focused on non-destructive geophysical investigations, as well as microscopy and chemical stratigraphic characterizations of colored plasters, and the results were obtained by

---

C. Gallo (✉) · N. Messuti · C. Napoli · E. Caliano
Istemi S.r.l., Via dei Lombardi 23, 84085 Mercato San Severino, SA, Italy
e-mail: c.gallo@istemi.it

N. Messuti
e-mail: n.messuti@istemi.it

C. Napoli
e-mail: c.napoli@istemi.it

E. Caliano
e-mail: e.caliano@istemi.it

L. D'Agostino · M. Quarta
Building Area—Building Plan Process Unit, University of Florence, Piazza Indipendenza 8, 50129 Florence, Italy
e-mail: luciano.dagostino@unifi.it

M. Quarta
e-mail: marco.quarta@unifi.it

D. Valentini
Firm Valentini-Ventura Restauro d'opere d'arte Srl, Firenze, Italy

means of several analytical techniques. The overall results have shown the importance and suitability of a multianalytical diagnostic approach by using structural and geophysical investigations, as well as archaeometric analyses, by revealing important information which could be useful to support future restoring and maintenance activities for the Biblioteca Umanistica of the University of Florence.

Keywords Cultural heritage conservation · Geophysical survey · GPR · Stratigraphic investigation · Optical microscopy · FT-IR spectroscopy

13.1   Introduction

Study of structures, construction materials, and plasters of cultural properties represents an important role in the knowledge of historical sites and monuments, providing essential information about building technologies used in the past, as well as construction phases, materials feature, and their composition for restoration purposes. In particular, many types of materials, mortars, and plasters are constantly investigated by detecting and monitoring their performances over the time. The durability of these materials, enduring from centuries in every situation, is primarily due to the excellent majesty of workers and their capacity to combine several construction products for the building of monuments. However, it is well known that the presence of degrading substances induces deterioration, even in the case of the most durable material, since physical, mechanical, and chemical processes lead to modifications of material properties [1, 2], as well as anti-esthetic effects due to subsequent maintenance interventions [3].

The increasing attention is being paid to the multidisciplinary approach aimed at restoration and maintaining purposes, focused on the using of non-destructive in situ investigation and laboratory analytical techniques, which allows both preventive conservation and a more invasive investigation. Nowadays, structural non-destructive tests (NDT) and micro-destructive surveys are a necessary tool in the field of cultural heritage, which is focused on the characterization of materials, detection of degradation forms, assessment of the effectiveness of interventions, and evaluation of compatible materials and processes applications [4]. In addition, it is worth noting that careless periodical city maintenance practices, over the years, are often performed without taking attention to the pre-existing materials, mortars, and plasters used, as well as colored-finishing layers applied on surfaces. This could be a further cause of degradation of the surfaces and masonries, in addition to natural atmospheric weathering and environmental pollution [3, 5].

Therefore, two main branches were considered and are reported in the present study: non-destructive structural investigations and stratigraphic investigation of the colored plasters of the Biblioteca Umanistica of the University of Florence. Data were obtained by a multianalytical approach, including autoptic, endoscopic, GPR, and geoelectrical surveys, as well as microscopic and chemical investigations of the colored layer samples. The overall results have shown the importance and suitability

of the multidisciplinary diagnostic approach by using structural, geophysical, and archaeometric investigations on materials. By revealing information on mechanical properties and homogeneity, as well as the state of preservation of the structures and the stratigraphic succession of plasters and the colored layers, this study could be useful as a support for future restoring and maintenance activities for the Biblioteca Umanistica of University of Florence.

13.1.1   Historical Background

The Biblioteca Umanistica was built in 1295 as a monastery (i.e., Complesso degli Angeli) [6], as a small and humble refuge for hermits, and it expanded by purchasing houses and neighboring lands. As early as 1300 s, it became a prestigious monastery, equipped with cloisters [7], noble chapels, and a large chapter room, and it was an important center of miniature and pictorial art [8, 9], even placing works of arts by main artists as Masaccio, Paolo Uccello, Beato Angelico, Lorenzo Ghiberti, Andrea del Castagno. Then, Brunelleschi worked on the design and partial realization of the famous Rotonda temple, as well as Ridolfo del Ghirlandaio, who executed its Cenacolo into the refectory of the monastery. From the end of 1500 s, a continuous change and renovation of the monastery and the cloisters occurred, implying both structural and decorative works, and by using different esthetic tastes, materials, and techniques depending on the historical era. During the centuries, and particularly from 1950s, new renovation led to the current aspect of the building, by adding different structures to the original body (Fig. 13.1a), and which currently seats the university classrooms of the Faculty of Literature and Architecture of the University of Florence.

Diagnostic investigations of the present work were performed by taking into account the original places of the complex, which nowadays is represented by the central part of the entire construction (Fig. 13.1b). In particular, five main locations were considered for the present work: (i) the minor cloister known as "Chiostro di Levante" or "Chiostro Nigetti" (1628–33); (ii) the major cloister (built in 1635); (iii) the Brunelleschi corridor, which links the two cloisters; (iv) the room named as "Sala Comparetti;" and (v) the rooms of the 1st floor.

13.2   Materials and Methods

13.2.1   In Situ Structural Investigations

In situ structural investigations performed in this study were focused on preliminary autoptic investigation, as well as endoscopy, ground-penetrating radar (GPR), and geoelectric surveys, aimed at the diagnosis of the state of preservation and assessment
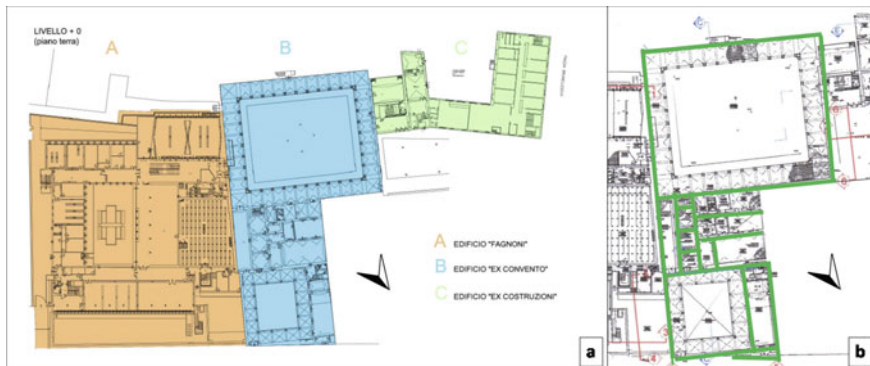
Fig. 13.1 Planimetry of the Biblioteca Umanistica of the University of Florence (Italy): **a** subdivision of the areas including the original central part (i.e., the ancient monastery—blue) of the complex, and the parts of structure added in the following centuries (orange and green); **b** detail of original central part considered for investigations, including two main cloisters, corridors, and rooms both from ground and first floors

of conservation interventions. The main purpose of the aforementioned diagnostic activities was to find and map the infiltrative phenomena detected inside the cloisters, defining their cause and size. Results were processed by Res2Dinvx, Res3Dinvx, Surfer 2D, and Voxler 3D software, in order to support strategic planning for the conservation interventions on monument scale and environmental impact assessment for the protection, management, and sustainable development of the construction. The surveys were carried out in several points of the Biblioteca Umanistica, including two main cloisters, corridors, and rooms both from ground and underground floors. In this study, representative investigations performed on the bigger cloister, called Nigetti cloister, are reported.

13.2.2 Stratigraphic Investigations on Colored-Finishing Layers

As for plaster samples, preliminary stratigraphic tests were carried out by using a scalpel, aimed at identifying the original colored layers of the internal wall surfaces. Then, sampling of plasters preserving colored layers was performed, by considering representative portions of materials and in order to minimize invasiveness of the operation, by taking micro-samples from the monument surfaces. Particularly, the samples were collected by considering the colored layers detected below the current ones, which could be related to the original colors of the ancient structure. Stratigraphic tests and sampling of the plasters were made in cooperation with the restorers and under the supervision of the project responsible of the University of Florence. A number of 15 samples were collected in different areas of the site, including the

Table 13.1 Samples collected from the Biblioteca Umanistica of the University of Florence (Italy) where not specified, sampling points were performed in correspondence of the ground floor

Sample	Description	Sample point
C.6	Thin pictorial film with dark color	Vault lunette, room n. 16 (1st floor)
C.12	Plaster with white layer	Vault lunette of the major cloister
C.14	Plaster with ochre layer	Vault lunette of the minor "Nigetti" cloister

two cloisters, corridors, rooms and vault ceilings, both from ground and first floors, and they were analyzed by means of the following described analytical techniques. Above the sample collection, three representative samples (summarized in Table 13.1) are reported in the present paper.

Micro-stratigraphic investigation. Samples were preliminarily observed by using a Kern OZP 558 stereomicroscope equipped with a Canon EOS 760D camera, in order to define the morphological characteristics of each fragment. Subsequently, a small portion (<15 × 15 mm) of each sample collected was embedded in a bicomponent epoxy resin (Hardrock 554), then prepared in cross-section. Optical microscopy observations were performed under visible and ultraviolet (UV) reflected light mode, by using a Zeiss Axioscope 5 microscope, equipped with an Axiocam 208 color camera for the image acquisition. By means of microscopic observations, the stratigraphic succession of the finishing layers of the samples was identified, as well as thicknesses, state of preservation, and degree of homogeneity of layers and substrates. Moreover, observations of the samples in UV light conditions have allowed the identification of organic compounds, through the occurrence of characteristic fluorescence phenomena of the materials.

Fourier Transform Infrared (FT-IR) spectroscopy investigation. FT-IR spectroscopy is a technique able to detect both inorganic and organic compounds eventually present in the samples. Hence, FT-IR analyses were performed in order to obtain information about pigments and materials used in the colored layers and plaster fragments. FT-IR investigations were carried out on the colored layers which were identified as the originals in the samples examined, by selecting the interesting portion and carefully removing by using a scalpel. The analyses were carried out by means of a Perkin Elmer Spectrum Two spectrometer, in attenuated total reflectance (ATR) mode. Spectra were collected in the 4000–450 cm^{-1} range, with a resolution of 4 cm^{-1}. A total of 16 scans were signal averaged to reduce the noise. Spectra are reported as wavenumber (cm^{-1}) versus absorbance (a.u.).

13.3   Results and Discussion

13.3.1   *In Situ Structural Investigations*

The combined processing of various diagnostic techniques which were used have allowed to univocally define the defectological picture present within the area under investigation. In particular:

- By GPR survey, it was possible to map the network of underground services present within the area;
- Endoscopic investigation has allowed to verify the presence of interruptions, occlusions, and ruptures inside the implants previously found (Fig. 13.2a);
- Geoelectric survey defined the location and extension of the areas subject to infiltration phenomena (see Figs. 13.2b and 13.3).

In order to interpret the results obtained from the various survey techniques used, a three-dimensional model was developed. Inside the model has been reported:

- the evidence obtained from the GPR relating to the anomalies found and attributable to the complex system of pipes present in the subsoil;
- video acquisitions relating to inspections carried out inside the pipes;
- the two-dimensional map of the resistivity values of the ground.

From the model, it was possible to detect how the infiltrative phenomena found on the surface are perfectly aligned with the anomalies found on the water drainage systems, and, in correspondence with the latter, how the soil resistivity values are significantly low. This testifies to a widespread percolation of water from the systems with consequent imbibition both of the garden inside the cloister and of the wall portions immediately behind the areas affected by these filtering motions.

Fig. 13.2 Execution of the investigations inside the Nigetti cloister: **a** endoscopic investigation inside the pipes found; **b** geophysical investigations for the characterization of infiltrative phenomena
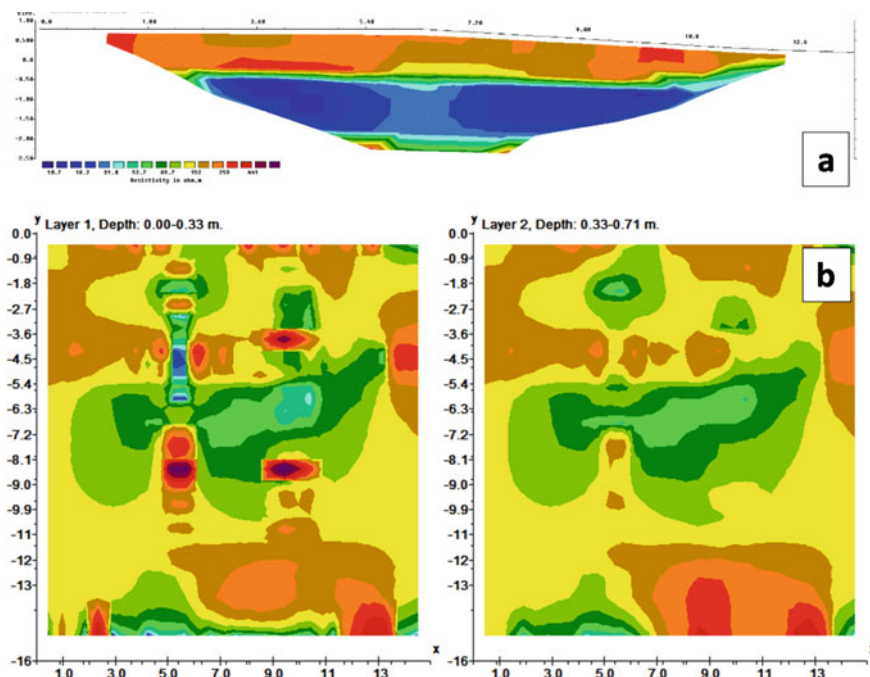
Fig. 13.3 Extract from the elaboration of the three-dimensional model: **a** one-dimensional electrical tomography with evidence of the different resistivity values (expressed in ohms) measured inside the ground (the area affected by infiltrations in blue); **b** defined two-dimensional electric tomography for successive slices

13.3.2 Stratigraphic Investigations on Colored-Finishing Layers

Preliminary stratigraphic tests have allowed to reveal colored layers in all the places investigated, possibly attributable to both original colors and related to maintenances operation of the structures. Particularly, interesting three samples were collected from the following locations: (i) sample C.6, a pictorial film fragment collected from the vault lunette of room n. 16 (1st floor), (ii) sample C.12, a white plaster collected from the main cloister, and (iii) sample C.14, ochre plaster collected from the Nigetti cloister (Fig. 13.4).

Microscopic observations and FT-IR analysis performed on samples C.6, C.12, and C.14 are reported in Figs. 13.5, 13.6, and 13.7, respectively.

Microscopic observation of sample C.6 (see Fig. 13.5a) has revealed a stratigraphy constituted by 4 layers, from the internal substrate to the surface. In particular, the white substrate has a porous and microcrystalline texture, with white crystals immersed into the matrix (thickness 0.3 mm). The second white layer appears dense and homogeneous (thickness 0.02 mm). The third layer appears as a light pinkish
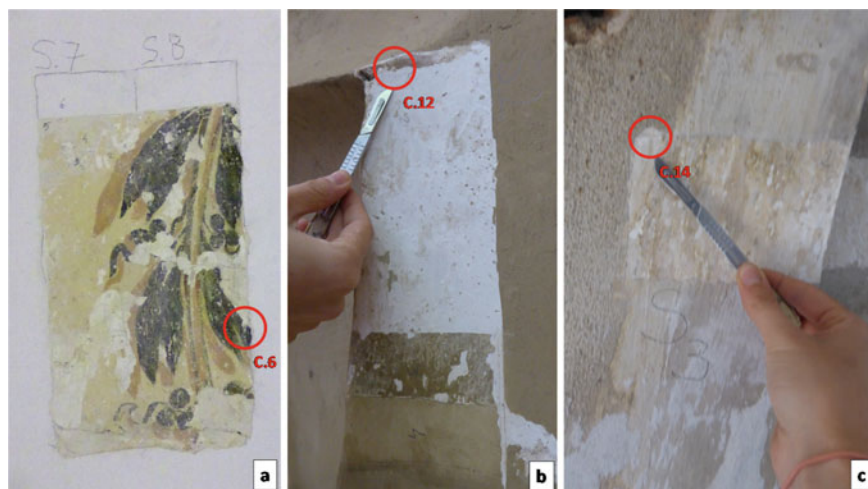
Fig. 13.4 Sampling points of **a** sample C.6, pictorial film fragment, **b** sample C.12, plaster with a white layer, and **c** sample C.14, plaster with ochre layer

color, dense and homogenous, with micrometric yellow and dark grains immersed in its matrix (thickness 0.05 mm). Lastly, the above layer appears as a thin dark-colored film; it is discontinuous on the surface, and it is 0.01 mm thick; it represents the colored pictorial film of the vault decoration.

FT-IR spectrum performed on this superficial layer (Fig. 13.5b) clearly indicates the presence of green earth [10], a pigment widely used by artists in Florence even before Renaissance [11], and constituted by calcium carbonate (712, 872, 1417 cm^{-1}), gypsum (601, 671, 1033, 1115, $\approx$3500 cm^{-1}), iron, aluminum, potassium, and manganese silicates and oxides (467, 524, 779, 797, 873, 915, 1011, 1428 cm^{-1}). In addition, a huge amount of calcium oxalates (i.e., whewellite and weddellite), was detected, evidenced by the absorbance bands at 516, 781, 1315, and 1641 cm^{-1}. As widely reported in literature, the oxalate formation is due to precipitation and crystallization of protein binders [12], especially in places where moisture occurs [13, 14]. Then, the presence of oxalates could be attributable to some protein-based compound used, for instance, as a binder for the pictorial decoration of the surface layer, otherwise the employment of organic products during restoration or maintenance activities carried out after the date of its realization.

As for sample C.12, collected from the main cloister, the microscopic observations have revealed the presence of two layers, placed above a lime-based plaster (Fig. 13.6a). The layers present a white color, and they are constituted by a lime matrix, with a thickness of 0.2 mm for each layer. The plaster substrate has a white color and has rounded silicate aggregates dispersed in the matrix, having size of 0.2 mm and homogeneously distributed. In addition, some vegetable fibers were detected in the lime matrix, appearing fluorescent under UV light mode (Fig. 13.6a').
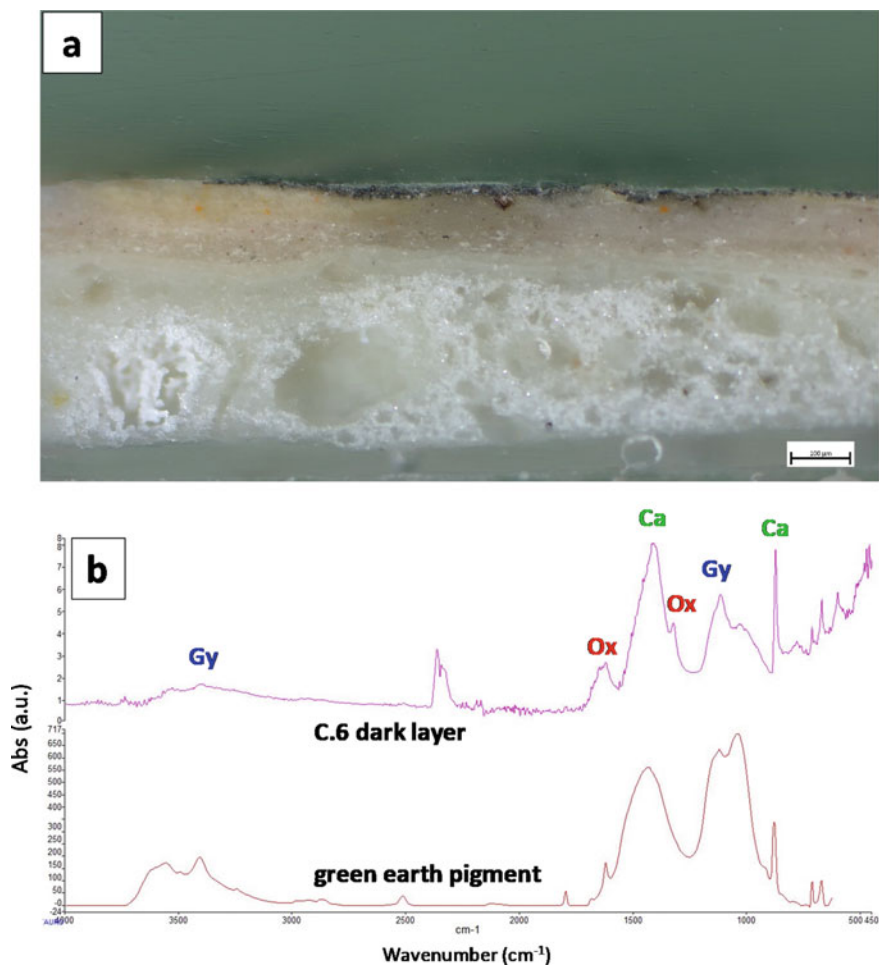
Fig. 13.5 Optical microscopy image **a** cross-section, 200x, reflected light mode, and FT-IR spectra of the dark thin layer **b** of sample C.6

FT-IR spectra performed on fibers (see Fig. 13.6b) clearly shown an organic nature, cellulosic fibers possibly comparable with hemp [15] or flax [16] fibers. Taking in consideration the results obtained, this is possibly related to the employment of fiber-reinforced plasters in occasion of restoring activities: In fact, reinforced mortars and plasters are widely used nowadays, representing an important resource for ancient masonry restoration [17].

Finally, sample C.14, which was collected from the Nigetti cloister, is a plaster fragment with white layer on its surface. Microscopic observations (Fig. 13.7a) have shown a lime-base matrix, very similar to those one detected in sample C.12 (Fig. 13.6a). Rounded silicate aggregates are analogously present (thickness
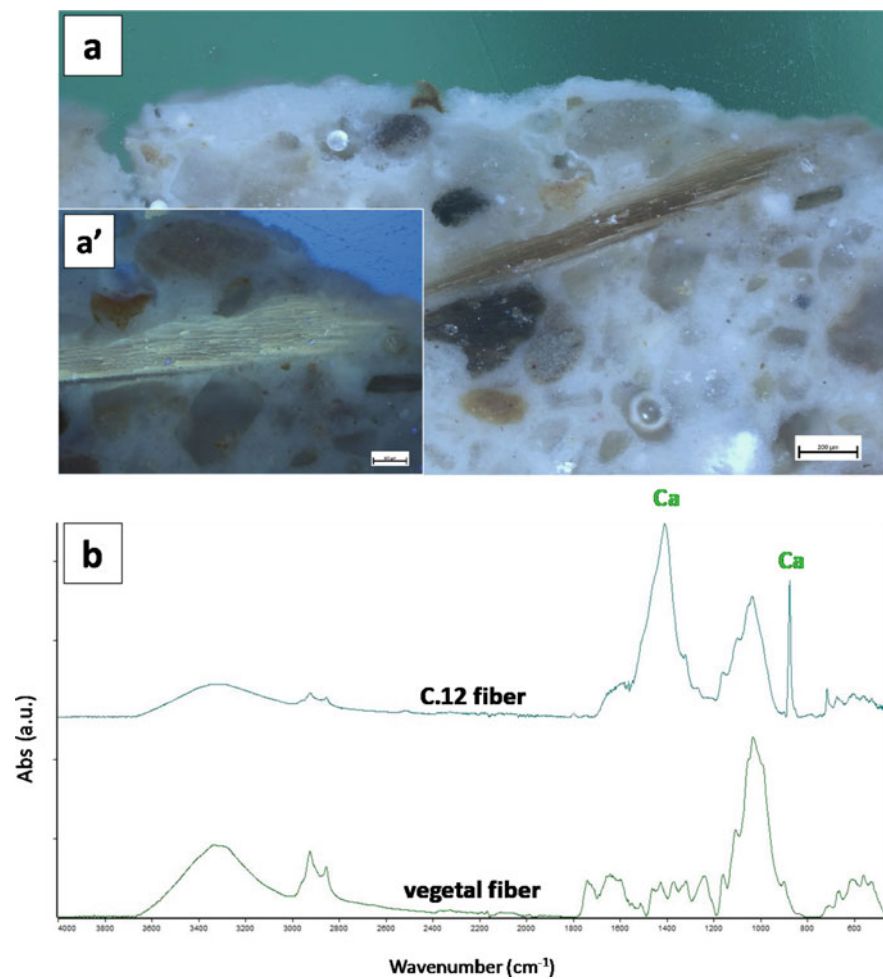
Fig. 13.6 Optical microscopy images—cross-section, 100x, reflected light mode **a**, UV light mode **a'**, and FT-IR spectra of the reinforcing fibers detected in the matrix **b** of sample C.12

of 0.2 mm). Above it, a succession of 4 white layers was detected, which are characterized by a homogeneous and dense texture without aggregates.

FT-IR spectra performed on these superficial layers (Fig. 13.7b) indicate a matrix mainly composed by calcium carbonate (711, 875, 1420 cm^{-1}). In addition, analogously to what was reported for sample C.6, oxalates were detected (516, 781, 1315, 1641 cm^{-1}), possibly indicating the employment of organic products [12–14] in occasion of potential restoring activities carried out after the date of monument construction.
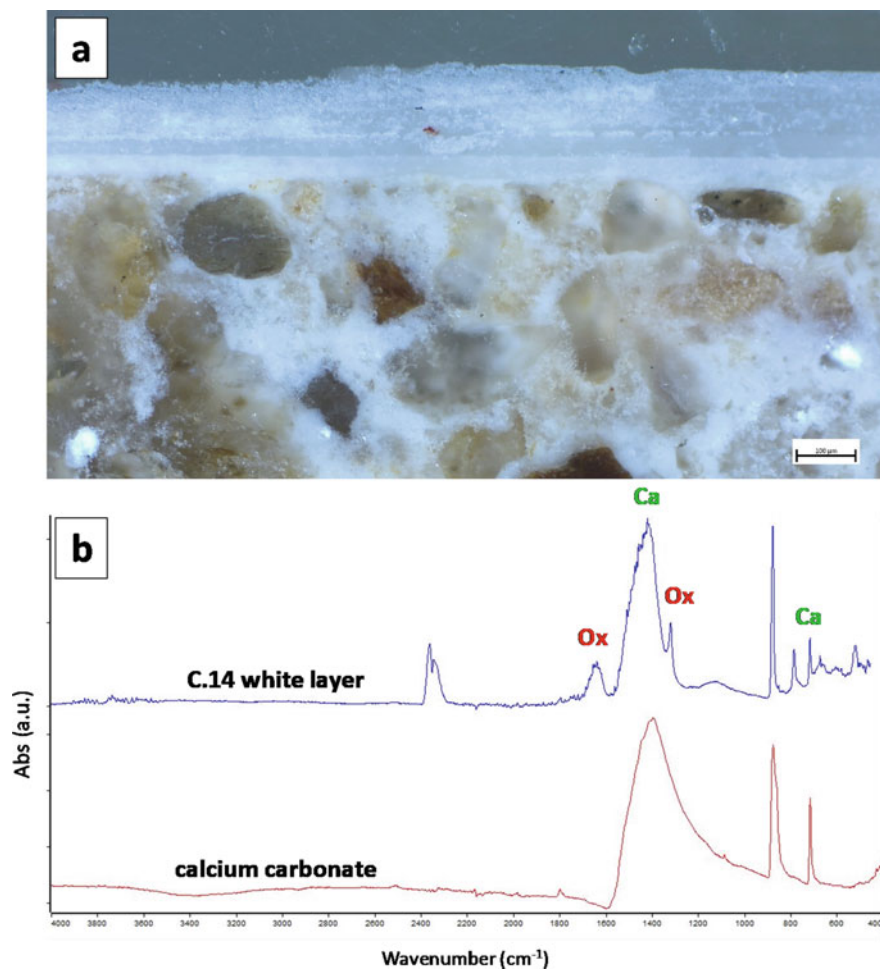
Fig. 13.7 Optical microscopy image **a** cross-section, 200x, reflected light mode, and FT-IR spectra of the white layers **b** of sample C.14

13.4   Conclusions

In the present paper, structural investigations on different materials and colored plasters of the historical Biblioteca Umanistica of the University of Florence were reported. Results were obtained through a multidisciplinary diagnostic plan, focused on structural investigations based on endoscopic and geophysical surveys, as well as microscopic and chemical stratigraphic characterizations of colored layers detected on the monument surfaces, by means of several analytical techniques.

Particularly, NDTs, performed on the monument areas, have allowed a complete mapping of the underground service network, by revealing the presence of interruptions and ruptures inside the implants, and detecting location and extension of infiltrations phenomena, giving valuable information on the state of preservation of the monumental construction. Moreover, microscopy and FT-IR investigations performed on colored plasters have evidenced a stratigraphic succession of layers placed on lime-based plaster binder, sometimes presenting reinforcing vegetal fibers. Finishing layers applied on substrate are mostly composed by calcium carbonate, while the analysis of a pictorial film discovered on a decorated vault lunette have revealed the use of green earth pigments, commonly used in Florence even before the Renaissance. In addition, the presence of oxalates was detected, possibly indicating the use of organic products as pictorial binders rather than restoring and maintenance activities performed over time.

The overall results have shown the importance and suitability of a multianalytical diagnostic approach by using structural and geophysical NDTs, as well as archaeometric analyses, in order to obtain accurate results and information useful at supporting future restoring and maintenance activities for the Biblioteca Umanistica of the University of Florence.

References

1. Camuffo D (1998) Microclimate for cultural heritage. Elsevier, The Netherlands, Amsterdam
2. Camuffo D, Fassina V, Havermans J (2010) Basic Environmental Mechanisms Affecting Cultural Herit. Nardini Ed, Firenze
3. Caliano E, Gallo C, Messuti N, Napoli C (2022) Colors, materials, and techniques in historical buildings in Rome: diagnostic investigations and case studies. In: Studies in conservation
4. Moropoulou A, Labropoulos KC, Delegou ET, Karoglou M, Bakolas A (2013) Non-destructive techniques as a tool for the protection of built cultural heritage. Constr Build Mater 48:1222–1239
5. Comite V, Ricca M, Ruffolo S, Graziano SF, Rovella N, Rispoli C, Gallo C, Randazzo L, Barca D, Cappelletti P, La Russa MF (2020) Multidisciplinary approach for evaluating the geochemical degradation of building stone related to pollution sources in the historical center of Naples (Italy). Appl Sci 10
6. Nencioni R, Savelli D (2008) Il chiostro degli Angeli: storia dell'antico monastero camaldolese di Santa Maria degli Angeli a Firenze. Polistampa ed, Firenze
7. Cricchio M (2014) Santa Maria degli Angeli a Firenze. L'evoluzione del monastero camaldolese attraverso la genesi dei suoi chiostri. Figure 2, Rivista della Scuola di Specializzazione in beni storico-artistici dell'università di Bologna, pp 47–55
8. Levi D'Ancona M, Dillon Bussi A (1994) The illuminators and illuminations of the choir books from Santa Maria degli Angeli and Santa Maria Nuova and their documents. Centro Di ed, Firenze
9. Levi D'Ancona M, Dillon Bussi A, Fantoni AR, Savelli D (1995) Corali del monastero di Santa Maria degli Angeli e le loro miniature asportate. Centro Di ed, Firenze
10. Montagna G (1993) I pigmenti. Nardini ed, Firenze
11. Puett SB, Puett JD (2016) Renaissance art and science at Florence. Truman State University Press, Kirksville, Missouri

12. Possenti E, Colombo C, Realini M, Song CL, Kazarian SG (2021) Insight into the effects of moisture and layer build-up on the formation of lead soaps using micro-ATR-FTIR spectroscopic imaging of complex painted stratigraphies. Anal Bioanal Chem 413:455–467
13. Del Monte M, Sabbioni C, Zappia G (1987) The origin of calcium oxalates on historical buildings, monuments and natural out-crops. Sci Total Environ 67:17–39
14. Russ J, Kaluarachchi WD, Drummond L, Edwards HGM (1999) The nature of a whewellite-rich rock crust associated with pictographs in southwestern Texas. J Stud Conserv 44(2):91–103
15. Dai D, Fan M (2010) Characteristic and performance of elementary hemp fibre. Mater Sci Appl 6(1):336–342
16. Jiang Y, Lawrence M, Hussain A, Ansell M, Walker P (2019) Comparative moisture and heat sorption properties of fibre and shiv derived from hemp and flax. Cellulose 26:823–843
17. Iucolano F, Liguori B, Colella C (2013) Fibre-reinforced lime-based mortars: a possible resource for ancient masonry restoration. Constr Build Mater 38:785–789

Chapter 14
Traditional or Innovative Systems for the Reproduction of Decorative Elements

Carlos José Abreu da Silva Costa and Marta Alexandre da Costa Frade

Abstract The reproduction of historical-artistic elements is a central reason for reflection during a conservation and restoration intervention, both from a technical and an ethical point of view. The solution and the replication system to be adopted can contribute to a more thoughtful and grounded decision from the standpoint of intervention criteria. The Jeronimo's Monastery, in Lisbon/Portugal—classified as a World Heritage Site by UNESCO and the most visited monument in the country—obliges by itself that all intervention processes show themselves to be reputable and judicious; the project to recover the decorative ceiling of the noble staircase was an important challenge, especially in relation to the reproduction of decorative elements in relieved stucco, which were absent and in need of replication. Traditional reproduction techniques such as wax molding were considered, and other innovative replication systems were tested, based on the use of numerous types of chemically inert composite materials, and when deciding on what to reproduce and how, all ethical precepts of conservation and restoration were guaranteed: compatibility, discernibility and reversibility.

Keywords Reproduction · Stuccoes · Replicas

C. J. A. da Silva Costa
Atelier Samthiago Manager, Braga, Portugal
e-mail: ccosta@samthiago.com

M. A. da Costa Frade (✉)
Faculdade de Belas-Artes, CentrodeInvestigaçãoEEstudosEmBelas-Artes, CIEBA, Largo da Academia Nacional de Belas-Artes, Universidade de Lisboa, 1249-058 Lisboa, Portugal
e-mail: m.frade@belasartes.ulisboa.pt; martacostafrade@gmail.com

Fig. 14.1 General view of the National Museum of Archeology

14.1 Reproduction of Decorative Elements—A Case Study

14.1.1 Introduction

The Jerónimos Monastery is currently one of the most important and visited monuments in Portugal. Classified as a UNESCO World Heritage Site, it periodically receives conservation interventions, and in many cases, urgent work is needed, given the nature and evolution of existing degradation pathologies. In 2020, by decision of the General Directorate of Cultural Heritage, there was a need to carry out a series of urgent works to resolve pathologies and minimize damage. The ensemble to be worked on needed complementary work in order to stabilizing essential visiting areas for the National Archeology Museum were: restoration of the ceiling of the noble staircase, consolidation of the detached surfaces of the vaults on the ground floor of the Museum's east wing, repair of walls and ceilings in the Bustorff Room and external overhaul work—coverings and facings (Figs. 14.1 and 14.2).

14.1.2 The Jerónimos Monastery and the Noble Staircase of the National Archeology Museum

The Jerónimos Monastery, built at the end of the fifteenth century by King Manuel I, is located in the city of Lisbon. It has been classified as a National Monument since 1907 and, in 1983, it was classified as a World Heritage Site by UNESCO. On the July 7, 2007, it was elected one of the seven wonders of Portugal and is today one of its most important tourist attractions, with approximately 1 million visitors each year.
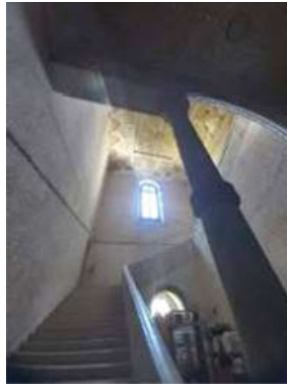
Fig. 14.2 General view of the access portal to the National Museum of Archeology and the staircase

The original plan followed the typical layout of a monastic house, including the church, cloister and outbuildings. What can still be found in Belém today preserves the essential aspects of the original design from the sixteenth century, being also a compilation of the numerous alterations and additions made in the following centuries, being outstanding of the remodeling carried out in the nineteenth century and which included the construction of the long neo-Manueline building to the west of the monastery, in the former monks' dormitory at the monastery. The National Archeology Museum has been installed here since 1903 (Fig. 14.3).

The museum's collection includes pieces from the founder and archaeologist Estácio da Veiga, pieces that came from State departments, as such the archeology collections of the former Portuguese royal house, incorporated after the establishment of the Republic in 1910, archeology collections from the former Museum of Fine Arts, and also by donation or legacy from collectors and friends of the museum. It should be noted that the museum has the largest concentration of goods classified as "National Treasure".

At the end of the nineteenth century and beginning of the twenty-first, several works were carried out throughout the monumental ensemble that would culminate in the great initiative of the Estado Novo, which was the Exhibition of the Portuguese World, in 1940. The "Noble Staircase", which at the center bears the coat of arms
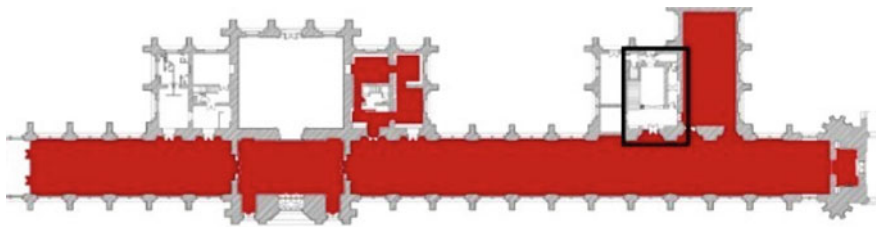
Fig. 14.3 Plan and location of the intervention site, at the National Archeology Museum

Fig. 14.4 Comparison of
other representations of the
Casa Pia coat of arms

of Casa Pia Children Institution, was possibly renovated at the end of the nineteenth
century, when this whole Wing of the Monastery was granted to that institution. In
1940, there was a project to play a central point and a reference point in welcoming
people to visit the great Exhibition of the Portuguese World. Throughout the span,
symbols of the new state proliferated, many of them were removed or destroyed
(Figs. 14.4, 14.5 and 14.6).

Fig. 14.5 Casa Pia coat of
arms
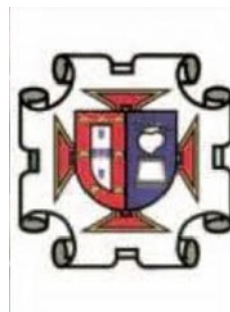
Fig. 14.6 Comparison of
other representations of the
Casa Pia coat of arms

14.1.3 The Intervention of Conservation and Restoration

This intervention to the urgent resolution of various pathologies, initially foresaw the resolution of problems related to infiltration in the staircase noble and in the Bustorff Room. Rooftops were revised, rainwater drainage systems unclogged and cleaned, walls and some window frames and spans were revised. Only by solving the origin of these problems, it would be possible to successfully complete the restoration interventions to be carried out in the interior, most of which are related to this same issue: the prolonged and systematic inflow of rainwater.

The relieved stucco ceiling was in a very poor state of conservation, with numerous detachment areas, gap areas, flaws in the stucco and areas with detachment of pictorial layer. There were also visible wetlands. There was an absence of crown molding at two different points on the ceiling, such as some of the finishing corbels. In that same zone where there is no coving, where there is an area of stucco gap, the inexistence of deliveries to the facings—which support the structural crankshafts of the roof and which in turn support the lath—were also missing.

In the other rooms that were interventioned, the problems were similar, also related to the presence of leaks and the consequent loss of support material (Figs. 14.7 and 14.8).

Once the anomalies and the origin of the pathologies had been resolved, it was important to restore the dignity and reading that this noble space in the building once have had. Cleaning work was carried out through the upper surface and the chromatic surface, structural reinforcement and support recovery work, and finally color and shape reintegration. Indeed, in a set, where three-dimensionality is central to the perception and reading of space, all the missing elements should be reproduced. Only in this way would it be possible to recover the historical and aesthetic potential

Fig. 14.7 Detailed view of some of the pathologies identified on the ceiling of the noble staircase and in other adjoining rooms

Fig. 14.8 Detailed view of one of the pathologies on the ceiling

of the space, trying to ensure its transmission and perception that would reflect something of its original aspect, despite being altered by the passage of time.

All the techniques and materials used were chosen taking into account their compatibility with the original objects, their stability over time and their reversibility, thus safeguarding the physical integrity of the original object. Therefore, there were chosen and used materials compatible with the original ones, which degraded as little as possible—either from a physical or a chemical point of view—and those that, more easily and in greater percentage, could come to be eliminated in the future without prejudice to the piece.

The procedures followed were elected, always having as a starting point that we are dealing with works that constitute a set and what was intended was a final work with a unitary and homogeneous character. All procedures followed the current parameters and deontological and professional codes of conservation and restoration.

14.2   The Reproduction of Decorative Stucco Elements

In the area of conservation and restoration of decorative plaster stuccoes, the conservator-restorer should have the utmost knowledge of the traditional techniques. This knowledge will allow to intervene properly in the asset and continue a *know-how* that is being lost. Currently, in the conservation and restoration of plaster stuccoes, the relevance of the use of traditional construction techniques allows us to raise the quality of the intervention. The awareness through this knowledge allows understanding the historical and artistic heritage "a world that stems from multiple encounters: from thinking, feeling and acting for the preservation of a memory" [1: 8].

14.2.1 The Relieved Stucco Ceiling and the Need to Reproduce New Elements

The ceiling of the noble staircase of the National Archaeological Museum, in the Jerónimos' Monastery, presented some volumetric gaps, both in terms of architectural decorative elements—warhead frames and small corbels (Figs. 14.9 and 14.10).

In this ceiling, the ornamentation was composed with geometric lines, straight, curved and mixed, drawing rhythmic subdivisions. In this example, the empty spaces were only filled by a smooth stucco. The small cordons, ornamented with acanthus leaves, hold the function of trim with the illusion of sustaining them. The straight frames that joined the cordons are decorated with balls. All these elements feature a decorative painting imitating stone.
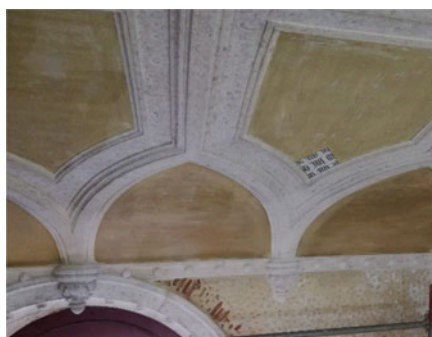
Fig. 14.9 Structure of the intervention roof

Fig. 14.10 Detailed view of the structure of the intervention roof, in noble staircase

14.2.2   Reproduction Techniques

> The mold is the presence of the absence of the form, the negative!
>
> (Frade [2]: p. 73)

In the area of conservation and restoration, molds are one of the fundamental processes for the return of reading and of stability of the work. Making a template through a fragment, or a unique element brings enough responsibilities to the conservative-restorative.

14.2.2.1   Reconstitution of Plain Elements

In the area of absence of support, we chose a traditional treatment (bare and mortar) and not resort to more contemporary methodologies such as plasterboard, which consists of a plate that does not exceed the thickness of one and a half centimeters, and is composed of plaster, sisal and bare. In rehabilitation, it turns out to be widely used because it is a lighter and cheaper solution. During the intervention, it was possible to identify the use of plasterboard of old restorations on a ceiling next to the staircase—see Fig. 14.12. However, where possible, the traditional process should be used (Fig. 14.11).

In this traditional process, the bar is placed perpendicular to the structural beam, supporting a layer of mortar (sketch), and finally, filled by a layer of smooth stucco (lime and plaster)—see Fig. 14.11.

All stucco gaps were filled, with traditional stucco, made with plaster stucco and lime in paste, as in larger areas. This traditional putty is used because the lime will allow it to be molded directly in place, delaying the plaster setting while the plaster sets, increasing its plasticity, consistency and resistance.

Fig. 14.11 Placement of the bar perpendicular to the main beam
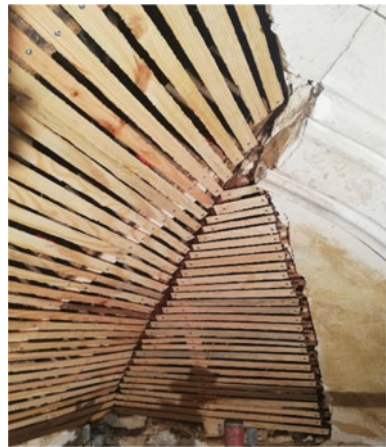
Fig. 14.12   Example of applying a plasterboard resulting from an old restore

Füller [3: p. 13] Thus, with the use of traditional masses, it is avoided the use of synthetic masses, as initially thought to use, in relation to the saved elements, these were replaced again—see Fig. 14.13.

The more original traces we leave, the more opportunities for future investigations will arise on the materials and techniques applied over time [4: p. 160].

Fig. 14.13   Elements saved from the warhead frame

Fig. 14.14 On the left a replica of the corbel and on the right the mold in beeswax

14.2.2.2   Reconstitution of Volumetric Elements

> Must respect the original as much as possible, in the art of making molds there must be consensus, and *common sense, of not having the abuse of substitution of originals.*
>
>   (Frade [2]: p. 74).

In areas, where there was a lack of volumetric elements, such as frames and corbel, they were reproduced through wax (corbel) and cércea (frames) molds.

The case of the cordons was adopted a traditional technique, the wax mold, because only a few replicas were needed. This mold, similar to gelatin, needs a component that gives it some plasticity such as glycerin (Fig. 14.14).

> The wax mold is carried out with beeswax, an ancient method, which the master plasterers still use. Through the heat the beeswax becomes liquid, with its cooling it gains a moldable consistency, becoming solid with the same cooling, gaining the shape of the ornament to be reproduced. (Samthiago® [5]: p. 22)

However, nowadays, the silicone mold is frequently chosen because, in the means of reproduction of replicas, we must be careful not to contaminate the original element. This silicone mold allows the execution to be made in situ, directly on the wall or ceiling, or through a detached piece and without the use of a release. In the event that the original element has been used to carry out the mold in another place*,* after the completion of the element, it must be returned to its place. Hence, the importance of not using a release.

> It is the mold maker's duty to choose the most appropriate method and product allowing for a complete reversibility and avoiding any contamination of the art work by product. Every material breathes and must be allowed to do so without obstruction. The life of an original depends on how it is treated. (Delpech and Figueres [6]: 26)

Fig. 14.15 Reinforcement in the decor back part, through metallic elements, for fixation on the wall

The silicone is made up of two components (within the percentages recommended by the supplier) and is poured, covering the entire original part, thus keeping all the details, including marks, signatures or fingerprints. In this work, because it is a roof, the silicone would have to be applied with a spatula, which requires that, in addition to the catalyst, we add a third element—the thixotropic—a thickening material that will allow the silicone to be placed vertically without draining. Once executed, the replicas were improved and cleaned. For its placement, the back part has been scratched just like the place to be applied and both moistened. For fixation, plaster-glue was used, and the ornament was immediately tightened to the support, then was cleaned all the excess that comes out by the sides of the piece. In the fixing of ornamental elements with some weight and protruding, in its back parts placed a reinforcement for the laying—see Fig. 14.15.

For geometric elements, as mentioned above, it was used the mold of cércea or commonly known as sliding mold; they are profiles that allow the realization of geometric elements such as frames—straight or circular, crown molding, balusters) [4: p. 78] for the realization of the gaps in the warhead's frames.

This mold consists of a cut-out and lime metal plate, "attached to the inside of a wooden box" [7: p. 12] that supports the zinc plate, is the same cut-out, but with a chamfer so that the zinc sheet is more protruding. This mold is run on a bench, in which "the mass of the plaster is put in its place until it reaches the height of the profile" [3: 69]—see Fig. 14.16.

Whether on a bench or on a wall or ceiling, when running the cércea mold there must always be a wooden board to serve as a guide.

Sometimes, in construction, we do not have the material indicated to carry out the mold of cércea with zinc plate or because the element to be reproduced does not require the realization of a complete mold. Thus, in point reproductions, we can replace it with dental wax plates demonstrating that the conservative-restorer must have spontaneity and creativity in the search for solutions [4: p. 211].

Fig. 14.16 Process of running a frame on a workbench. © Füller [3: 69]
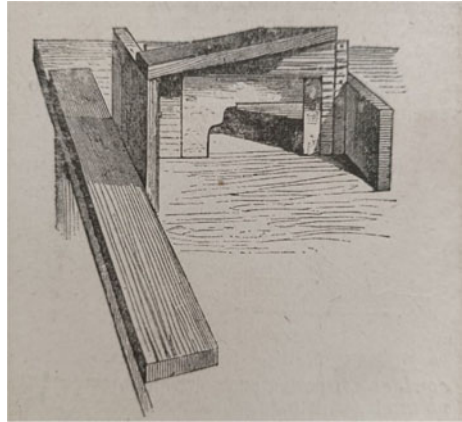
14.3 Conclusion

In the protection and safeguarding of heritage in plaster, it is emerging to preserve for the present generations and for the future this heritage of value and historical-artistic significance. This intervention preserved not only the material but also the immaterial heritage, the *know-how* that is being lost. The absence of this knowledge may put at risk the assets to be intervened.

In the choice to restore, the aesthetic unit of the decorative ceiling assembly was considered the traditional techniques as well as the use of material closer to the nature of the original, as there is greater compatibility and for having the same type of behavior as the original, always meeting the deontological code of conservation and restoration.

We guarantee the safeguarding of this heritage, whose conservation is legitimized due to its power to transmit information to an entire community and society, thus making it into a historical and scientific heritage.

References

1. Teixeira GB, Belém MC (1998) Diálogos de Edificação: estudos de técnicas tradicionais de construção. Centro Regional de Artes Tradicionais, Porto
2. Frade M (2016) A importância do ensino dos moldes na reabilitação, conservação e restauro de estuques decorativos em gesso—técnicas tradicionais e modernas. In: Matéria-Prima—Práticas Artísticas no Ensino Básico e Secundário
3. Füller J (s/d) Manual do Estucador e Formador. Colecção Biblioteca de Instrução Profissional, Dir. por Thomaz Bordallo
4. Frade M (2018) Conservação e Restauro de Escultura em Gesso. Valorização, metodologia, ensino, vol I. Lisboa

5. Samthiago® (2020) Museu Nacional de Arqueologia—conservação e restauro do teto da escadaria nobre e outros trabalhos urgentes—Direção Geral do Património Cultural. Relatório da intervenção realizada
6. Delpech J-P, Figueres M-A (2003) The Mouldmaker's handbook. A&C Black Publishers, London
7. Chavarria J (2000) Moldes. Coleção Aula de cerâmica. Editorial Estampa, Lda, Lisboa, p 12. ISBN 84-342-2217-5

Stone Material Assessment and Facades analysis

Chapter 15
System Integration for Masonry Quality Assessment: A Complete Solution Applied to Sonic Velocity Test on Historic Buildings

Irene Centauro ⓘ **, Sara Calandra** ⓘ **, Teresa Salvatici** ⓘ **, and Carlo Alberto Garzonio** ⓘ

Abstract The preservation of Built Cultural Heritage requires a careful diagnosis of the problems that characterize the historical masonries, through investigations aimed at assessing the quality of natural or artificial stone materials of which they are made. In particular, the diagnostics of masonry through Non-Destructive Techniques (NDT) is useful to deepen the knowledge of the construction characteristics, evaluate the state of conservation, and to monitor the effectiveness of the restoration interventions. Among the NDTs, the Sonic Velocity Test is largely used for evaluating the consistency of masonry and allowing the on-site identification of internal defects like fractures, voids, and detachments. The research involves the development of a complete management solution for the sonic measurements of different types of masonry and load-bearing elements. This solution consists of a website-based collaborative platform, a mobile/desktop application, and a reporting tool, which allows data processing from the on-site survey to their visualization and dissemination. The application of this system has been carried out by the LAM Laboratory of the Department of Earth Sciences (University of Florence) to evaluate the masonry quality in several historical civil and religious buildings and to improve the approach to diagnostics of Cultural Heritage.

I. Centauro (✉) · S. Calandra · T. Salvatici · C. A. Garzonio
Department of Earth Sciences, University of Florence, Florence, Italy
e-mail: irene.centauro@unifi.it

S. Calandra
e-mail: sara.calandra@unifi.it

T. Salvatici
e-mail: teresa.salvatici@unifi.it

C. A. Garzonio
e-mail: carloalberto.garzonio@unifi.it

S. Calandra
Department of Chemistry, University of Florence, Florence, Italy

15.1 Introduction

Historic buildings consist of different types of masonry, characterized by different materials and construction techniques, depending on their typology and use. A masonry is a highly differentiated system both for the constituent materials and for the construction technique; other determining factors are the time of realization, the geographical area, the economic and social conditions, and the function of the artifact [1–3].

Assessing the structure and texture of a historic masonry is a complex issue, and some mistakes can be made. For example, a wall that looks like regular outside can hide internal inhomogeneity; on the contrary, an irregular arrangement of the elements can instead correspond to a well-clamped masonry [4].

Due to this complexity of materials and construction characteristics, the use of the Non-Destructive Technique (NDT) Sonic Velocity Test (Fig. 15.1) allows inspecting in-depth the historical walls, identifying defects, inhomogeneity, and voids. Moreover, this test represents an important starting point to deepen the knowledge of the structures and direct further and targeted investigations and restoration interventions [5–9]. Because of its non-invasive features, depth of inspection, and ease of use, the sonic survey is particularly suitable for the investigation of cultural heritage. On-site diagnostic tests can also achieve the L2 level of knowledge required by Italian National Code (NTC 2018) [10, 11].
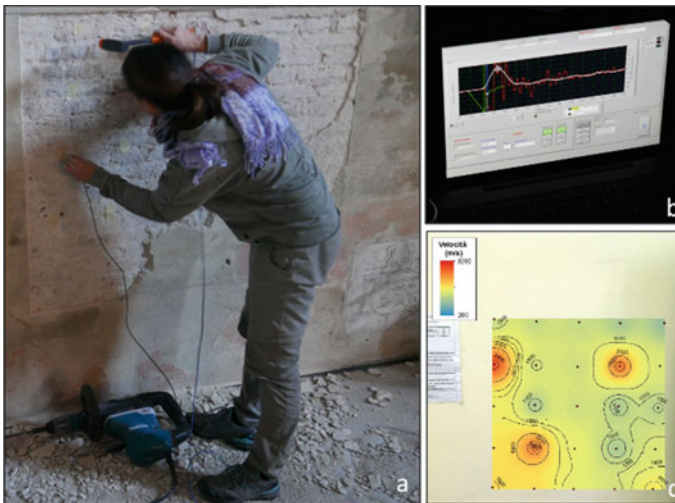
Fig. 15.1 Sonic Velocity Test: **a** on-site investigation, **b** diagram for time-of-flight analysis, **c** representation of velocity distribution through GIS software

However, to obtain useful and effective information, it is often necessary to adapt the survey method to the instrumentation features. Moreover, we also need to compare the velocity values with further investigations, so it is essential to standardize and optimize the data collection process [12, 13].

Because of the large amount and complexity of data on heritage buildings, the sustainable management of information requires a proper IT system that provides the means of collection, analysis, and manipulation of the Sonic Velocity Test results performed on masonry [14, 15].

A specific survey methodology, ranging from the on-site data entry to the dissemination of the results, which is scalable and repeatable over time, can represent an important support to the monitoring of the state of conservation of the structures. In addition, this solution can provide a critical contribution to the diagnostics of the Built Cultural Heritage.

15.2 Methods

15.2.1 Sonic Velocity Test Methodology

The Sonic Velocity Test exploits the propagation in the material of elastic compression waves generated by a short elasto-mechanical impact on the surface to investigate the condition of the material in its interior.

The propagation velocity of the waves is influenced by geometry and physical–mechanical characteristics of the material: lower values of velocity mean an increase in internal defects, voids, lower density, and thus a poor state of conservation of the investigated material.

The test involves the generation of elastic waves (hammer with a frequency range of 20 Hz–20 kHz) through a punctual mechanical impulse, which is read by an accelerometer. The measured value obtained in a Sonic Test is the time of flight, i.e., the time it takes the wave to pass through the sample. Starting from the time of flight (t) and the thickness of the material (L), velocity of the wave (v) can be measured (15.1).

$$v = L/t \tag{15.1}$$

The measurement methods can be of 3 modes (Fig. 15.2): direct transmission (in which hammer and accelerometer are placed on opposite faces), indirect transmission (in which hammer and accelerometer are placed on the same face), semi-direct transmission (in which hammer and accelerometer are placed on adjacent faces).

The Sonic Test is usually performed by direct transmission and was codified for surveys on concrete by ASTM in 1991 [16].
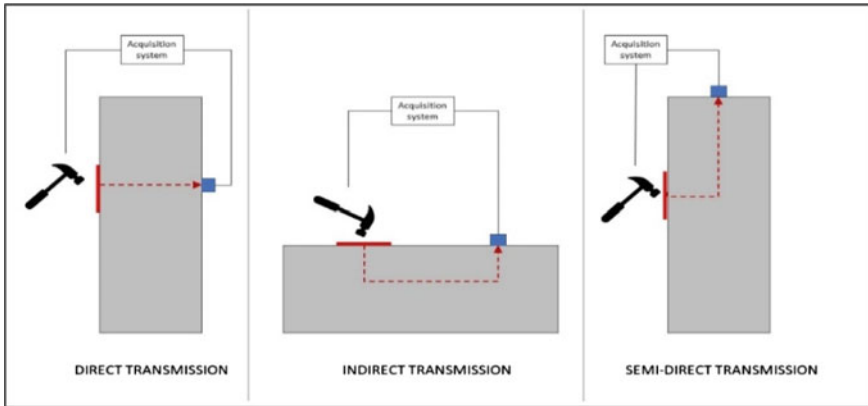
Fig. 15.2 Representation of the 3 different measurement methods for Sonic Velocity Test

For this work, the instrumentation used is Novasonic U5200 CSD of IMG Ultra-suoni Srl, consisting of a hammer with a load cell in the impact head, source of the acoustic wave; the time–amplitude function of the force applied in the impact is recorded through a detection system directly connected to the hammer.

15.2.2 Data Management System

Mechanical characterization of a masonry, according to the Italian seismic code, must be defined based on available data analysis, visual surveys, and on-site experimental investigations [17]. Sonic investigation involves the acquisition of numerous data; moreover, for a more in-depth knowledge of masonry, it is also advisable to collect information on materials, images, as well as the result of other investigations.

This large amount of information implies the need to make the data easily accessible and meaningful for analysis and monitoring purposes. Research must also focus on the integration and understanding of multi-analytical data, aimed at the re-use of knowledge [18]. In addition, leveraging mobile devices to create a portable lab represents a very interesting tool, even in the scientific field [19]. For this reason, a management system for data collection and analysis has been designed and set up for the LAM Laboratory of the Department of Earth Sciences of University of Florence. The data management system consists of 3 different tools to meet the need to develop a solution that compares a great variety of information:

- Website-based collaborative platform for sharing documents.
- Customized application for on-site data entry.
- Data visualization and analysis tool.

The first one is a customized private Microsoft SharePoint Website that allows storing, organizing, accessing, and sharing data and other contents managed by the research group. This platform hosts the survey campaign database and allows simultaneously working across different devices.

The mobile/desktop app has been built through a development platform for mobile and Web apps, adapting it to specific laboratory needs. The app is accessible both from a desktop workstation and from a mobile device (e.g., tablet or smartphone). An ontology-based data collection logic is effective for multi-field analysis of architectural heritage buildings [20], so data are collected according to a specific hierarchy (Fig. 15.3): campaign analysis/survey > sample/elements > specimen (if any). According to this logic, a unique ID is assigned for each record and level, to avoid duplicated or overwriting. Finally, the app allows the import of CSV files obtained from other tools or software to storage them properly in the system. The app uses the Microsoft Power Fx, which is an open-source programming language based on spreadsheet-like formulas. It is classified with the following paradigms: low-code, strongly typed, imperative, declarative, and functional [21].

Fig. 15.3 Data entry workflow scheme of the management system
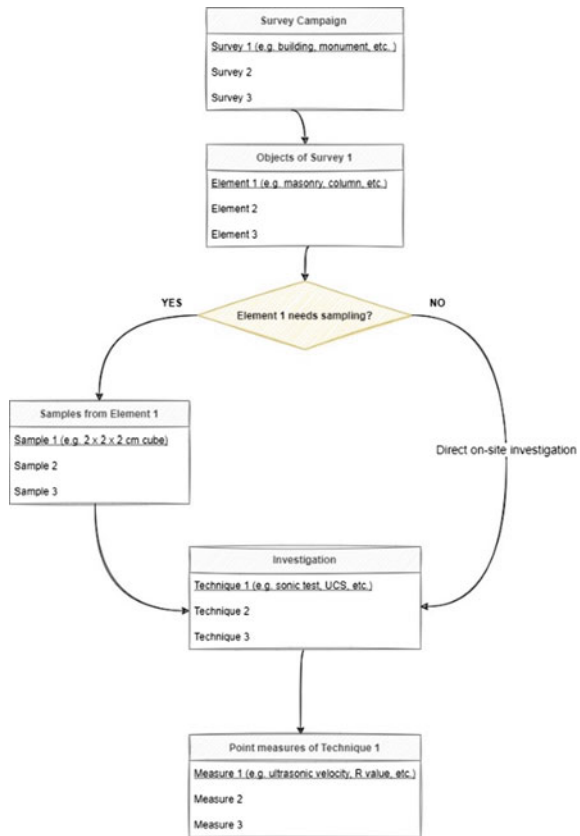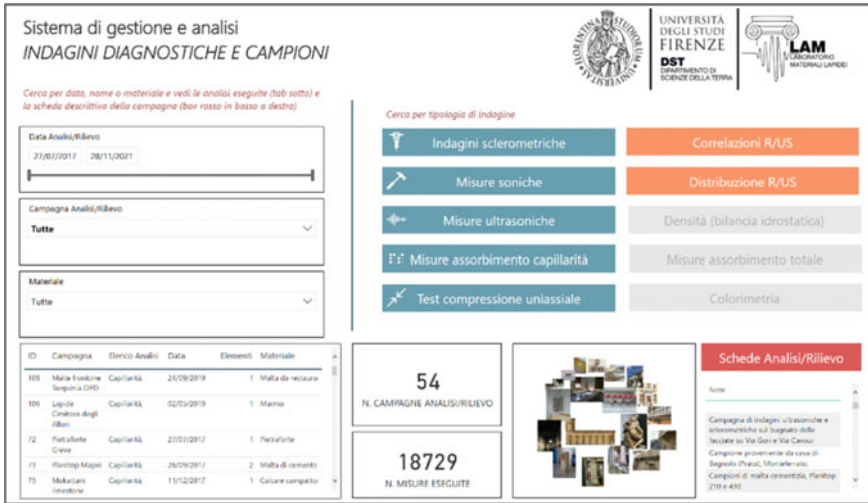
Fig. 15.4 Home page of the reporting tool of LAM laboratory

The reporting tool allows querying the collected data and generating reports consisting of maps, graphs, and interactive real-time dashboards (Fig. 15.4). Through this tool, it is possible to: harness data and gain insights, conduct an integrated analysis of surveys, quickly build graphs and reports, and share information. The reporting tool integrates several data languages including DAX, M, SQL, MDX, and R.

For the sonic measurements, a dedicated survey form has been developed (Fig. 15.5); the data entry procedure starts from the survey campaign section, which contains geographical and general information about the building.

One or more areas may be investigated for each survey campaign: information on the date of the survey, measurement method, and materials collected with images/photos automatically linked to that area.

Velocity data must be acquired according to a grid scheme, so the point measure names follow a row/column path, displayed as a table (e.g., A1, A2, etc.). For each point, the distance between hammer and accelerometer, in meter, and at least 3 ToF, in μs, are recorded; instantly, the ToFs are converted into seconds, and the velocity value in m/s, resulting from the average of 3 ToFs, is obtained. This calculated field automates the manual calculation operation and thus allows having useful information in real time.

Collected data can be immediately exported in tabular format (CSV or xls), for their subsequent processing, such as through GIS software, for the graphical representation of velocity distribution.

Moreover, the app makes it possible to insert one or more images (as well as other types of attachment) for each investigated area, either directly taking the photo or uploading it from an existing gallery.
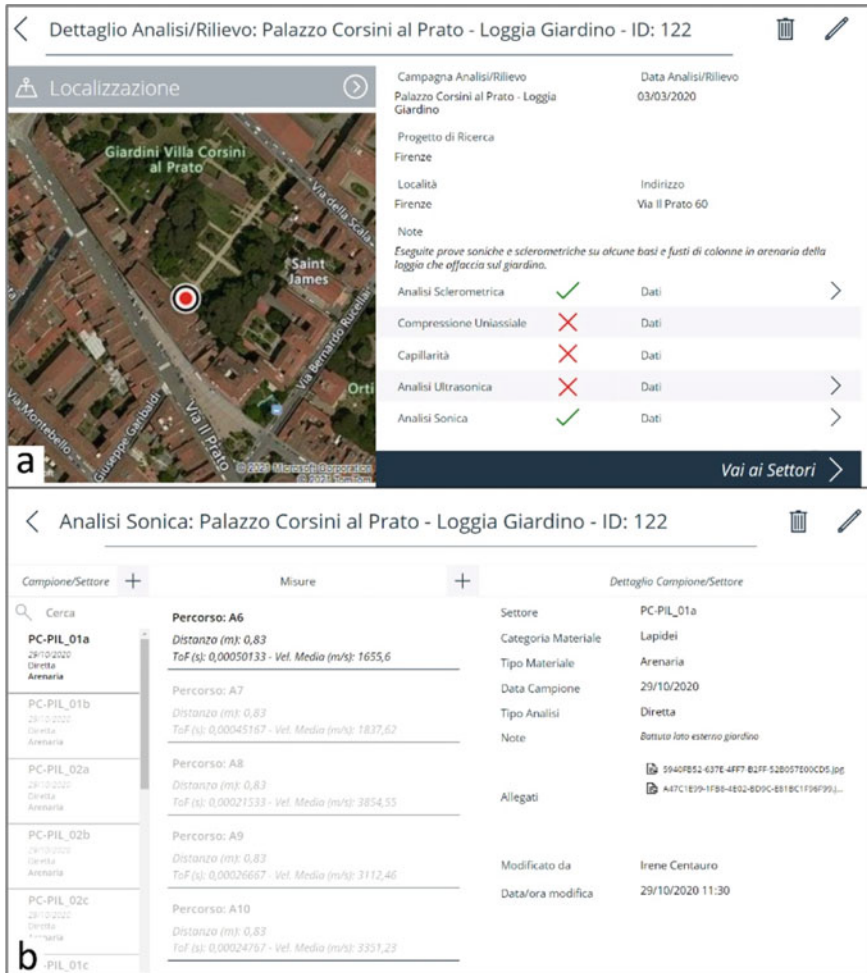
Fig. 15.5 Screenshots of the data entry app for Sonic Velocity Test: **a** the survey campaign form, **b** the sonic measurement form

Data can be immediately verified through interactive reports, thanks to real-time or daily scheduled updates. It is possible to query and filter information by date, type of survey, type of material, etc. It is also possible to display images or other elaborates next to the results table. Moreover, each cell of tables can be filled with a color scale, based on conditional formatting, to better highlight the different distribution of velocity.

By linking other information to each investigated material, such as mean reference velocity values, it is also possible to have a quick and useful comparison with the results obtained from the survey.

Whether other types of survey have been carried out on the same areas, these can be quickly compared with the sonic measurement, filtering them by the area name/ID.

A further advantage given by using this system is the easy dissemination of results, since the reports produced, and the related real-time updates can be shared externally through a simple link.

Finally, the data entry logic allows monitoring over time because it enables to compare areas with the same name/ID but different survey dates.

15.3 Experimental Campaigns

15.3.1 Case Studies/Investigation Procedures

The proposed methodology has been applied for the Sonic Velocity Test performed on different types of masonry. In this paper, we propose a representative selection of different cases:

- Indirect measurements on frescoed walls.
- Comparison of direct and indirect measurements on plastered mixed masonry.
- Direct measurements on stone columns.

For each case study, the velocity distribution tables of the interactive reports are compared with the maps obtained from data processing with GIS software. In GIS, the point values have been interpolated to provide a 2D false-color map of the velocity values distribution, according to the Spline function.

Indirect measurements on frescoes walls. Investigations have been conducted on different areas of frescoed masonry (dating XV century) of a church, in which the main need was to verify the adherence of the pictorial plaster to the substrate. The Sonic Tests have been performed on 4 sample areas of the frescoes, in correspondence with fractures of coating, infill masonry, and close to openings (doors, windows). These investigations aimed at assessing the state of consistency of the plaster coating, locating the possible presence of detachments, discontinuities, and voids. The test has been performed in indirect transmission, according to a horizontal measurement scheme. In addition to Sonic Velocity Tests, this investigation campaign also included pacometric tests, thermo-hygrometric measurements, and the determination of the absorption coefficient by the contact sponge method.

Comparison of direct and indirect measurements on plastered masonry. Investigations related to this survey campaign have been performed on 4 sample areas of 4 different internal walls (stone, brick, and mixed masonry) of an early XX century building, comparing the indirect and direct measurement. The survey aimed to evaluate the homogeneity of different walls and to assess the contribution of the

plaster coating in signal transmission. All areas have been investigated according to a horizontal measurement scheme.

Direct measurements on stone columns. Investigations have been carried out to verify the stability and safety of the 4 columns of a XVII century *loggia*. These analyzes provided for the integrated use of sonic and sclerometric NDTs to verify the physical–mechanical degradation of sandstone of which the columns are made. Both types of investigation have been performed on the same points, to achieve a correlation between the elocity values, that investigated the thickness of the structure, and the rebound index, that collected surface information. The columns, two of which were square, and the others were circular, were investigated in full thickness in direct mode regarding the sonic survey. Similarly, sclerometric test was performed on the entire surface development of the elements.

15.4   Results and Discussion

Indirect measurements on frescoed walls. The results obtained on one of the 4 analyzed areas are reported as an example (Fig. 15.6).
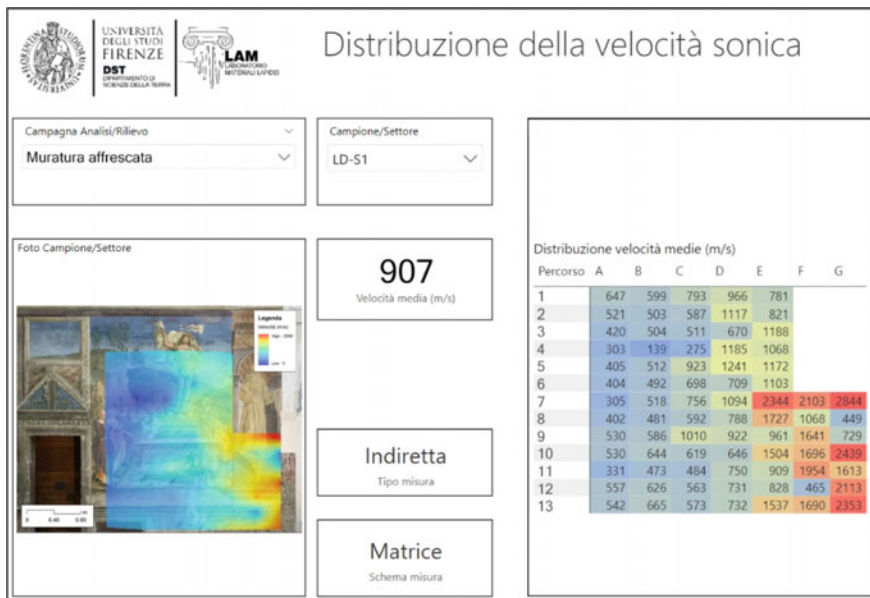
Fig. 15.6 Indirect measurements on frescoed walls. Interactive report page of the Sonic Test results obtained in a sample area, which made it possible to compare the table of the velocity values distribution with the interpolation map elaborated in GIS, attached to the record

The comparison between the color map and the results' table shows that the lowest velocity values are distributed on the left portion of the area, while in the right part, the values are higher. This separation is found in correspondence with a discontinuity in the cladding plaster under which there was an infill, near to a door.

The hygrometric measurements, following the same grid points used for sonic investigations, showed that the humidity of the plaster increases going down and toward the edge. This series of surveys thus show a partial detachment of the plaster layer and a different composition of the infill that constitutes the masonry apparatus in this area.

Comparison of direct and indirect measurements on plastered mixed masonry. The results obtained on one of the 4 analyzed areas are reported as an example (Fig. 15.7). The area corresponds to a brick masonry; comparing the results obtained in direct and indirect transmission, it emerges that two buffered holes are visible only through direct measurements. The velocity values obtained, excluding the two buffered holes, are comparable with the average values characteristic of regular masonry [8]. Furthermore, the velocity values obtained with the indirect measurements are lower than those obtained with the direct method, because only the surface part of the wall is investigated. These results are in line with the reference values for indirect tests conducted on a regular masonry [8].

Comparing the results obtained on brick and mixed walls has been observed that regular brick walls have higher mean velocity values than irregular mixed masonries. This result can be explained by the fact that mixed walls contain both stones that perform high velocity and parts consisting of bag mortar where the values are lower. In addition, solid brick walls have a regular texture and uniform structure, so velocity values are more homogeneous and higher than those obtained on mixed masonry.

Direct measurements on stone columns. The results obtained on one of the 4 sandstone columns investigated are reported as an example (Figs. 15.8 and 15.9). Sonic and sclerometric analyzes have been conducted to define the physical–mechanical degradation and the state of conservation of the sandstone. The comparison between the two investigations allowed a more accurate analysis of the decay phenomena.

Velocity values recorded on the stem are higher than those obtained on the base and comparable to the reference values for a regular stone wall measured in direct transmission [8]. In addition, from the comparison between the NDTs, widespread criticality emerged at the bases of columns: in particular, sonic investigations highlight areas of detachment of crusts and fractures even where the rebound values were good: this indicates the presence of inhomogeneity in deeper layers.
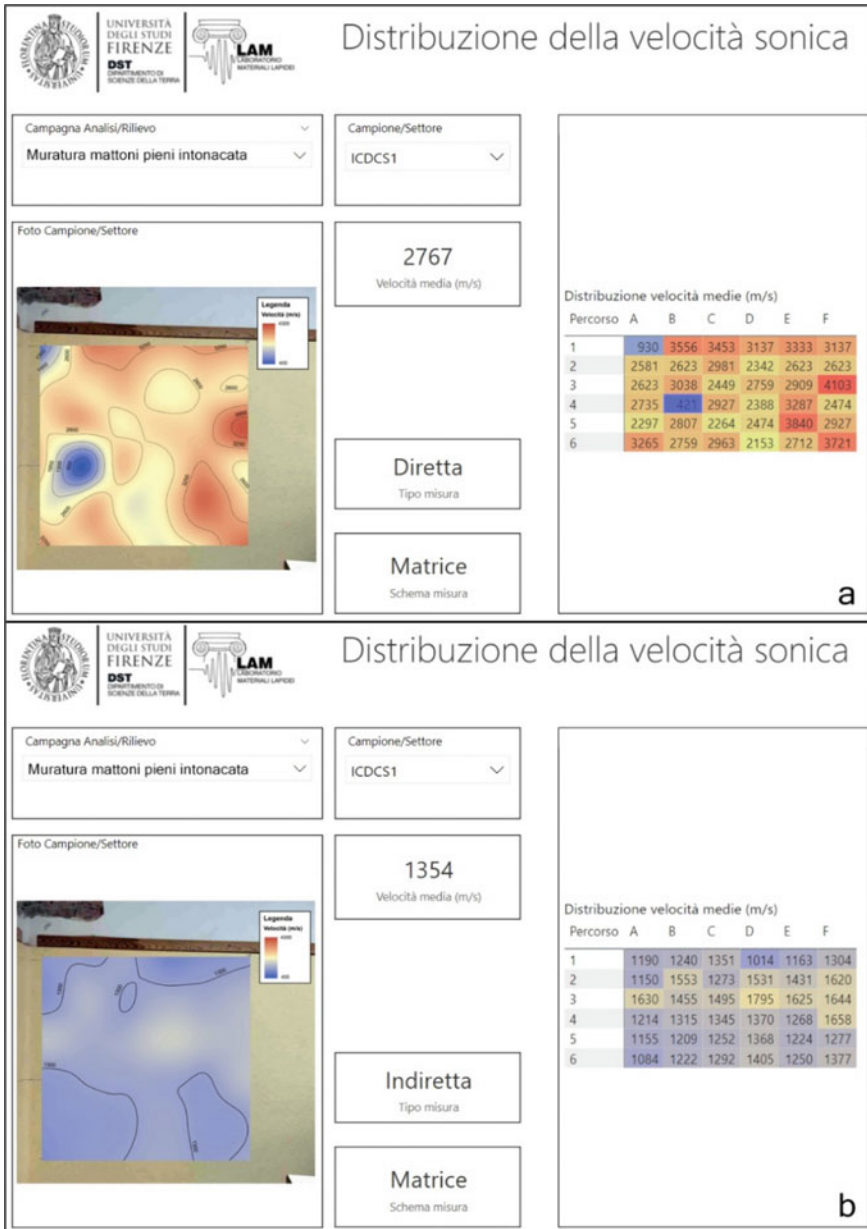
Fig. 15.7 Comparison of direct and indirect measurements on plastered mixed masonry. Interactive report page of the Sonic Test results obtained in a sample area, which made it possible to compare the table of the velocity values distribution with the interpolation map elaborated in GIS, attached to the record. The two buffered holes are visible only in direct transmission (a)
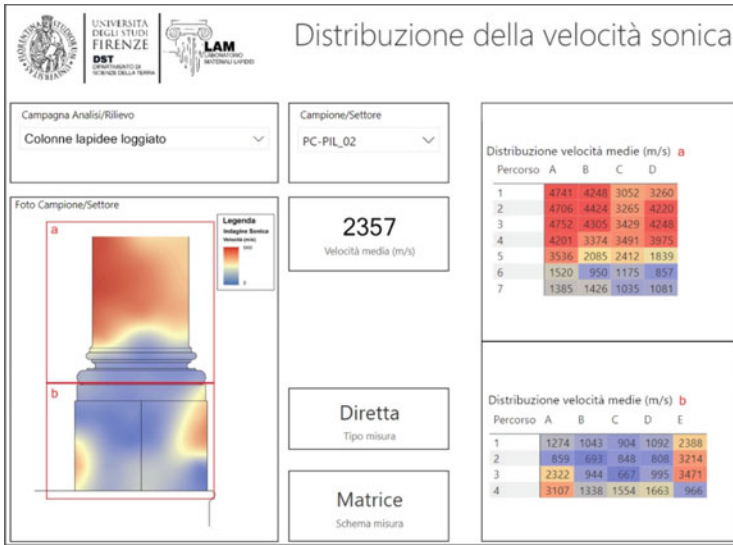
Fig. 15.8 Direct measurements on stone columns. Interactive report page of the Sonic Test results obtained in a sample area, which made it possible to compare the table of the velocity values distribution with the interpolation map elaborated in GIS, attached to the record. It is visible that the state of conservation of the base of column (b) is worse than the stem (a)
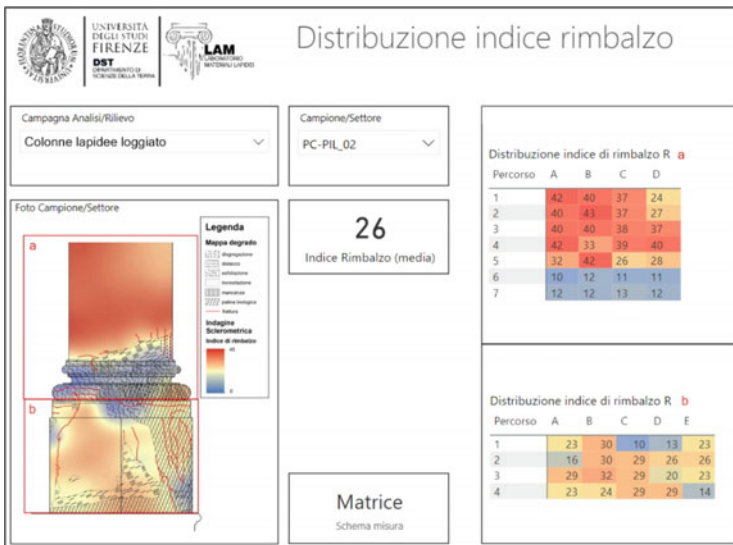
Fig. 15.9 Direct measurements on stone columns. Interactive report page of the sclerometric test results obtained in a sample area, which made it possible to compare the table of the rebound index distribution with the interpolation map elaborated in GIS, attached to the record. The base of the column has consistent crusts on the surface, which have good rebound index values, but are detached from the substrate, as emerged from the sonic investigations

15.5 Conclusions

Historical masonries are complex and heterogeneous elements and are often the result of a stratification of interventions over time. Their in-depth knowledge is essential for the safety of buildings and the protection of Cultural Heritage since a full understanding of the structural and material characteristics is required in conservation practice [13].

Sonic investigations represent a useful technique because it is not destructive and therefore respectful of the artifact, and because it provides a fundamental preliminary screening useful to better address further insights.

To be effective, however, measures must be conducted systematically and following a standard methodology, repeatable over time, suitable for different types of structures, and interoperable with other investigations.

The proposed methodology allows the standardization of the data entry workflow, and it is adaptable to different types of masonry; moreover, this system provides real-time verification of data, optimizes survey and analysis times, and reduces errors.

It has been successfully applied on 3 different case studies: frescoed walls, investigated in indirect transmission; plastered masonries with a comparison between direct and indirect transmission; stone columns, investigated in indirect transmission. This methodology has made it possible to highlight decay phenomena, such as plaster detachments and fractures, and to identify areas characterized by heterogeneous materials, such as infills or mixed walls.

This solution is also suitable for monitoring over time and allows the rapid dissemination of results. As a future development, the platform can be integrated with machine learning models for implementing forecasting processes analysis or for using clustering algorithms to better classify multidisciplinary data.

The solution presented is, therefore, a valuable contribution to the diagnostics of the Built Cultural Heritage.

References

1. Cardani G, Binda L (2013) Guidelines for the masonry quality evaluation in built heritage. In: Boriani M, Garabaglio R, Gulotta D (eds) BH2013-built heritage 2013 monitoring conservation management. Politecnico di Milano, Centro per la Conservazione e Valorizzazione dei Beni Culturali, pp 1–6
2. Giuffrè A (2000) Sicurezza e conservazione dei centri storici: il caso di Ortigia. 3rd edn. Laterza, Bari
3. Anzani A, Cardani G, Condoleo P, Garavaglia E, Saisi A, Tedeschi C, Tiraboschi C, Valluzzi MR (2018) Understanding of historical masonry for conservation approaches: the contribution of Prof. Luigia Binda to research advancement. Mater Struct 51(6):1–27
4. Binda L, Saisi A, Tiraboschi C (2000) Investigation procedures for the diagnosis of historic masonries. Constr Build Mater 14(4):199–233
5. Valluzzi M, Cescatti E, Cardani G, Cantini L, Zanzi L, Colla C, Casarin F (2018) Calibration of sonic pulse velocity tests for detection of variable conditions in masonry walls. Constr Build Mater 192:272–286

6. Cantini L (2016) The diagnostic investigations plan for historic masonry buildings: the role of sonic tests and other minor destructive technique. In: Modena C, Da Porto F, Valluzzi MR (eds) IB2MAC2016, 16th international brick and block masonry conference. CRC Press, London, pp 1469–1476

7. Binda L, Saisi A (2001) Application of NDTs to the diagnosis of historic structures. Non-destructive testing in civil engineering. NDT & E Int 34(2):123–138

8. Miranda L, Cantini L, Guedes J, Binda L, Costa A (2013) Applications of sonic tests to masonry elements: influence of joints on the propagation velocity of elastic waves. J Mater Civ Eng 25(6):667–682

9. Van Eldere H, Ramos LF, Verstrynge E, Shetty N, Van Balen K, Barroso CE, Oliveira DV (2019) The application of sonic testing on double-leaf historical Portuguese masonry to obtain morphology and mechanical properties. In: Aguilar R et al (eds) Structural analysis of historical constructions, RILEM book series, vol 18. Springer, Heidelberg, pp 661–668

10. Italian Ministry of infrastructures and transport (2018) DM 17/01/2018. Aggiornamento delle Norme tecniche per le costruzioni—NTC 2018

11. Italian Ministry of Cultural Heritage and Activities (2010) Circolare n. 26/2010. Linee guida per la valutazione e la riduzione del rischio sismico del patrimonio culturale con riferimento alle Norme tecniche per le costruzioni di cui al decreto del Ministero delle Infrastrutture e dei trasporti del 14 gennaio 2008

12. Binda L, Saisi A (2009) Knowledge of the building, on site investigation and connected problems. In: Cosenza E (ed) Eurocode 8 perspectives from the Italian standpoint workshop. Doppiavoce, Napoli, Italy, pp 213–224

13. ICOMOS (2003) International council on monuments and sites. Recommendations for the analysis, conservation, and structural restoration of architectural heritage

14. Tiano P, Tibaut A, Kaucic B, Jardim-Goncalves R, Panetto H (2019) Knowledge based IT platform for heritage buildings. In: Martins J (ed) Innovation in intelligent management of heritage buildings (i2MHB). pp 41–55. 978-953-8250-04-0. https://doi.org/10.1484/M.DEM-EB.5.118097. hal-02163685

15. Autiero F, De Martino G, Di Ludovico M, Prota A (2021) Structural assessment of ancient masonry structures: an experimental investigation on rubble stone masonry. Int J Archit Heritage

16. RILEM TC (1996) 127-MS.D.1: measurement of mechanical pulse velocity for masonry. Mater Struct 29:463–466

17. Marghella G, Marzo A, Carpani B, Indirli M, Formisano A (2016) Comparison between in situ experimental data and Italian code standard values. In: Brick and block masonry: trends, innovations and challenges—proceedings of the 16th international brick and block masonry conference (IBMAC 2016), Padova, Italy. pp 1707–1714

18. Cacciotti R (2015) Integrated knowledge-based tools for documenting and monitoring damages to built heritage. In: International archives of the photogrammetry, remote sensing and spatial information sciences. 25th international CIPA symposium, 31 August–04 September 2015, Taipei, Taiwan. ISPRS Archives, vol XL-5/W7, pp 57–63

19. Daffara C, Marchioro G, Ambrosini D (2019) Smartphone diagnostics for cultural heritage. In: Proceedings SPIE 11058, optics for arts, architecture, and archaeology VII, 110581K

20. Tibaut A, Kaucic B, Dvornik Perhavec D (2018) Ontology-based data collection for heritage buildings. In: Ioannides M (ed) Digital cultural heritage, LCNS, vol 10605. Springer, pp 65–78

21. Microsoft Power Fx source code. https://github.com/microsoft/Power-Fx. Last accessed 25 Mar 2022

Chapter 16
Characterization of XVI Century Wall Paint and Lime Mortar in the Façade of the Cathedral of Santo Domingo, Dominican Republic

Virginia Flores-Sasso [ID], **Esteban Prieto-Vicioso** [ID], **Letzai Ruiz-Valero** [ID], **Gabriela Fernández-Flores** [ID], **and Luis Prieto-Prieto**

Abstract The Cathedral of Santo Domingo (1521–1541), is the oldest in the New World. The main façade was finished in 1540 by Spanish builders from the Kingdom of Castile, Spain, built with Coralina limestone ashlars joined with lime mortar and as a finishing, color was applied directly to the stone, served as decoration and protection. Over time the color and the plaster has been lost, leaving few traces. For this reason, the aim of this research is to characterize a XVI century wall paint and lime mortar on the façade of Cathedral of Santo Domingo using Polarized Light Microscopy (PLM), Scanning Electron Microscopy/Energy Dispersive Analysis X-ray (SEM/EDX), and X-ray Diffraction (XRD). For this purpose, two micro samples were taken, one of paint and one of mortar. In conclusion four layers were found in the paint sample. Three of them were paint (orange, orange, and dark brown) and one is plastering mortar, which corresponds to the base (whitish). Regarding the mortar sample, it has a light beige in color and a microcrystalline texture with abundant porosity. It is composed mainly of calcite, with a small amount of gypsum.

V. Flores-Sasso (✉) · L. Ruiz-Valero · G. Fernández-Flores
Pontificia Universidad Católica Madre y Maestra (PUCMM), Santiago de los Caballeros, Dominican Republic
e-mail: virginiaflores@pucmm.edu.do

L. Ruiz-Valero
e-mail: letzairuiz@pucmm.edu.do

G. Fernández-Flores
e-mail: ga.fernandez@ce.pucmm.edu.do

E. Prieto-Vicioso
Universidad Nacional Pedro Henríquez Ureña (UNPHU), Santo Domingo, Dominican Republic
e-mail: eprieto@unphu.edu.do

L. Prieto-Prieto
Asociación Cultural Hornos de la Cal de Morón y Museo Cal de Morón, Seville, Spain

International Network for Traditional Building, Architecture and Urbanism (INTBAU), London, UK

16.1 Introduction

For the conservation of historical buildings, it is important to define each element with the purpose of preserving and protecting. There has been an interest in studying the pictorial coatings of historic buildings, especially the paintings on stone of artificial or anthropogenic origin, which were applied outside the buildings [1]. This characterization facilitates obtaining and recording important information on the repairs that the building has undergone throughout its life, as well as providing data on how to carry out a proper maintenance for the building conservation. For these reasons, the characterization of these elements is becoming increasingly important for the restoration of historic monuments [2, 3].

Duran et al. [4] studied Roman and Arabic wall paintings in the Patio de Banderas of Reales Alcazares' Palace of Seville (Spain) using non-destructive X-ray diffraction, scanning electron microscopy/energy dispersive analysis X-ray (SEM–EDX) and complementary techniques [4]. Torres et al. [5] carry out an analysis of the color of the Torres de Quart in Valencia (Spain), where the study of the physico-chemical composition of mortars and polychrome layers was carried out by X-ray diffraction (XRD), optical microscopy (OM), and scanning electron microscopy with X-ray energy dispersion microanalysis (SEM/XRE) [5]. Pelosi et al. [6], studied the painted silk panels of the Barberini Palace in Rome, where they used various techniques such as scanning electron microscopy (SEM), fourier-transform infrared spectroscopy, micro-Raman spectrometer, UV lighting, and among others [6].

Llopis et al. [7], studied the old town of Valencia (Spain) for chromatic image preservation, using a scanning electron microscope (for morphological study of the samples), and X-ray diffraction, and scanning electron microscopy with X-ray energy dispersion microanalysis (SEM/XRE) for mineralogical analysis of samples [7]. Garofano et al. [8], carry out a study that establishes the advantages and limitations of the combined use of portable UV–Vis equipment with fiber optics, fluorescence, and X-ray diffraction for the non-invasive characterization of the pigments of Roman wall paintings in Seville, Spain [8]. Auger and McLoughlin [9] conducted research on experimental and theoretical studies of perceptible discoloration of decorative paints composed of mixed pigments [9].

Gulzar and Burg [10] carried a preliminary research of late Mughal period wall paintings from historic monuments of Begumpura, Lahore, Pakistan using XRD and SEM–EDS to identify damage and understand the mechanisms to prevent it [10]. Taglieri et al. [11] studied a Byzantine fresco discovered in the rural monastery of Santa Maria del Rogato of the Dormitio Virginis from Sicily (Italy) using optical, polarization-fluorescence, electron microscopies, elemental analyzes, and X-ray diffraction [11].

Stamboliyska et al. [12] studied the altar wall paintings of "The Nativity of the Virgin" at Rila Monastery, Bulgaria by vibrational spectroscopic techniques complemented by EDX, XRD, and TGA analysis [12]. Also, Prieto et al. [13], carried out a study on the polychromies of the stone of the Gothic portal of the Cathedral of Santo Domingo, using a transmission polarized light microscopy (TPM), spectracopy fourier (FTIR), scanning electron microscopy/elemental Analysis elemental X-ray analysis (SEM/EDX), gas chromatography (GC), X-ray diffraction (XRD) and the Munsell color system [13]. Malletzidou et al. [14] carried out a research of wall painting which survives on the missing eastern part of mosaic composition in the interior of Rotunda, Thessaloniki, Greece using optical microscopy, fourier-transform infrared micro spectroscopy, scanning electron microscopy, X-ray diffractometry, and X-ray photoelectron spectroscopy [14].

For this reason, the aim of this research is to characterize an XVI century wall paint and lime mortar on the façade of the Cathedral of Santo Domingo by using three techniques: Polarized light microscopy (PLM), scanning electron microscopy/energy dispersive analysis X-ray (SEM/EDX), and X-ray diffraction (XRD).

16.2 Main Façade of the Cathedral of Santo Domingo

The Cathedral of Saint Mary of the Incarnation, known as Cathedral of Santo Domingo, is the oldest in the New World (1521–1541) and the most important colonial building in the city of Santo Domingo, Dominican Republic, declared by UNESCO World Heritage Site in 1990 [15]. Over time, the cathedral has undergone minimal interventions and modifications. However, is not protected from the progressive degradation and/or deterioration that all materials naturally suffer over time, due to the pollutants in the atmosphere and environment [16].

This cathedral is a Late Gothic church. Inside is a hall church, German *Hallenkirche*, or *Dreischiffige Kirche*, church with a nave and aisles approximately equal height. The three naves covered by stone vaults and the walls built of Coralina limestone, from the Santa Bárbara quarries, about 800 m from the Cathedral. It has fourteen side chapels located seven on each side between buttresses, a choir over the south door, a sacristy, a room for the ecclesiastical council located on the north portal and the bell tower on the base of the tower that was left unfinished. The Bass choir was demolished in 1877 [17].

The main façade is the most elaborate colonial façade in the Antilles (Fig. 16.1). It is oriented to the west following the astronomical criteria on which religious buildings of the time were created. It has a frontispiece framed by two pillars that act as abutments or buttresses which width is reduced, while advancing toward the front forming angles. These pillars are robust, have subdivisions with decorated fields on their different sides. In the first body there are niches that house the figures of the evangelists Saint Matthew, Saint Mark, Saint Luke, and Saint John, each with their corresponding canopies. In the second body, there are two niches, where are Saint Peter and Saint Paul [18]. In the center, at the top of the facade, is the coat of arms

Fig. 16.1 View of the main façade of the Cathedral (2019)

of Emperor Charles V of Germany and I of Spain, and to the right is a representation of the Pillars of Hercules and to the left of the Golden Toison.

The entrance has flared arches or ox-horns, decorated inside with carved coffers with floral motifs and other objects such as chalices and candlesticks, among others. Above these arches and horizontally crossing the entire area, the entablature composed of the architrave, frieze, and cornice is placed, suspended over the pilasters in which the façade is framed. The triangle that finishes off the cover replaces the pediment. The frieze is completely carved with human figures (Cupid), puttis, zoomorphic, grotesques, floral shapes, and objects such as fountains and flamer and intertwined with branches. In its center, it has a medallion with a Minerva's face [14, 17].

16.3 Materials and Methods

To carry out this investigation, two micro samples were taken on October 29th, 2019, from the main façade of the Cathedral of Santo Domingo, one of paint and the other one of mortar. A series of in laboratory studies were carried out: Polarized light microscopy (PLM), scanning electron microscopy/energy dispersive analysis X-ray (SEM/EDX), and X-ray diffraction (XRD).

16.3.1 Polarized Light Microscopy (PLM)

This analysis was performed with optical microscopy and polarized light, incident, and transmitted light were used. Halogen light and UV light, using the OLYMPUS BX41 Optical Microscope with attached camera and MPlan 10X/0.30 [19].

16.3.2 Scanning Electron Microscopy/Energy Dispersive Analysis X-ray (SEM/EDX)

The scanning electron microscope is a flexible, general purpose, and simple-to-use instrument that can be operated in either regular high-vacuum or low-vacuum modes, enabling users to image a wide variety of samples [20]. The FEI Quanta 200 scanning electron microscope was used to make this analysis. Operated in low vacuum with a pressure of 30 Pa with acceleration voltage of 22 kV-Oxford Instruments.

16.3.3 X-ray Diffraction (XRD)

The samples are analyzed by X-ray diffraction (powder method) to obtain the characterization and the semi-quantitative relationship of the mineralogical phases of the sample. XRD analysis are carried out using a Philips PW 1830 diffractometer, with copper (Cu) cathode with wavelength $K\alpha = 1.54051$ Å. The angular scan was recorded from 3° to 65° 2θ with a Philips PW 1710 digital recorder. The diffractogram obtained from the samples was studied with the X Powder software, version 2017 for both qualitative and quantitative analysis [21].

16.4 Results and Discussion

16.4.1 Polarized Light Microscopy (PLM)

In Fig. 16.2a an image of the cross-section of the paint micro-sample is shown. While in Fig. 16.2b the image obtained with the optical microscope of the cross section illuminated with UV light is presented. The numerical order indicated in Fig. 16.2 is the one that appears in Table 16.1.

Table 16.1 demonstrates the different layers found in the paint micro-sample. Its color, width, pigments, weight, and observations.

In the case of the mortar sample (Fig. 16.3), it has a light beige color and is easily disintegrable. It has a crystal, like texture with a vast porosity.
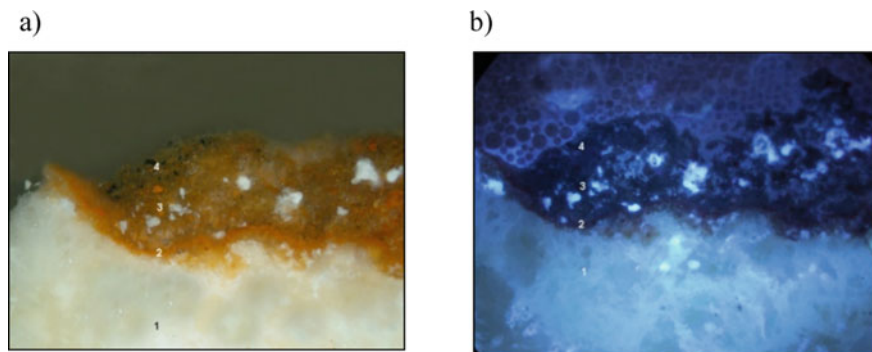
Fig. 16.2 **a** Image of micro-sample under the light microscope, **b** image of microsample under the light microscope illuminated with UV light

Table 16.1 Characteristics of reference paint layer from microsample

Layer	Color	Thickness (µm)	Pigments	Comments
4	Dark brown	10–60	Gypsum, red earth pigments, bone black	Paint layer
3	Orange	20–90	Gypsum, red earth pigments	Paint layer
2	Orange	≈20	Gypsum, red earth pigments, bone black (v. l. p.), shade earth pigments	Paint layer
1	White	>500	Calcium carbonate, silicates	Mortar
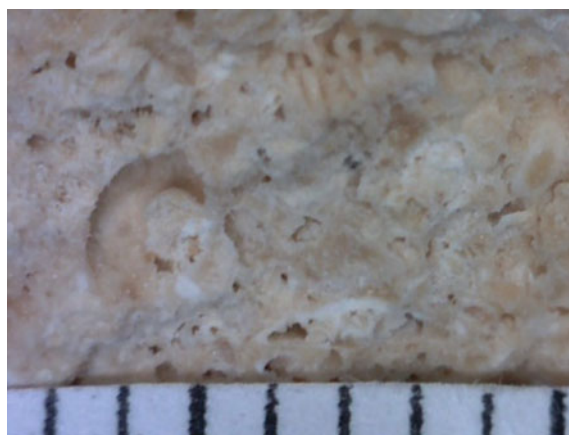
Fig. 16.3 Image of the mortar microsample with microscope

16.4.2 Scanning Electron Microscopy/Energy Dispersive Analysis X-ray (SEM/EDX)

Figure 16.4a shows the image obtained with a scanning electron microscope with a backscattered electron detector (BSE—Back Scatter Electron) (100X) of the cross section of the paint microsample. The numerical order indicated is that which appears in Table 16.1. Figure 16.4b–f presents the EDX spectrum obtained from the analysis carried out on each of the layers of the paint microsample.

a) microscope

b) Layer 1

c) Layer 2

d) Grain of paint micro-sample

e) Layer 3
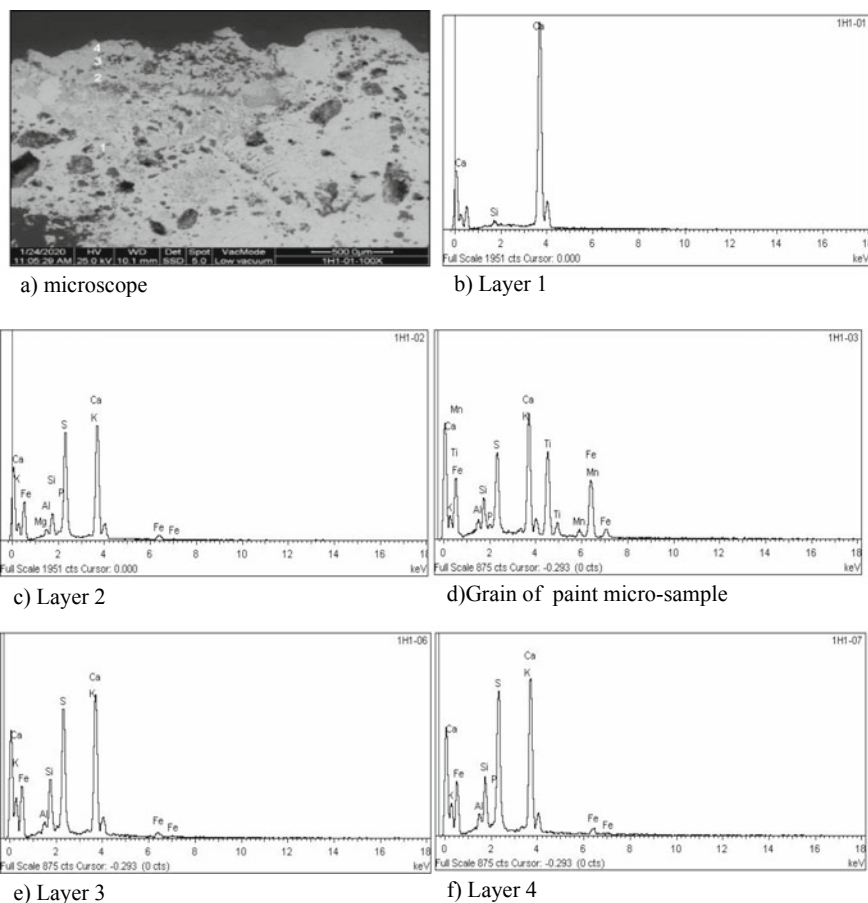
f) Layer 4

Fig. 16.4 a Image of the paint micro-sample obtained with the SEM; **b** EDX of layer 1; **c–f** EDX spectrum of the sample
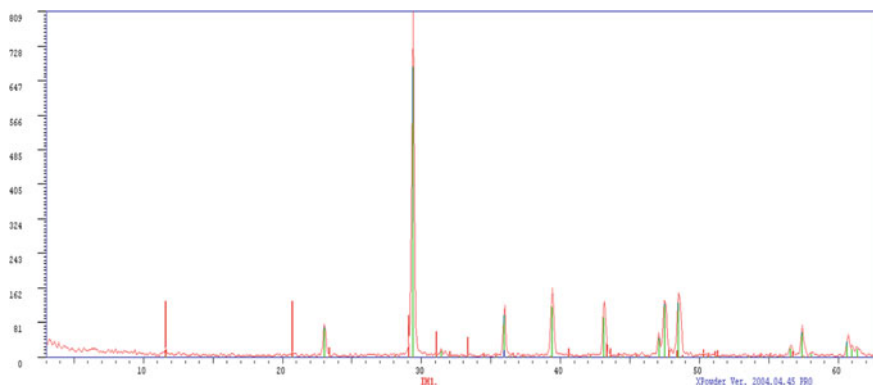
Fig. 16.5 XRD of the mortar microsample

16.4.3 X-ray Diffraction (XRD)

The mortar sample is mainly composed of calcite (99.0%), with a small amount of gypsum (1.0%) (Fig. 16.5).

16.5 Discussion

The base or plastering mortar is in contact with the stone, without the thin layer that plasters placed as repairs which are usually present. The hypothesis of an original mortar can be made. Its calcite composition indicates that the aggregate used is calcareous. Its formula is approximately one limestone, three calcareous aggregates, this data is difficult to determine because it has impalpable calcareous, and the carbonation is perfect. Parts of the lime paste turned into limestone. Lime used was lime paste, due to the presence of microcrystals (only lime has them).

On the other hand, it does not react with phenolphthalein, this implies that carbonation is perfect. The presence of gypsum in 1% can be due to several factors: contamination by CO_2 and sulfur alters the lime, transforming it into plaster, in any case the alteration is very low by comparing samples from other buildings (in Spain); the natural presence of gypsum in limestone is common; a small addiction, current in places of strong wind, to retain moisture and aid carbonation. With this proportion of 1% it would be sufficient and safe.

The porosity that it presents can be due to various factors: the original stone, there are limestone stones and mortars that can be very porous or less porous depending on the origin of the stone and the construction needs, a porous mortar evaporates water better and is usually more elastic; or the gradual dissolution of the softer parts of the mortar by the action of atmospheric agents, rain.

The colors used are natural earth, washed and grounded, ocher, reddish, and orange. Probably local minerals. In this case, the presence of yeso is not due to the presence of lime that it does not contain, but rather it is an addiction. Note that there is not a low proportion, nor a very low proportion, that is, the presence is greater. No organic binder has been found. The presence of plaster may be due to the following hypotheses: adulteration, historically very common; use it as an esthetic factor to mute the color, unlikely given that they have used the fresco technique; or natural pollution, but more comparative studies are needed from other places.

The technique used is fresco painting, probably mixing the pigments with lime water and patinated or aged with shadow earth and bone (a very low proportion is sufficient in these colors).

16.6   Conclusions

To characterize an XVI century wall paint and lime mortar on the façade of the Cathedral of Santo Domingo, the following analyzes were carried out: Polarized light microscopy (PLM), scanning electron microscopy/energy dispersive X-ray analysis (SEM/EDX), and X-ray diffraction (XRD). All these studies were carried out on microsamples of paint and mortar.

Four layers were identified in this research. The most superficial layer is ochre dark brown, followed by two more layers, one reddish and the other orange. The last one is a beige layer that corresponds to mortar as base material, which is in direct contact with the stone, without the thin layer that is usually present in renders placed as a repair, which is why we believe it to be the original mortar. The colored layers are natural earths, washed and ground. They are probably local earths, which could be located to reproduce the colors in the future restorations. Gypsum is present in the paintings, but in this case the gypsum is not due to the presence of lime, which it does not contain, but is an additive. No organic binder has been found.

The technique used is fresco painting, probably by mixing the pigments with lime water and patinated or aged with shadow earth and bone black (m.b.p. is sufficient in these colors).

The mortar has a microcrystalline texture with abundant porosity due to the lime used, which came from the Coralina limestone. The presence of 1% gypsum may be due to CO_2 and sulfur contamination which alters the lime transforming it into gypsum. The mortar is the original and is composed of fat lime and calcareous sand, painted and patinated al fresco. Of porous origin and deteriorated by atmospheric agents. It is assumed that it was made as a protector of natural stone, with a high aesthetic character.

Original mortar of fatty lime and calcareous sand painted and patinated in fresco. Porous in origin and deteriorated by atmospheric agents. It was probably made to protect the natural stone, with a high aesthetic character.

References

1. Flores Sasso V, Ruiz Valero L, Pérez Alvarez G, Frutos Vázquez B, Prieto Vicioso E, Martín-Consuegra F (2018) Determining the patina colors applied UV-VIS-NIR spectroscopy and Munsell systems in the main facade of the Cathedral of Santo Domingo, Dominican Republic. In: REHABEND 2018. Construction pathology, rehabilitation technology and heritage management, Cáceres, Spain

2. Garcia-Codoñer A, Llopis Verdú J, Torres Barchino A, Villaplana Guillén R, Serra Lluch J (2009) Colour as a structural variable of historical urban form. COLOR Res Appl 34:3

3. Barone G, La Russa M, Lo Giudice A, Mazzoleni P, Pezzino A (2008) The Cathedral of S. Giorgio in Ragusa Ibla (Italy): characterization of construction materials and their chromatic alteration. Environ Geol 55:499–504

4. Duran A, Perez-Rodriguez JL, Jimenez de Haro MC, Franquelo ML, Robador MD (2011) Analytical study of Roman and Arabic wall paintings in the Patio De Banderas of Reales Alcazares' Palace using non-destructive XRD/XRF and complementary techniques. J Archaeol Sci 38(9):2366–2377

5. Torres A, Serra J, Llopis J, Higón JL, García A, Sáiz B (2012) Análisis del color y el soleamiento en las Torres de Quart de Valencia (España). Inf Constr 64(527):261–274

6. Pelosi C, Falletta G, De Dominicis B, Baraldi P (2013) The painted silk panels of Palazzo Barberini at Rome. The scientific investigation and preservation challenge. Procedia Chem 8:248–257

7. Llopis et al (2015) The preservation of the chromatic image of historical cities as a cultural value. The old city of Valencia (Spain). J Cult Heritage 16(5):611–622

8. Garofano I, Perez-Rodriguez JL, Robador MD, Duran A (2016) An innovative combination of non-invasive UV–visible-FORS, XRDand XRF techniques to study Roman wall paintings from Seville, Spain. J Cult Heritage 22:1028–1039

9. Auger JC, McLoughlin D (2017) Experimental and theoretical studies of perceptible color fading of decorative paints consisting of mixed pigments. J Quant Spectrosc Radiat Transfer 187:322–332

10. Gulzar S, Burg JP (2018) Preliminary investigation of late Mughal period wall paintings from historic monuments of Begumpura, Lahore. Front Architectural Res 7:465–472

11. Taglieri G, Rigaglia D, Arrizza L, Daniele V, Macera L, Rosatelli G, Romè V, Musolino G (2019) Microanalytical investigations on a Byzantine fresco of the Dormitio Virginis from Sicily. J Cult Herit 40:155–162

12. Stamboliyska B, Tapanov S, Velcheva E, Yancheva D, Rogozherov M, Glavcheva Z, Lalev G, Dimitrov M (2020) The Altar wall paintings of the Catholicon "The nativity of the virgin", Rila Monastery, Bulgaria: identification of the painting materials by means of vibrational spectroscopic techniques complemented by EDX, XRD and TGA analysis. Spectrochim Acta Part A Mol Biomol Spectrosc 247:119087

13. Prieto Vicioso E, Flores Sasso V, Ruiz Valero L, García de Miguel JM (2020) The colour of architecture. Physical-chemical análisis of polychomy on stone in a 16th century gothic Portal at the Cathedral of Santo Domingo. In: International conference Florence Heri-Tech. The Future of Heritage Science and Technologies, Florence, Italy

14. Malletzidou L, Zorba TT, Kyranoudi M, Mastora P, Karfaridis D, Vourlias G, Pavlidou E, Paraskevopoulos KM (2021) The dome of Rotunda in Thessaloniki: investigation of a multi-pictorial phase wall painting through analytical methods. Spectrochim Acta Part A Mol Biomol Spectrosc 262:120101

15. Pérez-Cuevas J, Flores-Sasso V, Prieto-Vicioso E, Ruiz-Valero L, Senén S (2021) Application of geophysical prospecting methods for soil structure characterization of the cathedral of Santo Domingo, Dominican Republic. In: Roca P, Pelà L, Molins C (eds) 12th international conference on structural analysis of historical constructions SAHC 2020, Barcelona, Spain

16. Prieto Vicioso E (2011) Restauración, en "Basílica Catedral de Santo Domingo". Patronato de la Ciudad Colonial de Santo Domingo, Centro de Altos Estudios Humanísticos y del Idioma Español, Coeditor, Editora Amiga del Hogar, Santo Domingo, Dominican Republic

17. Flores Sasso V, Prieto Vicioso E (2016) Estudio de los Materiales Constructivos de La Catedral de Santo Domingo, Primada De América. In: REHABEND 2016. Construction pathology, rehabilitation technology and heritage management, 6th REHABEND, Burgos, Spain

18. Flores Sasso V, Prieto Vicioso E (1992) El modelo Hallemkirche o iglesia salón en el reino de Castilla de Ultramar. La Catedral de Santo Domingo. In: Obra Congrua, 1416. 500 Aniversario de la consulta de la Catedral de Girona, Universidad de Girona, Departamento de Arquitectura e Ingeniería de la Construcción, Colegio de Aparejadores, Arquitectos Técnicos e Ingenieros de la Edificación de Girona, 2017, p 183

19. Olympus. https://www.olympus-lifescience.com/en/microscopes/upright/bx43/, last accessed 2021/10/26

20. The Ohio State University. Center for Electron Microscopy and Analysis (CEMAS). https://cemas.osu.edu/capabilities/quanta-200-sem-formerly-produced-fei, last accessed 2021/10/29

21. Martin JD (2008) XPowder. A software package for powder X-ray diffraction analysis. Qualitative, quantitative and micro texture. User guide

Chapter 17
Laboratory and In Situ Control of Cleaning Techniques and Solutions Performed on Stone Façade of the Serbian National Theatre Building

Snežana Vučetić , **John Milan van der Bergh** , **Helena Hiršenberger** , **Bojan Miljević** , **Jonjaua Ranogajec** , **Ana Tomić** , **and Maria Tzoutzouli Malešević**

Abstract The aim of this paper is to show the holistic process of diagnosing issues on the façade of the Serbian National Theatre building which was used to make recommendations for subsequent cleaning and protection works done in 2021. The building of the Serbian National Theatre (Serbian: Srpsko narodno pozorište) is located in the city of Novi Sad, the cultural and administrative centre of Vojvodina, the northern Serbian autonomous province. The new theatre building was built in 1981, and apart from several ad hoc interventions on the façade of the building, for over 40 years no comprehensive cleaning had been done and there had been no consolidation or protection works on the delicate white stone. The Laboratory for Materials in Cultural Heritage was trusted with the task of preforming holistic characterisation of the façade stone, detecting deterioration mechanisms and proposing adequate conservation methodology. The laboratory's mobile equipment with non-destructive techniques and laboratory assessment enabled the complete analysis of the façade materials. Following the analysis of the obtained results, recommendation was made in which techniques and agents had to be used for the façade cleaning, ensuring good aesthetic and microstructural compatibility.

Keywords Stone façade · Marble · Cleaning · Protection · In situ

S. Vučetić (✉) · J. M. van der Bergh · H. Hiršenberger · B. Miljević · J. Ranogajec
Laboratory for Materials in Cultural Heritage, Faculty of Technology, University of Novi Sad, Bulevar cara Lazara 1, 21000 Novi Sad, Serbia
e-mail: snezanap@uns.ac.rs

M. Tzoutzouli Malešević
GP HGP d.o.o, Put Šajkaškog odreda 8a, 21000 Novi Sad, Serbia

A. Tomić
Faculty of Technology, University of Novi Sad, Bulevar cara Lazara 1, 21000 Novi Sad, Serbia

17.1   Introduction and Brief History

The building of the Serbian National Theatre (Serbian: Srpsko narodno pozorište) is located in the city of Novi Sad, the cultural and administrative centre of Vojvodina, the northern Serbian autonomous province. Although Novi Sad has never been the capital of the Serbian state, and for that matter was not even a part of Serbia at the time the Serbian National Theatre was founded, its rich and vibrant cultural atmosphere provided the perfect environment for avant-garde Serbian intellectuals and artists in the nineteenth-century Austrian Empire. The theatre was founded in 1861, in times of nineteenth-century European national awakening and the beginnings of the struggle for national freedom. Interestingly, until 1947 the theatre did not have its own central building but used various venues in the city and the region for practising and performing. In 1947, the theatre finally received a building from the state which it will use until 1981. The new theatre building was built in 1981 after an international architectural competition, won by Polish Architect Wiktor Jackievicz. The chosen location of the new building required intensive adaptation of the urban environment which included controversial demolishing of eighteenth- and nineteenth-century neighbourhood in the very heart of the city [1, 2]. Nevertheless, the new building now represents a new era in the urban development of Novi Sad, a city with continuously growing population and economy. Today, the Serbian National Theatre building is one of the central city landmarks with its characteristic hexagonal-based structure cladded with white marble stone façade slabs (Fig. 17.1).

Apart from several ad hoc interventions on the façade of the building, for over 40 years no comprehensive cleaning had been done and there had been no consolidation or protection works on the delicate white stone. Recently, the city government has begun an ambitious project of local heritage resurgence as Novi Sad has become the European Capital of Culture for 2022, together with Kaunas (Lithuania) and Esch-sur-Alzette (Luxembourg). The Laboratory for Materials in

Fig. 17.1 Southeast-facing façade with the main entrance to the Serbian National Theatre in Novi Sad, before cleaning and protection works done in 2021 (authors' photo)

Cultural Heritage, Faculty of Technology, University of Novi Sad, was trusted with the task of performing holistic characterisation of the façade stone, detecting deterioration mechanisms and proposing adequate conservation methodology. The laboratory's mobile equipment with non-destructive techniques and laboratory assessment enabled the complete analysis of the façade materials. Different types of degradation such as patina, dirt deposits, eroding surfaces, yellow layers and black crusts, large amounts of carbonaceous particles responsible for black shading of the stone surface, soluble salts, microbiological corrosion, residue of inadequate graffiti removal, façade paints, acrylic binders, as well as mechanical damage of the stone panels were identified [3]. The aim of this paper is to show the holistic process of diagnosing the façade issues which was used to make recommendations for subsequent cleaning and protection works done in 2021.

17.2 Methods

17.2.1 In Situ Investigation and Measurements

In situ investigation of the stone façade was done using laboratory's mobile equipment: digital microscope (PRO10-3, Vitiny, USA), colorimeter/spectrophotometer (CM-700D, Konica Minolta, Japan), Fourier transformed infrared spectrometer (ALPHA, Bruker Optics, Germany), X-ray fluorescence spectroscopy (ARTAX, Bruker, Germany), salt content analysis (Quantofix strips, Macherey–Nagel, Germany), and thermal imaging camera (T440bx, FLIR, USA).

17.2.2 Laboratory Investigation and Measurements

In order to complement the in situ measurements, additional laboratory analyses were performed on obtained representative samples of the stone façade: X-ray powder diffraction (PW 1710, Philips, The Netherlands), mercury intrusion porosimetry (Autopore IV 9500, Micromeritics, USA), drilling resistance measurement (DRMS, SINT Technology, Italy), and microbiological analyses by swabbing (total number of microorganisms and presence and number of fungi and yeasts).

17.3 In Situ and Laboratory Stone Characterisation

X-ray diffraction analysis (XRD) determined that the stone used for façade cladding of the Serbian National Theatre building was of calcite origin ($CaCO_3$) [4]. No other mineral components were identified in the samples of this stone. Mercury

(Hg) intrusion porosimetry gave insight into the pore size distribution and textural characteristics of the stone, which was the starting point for determining adequate filling and repair materials to be used (Table 17.1).

The entire area of the façade (Fig. 17.2) was mapped providing detailed information about observed deterioration patterns, such as cracks, graffiti stains, mechanical damage from previous graffiti removal attempts, soluble salts induced erosion, oxalate salt stains, synthetic resins and glues (from fixed placards), façade paint and paint-induced erosion and microbiological stains and erosion.

In total, four main zones (I: north west, NW, II: north east, NE, III: south east, SE, and IV: south west, SW, corresponding to the four cardinal directions the building façades are facing in general) with 33 subzones were selected for diagnostics mapping using previously described portable equipment for in situ analysis. Table 17.2 shows

Table 17.1 XRD and Hg intrusion porosimetry of the façade stone sample

X-ray diffraction (XRD)	Mercury (Hg) intrusion porosimetry
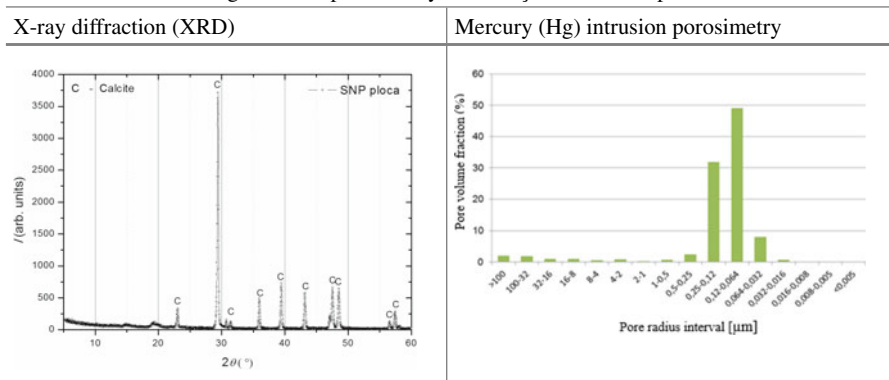
Fig. 17.2 Northwest-facing façade with the side entrance to the Serbian National Theatre building, before cleaning and protection works in 2021 (authors' photo)

several examples of results obtained in this way. Table 17.3 shows final systematic mapping of all observed damage and contamination (Tables 17.4 and 17.5).

17.4 Stone Cleaning and Protection

17.4.1 Selection of Cleaning Techniques/Laboratory Solutions

Commercially available techniques and solutions for cleaning stone materials investigated in the laboratory were selected based on the obtained results of the original stone material characterisation. Solutions were applied on the stone sample (taken from the theatre building façade) and analysed in laboratory conditions. After the analysis of the obtained results, the solutions that satisfied the basic compatibility criteria were applied and analysed on the selected zones of the building (in situ trials) with characteristic contaminations.

Laboratory testing was done on the original stone material sampled from the building façade itself. The material had visible traces of contamination and surface degradation. For a cleaning technique/solution to be selected as adequate, it had to satisfy the following conditions, which were not to cause: 1. further degradation of the stone material; 2. colour change of the surface; and 3. negative changes of microstructural characteristics of the surface.

Testing of the available techniques/solutions was done by dividing the original (dirty) stone material into several zones on which the techniques/solutions were applied (Figs. 17.3 and 17.4).

24 h after the treatment, every zone was visually inspected, and microscopically and colourimetrically analysed. The treated surface was cleaned using steam cleaner which partially removed grime. The colourimetric parameters recorded after the steam cleaning treatment ($L* = 89.71$; $a* = 0.67$; $b* = 5.48$) were used as the target aimed for future in situ treatments.
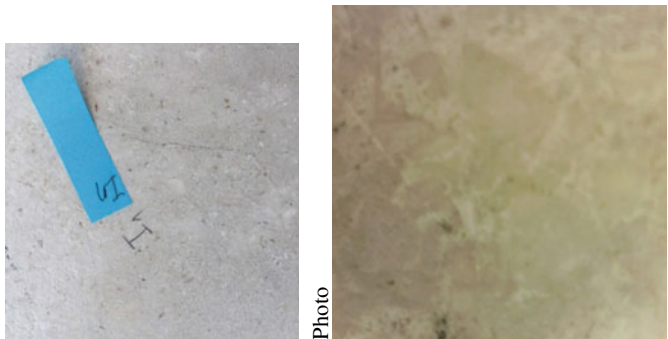
Next step included the treatment with soaps and graffiti removal solutions. All zones were then visually inspected and measured with microscope and colourimeter. The surface which was microscopically confirmed to be free of residual grime, and at the same time contained natural patina layer, was selected as the reference surface.

17.4.2 In Situ Cleaning Trials

After selecting adequate techniques/solutions in laboratory, trials were performed directly on the façade stone material in the chosen area of the building. Cleaning process consisted of machine cleaning using hot water/steam (Hot box, OERTZE
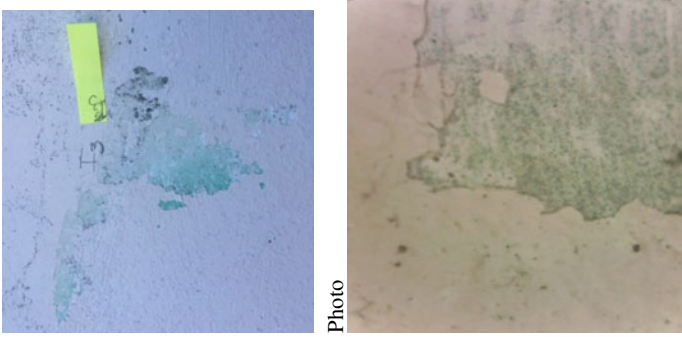
Table 17.2 Results of in situ diagnostics of the stone façade

Subzone	Photo/optical microscopy	Microbiological analysis (CFU/cm^2)	Colourimetry	Soluble salts (mg/L)
I.1	Photo Optical microscopy, 6.5× mag	No microbiota of significance detected	$L* = 73.90$ $a* = 1.83$ $b* = 11.56$	Cl^-: 500–1000 NO_3^-: 25 SO_4^{2-}: /

Table 17.2 (continued)

Subzone	Photo/optical microscopy	Microbiological analysis (CFU/cm^2)	Colourimetry	Soluble salts (mg/L)
I.3		No microbiota of significance detected	Green area (graffiti) $L^* = 87.28$ $a^* = -4.04$ $b^* = 3.44$ White area (façade paint) $L^* = 88.68$ $a^* = 1.70$ $b^* = 3.18$	Green area (graffiti) Cl^-: / NO_3^-: / SO_4^{2-}: / White area (façade paint) Cl^-: 0–500 NO_3^-: / SO_4^{2-}: /
	Photo Optical microscopy, 6.5× mag			

Table 17.2 (continued)

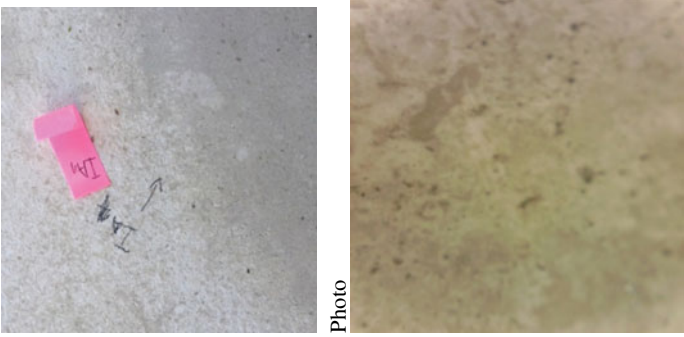| Subzone	Photo/optical microscopy	Microbiological analysis (CFU/cm^2)	Colourimetry	Soluble salts (mg/L)
I.4	Photo Optical microscopy, 6.5 × mag	Bacteria: 1 Fungi: 5	$L^* = 76.00$ $a^* = 2.59$ $b^* = 12.70$	Cl^-: 500–1000 NO_3^-: 25 SO_4^{2-}: /

Table 17.3 Systematic mapping of observed damage and contamination

Identified damage/contamination		Subzones
Surface-structural changes	Microbiological contamination	I.4, I.6, I.7, I.8, III.4
	Atmospheric contamination (surface grime without structural changes)	I.1, I.7, I.9, II.5, IV.1, IV.4
	Patina formation	I.1, I.4, I.9, I.10, IV.2, IV.4
	Surface contamination (clay, quartz sand)	I.1, I.2, I.4, I.5, I.6, I.7, I.8, I.9, II.1, II.5, III.4, III.6, IV.1
	Oxalates	I.1, I.4, I.6, I.7, II.5, III.4
	Rust	I.10
Paint layers	Acrylates	I.3, II.1, II.2, II.6, II.7, III.1, III.2
	Alkyds	I.3, II.3, III.2, III.3
Elevated levels of soluble salts contents	Chlorides	I.1, I.4, I.6, II.4, III.4, IV.2
	Nitrates	I.8, II.4, IV.2
Disintegration of material and fillings	Surface erosion	I.2, I.5, III.5, III.6
	Point surface defects and perforations	II.1, II.3, II.4, II.5, II.7, III.1
	Cracks	IV.3
	Fillings based on incompatible material	IV.3

2000, Germany; $t = 120\ °C$, $p = 60$ bar)—Fig. 17.5, and Schmutzlöser and Kiehl Li-Ex soap treatments.

Four treatment procedures were tested: MCL01—2.5% Schmutzlöser soap applied and left on the surface for 24 h, machine rinsing; MCL02—10% Schmutzlöser soap applied and left on the surface for 24 h, machine rinsing; MCL03—33% Kiehl Li-Ex soap applied and left on the surface for 24 h, machine rinsing; and MCL04—machine cleaning (Fig. 17.6). The results of the visual inspection of the trial surface are given in Table 17.6. These findings were confirmed with microscopic and FTIR analyses, and colourimetric evaluation of the trial surface.

17.4.3 Façade Stone Protection

Stone protection agents were tested in laboratory conditions before the selection for in situ trials. The agents were applied on previously steam cleaned stone surface in the laboratory. In situ trials also presumed application on cleaned stone surfaces (see Sect. 17.4.2). In order to satisfactorily resolve the issues identified in the diagnostics phase of the investigation, eleven agents with different functionalities were selected

Table 17.4 Overview of the cleaning techniques/solutions tested in the laboratory

Cleaning technique/solution	Producer	Product image	Purpose	Application instructions (given by the producer)
Steam cleaner Cleansy	Zepter International, Switzerland		Laboratory steam cleaner	Slightly alkalised water, $t = 100\ °C$, $p = 4.5$ bar, power $= 1.3$ kW
Schmutzlöser soap	Remmers, Germany		Grime removal	Apply with rough sponge and rinse with water; 1:40 soap to water ratio; 1:10 soap–water ration for persistent grime
Kiehl Li-Ex soap	Hygi, Germany		Grime removal	Apply with rough sponge and rinse with water; 1:8 soap to water ratio; 1:3 soap–water ratio for persistent grime
AGE	Remmers, Germany		Graffiti removal	Apply thick layer using a spatula, leave for 24 h and then remove using steam cleaner
Easy-off	Urban Hygiene Ltd, UK		Graffiti removal	Apply with sponge and rinse with water

(continued)

Table 17.4 (continued)

Cleaning technique/solution	Producer	Product image	Purpose	Application instructions (given by the producer)
Potassium-based soap	Beohemik, Serbia		Grime removal	Apply with sponge and rinse with water

for testing: 1. hydrophobisation function; 2. self-cleaning function; and 3. anti-graffiti function.
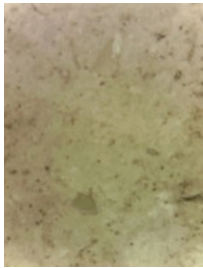
Pre-trial elimination of agents. Elimination of protection agents was done according to the same aesthetic and functional criteria used for cleaning techniques/solutions. Five tested protection agents did not satisfy the colourimetric requirements (namely, the colour change ΔE was greater than 3) or they left film deposits on the stone. Therefore, the remaining six agents were selected for in situ trials.

Hydrophobisation function. Hydrophobisation function of protective agents was evaluated via contact angle measurements. The agents were applied to the test surface and left for 48 h, after which time the contact angle (using glycerol as a testing fluid) was measured. The angle measurements were compared with untreated surface, and the results are given in Table 17.7.

Self-cleaning function. Photocatalytic material NANOFAS was chosen for self-cleaning function tests, as relevant scientific results [5, 6] and the Laboratory for Materials in Cultural Heritage expertise indicated that this material could potentially be compatible with the original stone material. The compatibility was indeed proven in the laboratory by colourimetric and microscopic analysis of the stone substrate after NANOFAS was applied on it. NANOFAS agent was applied using spray technique in two layers, with 3 min pause between applying the layers. Self-cleaning function was investigating by measuring the photocatalytic activity of the surface before and after the application of the agent, using rhodamine B as a model organic pollutant. The results are given in Table 17.8. It can be concluded that there was a significant decomposition of the model pollutant, which indicates good photocatalytic activity of the NANOFAS material.
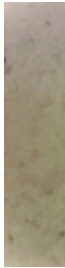
Anti-graffiti function. Methodology of the anti-graffiti function testing was established in accordance with the standard practice [7, 8] and contained the following steps: 1. Applying the protective agent onto the cleaned stone surface; 2. after 24 h, applying car spray paint graffiti on the treated surface; 3. after 24 h, removing (cleaning) the car spray paint graffiti: (a) step one—using sponge and water and (b)

Table 17.5 Evaluation of the cleaning solutions tested in the laboratory

Zone (Figs. 17.3 and 17.4)	Solution	Microscopy image	Change of colour (colourimetry)		Comment	Selected for in situ?
2	Potassium–based soap		ΔE	4.53	Detrimental effect on colour characteristics; grime is not removed	No
			Δa	0.57		
			Δb	0.85		
			ΔL	−3.41		
3	Schmutz-löser soap		ΔE	1.80	No detrimental effect detected; grime is removed	Yes
			Δa	0.35		
			Δb	0.89		
			ΔL	−1.52		
4	Kiehl Li-Ex soap		ΔE	1.82	No detrimental effect detected; grime is removed	Yes
			Δa	0.40		
			Δb	0.76		
			ΔL	−1.68		

(continued)

Table 17.5 (continued)

Zone (Figs. 17.3 and 17.4)	Solution	Microscopy image	Change of colour (colourimetry)		Comment	Selected for in situ?
5	AGE		ΔE	2.56	No detrimental effect detected	Yes
			Δa	0.50		
			Δb	0.47		
			ΔL	−2.47		
6	Easy-off		ΔE	0.32	No detrimental effect detected	Yes
			Δa	0.20		
			Δb	0.09		
			ΔL	−0.23		

Fig. 17.3 Stone material divided into testing zones, after application of cleaning techniques/solutions; zones: 1—steam cleaning; 2—potassium-based soap + steam cleaning; 3—Schmutzlöser soap + steam cleaning (3a—1:40 water–soap ratio, 3b—1:10 water–soap ratio); 4—Kiehl Li-Ex soap + steam cleaning. Surface above zone 1 was not treated

Fig. 17.4 Stone material divided into testing zones before (left) and after the treatment (right); zone 5—steam cleaning + AGE; zone 6—steam cleaning + easy-off solution

step two—using steam cleaner; 4. visual, microscopic and colorimetric inspection of the treated and cleaned surface (Fig. 17.7).

The results showed that sponge and water cleaning expectedly did not give any results in removing the graffiti, whereas steam cleaning successfully removed the graffiti from the surface treated with Funcosil-FC and partially from the surface

Fig. 17.5   Hot box machine (left photo) and hot box cleaning process (middle and right photos)

Fig. 17.6   Trial surface before treatment (left) and after treatment with the soaps (right photo, 2.5% Schmutzlöser—left slab, 10% Schmutzlöser—middle slab, 33% Kiehl Li-Ex—right slab)

treated with Sikagard 703 W. Therefore, it was recommended that these two protective agents should be applied in lower regions of the theatre façade as anti-graffiti protection. These results were confirmed by microscopic and FTIR analyses. They presented the basis for in situ trials final optimisation of the application process.

17.5   Conclusion

Combining several diagnostic techniques (in situ and laboratory), it was possible to determine the state of the original stone material and its degradation degree, which represented the basis for selecting cleaning techniques in laboratory and in situ. The main objective was to choose adequate technique and solution for façade cleaning

Table 17.6 Visual inspection of the trial surfaces

Photo of the trial surface before/during the treatment	Photo of the trial surface after the treatment
2.5% Schmutzlöser soap + rinsing	

Table 17.6 (continued)

	Photo of the trial surface before/during the treatment	Photo of the trial surface after the treatment
10% Schmutzlöser soap + rinsing		

Table 17.6 (continued)

	Photo of the trial surface before/during the treatment	Photo of the trial surface after the treatment
33% Kiehl Li-Ex soap + rinsing		

Table 17.6 (continued)

	Photo of the trial surface before/during the treatment	Photo of the trial surface after the treatment
Machine cleaning (no soap)		

Comment: Machine cleaning using hot box is recommended in all zones of the façade. In the parts of the façade not containing yellow stains, hot box machine process satisfactorily cleaned the surface (MCL04). In the areas of the façade where the yellow stains were present, it was necessary to treat the surface with the soap before machine cleaning. Schmutzlöser soap was not able to remove yellow stains (MCL01 and MCL02), while Kiehl Li-Ex soap managed to remove the stains (oxalate deposits)—MCL03. After the grime was removed from certain areas of the façade, erosion of the stone material was noted. These eroded surfaces present vulnerable spots for future rapid degradation of the material, the reason to be adequately protected

Table 17.7 Results of contact angle measurements

Protective agent	Measured contact angle
None (untreated surface)	26.6°
Funcosil-SNL	105.3°
Funcosil-AG	90.3°
Funcosil-SN	118.8°
Funcosil-FC	101.0°
Sikagard 703 W	94.3°

Comment: All tested protective agents expressed adequate hydrophobisation functionality as the measured contact angle after the treatment was higher than 90°

Table 17.8 Photocatalytic activity measured using model organic pollutant (Rhodamine B) decomposition during 24 h

	Photocatalytic activity (%)				
Sample	0.5 h	1.5 h	2.5 h	3.5 h	24 h
Stone material	4	6	6.5	6	6.5
Stone material with NANOFAS applied	4	8	13	16.5	19
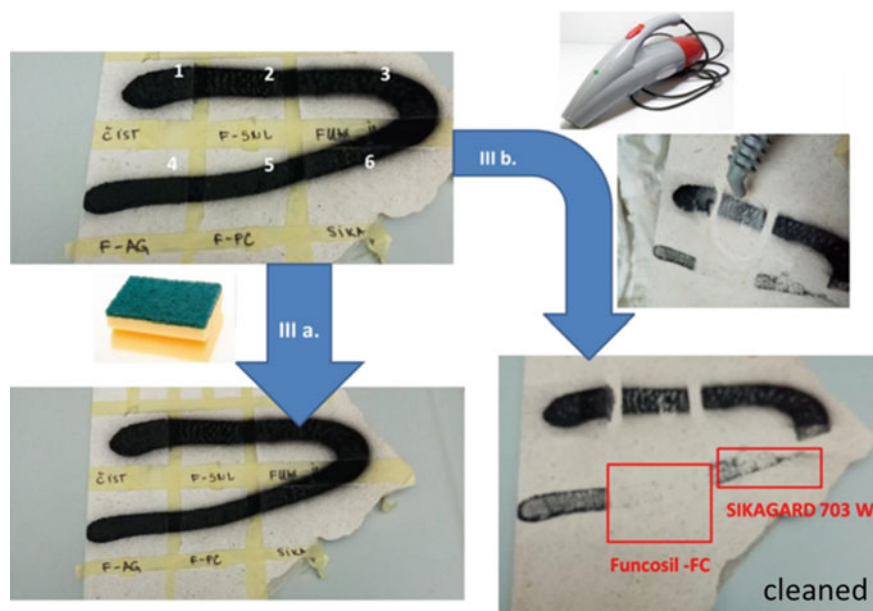
Fig. 17.7 Overview and visual inspection results of the anti-graffiti function testing: 1—untreated surface, 2—Funcosil-SNL, 3—Funcosil-SN, 4—Funcosil-AG, 5—Funcosil-FC, 6—Sikagard 703 W

that would be the most efficient, but at the same time would not contribute to further degradation of the façade, including aesthetics and microstructural integrity.

In situ analyses determined a dominantly present patina of various colouration and several types of grime and soil, as well as material degradation as a consequence of environment and previous repair interventions. There is a generally homogeneous layer of patina, most commonly accompanied with surface grime (atmospheric origins), although with no significant impact on the stone surface. In some zones, microbiological infiltration (bacteria, fungi) was determined, as well as lichens and moss presence, which indicated advanced microbiological corrosion characteristic for high levels of humidity (more than 80%), usually in the foundation layers of the building. More intensive yellow tones were due to high chloride contents and/or oxalate salts (which are known to be formed by microbiological metabolic pathways), confirmed by FTIR analysis. Several zones exhibited significant surface erosion, with visible perforations, point defects and microcracks.

Following the analysis of the obtained results, recommendation was made for machine cleaning with pressurised water/steam in all façade zones to be used, with additional use of commercially available soaps for certain zones with specific grime. Additionally, graffiti removal technique and future anti-graffiti protection were determined. Furthermore, based on colourimetric analysis, visual compatibility and proven functionality, commercially available NANOFAS solution with self-cleaning function was selected for long-term protection of the façade.

In situ trials on the actual façade were done for recommended cleaning and protection techniques and agents, as well as for periodic in situ control of the treated surfaces after the treatments. These in situ investigations confirmed the adequacy and compatibility of the selected techniques and agents.

References

1. Leskovac M (n.d.) History of SNP (in Serbian). https://www.snp.org.rs/?page_id=238
2. N.S. (n.d.) SNP buildings (in Serbian). https://www.snp.org.rs/enciklopedija/?p=17788
3. Cariati F, Rampazzi L, Toniolo L, Pozzi A (2000) Calcium oxalate films on stone surfaces: experimental assessment of the chemical formation. Stud Conserv 45:180–188. https://doi.org/10.2307/1506764
4. RRUF (n.d.) Calcite R050128. https://rruff.info/Calcite/R050128
5. Joo H-C, Lim Y-J, Kim M-J, Kwon H-B, Han J-H (2010) Characterization on titanium surfaces and its effect on photocatalytic bactericidal activity. Appl Surf Sci 257:741–746. http://doi.org/10.1016/j.apsusc.2010.07.054
6. Pondelak A, Kramar S, Ranogajec J, Škrlep L, Vucetic S, Ducman V, Sever Škapin A (2019) Efficiency of novel photocatalytic coating and consolidants for protection of valuable mineral substrates. Materials 12:1–15. http://doi.org/10.3390/ma12030521

7. Moura A, Flores-Colen I, de Brito J, Dionisio A (2017) Study of the cleaning effectiveness of limestone and lime-based mortar substrates protected with anti-graffiti products. J Cult Herit 24:31–44. http://doi.org/10.1016/j.culher.2016.04.004
8. Gomes V, Dionísio A, Pozo-Antonio JS (2017) Conservation strategies against graffiti vandalism on cultural heritage stones: protective coatings and cleaning methods. Prog Org Coatings 113:90–109. http://doi.org/10.1016/j.porgcoat.2017.08.010

Chapter 18
Design of Compatible Mortars for a Late Roman Tomb in Serbia

Snežana Vučetić ⓘ**, Emilija Nikolić** ⓘ**, Mladen Jovičić** ⓘ**, Ivana Delić-Nikolić,**
Ljiljana Miličić, Jonjaua Ranogajec ⓘ**, and Helena Hiršenberger** ⓘ

Abstract Design of conservation mortars for architectural heritage is always an ambitious and inspiring task, asking for many diverse requirements to be successfully harmonised. Principally, conservation mortars need to comply with demanding chemical, mineralogical, textural, and mechanical compatibility criteria. The main aim of this paper is to show the design and development of compatible mortars for conservation of a late Roman tomb in Serbia, situated around the former Danube Limes. It is only a fragment of the MoDeCo2000 project which deals with the research of mortars from the archaeological sites along the Limes, dated to the period from the first to the sixth centuries. Laboratory activities for the sampled mortars included visual observations, stereo-optical and digital microscopy, spectrophotometry and colourimetry, mineralogical and petrographic analyses, physical–mechanical tests, thermal characterisation, mechanical and chemical separation of aggregates and binders, and characterisation of samples, binders, and aggregates using FTIR, Raman, XRF, and XRD. The obtained results enabled designing of conservation mortars mixtures based on local raw materials. Following laboratory preparation of mortar models and several cycles of mixtures optimisation, the newly developed mortars for the Roman tomb were artificially aged and compared with original samples. The models which successfully fulfilled requirements qualified for application on small test areas of the historical building, and their behaviour was closely monitored in situ. The promising research results directly led to production of compatible mortars for upcoming conservation actions on the Danube Limes in Serbia and contributed to the universal body of knowledge about Roman mortars and architecture.

S. Vučetić (✉) · J. Ranogajec · H. Hiršenberger
Laboratory for Materials in Cultural Heritage, Faculty of Technology, University of Novi Sad, Bul. cara Lazara 1, Novi Sad 21000, Serbia
e-mail: snezanap@uns.ac.rs

E. Nikolić · M. Jovičić
Institute of Archaeology, Kneza Mihaila 35/IV, Belgrade 11000, Serbia

I. Delić-Nikolić · L. Miličić
Institute for Testing of Materials, Bul. vojvode Mišića 43, Belgrade 11040, Serbia

18.1   Introduction

An in-depth scientific understanding of historical building materials and technologies is essential for the design of sustainable preservation solutions. Despite the crucial role of Roman mortars in building history, there is a lack of comprehensive research of their creation and use in Roman buildings along the Danube Limes in Serbia.

Mortars are essential artificial material of most historical buildings, and its durability is related to the nature of its components, manufacturing methods, and conditions it is later exposed to. The study of historical mortars offers evidence about the choice of raw materials and their provenance, as well as on the manufacturing technology and the chronological phases of the structures to which they belong [1]. Design of conservation mortars for the historical constructions is always an ambitious and inspiring task, asking for many diverse requirements to be achieved and successfully harmonised. Principally, conservation mortars need to comply with demanding chemical, mineralogical, textural, and mechanical compatibility criteria. Additionally, to be applied in situ, under real environmental conditions, specific preconditions regarding the formation of the contact zone (between conservation and original material), tensile strength, porosity, and visual properties (colorimetric parameters) must be fulfilled as well. Compatibility criteria are always related to the properties of the repair mortar compared to those of the original material [2].

Since 2020, three research organisations in the Republic of Serbia, the Institute of Archaeology, Faculty of Technology Novi Sad, and Institute for Testing of Materials, formed a team that has been conducting a two-year research project Mortar Design for Conservation—Danube Roman Frontier 2000 Years after (MoDeCo2000). The main aims of the project were research of historical mortars and design with development of highly compatible mortars for future conservation of the Roman buildings along the Danube Limes in Serbia (Fig. 18.1). All available archaeological sites and cultural monuments of the Limes were visited. More than 120 different samples of historical mortars, stones, and bricks originating from the building structures dated between the first and sixth centuries were collected. Based on detailed research works of on historical mortar samples, a number of mortar mixtures were designed based on local raw materials and traditional technologies, tested, and applied on the experimental and original historical walls.

Bearing in mind the great number of visited historical buildings on the Danube Limes in Serbia and collected mortar samples (photo-documentation consists of 20,000 laboratory photos and more than 5000 field photos), and that every mortar sample represents a specific case for the analysis, according to its age and function, composition, and technology of manufacture, the project database offers many valuable insights for further research. This paper focuses on one research case, that is the late Roman tomb in the village of Brestovik near Belgrade, a unique example of
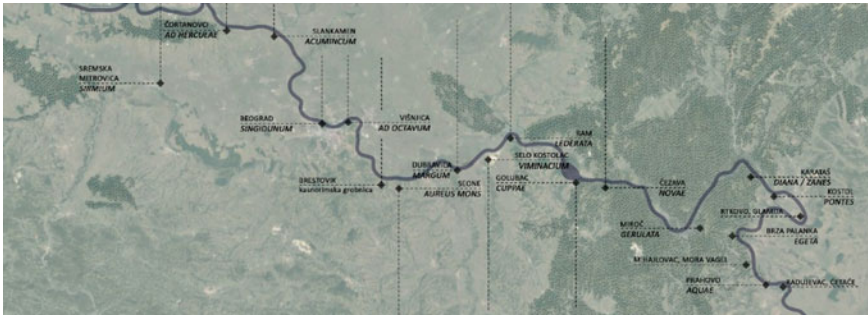
Fig. 18.1 Map of the sampled Roman archaeological sites along the Danube Limes in Serbia (Documentation of the MoDeCo2000 project, author: Danica Petrović)

Fig. 18.2 Late Roman tomb in Brestovik (Photo-documentation of the MoDeCo2000 project)

the ancient funerary monument in Serbia whose conservation is planned for the near future (Fig. 18.2).

18.2 Materials and Methods of the Research

After the detailed research works performed both in situ and under laboratory conditions, the project team revealed main characteristics of all historical mortar samples. Several mortar mixtures were designed based on local raw materials and traditional technologies and tested in laboratory using different characterisation techniques,

comparing their properties with those of the original samples. The most promising recipes (mortar models) were chosen after weathering in laboratory conditions, artificial weathering in the climate chamber, and followed by the application of new conservation mortars in real environmental conditions (experimental walls). Finally, the chosen conservation mortars were tested on small areas of the original historical walls. The behaviour of the applied mortars and their contact with the original ones have been continuously monitored in situ.

The methodology procedure used in the project includes five main steps:

Cabinet research on architectural, archaeological, geological, and technological aspects of the materials that have been potentially used for the preparation of original mortars;

In situ characterisation and sampling of the mortars from the reachable archaeological sites;

Laboratory characterisation of historical mortars;

Design, artificial weathering, comparative characterisation, and selection of the promising conservation mortars; and

Application of designed mortars on the experimental and original walls and monitoring of their behaviour.

18.2.1 Archaeological and Architectural Context of the Research

The Roman conquest of the territory of present-day Serbia had finished in year 15 AD when the territory was incorporated into the provinces of Pannonia and Moesia [3]. The establishment of the fortified Roman border on the right side of the Danube (Limes), with a series of fortresses and forts for legions, cohorts, or auxiliaries, connected by roads, was completed during the first century after which large civil settlements were developed in the vicinity of military camps. Life in the Limes had several phases, from its establishment to its destruction during the Hun invasion in 441/443 AD, after which short renovation in the sixth century occurred, finally ending with Avar and Slavic conquests of the Danube region [4]. The research of the frontier along the Danube on the territory of present-day Serbia has been conducted for over 130 years, and so far, a great number of sites have been explored [5]. Some of the sites were flooded during the construction of the hydroelectric power plant Đedrap I and II during the 1970s and 1980s, but a large number of archaeological remains are still reachable today. Thus, the mortars sampled through the MoDeCo2000 project originate from legionary fortresses Viminacium (Stari Kostolac) and Singidunum (Belgrade), auxiliary forts and smaller fortifications, such as Lederata (Ram), Novae (Čezava), Diana (Karataš), and Egeta (Brza Palanka), Roman villas and civil buildings, as well as from the remains of the Trajan's Bridge (Kostol) (Fig. 18.1).

The remains of a tomb in the modern-day village of Brestovik keep one of the best-preserved examples of Roman funeral art in the region. The tomb represents a family mausoleum that belonged to the private property of a surrounding villa [6] and dates back to the period from the late third to the early fourth centuries [6–8]. Archaeological excavations of the tomb were conducted in 1895 and 1955 [7, 8], with conservation and restoration of architecture and wall paintings performed in 1964 [9]. The tomb, built of stones and bricks, is oriented east–west and consists of the vaulted grave chamber with masonry graves, completely decorated with wall paintings; the central room with two side apses and painted walls, decorated with stone sculptures, and used for cult funeral services; and the entrance area with access corridor [10]. The wall painting of the tomb is one of the finest examples of late antique art in the territory of modern-day Serbia and consists of geometric, vegetation, and zoomorphic motifs [11]. The architectural composition, sculptures, and wall paintings confirm that it is the tomb of a high-ranking Roman and his family, probably a military commander or a civilian official [10]. Its architecture and painting can be connected with analogous examples in the Middle East, on the southern coast of the Black Sea and North Africa [11].

18.2.2 Characterisation of Historical Mortars from the Tomb

Four samples of lime mortar were collected from this tomb—floor mortar from the grave chamber, mortar belonging to the wall painting from the central room, and two masonry mortars from the entrance area. Laboratory characterisation of mortar samples was performed using sieving, wet chemical analysis, stereo-optical microscopy with colourimetry, chemical–mineralogical analysis (XRF/XRD), mechanical tests (drilling resistance measurements and compressive strength), thermal analysis (DTA/DSC/TG/MS), FTIR and Raman spectroscopy analysis, and identification of binder–aggregate ratio (wet chemical analysis and interpretation of petrography and thermal analysis) [12]. Data obtained in situ and by laboratory tests presented the basis for the development of compatible conservation mortars (Fig. 18.3).

18.2.3 Design of Conservation Mortars for the Tomb

The mixture composition and production technology of the conservation mortars for the Brestovik tomb was established based on the results of a comprehensive historical mortars characterisation. The models of conservation mortars were prepared in the laboratory and artificially aged using a weathering chamber (KBWF 240, Binder, Germany). The comparative characterisation was performed for historical and aged conservation mortars to examine their compatibility (colour, mechanical properties, and formation of contact zone between designed systems and historical ones).

Fig. 18.3 Sampling position, masonry mortar sample Br1, late Roman tomb in Brestovik (Photo-documentation of the MoDeCo2000 project)

Mechanical properties were determined by a Drilling Resistance Measuring System (DRMS, SINT Technology, Italy), while colour characteristics were measured with a spectrophotometer (CM-700D, Konica Minolta, Japan) and calculated in Commission International de l'Eclairage (CIE) colour space. Interaction between the prepared conservation mortars and the original historical samples, and their cohesion was studied in laboratory during artificial ageing of the samples (original fragments were inserted in fresh models of the conservation mortars). Moreover, monitoring of cohesion and formation of contact zone was performed in situ after the application on historical walls, periodically after the application, by digital optical microscopy, using a digital optical microscope (PRO10-3, ViTiny, USA).

18.3   Results and Discussion

18.3.1   Characteristics of Historical Mortars

Based on the results given in Table 18.1, the binder to aggregate ratio was calculated as 1:2.5 (mass ratio), while the chemical analyses revealed that sand, gravel, and a very small amount of crushed bricks take up 72.02% m/m of the mixture. This explains that the remaining 27.98% m/m is of carbonate origin, including a negligible amount of soluble SiO_2 (0.01% m/m.). Also, by visual, mineralogical, and petrographic analyses, aggregate was recognised to be natural, with semi-rounded to rounded shaped grains of quartzite (dominantly), granitoid, quartz and mica transparent white, yellowish, dark red, orange, light grey, dark grey, and black colour. Grain size is up to a maximum of about 30 mm, although such large grains are rare, and they are

dominantly about 3 mm in size. Lime lumps are rarely present, generally less than 1 mm in size.

Chemical analysis (XRF) and drilling resistance measurements were performed on the original compact samples, XRD analysis was done on insoluble residue, while FTIR analysis was performed on three separated fractions after the sieving analysis: (a) binder < 63 µm, (b) agglomerated binder > 710 µm, and (c) aggregate 710–500 µm (Table 18.2).

Based on the summarised results of the original mortar sample Br1 from the late Roman tomb in Brestovik, this sample could be classified as lime mortar, formed using lime and natural Danube river sand (carbonate or dolomitic aggregates were not found). Also, very small amount of lime lumps and crushed brick was found, while the interesting feature is the usage of gravel, however, in very small percentage.

18.3.2   Compatible Conservation Mortars

Mechanical and visual examinations of the historical mortar sample Br1, the composition of the conservation mortar mixture, and production technology were established based on the results obtained after the chemical–mineralogical analyses. The selected components for the conservation mortar mixtures were quicklime and slaked lime putty from the small village manufacturers, industrial hydrated lime, Roman crushed and ground brick, clay, kaolin, Danube river sand, and gravel.
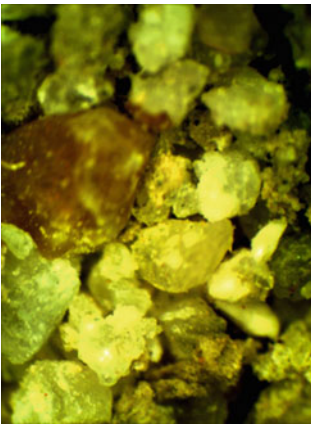
Nine different mixtures of conservation mortar were prepared in laboratory, with variations of type and percentage of lime and aggregate components (Table 18.3). To allow evaluation of compatibility between original historical mortars and laboratory designed conservation mortars, small fragments of sample Br1 were put in one set of fresh model samples and analysed during and after the artificial ageing (Fig. 18.4).

After the artificial ageing in laboratory, as given in Table 18.4, the mortar models were characterised, and the most promising recipes were applied on the experimental wall in the laboratory and monitored by optical microscopy (Table 18.5).

Based on the visual observation, only three systems developed in the laboratory were adequate for future considerations. It was concluded that samples Br4, Br5, and Br7 were compact, without visible cracks and with the appropriate difference in colour characteristics developed after ageing [13], compared with the original sample from the tomb (Table 18.4). However, in case of the designed mortar Br5, the contact zone was not well formed; therefore, only samples Br4 and Br7 were chosen for in situ testing, having the adequately formed contact zones, with no cracks found on the boundaries between newly designed and original mortars. After the application on the experimental wall in environmental conditions, only mortar Br7 was chosen for the use in conservation of the original wall in the tomb (after one month on the experimental wall, small cracks were identified in the case of sample Br4). The chosen sample was applied in situ on the authentic wall and has been monitored since. In situ optical microscopy of the conservation mortar, six months after application in real environmental conditions on the original structure, as given

Table 18.1 Wet chemical analyses and optical microscopy of historical mortar sample Br1

Wet chemical analyses/binder to aggregate ratio/optical microscopy

Optical microscopy—compact sample Br1, magnification ×10

Optical microscopy—insoluble residue after wet chemical analysis, magnification ×10

Treatment with HCl	
Soluble residue	27.98% m/m
Insoluble residue	72.02% m/m
Insoluble residue treated with Na_2CO_3	
Soluble SiO_2	0.01% m/m
Insoluble SiO_2 (sand)	72.01% m/m

Table 18.2 Summarised results of the chemical, mechanical, and mineralogical examination—original mortar sample

FTIR

FTIR analysis:
blue: binder <63 μm;
red: agglomerated binder >710 μm, and
green: aggregate 710–500 μm

Identification	Bands (cm⁻¹)	<63 μm	>710 μm	710–500 μm
Carbonate	1796	x		
	1410	x	x	x
	872	x	x	x
	712	x	x	x
Quartz	1170		x	
	1083		x	x
	798		x	x
	779		x	x
	695			
	520	x	x	
	460	x	x	
(alumo)silicates	1002	x		
Fe—O	530	x		

Table 18.2 (continued)

XRD/XRF

SiO_2, %	61.42
Al_2O_3, %	5.09
Fe_2O_3, %	2.00
CaO, %	18.32
MgO, %	1.13
Na_2O, %	0.69
K_2O, %	1.07
SO_3, %	0.22
P_2O_5, %	0.16
MnO, %	0.15
TiO_2, %	0.27
Cl, %	0.01
L.O.I. (1000°C), %	9.32
Total	99.85

XRD analysis:

Q - quartz; F - feldspat; M - muscovite;
Typical composition of Danube river sand

Drill resistance

BR 1

max. force 14.2 N; average force 4.8 N

Table 18.3 Sample markings and composition of the prepared mortar models (in parts)

Components	Sample marking—conservation mortar models								
	Br1	Br2	Br3	Br4	Br5	Br6	Br7	Br8	Br9
Sand 0.25–4 mm	3	2	2	2			3	0.5	0.5
Sand 0.125–2 mm	1	1	2		2	2	1		
Gravel 1–1.5 mm	0.5	1	1	0.3			0.5	4	4
Crushed and ground brick (up to 1 mm)		0.1	0.1	0.05	0.1	0.1			
Clay				0.6	0.5	0.5	0.5	1.5	1.5
Kaolin				0.4					
Slaked lime putty	2		2				2.5	4	
Quick lime		1	1	2					2
Hydrated lime					2				
Aggregate/binder	2.25:1	4.1:1	1.7:1	1.5:1	1.3:1	2.1:1	2:1	1.5:1	3:1

Fig. 18.4 Freshly prepared samples (left) and their artificial ageing in the chamber (right) (Photo-documentation of the MoDeCo2000 project)
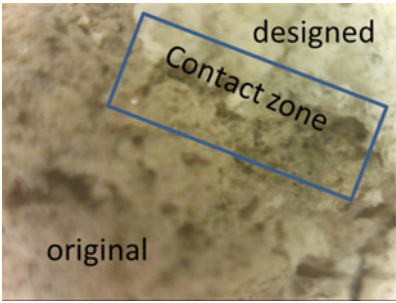
in Table 18.5, revealed very good contact between lime, sand, and coarse aggregate (gravel). Also, no structural or small cracks were identified. Moreover, contact zone between original and conservation mortar is well formed.

Table 18.4 Optical microscopy and total colour difference between mortar model after ageing and original sample—samples chosen for the application on the experimental walls

Sample	Optical microscopy, ×10	L	a	b	
Original Br1		66.14	3.65	12.81	

Sample	Optical microscopy, ×10	ΔL	Δa	Δb	ΔE
Br4		2.64	−1.50	−6.49	7.16
Br5		8.31	−0.98	−6.27	10.45

(continued)

Table 18.4 (continued)

eBr7		4.06	−0.90	−4.73	6.30

Table 18.5 Small area of the historical wall conserved with the designed Br1 mortar (Photo-documentation of the MoDeCo2000 project)

Conservation mortar 6 months after application on the original structures

Optical microscopy, magnification ×10

18.4 Conclusions

In this research paper, the methodology of the project MoDeCo2000 for design of compatible conservation mortars with targeted chemical, mineralogical, textural, and mechanical properties is presented on the case study of a late Roman tomb in Serbia. The steps in design and development, laboratory and in situ testing, and in situ monitoring of the mortars for future conservation of this tomb are shown.

Based on visual observations, stereo-optical and digital microscopy, spectrophotometry and colourimetry, mineralogical and petrographic analyses, tests of physical and mechanical characteristics, thermal characterisation, mechanical and chemical separation of aggregates and binders, FTIR, Raman, XRF and XRD, and comprehensive characterisation of the original mortar samples from the tomb were performed as a necessary input for the design of conservation mortars.

In parallel, identification and characterisation of raw materials for conservation mixtures took place. Following laboratory preparation of mortar models and several cycles of mixtures optimisation, the newly developed mortars were artificially aged, and a detailed comparative analysis of original and laboratory prepared models was done. The systems which successfully fulfilled all the requirements qualified for application on small test areas of the examined tomb, and their behaviour was closely monitored.

During all project research phases, many interesting points about ancient Roman building technologies characteristic for provincial architecture developed in the border area along the Danube were revealed. Many have confirmed initial hypotheses and others fine-tuned the approach, while some original samples still intrigue the research team with their exceptional properties. Moreover, they provide important insights and additional interdisciplinary results to be added to the knowledge base about Roman mortars on the whole area of the former Danube Limes. These results also navigate the discovery of some missing pieces of the story about the Roman architecture at the territory of today's Serbia. Likewise, this multidisciplinary research work proved that learning from the past, directly from the original historical mortars by using the most advanced scientific methods and equipment, can give valuable recognition of living habits and technological readiness of people from the distant past.

The obtained project results directly led to upcoming conservation actions with scientifically proven compatible mortar mixtures. The late Roman tomb in the village of Brestovik in Serbia is one of the monuments which is planned to be conserved in its entirety in the near future. The results of the research shown in this paper will be of huge importance, being offered as the study with tested and proven recipes for the conservation mortars.

Beside the production of compatible conservation mortars for upcoming conservation actions on the Danube Limes in Serbia, all results obtained greatly contribute to the Roman heritage preservation in Serbia. Moreover, obtained project results directly led to formation of a multidisciplinary database on archaeology, architectural and construction history, conservation science, geology and chemistry of raw materials,

as well as the technology of original mortars, contributing to the universal body of knowledge about Roman mortars and architecture used in further research and conservation. At the same time, the revealed ancient knowledge and deeper understanding of the origins of superior mechanical properties of some Roman mortar samples used in the buildings that stand for almost 2000 years have vast potential to shape our solutions for modern products that can effectively respond to the needs of the green and sustainable architecture of our future.

References

1. Alonso-Olazabal A et al (2020) Compositional characterization and chronology of Roman mortars from the archaeological site of Arroyo De La Dehesa De Velasco (Burgo De Osma-Ciudad De Osma, Soria, Spain). Minerals 10:393
2. Lubelli B, Nijland TG, van Heesa RPJ (2021) Characterization and compatibility assessment of commercial stone repair mortars. J Cult Heritage 49:174–182
3. Ferjančić S (2013) History of Roman provinces in the territory of modern day Serbia during Principate. In: Popović I, Borić-Brešković B (eds) Constantine the Great and the Edict of Milane 313. National Museum in Belgrade, Belgrade, pp 16–25
4. Petrović P, Vasić M (1996) The Roman frontier in Upper Moesia: archaeological investigations in the Iron Petrović, Beograd, pp 15–27
5. Korać M, Golubović S, Mrđić N, Jeremić G, Pop-Lazić S (2014) Roman Limes in Serbia. Institute of Archaeology, Beograd
6. Milošević-Jevtić G (2014) Architecture of 'The Family Mausoleums' on Danube Limes between Singidunum and Pontes. In: SGEM 2014 conference on anthropology, archaeology, history and philosophy, pp 323–330
7. Valtrović M (1895) Rimska grobnica u Brestoviku, Starinar, XII, pp 131–132 (in Serbian)
8. Stričević Đ (1957) Brestovik – Rimska grobnica. Starinar Tы VII-VIII (1956–1957), pp 411–413 (in Serbian)
9. Vujičić-Vulović M (1967) Rimska grobnica u Brestoviku (konzervatorsko-restauratorski radovi – prva faza). Zbornik zaštite spomenika kulture, Knjiga XVIII (1967), Beograd, pp 86–92 (in Serbian)
10. Milošević (2009) Funerary sculpture from the Brestovik tomb. In: Gaggadis-Robin V, Hermary A, Redde M, Sintes C (eds) Les ateliers de sculpture reginaux: techniques, styles et iconographie. Actes du Xe Colloque international sur l'art provincial gate area—main results. In: Romain P (ed) Roman limes on the middle and lower Danube. Arles et Aix-en-Provence, pp 741–751
11. Nikolić E, Rogić D, Anđelković Grašar J (2018) Architectural space in the wall painting of the Roman tomb in Brestovik. In: Korać M (ed) Vivere Militare Est, From Populus to Emperors—living on the frontier, vol II, Belgrade, pp 195–268
12. Pašalić S, Vučetić S, Zorić DB, Ducman V, Ranogajec J (2012) Pozzolanic mortars based on waste building materials for the restoration of historical buildings. Chem Ind Chem Eng Q/CICEQ 18:147–154
13. Rodrigues JD, Grossi A (2007) Indicators and ratings for compatibility assessment of conservation actions. J Cult Herit 8:32–43

Chapter 19
Development of a New Cleaning Product for Heavy Metals Containing Facades

Dipl.-Ing.Jens Engel

Abstract In inner cities, especially along highly trafficked roads worldwide high contents of heavy metals are found on all older facades. They are the result of dust and gaseous emissions of combustion and production processes. These include mainly arsenic, cadmium, chrome, mercury and nickel. But particularly high are the contents of lead, which is classified as toxic for reproduction–on one side the heritage of the time when gasoline was still leaded but on the other side a result of the abrasion of tyres and breaks. The heavy metals are often inseparably fused with other dirt particles that have accumulated over the course of decades–if not centuries–on the surface of the building materials. These dirt layers are usually not just an aesthetic problem but also damage the building. That is why facades should be cleaned regularly, but in a most delicate way and without releasing their heavy metals load to the environment. This article describes the development of an innovative cleaning product that allows a particularly delicate cleaning of facades whilst binding the heavy metals contained in it, and lead in particular, so that they cannot disperse uncontrollably into the environment. After cleaning the product usually can be disposed together with normal household waste since the lead and other heavy metals embedded are not to be considered critical according to the hazard criteria of the European Chemicals Regulation REACH and the classification of substances and mixtures at the UN level, the so called CLP Regulation. The Article gives particularly noteworthy examples by the cleaning of the Musée du Louvre and the Musée Carnevalet in Paris.

Keywords Cleaning · Facades · Poultice · Heavy metals · Lead

19.1 Introduction

Cleaning of cultural heritage is always associated with a certain risk. Therefore, the question of whether a monument should be cleaned again and again generates justified discussions. The reasons for cleaning a building are basically either aesthetic

Dipl.-I. Engel (✉)
Remmers GmbH, Bernhard-Remmers-Straße 13, 49624 Löningen, Germany
e-mail: Jengel@remmers.de

or technical. The aesthetic reasons will not be discussed here, even though they certainly play a major role in the decision to carry out a cleaning measure. The technical reasons are manifold. An important one is that dirt deposits on façades constitute reservoirs of moisture and pollutants. In many cases, the drying rate of the substrate is hindered by superficial deposits or even dirt crusts. Thus the stone surface remains moist for a longer time and the associated damage processes can have a greater effect. In addition, darker façades can also lead to more damage because they heat up more when exposed to sunlight and the associated temperature gradient in the façade´s building material is steeper.

Typical urban façade soiling also results from the deposition of suspended particles such as dust, diesel soot, tyre and brake dust, railway iron dust. Some of these contain heavy metals [1–3] and can react with the stone substance and destroy the original surface. However, when cleaning façades that are exposed to this kind of loads, the potential problem arises that these sometimes considerable amounts of heavy metals are emitted, depending on the cleaning method chosen, and can again significantly harm people and the environment.

19.2   "Clean Galena"—A Special Cleaning Process

In recent years, sensitivity to emissions that can arise during façade cleaning has rightly increased considerably but especially in France it is significantly higher than in the rest of Europe [4]. In this context, special attention is paid to the question of whether heavy metals can enter the environment in any form as a result of cleaning.

A good method to bind environmentally hazardous substances right under the cleaning process is the use of cleaning poultices.

These are pasty cleaning media that contain cleaning-active substances in addition to the carrier material. When they are used, impurities of the substrate are dissolved and migrate together with the solvents used into the compress, where they are bound. Once the cleaning process is finished, the compress dries out almost completely and can easily be removed.

In recent decades, the vast majority of the poultices used have been produced on site by restorers, i.e. by the applicators themselves, and applied immediately [5].

19.2.1   Significance of Metal Ions in Connection with Cleaning

The active ingredients most frequently used for cleaning purposes are surfactants. Many of them are impaired in their surface-active property by hardness-forming metal ions. Metal ions improve the adhesion of dirt to surfaces and increase the cohesion of dirt particles.

Positive metal ions can serve as "mediators" between negatively polarised surfaces and negatively polarised dirt components; explained differently: In dirt, metal ions can be complexed as a central atom, which makes the swelling of protein-containing dirt, which is important for cleaning, more difficult because the negatively polarised molecular groups of the protein are not available for interaction with water due to the bond to the metal ion.

Soiling is therefore easier to remove if the metal ions are removed from it!

The newly developed poultice was originally designed for the complexation and emission-free removal of metal ions, especially lead ions, from façade surfaces. In addition, so to speak as a side effect, the so called "Clean Galena" often has a cleaning effect as well, as the removal of metal ions influences the cleaning positively in various ways:

- Destabilisation of gypsum and lime deposits,
- Improvement of the swelling capacity of organic dirt,
- Facilitated dispersion of dirt particles. The dispersing effect of certain complexing agents is based less on the removal of metal ions from dirt than on the adsorption of negatively charged ions on dirt particles. This causes the dirt to become negatively charged. The identically charged dirt particles easily disintegrate into even smaller components and also repel each other. Dirt is also repelled from negatively charged or polarised surfaces.

All these mechanisms of action are made usable for façade cleaning with this poultice. Therefore, in addition to the (invisible) complexation and integration of the metal ions, especially lead ions, into the material, a simultaneous cleaning effect is generally achieved.

19.2.2 Composition and Mode of Action

The main active ingredient in "Clean Galena" is a special clay mineral that occurs naturally. The bentonite used is a layered silicate and functions as a binder and active ingredient. Due to the characteristic building elements SiO_4 and AlO_6 contained in it, a stratification exists which is neutralised by the incorporation of cations. The poultice thus has a special type of swellable clay minerals with a very large specific surface to which pollutants can be bound by adsorption and electrochemical processes. It also regulates moisture transport processes during the cleaning process.

Another component of the innovative cleaner is a derivative of easily biodegradable succinic acid, which in turn complexes alkaline earth and polyvalent heavy metal ions (e.g. lead) in combination with water. It is also used to remove limescale deposits.

This chemical reaction is further supported by natural fruit acid derivatives, which in turn form metal ion complexes. One of the fruit acids serves primarily to bind calcium and iron ions, another to purify iron or copper impurities.

Experiments have shown that these active ingredients only develop their full effect in combination, i.e. a synergetic effect is created that enhances the cleansing effect.

This explains why "Clean Galena" can achieve considerably better cleaning effects than "classic" ammonium carbonate compresses.

The poultice gets its stability from thickeners made from naturally renewable raw materials. An increase in strength is achieved by adding another special layered silicate.

It is free of hydrocarbons, chlorine and other halogen compounds.

All ingredients are carefully selected and coordinated.

19.2.3   Possible Side Effects

A critical point is a possible salt input into the subsoil in the course of cleaning.

If the product is used properly and as intended, salt input into the substrate is not to be expected. Depending on the application (e.g. substrate not sufficiently pre-wetted) and/or substrate (e.g. highly absorbent), small amounts of sodium cations may be introduced into the substrate to be cleaned via the necessary cleaning additives or active ingredients. Therefore, the sodium concentration in the product is kept as low as possible. The theoretical sodium concentration of the product can be calculated from the added amount of complexing agents, however, other small contents from thickeners, fillers and the added water may also be added, but these cannot be calculated exactly as no concentration data are available.

The maximum total mass content of sodium in "Clean Galena max", undiluted, as determined by laboratory tests, is less than 2.5 M.%.

Easily water-soluble anions, such as chlorides, sulphates and nitrates, which are harmful to the building fabric, are only contained to a minor extent in the poultice.

19.3   Individualisation of the Cleaning Effect on the Object

In order to be able to individually adapt the cleaning effect and, if necessary, the drying time of the poultice, which decreases with decreasing active ingredient content, to a specific substrate, there is a variant with the lowest possible active ingredient content in addition to the original standard variant "Clean Galena max" with "Clean Galena neutral". A formulation without any active ingredient at all is possible but leads to a strongly changed consistency when mixed with the standard material, which is why the active ingredient content has been minimised and not eliminated. Both variants can be mixed so that different active ingredient concentrations can be created. It is recommended to create sample areas with different mixing ratios.

After selecting a suitable mixing ratio, the mixture can be prepared by the contractors themselves on site for smaller areas; for larger areas, an individual poultice can be provided by the factory in the appropriate mixing ratio. This special mixture is

then called "Clean Galena individual" and can be ordered from a minimum order quantity of 1 tonne.

19.4 Processing

19.4.1 The Procedure in Detail

- In a first step, the surface to be treated must be cleaned of loose and adhesion-reducing components, usually by hand with a broom resp. brush or paintbrush.
- Before applying the poultice, the substrate should be pre-wetted to fill the capillary active pores near the surface with water. This prevents the active ingredients of the poultice from being absorbed too deeply into the substrate or, in the worst case, from migrating and not returning into the poultice.
- Clean Galena must be homogenised immediately before application.
- Machine application has proven to be the most economical and technically effective application method. Coating thicknesses exceeding 2 mm do not increase the cleaning success, but the drying time and thus the waiting time until removal is often significantly increased.
- After one to three days, even at rather low temperatures, the poultice is dry and detaches from the substrate.
- After dry removal of the poultice, the surface can be washed slightly. Any remaining dirt that has been destabilised by the metal ion removal can usually be easily removed now.
- The dried, removed material must be disposed of according to municipal regulations; if necessary, the heavy metal load of the compress must be examined for this purpose. The dried compress material itself is not considered critical.

19.4.2 Disposal

According to the REACH Committee decision of February 2016 and the publication of the 9th amendment to the CLP Regulation, lead metal has been classified as toxic for reproduction category 1A since 1 March 2018. The classification was later further clarified and includes, as of today, a general concentration limit (GCL) for solid material and mixtures of 0.3% and a specific concentration limit of 0.03% for powder form (< 1 mm).

For other "non-massive" wastes, such as slags or filter dusts, the hazard criteria of the Waste Framework Directive (HP criteria) are to be applied [6]. Here, for substances toxic to reproduction of category 1A and 1B, a waste classification is to be made from contents of 0.3% (Pb particle diameter > 1 mm) and 0.03% for the powder form (particle diameter < 1 mm) (HP 10).

With regard to the maximum amount of Pb produced during cleaning with the newly developed poultice, percentages of 0.0021% Pb were achieved in the dried compress. Thus, even in the extreme case that has occurred so far, nothing stands in the way of a "simple" dumping of the used and dried material.

19.5   Projects

19.5.1   Hotel de Rohan, Paris

Construction work on the original building began in the second half of the fourteenth century. The baroque façades that can be seen today were essentially created at the beginning of the eighteenth century after several alterations.

Today, the Hotel Rohan houses part of the French National Archives. Between 2015 and 2017, the building's façades were restored; the simultaneous use of the areas for laying out sample surfaces was therefore unproblematic.

After a series of laboratory tests, sample areas were laid out on site in February 2016. The main objective of the sample areas was to test the effectiveness of the compress in reducing lead exposure. In addition, the processing properties and parameters useful for the application were to be determined.

After one day, even at rather low temperatures, the poultice had dried and detached from the substrate. On one of the sample surfaces, the compress was applied in different layer thicknesses, continuously increasing from 2 to 6 mm. Here it was shown that with layer thicknesses exceeding 2 mm, no increasing cleaning success can be achieved, but the drying time and thus the waiting time until removal is significantly increased.

An unplanned, but not undesirable side effect of cleaning with the compress material was a clear brightening of the natural stone surfaces that went beyond the removal of the heavy metal load (Figs. 19.1 and 19.2).

19.5.2   Musée du Louvre, Paris

After the extremely positive results at the Hotel de Rohan, the French authorities decided to test the cleaning poultice again on an in terms of monument preservation even higher-ranked object, the Musée du Louvre. These tests were also used to draw comparisons between the newly developed poultice and a proprietary poultice of the restoration company carrying out the work (Fig. 19.3).

The decision was made in favour of the material that had already been successfully tested at the Hotel de Rohan, on the one hand due to the better cleaning effect and on the other hand in accordance with the city's wish to use a material that had been

Fig. 19.1 Sample surfaces to determine the optimal application thickness (continuously increasing within an area of 2 mm to 6 mm) or application quantity one day after application. The self-detaching effect at low film thickness is clearly visible. [Photo: Remmers]

Fig. 19.2 Cleaning results on sample surfaces with different natural stone substrates. [Photo: Remmers]

pre-produced and quality-assured in a factory. For use at the Louvre, the poultice was commercialised under the name "Clean Galena".

Unfortunately, the collection of samples from the test areas at the Musée du Louvre was restricted to a minimum; only two pyramidal samples with a base area of 10 × 10 mm were allowed to be taken for our own laboratory tests. Sample 1 before cleaning and sample 2 after cleaning.

Fig. 19.3 Cleaning sample areas at the Louvre, Paris [Photo: Tollis]

These samples were tested in cooperation with the Material Prüfanstalt Bremen, Mr. Frank Schlütter (Figs. 19.4 and 19.5).

The work was carried out by Tollis, company Lefevre's sculpture specialists. The cleaning poultice was sprayed on, using the airless method, and removed from a mobile scaffold that was not allowed to be anchored to the façade (Fig. 19.6).

By airless spraying, the material showed rapid drying, even in relatively poor climatic conditions, which usually cannot be achieved by manual application.

The poultice used showed on the natural stones of the Louvre that it is capable of cleaning the façade in such a way that no further cleaning step needs to take place–as was the case in all the preliminary tests. Taking more samples from the Louvre façade
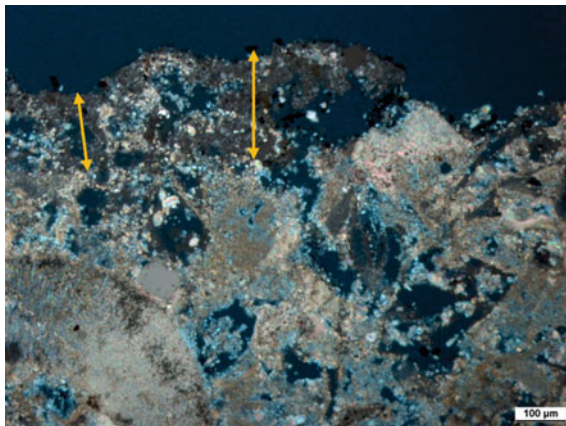
Fig. 19.4 PolMi image, under crossed polarisers, sample 1, uncleaned. There are dirt particles in depressions in the surface (area 3). Plastering on the surface and in the microstructure section near the surface (arrow mark) [Photo: MPA Bremen]
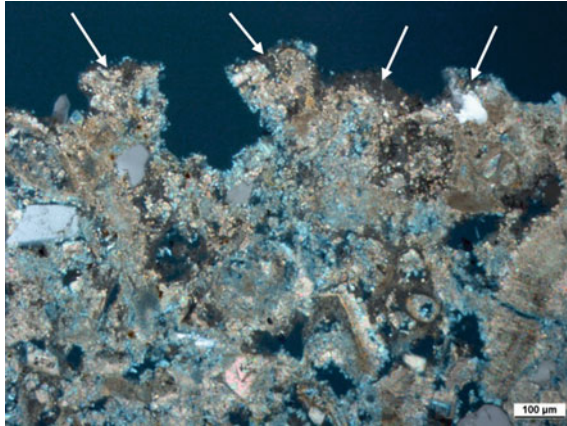
Fig. 19.5 PolMi image, under crossed polarizers, sample 2, cleaned. No dirt particles are visible on the surface. The plastering (arrows) on the surface does not appear to have been altered by the cleaning. [Photo: MPA Bremen]

Fig. 19.6 Scaffolding on the Louvre façade, during cleaning [Photo: Remmers]

was not permitted. In spring 2017, a first construction section of the Louvre, about 200 m of the façade along the Seine, was cleaned with the novel compress. To date, two further construction sections have been processed (Fig. 19.7).

Fig. 19.7 First section of
the Louvre façade cleaned
with "Clean Galena" [Photo:
Remmers]

19.5.3   Musée Carnavalet, Paris

Between October 2017 and February 2019, the Facades of the Museum "Carnavalet" in Paris have been cleaned and restored by company H. Chevalier.

The Museum is the major historical museum of the City of Paris. Its collections, which include more than 600,000 works and makes it one of France's leading museums, are presented in the exceptional historical setting of two townhouses in the heart of the Marais (Fig. 19.8).

The French labour code specifies that before any cleaning of a stone facade a test in order to identify a potential lead pollution must be carried out.

Fig. 19.8 Musée
Carnavalet, the major
historical museum of the
City of Paris [Photo: H.
Chevalier]

In case that a lead content of more than 1000 μg/m^2 is detected, the French public health protection act prescribes the following:

- No sandblasting is allowed anymore,
- workers must be equipped with specific protections and
- workers have to undergo tests to determine the lead level in their blood.

On the facades of the Musée Carnavalet tests to determine the lead exposure have been carried out on five spots. Three of these spots showed more than 1000 μg/m^2.

At one of these spots a lead content of 28,000 μg/m^2 was measured.

After the treatment with the compress the lead content of all the sample areas was significantly reduced. Just at the spot with the highest led content it has not been possible to reduce it to a content below 1000 μg/m^2 (Fig. 19.9).

The cleaning effect of the compress has been very sufficient in all test areas (Fig. 19.10).

At the Musée Carnavalet the poultice was as well applied by airless spraying. Due to the local recommendations the workers had to wear protective suits to avoid them from getting in contact with lead containing dust (Figs. 19.11 and 19.12).

One day after the application the compress has already dried and could be removed very easily. Beyond application of the compress further cleaning of the facades hasn't been necessary. The dried, removed material must be disposed of according

| REFERENCE DES ECHANTILLONS	DESIGNATION		TENEUR EN PLOMB ACIDO-SOLUBLE (µG/M²)
PMH171271 – 1	Lingette référencée : « 1 »		563
PMH171271 – 2	Lingette référencée : « 2 »		1 043
PMH171271 – 3	Lingette référencée : « 3 »	Avant pose de cataplasme Clean Galéna	280 00
PMH171271 – 4	Lingette référencée : « 4 »		3 560
PMH171271 – 5	Lingette référencée : « 5 »		739
PMH171271 – 6	Lingette témoin		< LQI
PMH171278 – 1	Lingette référencée : « 1 »		42
PMH171271 – 8	Lingette référencée : « 2 »		126
PMH171278 – 2	Lingette référencée : « 3 »	Après application de cataplasme Clean Galéna	11 512
PMH171278 – 3	Lingette référencée : « 4 »		161
PMH171278 – 4	Lingette référencée : « 5 »		137
PMH171278 – 5	Lingette témoin		<LQI

Fig. 19.9 The determination of acid-soluble lead on dust is carried out by atomic emission spectrometry according to French standards NF X 46-032 and FD T 90-112 [Photo: H. Chevalier]

Fig. 19.10 Cleaning test area at the Musée Carnavalet in Paris [Photo: H. Chevalier]

Fig. 19.11 Application of the cleaning compress at the Musée Carnavalet, Paris [Photo: H. Chevalier]
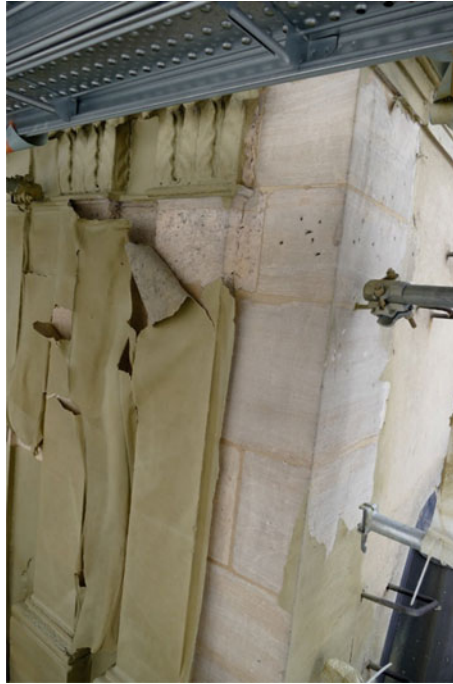
Fig. 19.12 Dried compress is self-peeling that means that it is very easy to remove [Photo: H. Chevalier]

to municipal regulations; if necessary, the heavy metal load of the compress must be examined for this purpose. The dried poultice material was not considered critical and could be disposed of as "household waste" without special treatment (Fig. 19.13).

19.6 Conclusions

Cleaning of natural stone facades is a field that is influenced by many parameters. The interaction between the properties of the substrate, the "dirt" to be removed and the process used is extremely diverse and always at risk.

The new technology presented in this article offers the chance to remove heavy metal loads on facades, an increasingly relevant problem, efficiently and "cleanly"; at the same time, it seems that gentle cleaning of many natural stone substrates is possible with it as well. Although the method has already been successfully used on some outstanding monuments, it is still far away from being sufficiently investigated to be able to make general statements about the necessary boundary conditions to achieve positive results. Further investigation and modifications of the material have already started or are planned for the future.

Fig. 19.13 Facade of the Musée Carnavalet after cleaning [Photo: H. Chevalier]

Meanwhile the cleaning of facades at Westminster Palace including Big Ben has started (Fig. 19.14).

Fig. 19.14 Cleaning of a tracery at Westminster Palace, London [Photo: Remmers]

References

1. Zier H-W (2005) Dust exposure on building surfaces. In: Stein Zerfall und Konservierung, Institut für Steinkonservierung e.V
2. URL: https://www.umweltbundesamt.de/blei-im-feinstaub#textpart-1, 24.03.2020, 11:36
3. Harrison RM, Laxen DPH (1981) Lead pollution, causes and control. Chapman and Hall Ltd, London
4. Compare: Articles R.1334-8 and R.1334-13, Code de la santé publique, France, Sept 2006
5. Woolfitt C, Abrey G (2000) The building conservation directory
6. https://eur-lex.europa.eu/legal-content/DE/TXT/?qid=1530028986315&uri=CELEX:32018L0851, 01.03.2022, 10:17

Chapter 20
IRT Survey of Historic Building Façades for Focusing the Diagnostic Analysis

Sofia Brizzi , **Emma Cantisani** , **and Cristiano Riminesi**

Abstract In the framework of conservation of historical buildings, the infrared thermography (IRT) is a valuable tool for the image diagnostic on façades. This non-destructive technique allows to discover structural defects on masonries—such as detachments, cracks, inhomogeneity in the wall texture, or to determine heat dispersion, raising dampness, and water infiltrations—by the detection of the surface temperature. In the present work, the IRT technique was applied to investigate the painted façades of the Lenzi palace in Florence. The palace currently houses the French Institute in Florence and it has undergone several renovations and restorations over the years, the last one in 1984. The target of the IRT survey has been to highlight the areas affected by decay phenomena, including those already restored. This result was used to direct the sampling for the laboratory analysis, thus reducing the number of samples and optimizing the sampling procedure. The laboratory analysis, consisting of FT-IR, XRD, optical and electronic microscopes investigations, allowed the identification of the executive technique, the products of past restoration and the alteration/decay products. Through the experience of the case study of palazzo Lenzi, it was possible to check the effectiveness of the IRT technique in supporting a multi-disciplinary approach to focus the diagnostic analysis and verify the efficacy and duration of conservation interventions by remote way identifying areas subject to new degradation phenomena.

Keywords "Graffito" technique · Infrared thermography · Multi-disciplinary diagnostic approach · Preventive conservation

S. Brizzi (✉) · E. Cantisani · C. Riminesi
National Research Council of Italy—Institute of Heritage Science (CNR-ISPC), Via Madonna del Piano 10, Sesto Fiorentino (FI), Tuscany, Italy
e-mail: sofia.brizzi@ispc.cnr.it

E. Cantisani
e-mail: emma.cantisani@cnr.it

C. Riminesi
e-mail: cristiano.riminesi@cnr.it

20.1 Introduction

The conservation of painted façades of the historical building represents a complex process, dealing with extremely heterogeneous elements and with different and stratified layers. The Lenzi palace, which has the front elevation in Ognissanti square and the side elevations in the streets Montebello and Borgo Ognissanti, represents an important proof of the Florentine Renaissance architecture, with the façades painted in 1456 using the *graffito* technique. The *graffito* was realized by applying layers of plaster tinted in contrasting colors to a moistened surface and then scratching the superficial layer so as to reveal parts of the different colored ground [1, 2]. From past interventions have been discovered that a stratigraphy is present. Under the present painted façade, there are both portions of an older *graffito* and, at an even deeper level, a coarse and rough plasterwork, scratched with various motifs, revealed by significant mortar losses.

In this research activity, the infrared thermography technique was used to investigate the "footprint" of previous interventions that have changed the appearance of the palace occurred during the centuries. Given the excellent quality of the *graffito* material, a diagnostic survey of the mortars was carried out, defining a careful and accurate historical-documentary research of the palace, in order to solve its "enigmas" and define its precarious state of conservation.

20.1.1 Historical Background

Firstly, and for a long time, the *graffiti* was attributed to Andrea Feltrini, at the beginning of the XVI century. After, it has been backdated to 1494, suggesting that it was commissioned by Lorenzo Lenzi. The palace became the property of the patrician florentine family Quaratesi in 1763. In the last decades of the nineteenth century, it was acquired and restored by the Pisani family following the project of the architect Luigi Del Moro (1885–1887). During this intervention, the original plasters were brought to light [3]. In 1908, the palace became the headquarters of the French Institute of the University of Grenoble, which promoted further works, especially to adapt the interior to its new function. In 1927, when it was still owned by the Pisani family, the windows on the ground floor were reduced to "shop windows", as attested by the request for work kept in the historical archives [4]. In particular, the ground floor was reworked during the conservation works of the XIX century and only the central entrance left original, while all the other entrances, including the one facing on Borgo Ognissanti Street, were opened by replicating the shape and proportions of the model (an image of the building before these interventions is given by Giuseppe Zocchi in 1744, Fig. 20.1) [5]. In 1950, the building was acquired by the French government and the façades were again restored in 1950 and 1965.

The last intervention has been done in 1984, and it consisted of the integration of the new *graffito* with aerial mortar and manganese oxide, then, again with fresh

Fig. 20.1 Representation of Ognissanti square, on the left the Lenzi Palace

plaster, the entire surface was colored with several coats of white layers, sprinkling the decorative motif found in real life and recomposed on the basis of the remaining original decoration. Finally, the surface was scratched, following the lines of the dusted design and consolidated by the application of barium hydroxide [6].

20.2   Methods and Materials

20.2.1   IR Thermography Survey

The front elevation and the side elevations on Via Montebello and Borgo Ognissanti façades were investigated by IRT. The surveys were performed in passive modality [7, 8] during different periods, in particular autumn and winter, i.e., exploiting the different thermal capacity of the materials composing the masonry and the exchange that can occur between them in certain period of the day as a result of the weather/environmental condition of the seasons.

The aims are the following:

- to confirm the transformations carried out over the years and described in the previous paragraph (plugging of windows, modifications to openings—doors and windows) [9–11];
- to determine the presence of detachments, water infiltrations/leaks from the downpipes [12, 13].
- to allow a stratigraphic reading of the building by non-destructive way which is useful to guide further analytical investigations performed by sampling.

The device used for the IRT survey is the FLIR infrared camera T540, with a resolution of 464 × 348 pixels, thermal sensibility of (NETD) < 30 Mk a 30 °C

(optic lens of 42°) di 50 mK, temperature range from −20 °C to + 350 °C, and accuracy of ± 2%. The thermal image was elaborated by FLIR software, and the mosaic reconstruction was performed by Adobe Photoshop software.

20.2.2 Laboratory Analysis

The chemical, mineralogical, and petrographic characterization of plasters was carried out for all samples, using the following analytical methodologies [14–18]:

- Optical microscopy (OM) was used to observe macroscopic features of the mortar samples, as well as by the naked eye, also by means of a stereomicroscope up to 200 magnifications. A Nikon Eclipse E600 reflected-light optical microscope was also used, equipped with a high-resolution camera and NIS Elements software for managing the images and evaluating the morphometric characteristics of the material. It is particularity useful to verifying the presence of a stratigraphic succession in the samples, to assess their thickness, state of conservation, and adhesion characteristics. It also makes it possible to check for the presence of pigments, organic binders, and any surface alterations;
- petrographic investigation was carried out through observation in transmitted light of thin Sections (30 μm thickness) with an optical microscope. In case of mortars, the petrographic approach permits accurate characterization of binder, aggregate, and inorganic additives and admixtures;
- X-ray powder diffractometry (XRPD) was employed on powders to determine the mineralogical composition using a powder X-ray diffractometer (Cu anticathode ($k = 1.54$ Å)), under the following conditions: current intensity of 30 mA, voltage 40 kV, and angular range $3° < 2\theta < 70°$;
- IR spectroscopy by Fourier transform infrared method (FT-IR) was used to determine the molecular composition of the samples and the possible presence of previous treatments. FT-IR measurements were carried out using an ALPHA Bruker portable spectrometer with a Globar SiC source and DTGS detector. Spectra were recorded by scratching small amounts of sample directly from the surface of the stones, using a platinum single reflection diamond module for attenuated total reflectance (ATR). Operating conditions: spectral range 4000–400 cm^{-1}, resolution 4 cm^{-1}, and 24 scans. The spectra were processed with OPUS 7.2 software.
- Scanning electron microscopy/energy dispersive X-ray spectroscopy (SEM–EDS) was used for morphological observation and elemental microanalysis of plasters, with an acceleration potential of 15 kV, beam current of 500 pA, and working distance between 9 and 8.5 mm.

20.2.3   Samples Description

The preliminary IRT survey, combined with a visual investigation, allows us to identify the most degraded areas, in which infiltration of water and plaster detachments were present (see sub-paragraph 3.1). During recent restoration works, ten samples were collected. The name of the samples and their location is shown in Fig. 20.2. Table 20.1 reports the samples description.
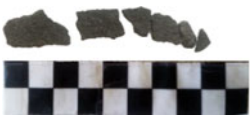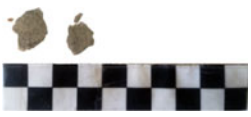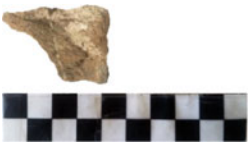

Fig. 20.2   Samples location

Table 20.1   Description of samples

Label	Sample description	Photo-macro
PL_01	Fragment of black and brown plaster with white mortar substrate	
PL_02_A	Fragment of black plaster with white mortar substrate	
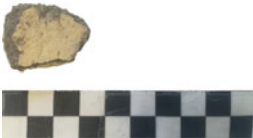
Table 20.1 (continued)

Label	Sample description	Photo-macro
PL_02_B	Portion of black plaster surface	
PL_03_A	Fragments of integration mortar	
PL_03_B	Fragments of integration mortar anchored to pietraforte	
PL_04	Fragment of black plaster with white mortar substrate	
PL_05_A	Fragment of pietraforte	
PL_05_B	Portion of mortar anchored to pietraforte with brick inserts	

Table 20.1 (continued)

Label	Sample description	Photo-macro
PL_06	Fragment of black plaster with white mortar substrate	
PL_07	Fragment of white superficial layer with black plaster and white mortar substrate	

## 20.3   Results and Discussions

20.3.1   Infrared Thermography

The IR images were collected on the frontal façade and on the side façades on Montebello and on Borgo Ognissanti Streets. Several critical elements were identified, and they should be taken into account during the restoration works. The result of the IR images merging is shown in Figs. 20.3 and 20.4.

The issues detected are summarized in the following:

- the thermal anomalies found above the first door and the second door on the frontal façade, from Montebello Street to Borgo Ognissanti, are due to the presence of detachment and loss of cohesion of the plaster (Fig. 20.3). These anomalies correspond with the pre-existing windows that were filled in during the works of the late 1800s, under the Pisani property. In fact, their presence in the past is also confirmed by Giuseppe Zocchi's drawing of 1744 (Fig. 20.1); the drawing shows four windows very similar, both in size and location, to the two windows still present on the right of the entrance door. The presence of windows above the first and second door is very slight and is probably superimposed with the loss of cohesion of the plaster (Fig. 20.5).
- presence of downpipes embedded in the masonry (hidden downpipes) between the first and second window and between the sixth and seventh window of the frontal façade, starting from Montebello street going to Borgo Ognissanti (see Fig. 20.3). The presumed downpipes went down from the roof to the ground, then have been probably interrupted above the first and fourth entrance door during a previous restructuration works. In both cases, a thermal discontinuity highlights a loss of cohesion of the plaster or the presence of detachment.
- the areas under the windows of the first and the second floors, that show a higher temperature (about 30 °C) than the surrounding area, are probably due to the presence of heating pumps (see Fig. 20.3).
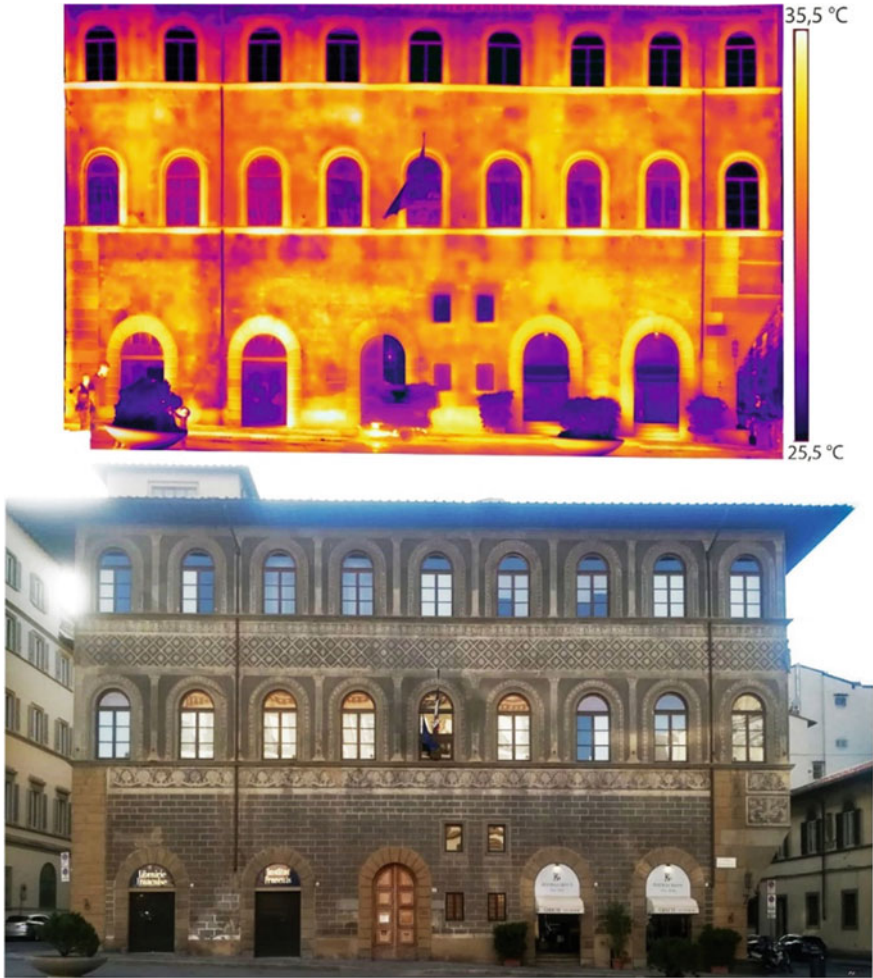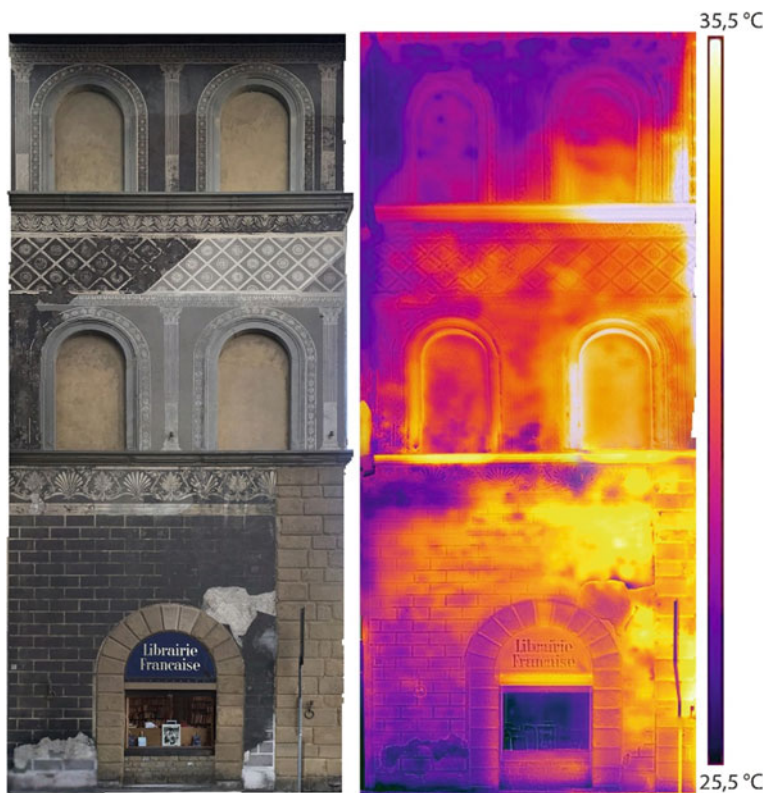
Fig. 20.3 IR and VIS images of the frontal façade (view from Ognissanti square)

- the windows on the top floor, although arched, show a rectangular internal frame (see Fig. 20.3).
- at the base of the building, the one in contact with the street level, the presence of capillary rising water phenomena is evident and it is still in progress (see Fig. 20.3).

As far as the IR images of Via Montebello are concerned, the area to the right above the door is characterized by the presence of a huge detachment, which has already resulted in large losses of material (see Fig. 20.4). Also in this case, the lower level, in contact with the ground, seems to have patches of moisture.

Fig. 20.4 IR and VIS image on the left façade (view from Montebello Street)
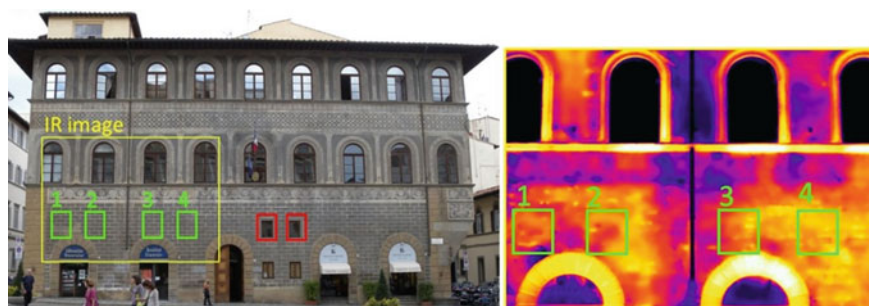
Fig. 20.5 Green line is highlighted the probable location of the four covered windows on the frontal façade. In red line, the existing windows

About the IR survey on the side elevation of Borgo Ognissanti Street no relevant defects is detected at the moment.

20.3.2 Chemical, Mineralogical, and Petrographic Characterization

The main chemical, mineralogical, and petrographic characteristics of analyzed samples are summarized in Table 20.2. Table 20.3 reports the XRD and FT-IR results.
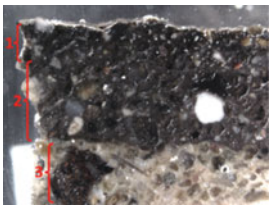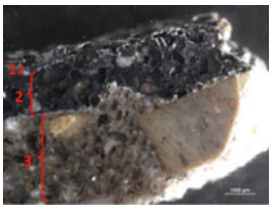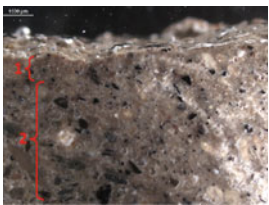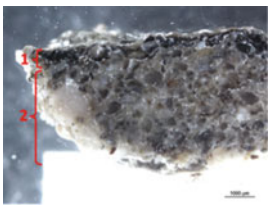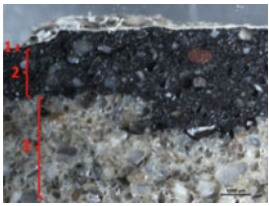
In order to examine the composition and microstructure of plasters, the thin sections of samples were analyzed under an optical microscope. The petrographic observation allows to identify the main features of each layer in terms of composition, microstructure and texture of binder, composition, grain size distribution and shape of aggregate and inorganic additives. According to the *graffito* technique, all the samples are composed at least by two layers, the first one with a typical dark color, the second one lighter. The analyzed plasters were realized by mixing an air hardening calcic lime with an aggregate of heterogeneous composition. Quartz mono and polycrystalline, plagioclases, K-feldspars, micas, carbonate, and silicate rock fragments were identified. Even if the mineralogical composition of aggregate in the analyzed plasters is quite similar, differences can be observed in the relative abundance of aggregate and in the grain size distribution. In the Fig. 20.6, as example, the different petrographic features of the first and second plaster layers for sample PL0_2A are reported.

Petrographic observations highlight also differences among the same layers of different samples in the composition of aggregate, relative abundance, and grain size distribution, proving the application of these materials at different times or by different workers. SEM morphological and microchemical analyses revealed that the black coloration of the upper layers is due to the presence of Mn and Fe compounds, finely dispersed within the binder, but differences among abundance, distribution and grain size of these compounds have been evidenced (Fig. 20.7).

In Fig. 20.7b, we can observe that Mn is in lamellar form both as an oxide (MnO_2, pyrolusite) and in agglomerates also containing Ba and traces of Pb, instead of the sample PL_01 (Fig. 20.7a), where Mn compounds presence is limited to the surface level and its distribution is not uniform. For sample PL _07 (Fig. 20.8a), the Mn is associated to iron in grain of size of almost 100 μm and the presence of a superficial thin layer enriched in Ti has been observed (Fig. 20.8b).

In the case of the sample PL_06, the Mn is concentrated in a very limited thickness of sample and associated to Fe compounds (Fig. 20.9).

Table 20.2 Description of analyzed samples

| Sample label	Cross section	Sample description	Performed analyses
PL_01		Layer 1: black plaster of 1 mm of thickness	OM, XRD, FT-IR, SEM-EDS
		Layer 2: layer in which the color changes from black to brown for a total thickness of 3 mm	OM, XRD, FT-IR, SEM-EDS
		Layer 3: layer of white mortar	OM, XRD, FT-IR
PL_02_A		Layer 1: white surface layer of approximately 50 μm of thickness	OM, XRD, FT-IR, SEM-EDS
		Layer 2: black plaster of 2 mm of thickness, with a finely dispersed black aggregates in the binder	OM, XRD, FT-IR, SEM-EDS
		Layer 3: white mortar very rich in aggregate, more heterogeneous than the surface plaster	OM, XRD, FT-IR
PL_05_B		Layer 1: superficial layer (ca 500 μm) poor in aggregate	OM, XRD, FT-IR, SEM-EDS
		Layer 2: internal mortar richer in aggregate than the superficial area Some areas are affected by the re-precipitation of calcite, with many shrinkage cracks	OM, XRD, FT-IR, SEM-EDS
PL_06		Layer 1: black superficial plaster (ca 500 μm)	OM, XRD, FT-IR, SEM-EDS
		Layer 2: white mortar very rich in aggregate, more heterogeneous than the surface plaster	OM, XRD, FT-IR
PL_07		Layer 1: thin white superficial layer (ca 50 μm)	OM, XRD, FT-IR, SEM-EDS
		Layer 2: black plaster of 2 mm of thickness, with a finely dispersed black aggregates in the binder	OM, XRD, FT-IR, SEM-EDS

Table 20.2 (continued)

Sample label	Cross section	Sample description	Performed analyses
		Layer 3: white mortar very rich in aggregate, more heterogeneous than the surface plaster	OM, XRD, FT-IR

Table 20.3 Results of XRD and FT-IR analysis

	XRD	FT-IR
PL_01		
layer 1–2	Quartz, calcite, gypsum, plagioclase, muscovite, k-feldspars	Quartz, calcite, calcium oxalate, gypsum
layer 3	Quartz, calcite, plagioclase, muscovite, k-feldspars	Quartz, calcite
PL_02_A		
layer 1–2	Quartz, gypsum, calcite, pyrolusite	Quartz, gypsum
layer 3	Quartz, calcite, plagioclase, k-feldspars	Quartz, calcite
PL_05_B		
layer 1	Quartz, calcium oxalate (weddellite), calcite, gypsum	Quartz, calcium oxalate, (weddellite)
layer 2	Quartz, calcite, gypsum	Quartz, calcite, gypsum
PL_06		
layer 1	Quartz, calcite, gypsum, plagioclase, k-feldspars, muscovite	Quartz, calcite, gypsum, calcium oxalate
layer 2	Quartz, calcite, gypsum, plagioclase, k-feldspars, muscovite, traces of gypsum	Quartz, calcite, traces of gypsum and calcium oxalate
PL_07		
layer 1	Quartz, calcite, gypsum, k-feldspars, albite	Quartz, calcite, gypsum, calcium oxalate
layer 2	Quartz, calcite, k-feldspars, traces of pyrolusite	Quartz, calcite, traces of gypsum
layer 3	Quartz, calcite, k-feldspars	Quartz, calcite
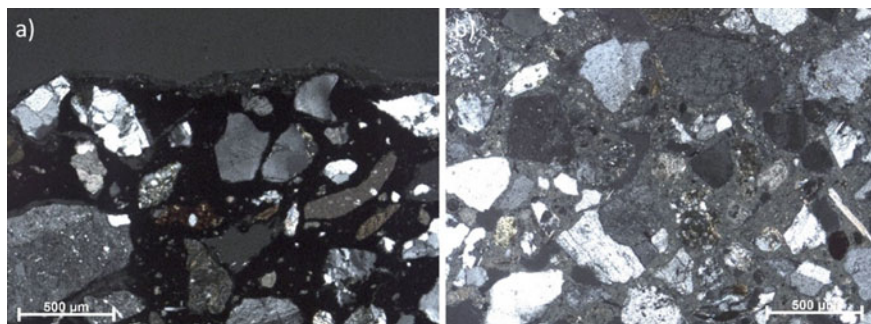
Fig. 20.6 Microphotographs of sample PL02A: first layer (left), second layer (right) under optical polarized microscope, cross nicols
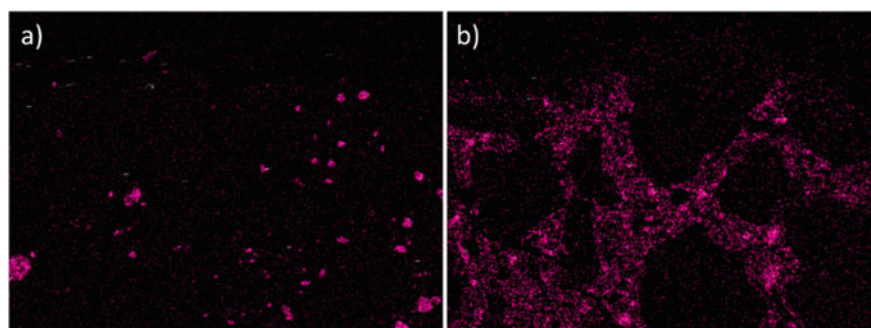
Fig. 20.7 Map of Mn distribution in the first 300 μm of the sample **a** PL_01 and **b** PL_02_A
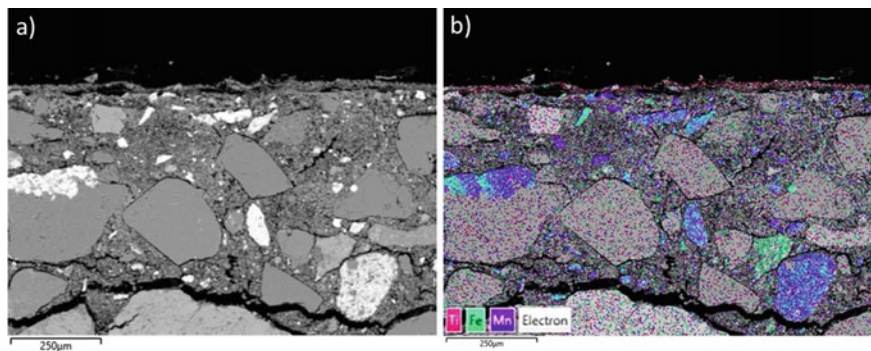
Fig. 20.8 SEM-EDS backscattered image of sample PL_07 (**a**) SEM–EDS combined map of Mn, Fe, Ti (**b**)

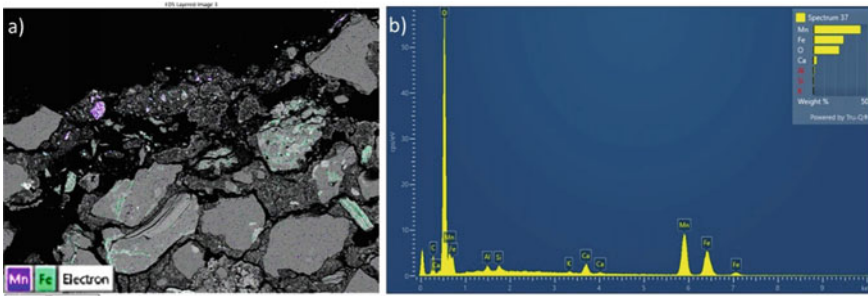**Fig. 20.9** SEM–EDS map of Mn and Fe for sample PL_ 06 (**a**) and relative EDS spectrum of selected grains (**b**)

20.4 Conclusions

The IRT survey provides a useful approach to focus the sampling for laboratory investigations on the degraded areas to better characterize the different construction phases. The laboratory techniques, chemical, mineralogical, and petrographic, allowed to characterize the materials composition and the technologies used for their preparation, so it has been possible to identify the different phases of intervention and restorations. In particular pyrolusite (MnO_2), which is present in all the analyzed samples, is due to the last restoration, however, the plasters composition differs in grain size and relative abundance, so they might belong to restorations that took place at different times or by different workers. With the available data, it is not possible to exclude an organic surface treatment as well, as suggested by the presence of calcium oxalates detected by XRD and FT-IR.

Sulphation phenomena (presence of gypsum) are also recurrent in the surface layers. With this multi-analytical approach, it has been possible to discover different construction restorations of Lenzi façade palace, even if the original *graffito* has not been found and seems to remain only in small traces probably on the last floor.

References

1. Menicali U (1992) I materiali nell'edilizia storica: tecnologia e impiego dei materiali tradizionali. Nuova Italia Scientifica
2. Bocchi-Cinelli (1677) Le bellezze della città di Firenze, dove a pieno di pittura, di scultura, di sacri templi, di palazzi, i più notabili artifizi, e più preziosi si contengono, scritte già da M.

Francesco Bocchi, ed ora da M. Giovanni Cinelli ampliate, ed accresciute, Firenze, per Gio. Gugliantini

3. Carocci G (1906–1907) I dintorni di Firenze, edizione completamente rinnovata, 2 vol., Firenze. Multigrafica Editrice

4. Ginori Lisci L (1972) I palazzi di Firenze nella storia e nell'arte, Firenze, Giunti & Barbèra

5. Zocchi G (1744) Scelta di XXIV vedute delle principali Contrade, Piazze, Chiese e Palazzi della Città di Firenze, Firenze, appresso Giuseppe Allegrini, tav. IX

6. Soprintendenza per i beni ambientali ed archiettonici per le provincie di Firenze e di Pistoia French ministry of foreign relations, restoration work on the facades of palazzo Lenzi, seat of the general consulate of France in Florence and the French institute no. 165/1°/1984, (1984)

7. BSI (1999) Thermal performance of buildings-qualitative detection of thermal irregularities in building envelopes-infrared method (ISO 6781: 1983 Modified); BSI: London, UK

8. Vollmer M, Mollmann KP (2017) Infrared thermal imaging: fundamentals, research and applications. Wiley, Hoboken, NJ, USA

9. Cabrucci A, Padovani S (2008) L'evoluzione dell'indagine termografica., Il cantiere della conoscenza, Arte Tipografica Editrice, Napoli

10. Glavaš H, Hadzima-Nyarko M, Haniˇcar Buljan I, Bariˊc T (2019) Locating hidden elements in walls of cultural heritage buildings by using infrared thermography. Buildings 9:32. https://doi.org/10.3390/buildings9020032

11. Grinzato E (2012) IR Thermography applied to the cultural heritage conservation. In: 18th World conference on nondestructive testing, Durban, South Africa, pp 16–20

12. Proietti N, Capitani D, Di Tullio V, Olmi R, Priori S, Riminesi C, Sansonetti A, Tasso F, Rosina E (2015) MOdihMA at Sforza Castle in Milano: Innovative Techniques for Moisture Detection in Historical Masonry, In: Toniolo L, Boriani M, Guidi G (eds) Built heritage: monitoring conservation management. Research for Development. Springer, Cham. https://doi.org/10.1007/978-3-319-08533-3_16

13. Vettori S, Bracci S, Cantisani E, Riminesi C, Sacchi B, D'Andria F (2016) A multi-analytical approach to investigate the state of conservation of the wall paintings of Insula 104 in Hierapolis (Turkey). Microchem J 128:279–287. https://doi.org/10.1016/j.microc.2016.05.006

14. Cantisani E, Calandra S, Barone S, Caciagli S, Fedi M, Garzonio CA, Liccioli L, Salvadori B, Salvatici T, Vettori S (2021) The mortars of Giotto's bell tower (Florence, Italy): raw materials and technologies. Sci Dir Constr Build Mater 2021(267):1–11

15. Sardella A, Canevarolo S, Marrocchino E, Tittarelli F, Bonazza A (2021) Investigation of building materials belonging to the ruins of the Tsogt palace in Mongolia, Heritage MDPI

16. Elsen J, Brutsaert A, Deckers M, Brulet R (2004) Microscopical study of ancient mortars from Tournai (Belgium), Mater Charact 53:289–294

17. Blaeuer C, Kueng A (2007) Examples of microscopic analysis of historic mortars by means of polarising light microscopy of dispersions and thin sections. Mater Charact 58(11–12):1199–1207

18. Pavía S, Caro S (2008) An investigation of Roman mortar technology through the petrographic analysis of archaeological material. Constr Build Mater 22(8):1807–1811

Chapter 21
Walking Through Florence to Discover the Stone-Built Cultural Heritage

A. P. Santo, I. Centauro, and E. Pecchioni

Abstract Bathed in the charm of centuries of history and architectural beauty, the city of Florence is a kind of open-air museum which represents the historical memory of the city, from the Middle Age to modernity. The countless masterpieces are mainly made of the rocks outcropping close to the city and surrounding areas. Thus, Florence is characterized by the colours of its stone-built cultural heritage, the warm ochraceous and the cerulean grey of the Pietraforte and Pietra Serena sandstones, but also the white of marbles, the green of serpentinites, and the red of limestones. In addition, other natural lithotypes, together with artificial materials, were used to realise columns, decorations, claddings, masonry finishing, etc. To deepen the knowledge of the stone materials of Florence, the progressive web app "Florence RockinArt" may help us; it is addressed to all those who are interested in discovering the monuments of Florence by carefully observing the stone materials that make up them. The web app contains short historical and architectural notes on the main monuments but, first of all, detailed geological, mineralogical, and petrographic characteristics of the natural and artificial materials of which they are constituted. The best way to visit this charming city is on foot, getting the chance to walk into the history. In this paper, we suggest a selection among the most significant and suggestive walks through the city such as, for instance, looking for the differences between the sandstones Pietra Serena and Pietraforte, the search for churches decorated with the three colours, white, red, and green, or the hunt for little used polychrome materials.

Keywords Florence · Progressive Web App · Stones · Cultural heritage · Walks

A. P. Santo (✉) · I. Centauro · E. Pecchioni
Department of Earth Sciences, via La Pira, 4, Florence, Italy
e-mail: alba.santo@unifi.it

21.1   Introduction

Florence is one of the most art-owned cities in the world; indeed, in 1982, the historic centre of Florence was declared a World Heritage Site by UNESCO. The architectural buildings and the works of art represent the historical memory of the city, the result of a continuous artistic creation that lasted over the centuries, from the Middle Age to modernity. One of the most distinctive features of Florence is, undoubtedly, the Renaissance architecture that in this city was born. However, other artistic periods left here their masterpieces, such as the Romanesque of Chiesa di San Miniato al Monte, the Gothic of Chiesa di Santa Croce, the Mannerism of Fontana del Nettuno and Giardino di Boboli, the Baroque of Chiesa di San Michele e San Gaetano and the Complesso di San Firenze, the Modern of the Santa Maria Novella train station, and the Artemio Franchi stadium.

The city represents, for the great variety of its artistic and architectural heritage, a kind of open-air museum. The works of art and monuments are mainly made of rocks outcropping close to Florence and surrounding areas; a close link, therefore, exists between monuments, geographical position of the city and its history. The use of rocks coming from the nearby outcrops allowed limited transport costs of material; indeed, the main stone materials used in the architecture of Florence are the sandstones (Pietra Serena and Pietraforte), extracted from the quarries in the Florentine hills. In many churches were used, also, for decorative purposes, various types of marbles, besides serpentinites and limestones; in addition to the natural stones, also artificial materials, such as plasters, mortars, and bricks were used to complete or cover the stone walls. Florence, like every city, is characterised by the colours of its stones: the warm ochraceous and cerulean grey of the Pietraforte and Pietra Serena sandstones, the white of marbles, the green of the serpentinites, and the red of limestones. To deepen the knowledge of the stone materials, the Progressive Web App (PWA) "Florence RockinArt" [1] was created and is available for iOS and Android devices (Fig. 21.1). It is addressed to all those who are interested in discovering the monuments of Florence by carefully observing the stone materials used during the different historical epochs in the Florentine architecture. It contains short historical notes and detailed geological, mineralogical, and petrographic characteristics of the natural and artificial materials of which the monuments are constituted.

Florence can be easily visited by walking, the possible routes are endless, studded with countless architectural and historical artistic highlights; we suggest here a selection among the most significant and suggestive (Fig. 21.2).

21.2   Looking for the Differences Between the Pietra Serena and Pietraforte Sandstones

One of the best ways to observe the Pietra Serena and Pietraforte sandstones is through a walk starting in Piazza della Santissima Annunziata and reaching Piazza
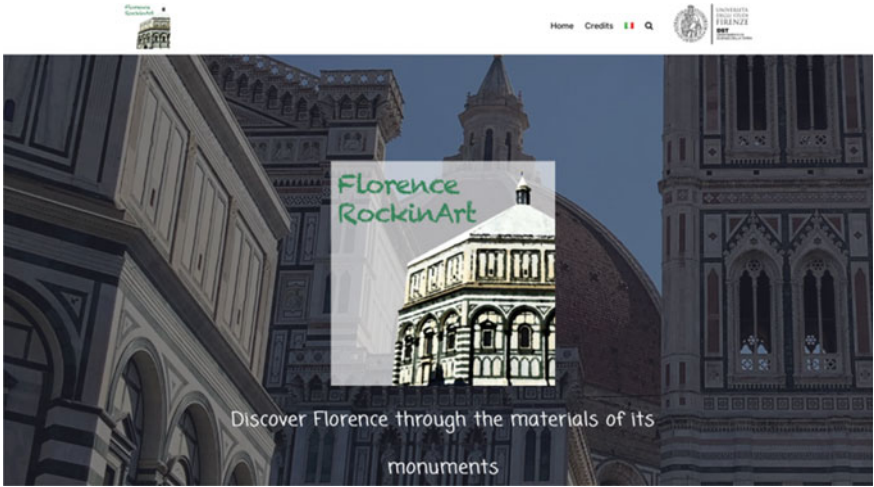
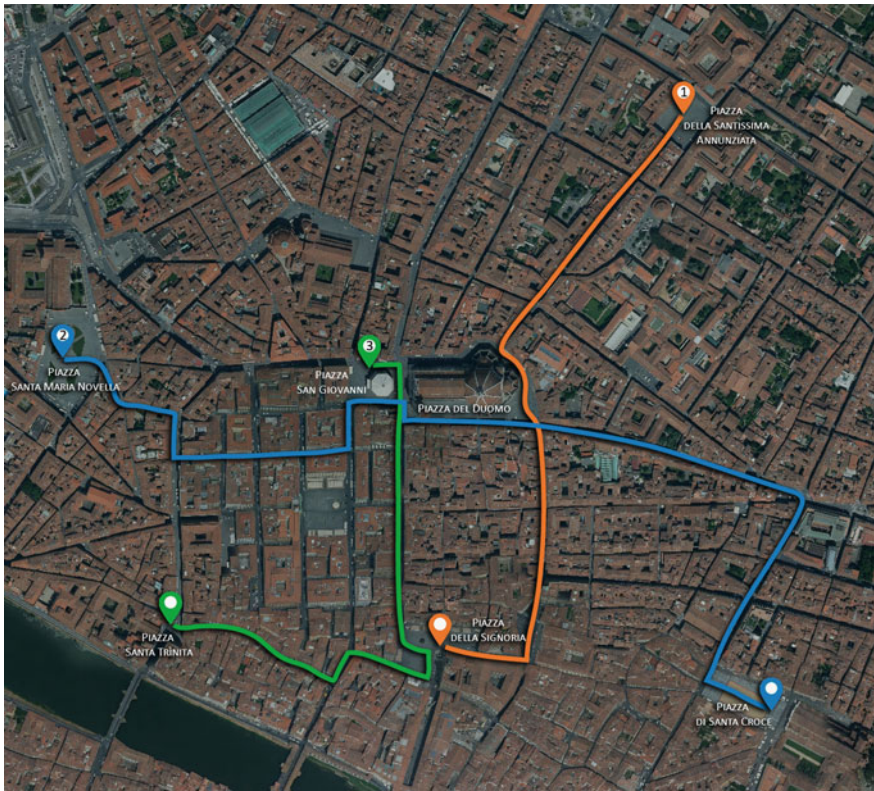**Fig. 21.1** Home screen of the Progressive Web App "Florence RockinArt"

Fig. 21.2 Map of Florence reporting the suggested three walk itineraries

della Signoria (walk number 1, Fig. 21.2). During the walk, we can see several buildings made of Pietraforte and Pietra Serena sandstones; in particular, in Piazza della Santissima Annunziata it is possible to look at the Basilica della Santissima Annunziata, the Loggiato dei Servi di Maria, and the Spedale degli Innocenti, briefly described as it follows. The second suggested stop during this walk is in Piazza della Signoria, entirely surrounded by Pietraforte sandstone buildings.

The Basilica della Santissima Annunziata (Fig. 21.3a) represents the main Marian sanctuary of the city. The construction of the church began in 1250 by the brotherhood of the Servi di Maria; the current name derives from the fresco of the Annunciation executed by the painter Bartolomeo and kept inside the church. Today's aspect is the result of three centuries of works; from 1280 until the first half of the fourteenth century, many internal modifications were done; successively the church was significantly enlarged. The external loggia (1601), by Giovanni Battista Caccini, was built to connect the façade with the arches of the Spedale degli Innocenti and the Loggiato dei Servi di Maria. In 1857, a great restoration was carried out by the architect Giuseppe Poggi. The columns, the arches, the tympanums, and the cornices are realised in Pietra Serena sandstone [1]. The floor of the loggia is in Apuan marble, Alberese limestone, and Colonnata black limestone [1–3].

The initial project, by Filippo Brunelleschi, of the Spedale degli Innocenti (Fig. 21.3b) started in 1419. After a long interruption, the works restarted in 1436 under the direction of Francesco Della Luna, and in 1445, the spedale was inaugurated. The spedale stands on a stairway in Pietraforte sandstone and is characterized by an arcade defined by nine large arches on columns having Corinthian capitals, and, on the sides, by two other arches flanked by grooved pilasters. On the upper part of the arcade, in 1487, ten white and blue glazed terracotta rounds, by Andrea della Robbia, were inserted. Many restoration and transformation interventions took place after the earthquake of 1842, when the damaged columns were replaced. The


Fig. 21.3 a Santissima Annunziata basilica; **b** Spedale degli Innocenti; **c** Loggiato dei Servi di Maria. Columns, capitals, and arches are in Pietra Serena sandstone, stairway is in Pietraforte sandstone (Spedale degli Innocenti) and in Pietra Serena sandstone of Firenzuola (Marnosa Arenacea Formation) [4] (Loggiato dei Servi di Maria). Images are from the PWA [1]

columns, the external arches, the capitals, the buttresses, the string course, the tympanums and the frames of the windows, and the corbels under the arcade are in Pietra Serena sandstone. The entire structure is in white plaster. Under the arcade, there are frescoes and busts in Apuan marble [1].

The construction of the Loggiato dei Servi di Maria (Fig. 21.3c), commissioned by the Servi di Maria order and designed by Antonio da Sangallo il Vecchio and Baccio d'Agnolo, began in the period between 1516 and 1525. The loggiato consists of an arc joining a series of houses each of which corresponds to one span. The house construction was very complex and lasted over the centuries until 1720 when the works were completed. The columns of the loggiato, the external arches, the corbels, the window and door frames are in Pietra Sera sandstone; and doors, the tympanum and window frames, the decorations, and the string courses above the loggiato are in Pietra Serena sandstone. The entire structure is finished by plaster. The steps of the entrance stairway are realized in Pietra Serena sandstone of Firenzuola (Marnosa Arenacea Formation) [4]. In the external loggiato, there are rounds realized with painted plaster and finishing in Pietra Serena sandstone [1].

In Piazza della Signoria, we can admire the Palazzo della Signoria (Fig. 21.4a) and several other monuments such as the Loggia dei Lanzi (Fig. 21.4b) and the Palazzo Uguccioni (Fig. 21.4c).

The Palazzo della Signoria (Fig. 21.4a) was originally known as Palazzo dei Priori; in the fifteenth century, it became the seat of the *signoria*, hence, the name of the palace and the homonymous square in which it is located. The first phase of construction began in 1299 on the design of Arnolfo di Cambio and ended in 1315. The building is the result of other subsequent constructions and enlargements completed in the sixteenth century; it has the appearance of an inaccessible fortress, in the form of a square parallelepiped, in a typical Gothic style. The structure is divided into three floors and has a balcony and a tower. The different floors are divided by thin frames; on the ground floor, there are single windows, while on the two upper floors,
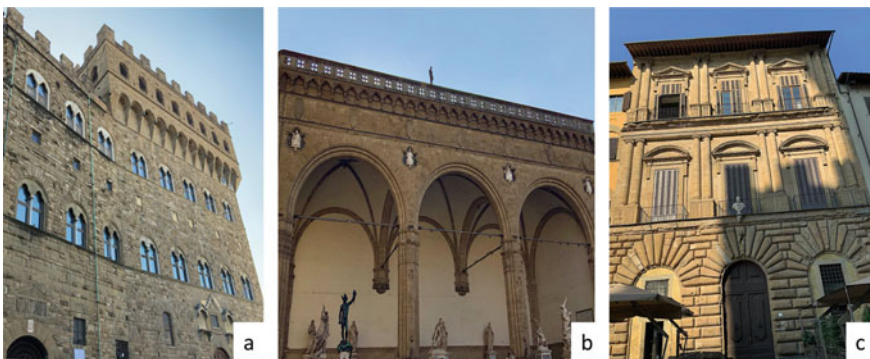
Fig. 21.4 **a** Pietraforte sandstone of the Palazzo della Signoria; **b** Loggia dei Lanzi entirely made in Pietraforte sandstone, with the balustrade of the terrace in Pietra Serena sandstone; **c** Façade of the Palazzo Uguccioni made of Pietraforte sandstone. Images are from the PWA [1]

there are mullioned windows displaying radial frames; the gallery is protected by square-shaped merlons and supported by brackets connected by round arches; below the arches are visible the large coats of arms (repainted several times in the centuries) reporting the symbols of the Florentine Republic. The Torre di Arnolfo, about 94 m in height, appears on the top right; it was edified in 1310 replacing the old tower, called della Vacca; the upper part of the bell tower displays swallowtail merlons. The palace and the tower are entirely made of Pietraforte sandstone. The mullioned windows and the radiant trigram of Cristo Re above the main door are in Apuan marble; behind the trigram there is a painted plaster (blue background with golden lilies). The coats of arms with the symbols of the Florentine Republic are painted on plaster [1]. The Loggia dei Lanzi (Fig. 21.4b) was built between 1376 and 1383 to accommodate the people's assemblies and public ceremonies; it was initially known as Loggia dei Priori or "dell'Orcagna", from the name of the artist who is thought to have designed it. Although it is a gothic building, the anticipation of the Renaissance style is already present in the round arches (Fig. 21.4b). From the sixteenth century, and in the following centuries, this space was destined to accommodate the bronze Perseus (by Benvenuto Cellini) and marble sculptures, dating back to the classical age, the Mannerist period and the nineteenth century, thus becoming one of the first exhibition spaces in the world.

The Palazzo Uguccioni (Fig. 21.4c) constitutes an exception in the context of the Medici city, as it is the only private building of that century exhibiting columns in relief on the façade. According to historical sources, the drawings of the project had origin in Rome (1549); anyway, some elements are also found in Florentine works and attributable to Raffaello and Michelangelo, while others date back to local tradition. The importance given to the architecture of the building is related to the arrangement of the Piazza della Signoria as commissioned by Cosimo I to increase its decor. The palace, realized in Pietraforte sandstone, is characterized by a base made of ashlar drawing three arches. The base is surmounted by two overlapping orders of semi-columns, Ionic (first level), and Corinthian (second level). Above the entrance door there is the marble bust of Francesco I de' Medici, attributed to Giambologna.

The described monuments are characterized by the Pietraforte sandstones used mainly as cladding material of most of the Florentine palaces due to its high resistance, while Pietra Serena sandstone has been widely used for decorative purposes due to its high ductility but low durability. The main differences between the two sandstones consist in a very fine grain size crossed by veins of calcite and presence of convoluted laminations in the Pietraforte sandstone, while the Pietra Serena sandstone, characterized by a medium coarse grain size, is more compact.

21.2.1 The Pietra Serena Sandstone

This sandstone (Macigno and Mt. Modino Formation) is dated to the upper Oligocene—lower Miocene. It is a quartz-feldspatic-micaceous sandstone in layers of different thickness (1–5 m) separated by thin levels of shales and siltites. The
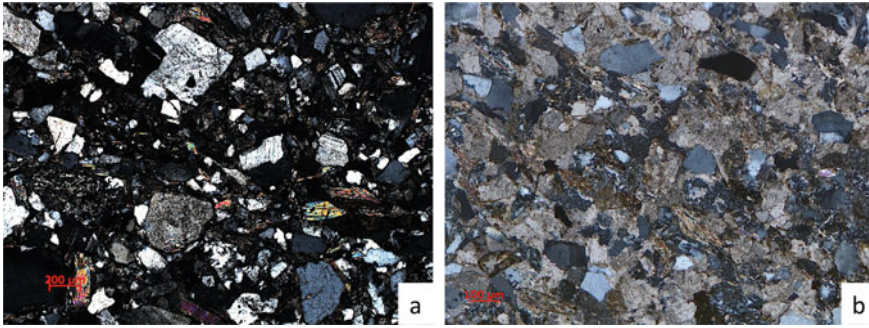
Fig. 21.5 Photomicrographs of thin section in crossed polarized light of **a** Pietra Serena sandstone, **b** Pietraforte sandstone. Images are from the PWA [1]

mineralogical composition consists of quartz, feldspars, fragments of metamorphic and magmatic rocks, muscovite, and biotite often transformed into chlorite; the sandstone is rich in clay matrix with a low amount of carbonatic cement (calcite) [5]. The sandstone is classified as a lithic arkose [6]. Figure 21.5a shows the typical aspect of this rock observed in thin section at the polarized microscope. Already employed in the Etruscan and Roman periods, it was used in Florence mainly during the Renaissance, for flooring, stairways, squares, columns, pilasters, cornices, and other decorative architectural elements.

21.2.2 The Pietraforte Sandstone

This turbiditic sandstone, belonging to the external Ligurian Domain, is dated to the Late Cretaceous. It is a feldspathic and carbonatic quartz sandstone; it occurs in thin layers (20–100 cm) alternated with silty argillites. The Pietraforte sandstone is mainly constituted by a clastic component made of quartz, feldspars, carbonate grains, and fragments of sedimentary, low-grade metamorphic, and acidic effusive rocks. The binder consists of recrystallised micritic calcite, a little amount of clay minerals, and a secondary calcite cement [7]. The sandstone is classified as a lithic arenite [6]. Figure 21.5b shows the aspect of this rock, observed in thin section by a polarized microscope. It was the most used building material in the mediaeval Florence, in ashlars of various sizes. The use continued during the Renaissance, also for the road paving.

21.3 Searching for Three-Colours Decorated Churches

The suggested walk (number 2, Fig. 21.2) starts from the Basilica di Santa Maria Novella (Fig. 21.6a), located in the homonymous square, continues in Piazza del Duomo where the Cattedrale di Santa Maria del Fiore is located, and ends in Piazza Santa Croce, where it is possible to admire the Basilica di Santa Croce.

The Basilica di Santa Maria Novella (XIII-XV centuries) is an important dominican religious and cultural centre. Its construction began in 1242 in the place where the small church of Santa Maria delle Vigne already existed. The project, according to controversial sources, is attributed to two Dominican monks, fra' Sisto da Firenze and fra' Ristoro da Campi, but fra' Jacopo Passavanti and fra' Jacopo Talenti also seems to have taken part in the building construction. The typically Renaissance façade in white Apuan marble, serpentinite, and red marly limestone was started already at the end of the thirteenth century; the tombs, the Gothic side doors, the ornamentation with panels, the blind arches up to the first cornice, and the rose window were placed during the sixteenth century. The façade was completed at the end of the fifteenth century by Leon Battista Alberti [1].

The Cattedrale di Santa Maria del Fiore (Piazza del Duomo; Fig. 21.6b) is the third church in width in the world (after San Pietro in Roma and Saint Paul in London). The cathedral is part of the great monumental complex of Santa Maria del Fiore which comprehends the namesake cathedral, the baptistery, and the Giotto bell tower. It lies on the foundations of the ancient cathedral of Florence, the small church of Santa Reparata. The first stone was laid on September 1296, on a project by Arnolfo di Cambio and it was consecrated to Santa Maria del Fiore in 1412. The different styles (Gothic, Renaissance, Neogothic) present in this church testify to the variation of
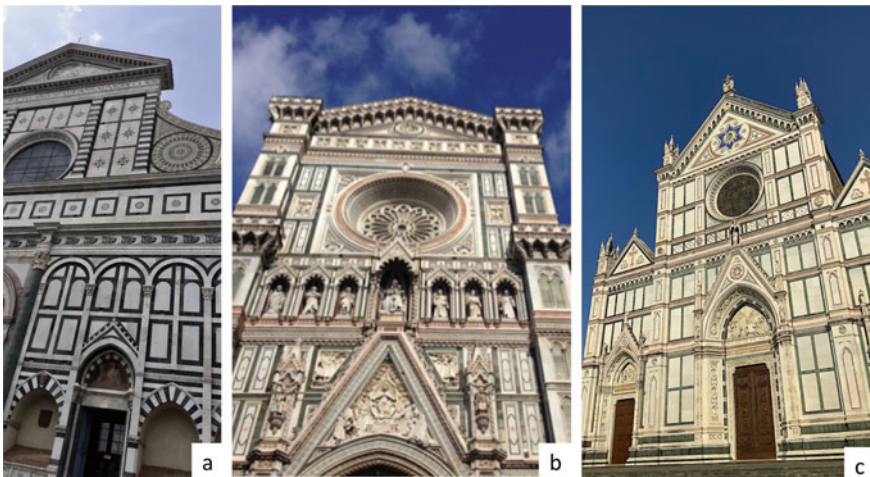
Fig. 21.6 Three-colours façades of **a** Santa Maria Novella, **b** Santa Maria del Fiore, **c** Santa Croce churches. Images are from the PWA [1]

the architectural tastes that occurred in the long period between its foundation and completion. The façade of the cathedral, by Emilio de Fabris, in polychrome stones, is from the modern era, dating back to 1884, and it represents an important example of Neogothic style in Italy. The base of the cathedral is in Pietraforte sandstone like the steps of the north side. The cupola is covered by red tiles made of brick, the ribs and the lantern are in Apuan marble; the two-colours coating of the drum consists of Apuan marble and serpentinite; the upper part of the drum is in Pietraforte sandstone [1].

The Basilica di Santa Croce (Fig. 21.6c) is one of the largest Franciscan churches and it is considered an example of Gothic style. The original complex dates back to the thirteenth century; the initial nucleus was enlarged, under the guidance of Arnolfo di Cambio; the works began in 1294 and lasted until 1385. The façade, however, remained incomplete and was built, in Neogothic style, by Niccolò Matas in the period 1853–1863; on the façade are remarkable the three lunettes of the portals, which recall the legend of the Vera Croce, to which the church is dedicated. The bell tower was built by Gaetano Baccani in 1847. The basilica is famous also because hosts the tombs of many important people such as Michelangelo Buonarroti, Galileo Galilei, Niccolò Machiavelli, Vittorio Alfieri, Ugo Foscolo, and Gioacchino Rossini. The claddings and the statues of the façade are realized in white Apuan marble; the decorations are made of Apuan marble and Sassetta ammonitic red limestone and red marly limestone; the frames and decorative strips at the base of the façade are in serpentinite; the coats of arms are in white and yellow Montagnola Senese marble. The side parts are in Pietraforte sandstone and plaster. The bell tower is in Pietraforte sandstone [1].

These three churches display an external revetment realised through the use of three colours, white, red, and green. The used rocks are Apuan marble, red limestones (ammonitic and marly limestones), and serpentinite, respectively.

21.3.1 Apuan Marble

Marble is a metamorphic carbonatic rock deriving from a sedimentary protolith having a limestone composition. The mineralogical composition of the Apuan marble is characterized by high content of calcite (> 95%); in some cases, dolomite is also present. In addition, various accessory minerals (quartz, albite, pyrite, mica) and pigments, which are responsible of the different varieties of Apuan marbles, can be found. Figure 21.7a shows the typical aspect of an Apuan marble observed in a thin section by a polarized microscope. The marble shows omeoblastic or heteroblastic micro-structure depending on the quarries of provenience [2]; the contacts among the calcite crystals can be rectilinear, lobate, sutured; granulometry and porosity of the rock display wide variability. Most of the marble used in Florence comes from the Apuan Alps, in Italy. The metamorphic event responsible for the marble formation occurred during the Oligocene–Miocene (27–10 Ma before present) at a temperature of 300–450 °C and a pressure of 5–6 Kbar. The extractive history of the
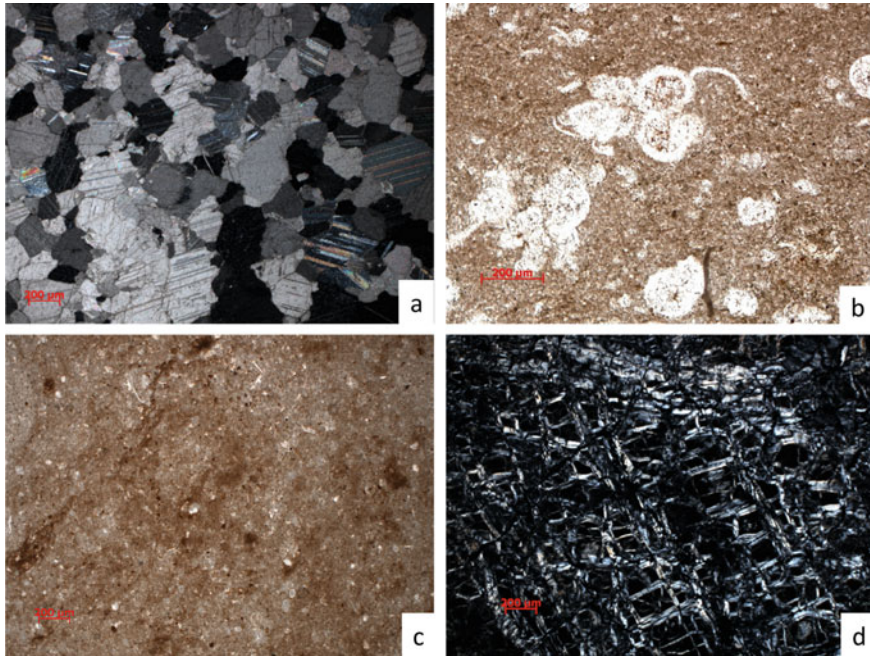
Fig. 21.7 Photomicrographs of thin sections of rocks observed in crossed polarized light. **a** Apuan marble, **b** Red ammonitic limestone, **c** Red marly limestone, **d** Serpentinite. Images are from the PWA [1]

Apuan marble began in Roman times when it was mainly used in the monumental architectures. The extraction continued over the centuries, due to the wide use of this rock in the decoration of many religious buildings, mainly Christian. During the Renaissance, the Apuan marble became a real distinctive feature of statuary art, with the consecration by Michelangelo of a lithotype that still today represents a real territorial excellence.

21.3.2 Red Ammonitic Limestone

The red ammonitic limestone belongs to the Red Ammonitic Formation of the Tuscan Series (Lower Jurassic). It is a sedimentary rock of chemical/clastic origin; it can be classified as a pelagic limestone more or less ammonitiferous or marly and nodular with haematitic pigment in variable concentration [8–11]. The rock consists of well stratified homogeneous calcareous layers, mostly pink or grey-pink in colour, and calcareous layers with a heterogeneous red to dark red colour and characteristic nodular appearance; the presence of wide-sized calcite veins and stilolitic joints containing clay minerals, iron oxides, and quartz crystals is evident. Figure 21.7b

shows the photomicrograph of this rock observed in crossed polarized light. This rock outcrops in several provinces of the Tuscany region and mainly in the area of Pistoia, Livorno, Pisa, Lucca, and Grosseto. The red ammonitic limestone is a material of great ornamental effect, used in Tuscany since the Renaissance period until the nineteenth century, in interiors and exteriors, mainly in religious architecture.

21.3.3 Red Marly Limestone

The red marly limestone belongs to the Tuscan Scaglia Formation of the Tuscan non-metamorphic sequence (Upper Cretaceous– Paleogene); it consists of several members including the "Marne del Sugame" member, where marly limestones of different colours, from dark red to grey-green, can be found. The red marly limestone is a sedimentary rock of clastic origin; it can be classified as a turbiditic micrite due to the presence of clay components and ferruginous pigment. Microfossiliferous content is evident. Bioturbations and thin veins of calcite are frequent; they differ from the surrounding mass for higher crystalline grain and the lack of pigment [9, 11]. Figure 21.7c shows the photomicrographs of this rock as observed in thin section under the petrographic microscope. As well as the red ammonitic limestone also this sedimentary rock comes from several outcroppings in the Tuscany region (e.g. Florence, Pistoia, Grosseto). This limestone, of ornamental effect, has been used both indoors and outdoors, mainly in Tuscan religious architecture from the Renaissance to the nineteenth century.

21.3.4 Serpentinite

In Italy, the serpentinite outcrops occur in the Alps and the Apennines. The serpentinite used in the Florentine architecture has been historically referred to the Ophiolitic Complex (Northern Apennine), outcropping in Tuscany in different localities such as Impruneta, Prato, Pistoia, Siena, and Volterra [12]. Serpentinite is a metamorphic rock forming at low (100 °C) to intermediate (700 °C) temperature, in many different geologic settings, by the hydration of olivine- and pyroxene-rich ultramafic rocks (peridotites). This rock consists mostly of serpentine-group minerals (antigorite, lizardite, and chrysotile), and subordinately, by magnetite, brucite, talc, calcite, and magnesite. During the serpentinisation process, the primary Mg-rich minerals (olivine, orthopyroxene, and clinopyroxene) are replaced by serpentine-group minerals. In Fig. 21.7d, the typical aspect of the serpentinite as observed in thin section and crossed polarized light is shown. The rock, with its typical bastite and mesh texture, is characterized by fine-grained serpentinitic minerals, in which chrysotile is recognisable in cross-fibre veins. Ghosts of pyroxenes are present together with accessory minerals as magnetite and spinel. This rock, worldwide used since ancient times for ornamental and building purposes, was employed in Tuscany

for the first time during the Middle Age. The so-called "Verde di Prato" represents one of the characteristic lithotypes of Florence architecture.

21.4   Hunting for Little Used Polychrome Materials

In addition to the main and widespread rocks described above, other rocks little used but no less interesting are noteworthy. The walk (number 3, Fig. 21.2), starting from the Colonna di San Zanobi and continuing to the Fontana del Nettuno, and to the Colonna della Giustizia, allows to observe some of these rocks.

The Colonna di San Zanobi (Fig. 21.8a) stands in Piazza San Giovanni, in front of the North door of the Battistero di San Giovanni. According to some historical sources, the column is a reconstruction of 1334; the terrible flood of 1333 that swept away all the bridges of Florence, inexorably destroyed it; other sources report that the column is the original, dated to the second half of the twelfth century; accordingly, the column was only restored after being overwhelmed by the flood of the Arno river. The column was built in the same place where a miracle, linked to the cult of San Zanobi, occurred; during the moving of the San Zanobi relics to Santa Reparata, a dry elm, in the middle of winter, at the contact with the sarcophagus, would be miraculously revived. In 1338, the column was crowned with the cross at the top, and in 1375, an inscription, recalling the legend of San Zanobi, was added. To date, the cross and the original pedestal are housed inside the Museo dell'Opera del Duomo, while above the column, there is a fibreglass copy. The column is made of Greek marble (Cipollino/Carystium) [1].

The Fontana del Nettuno (Fig. 21.8b), locally called "il Biancone", is located in Piazza della Signoria and represents the monument celebrating the power of Cosimo

Fig. 21.8   a Colonna di San Zanobi; **b** Fontana del Nettuno; **c** Colonna della Giustizia. Images are from the PWA [1]

I de' Medici as well as the maritime domain of Florence. The first project of the fountain was due to Baccio Bandinelli in 1549. At the death of Bandinelli, in 1560, Bartolomeo Ammannati took over the work that continued until 1565 when the fountain was inaugurated. In 1575, the bronze sculptures (attributed to Giambologna but, according to other sources, made by Ammannati and his assistants) of marine divinities (Doride, Teti, Oceano and Nereo), all flanked by pairs of satyrs and nymphs and the marble parts of the tub, were completed. The fountain is characterized by a large octagonal tub with bronze sculptures and many decorative elements along the edges. The statue of Nettuno, the tritons, the chariot, two horses, and the decorations on the tub are in Apuan marble; the tub and the other two horses are in Breccia di Seravezza. The marine divinities, the satyrs, and nymphs are in bronze [1].

The Colonna della Giustizia (Fig. 21.8c) was placed in Piazza Santa Trinita by order of the Grand Duke Cosimo I de' Medici to symbolise the virtues and glory of his family. It came from the monumental swimming pool of the Terme di Caracalla in Rome, and was donated by the Pope Pius IV to Cosimo I. It is a large monolithic column, 11.2 m high and weighing about 50 tons, arrived in Florence after a long journey, which lasted one year. The column was dedicated to Justice and, for this reason, at its top was placed a statue of Justice, originally made of wood and terracotta, then replaced by another made of ancient red porphyry. The processing of granite lasted about eleven years; six blocks, probably coming from ancient Roman columns, were assembled together to realize the statue (1581). The base of the column is obtained by using the Breccia di Seravezza and marble stones; the stem is made of granite; the Statua della Giustizia is made of red porphyry, an igneous silica-rich rock, containing large crystals of feldspar and quartz; the cloak is realised in bronze [1].

21.4.1 Carystium Marble

This metamorphic rock is an impure chlorite marble. It displays a light green or grey and yellowish background furrowed by veins, dark green to grey-blue in colour, with wavy shininess or parallel plane of variable thickness. Figure 21.9a shows the photomicrographs of this marble observed in thin section by crossed polarized light; a preferred orientation of elongated crystals and a heteroblastic micro-structure are evident. The quarry locations are in Greece, in southern Eubea. This marble was imported to Rome in the first century [13, 14].

21.4.2 Breccia Di Seravezza

The rock belongs to the Breccia di Seravezza Formation which is part of the metamorphic Tuscan Units. It is a polygenic breccia that has undergone low-grade metamorphism. Marble and dolomitic clasts of variable dimensions are generally set in
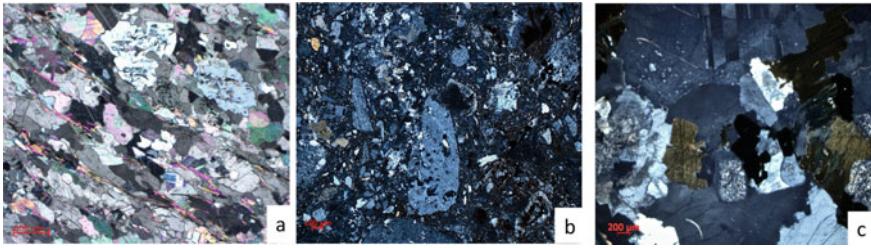
Fig. 21.9 Photomicrographs of thin sections of rocks observed in crossed polarized light. **a** Carystium marble (courtesy of Prof. F. Antonelli, IUAV University-Venice, Italy); **b** Breccia di Seravezza; **c** Granite. Images **b** and **c** are from the PWA [1]

a hematitic and filladic chloritoid matrix. The composition is mainly calcitic with a subordinate amount of dolomite; small quantities of pyrite, quartz, hematite, and phyllosilicates are also present. In Fig. 21.9b, the aspect of this breccia observed in a thin section in crossed polarized light is shown. The oldest quarries of this rock, exploited since the Medici time, are in Versilia, in the municipality of Seravezza and Stazzema (Lucca). The so-called Medicean Breccia was largely employed by Cosimo I de' Medici, Lord of Florence, who made this rock the symbol of his power. The Breccia di Seravezza was used in Florence mainly in coatings and interior decorations and for sculptures [15].

21.4.3 Granite

The granitic rocks have been little used in Florence; these rocks mainly come from different localities but, in particular, from different quarries (Mt. Capanne, Pomonte, Cavoli, Sant'Ilario, San Piero, etc.) in the Elba Island (Tuscany) [16]. Granite is a very common type of intrusive igneous rock that represents one of the main components of continental crust; much of it was intruded during the Precambrian age. It derives from the crystallization of magma within the crust where it is well insulated. Granite is a rock (Fig. 21.9c) containing between 20 and 60% of quartz by volume and at least 35% of the total feldspar consisting of alkali feldspar; femic minerals (Fe- and Mg-rich) as micas (mainly biotite) and amphiboles (commonly hornblende) are also present together with accessory amounts of cordierite, granato, apatite, titanite, zircone, allanite, and magnetite. The rock displays a holocrystalline, generally equigranular, faneritic texture (Fig. 21.9c). Crystals appear strictly in contact with each other. Quartz is typically anhedral and colourless, feldspar shows regular, well-developed faces. The word "granite" comes from the Latin granum = grain, with reference to the coarse-grained structure of such a holocrystalline rock. Due to its high hardness and durability, it has gained widespread use throughout human history as a construction stone, a very good material to prepare aggregate, for interior and exterior cladding and several other purposes. Elban granitic rocks are known and

used from prehistory; they were employed during the Etruscan times for artefacts, weapons, tombs, and defensive constructions; during the Roman Imperial time, these rocks were used for big constructions and were exported in the more important cities of the Empire.

References

1. Pecchioni E, Santo AP (2020) Florence RockinArt. https://books.fupress.com/catalogue/florence-rockinart/4343
2. Cantisani E, Pecchioni E, Fratini F, Garzonio CA, Malesani P, Molli G (2009) Thermal stress in the Apuan Marble: Relationship between microstruc-ture and petro physical characteristics. Int J Rock Mech Min Sci 46:128–137
3. Fratini F, Cantisani E, Pecchioni E, Pandeli E, Vettori S (2020) Pietra alberese: building material and stone for lime in the florentine territory (Tuscany, Italy). Heritage 3:1520–1538. https://doi.org/10.3390/heritage3040084
4. Cantisani E, Garzonio CA, Ricci M, Vettori S (2013) Relationships between the petrographical, physical and mechanical properties of some Italian sandstones. Int J Rock Mech Min Sci 60:321–332
5. Fratini F, Pecchioni E, Cantisani E, Rescic S, Vettori S (2015) Pietra Serena: the stone of the Renaissance. In: Pereira D, Marker BR, Kramar S, Cooper BJ, Schouenborg BE (eds) Global heritage stone: towards international recognition of building and ornamental stones, vol 407, no 1. Geological Society, London, Special Publications, pp 173–186
6. Folk RL (1974) The petrology of sedimentary rock. Hemphill Publishing Company, Austin, Texas, 182 p
7. Pecchioni E, Fratini F, Pandeli E, Cantisani E, Vettori S (2020) Pietraforte, the Florentine building material from the middle ages to contemporary architecture. Episodes 44(3):259–271. https://doi.org/10.18814/epiiugs/2020/020087
8. Fazzuoli M, Ferrini G, Pandeli E, Sguazzoni G (1985) Le formazioni giurassico-mioceniche della Falda Toscana a Nord dell'Arno: considerazioni sull'evoluzione sedimentaria. Mem Soc Geol It 30:159–201
9. Malesani P, Pecchioni E, Cantisani E, Fratini F (2003) Geolithology and provenance of materials of some historical buildings and monuments in the centre of Florence (Italy). Episodes 26(3):250–355
10. Abbate E, Fanucci F, Benvenuti M, Bruni P, Cipriani N, Falorni P, Fazzuoli M, Morelli D, Pandeli E, Papini M, Sagri M, Reale V, Vanucchi P (2005) Note Illustrative della Carta Geologica d'Italia alla scala 1:50.000, Foglio 248, La Spezia. APAT, Dipartimento Difesa del Suolo-Servizio Geologico d'Italia, Roma, pp 204
11. Pecchioni E, Magrini D, Cantisani E, Fratini F, Garzonio CA, Nosengo C, Santo AP, Vettori S (2019) 2021: A Non-Invasive Approach for the Identification of "Red Marbles" from Santa Maria Del Fiore Cathedral (Firenze, Italy). Int J Architectural Heritage 15(3):494–504
12. Santo AP, Pecchioni E, Garzonio CA (2018) The San Giovanni Baptistery in Florence (Italy): characterization of serpentinite floor. IOP Conf Ser Mater Sci Eng 364(012069):1–7
13. Lazzarini L (2004) Pietre e Marmi Antichi, Cedam, Padova Italy, 194 p
14. Antonelli F, Lazzarini L, Cancelliere S, Buffone L (2020) The coloured stones and marbles decorating the Odeion of Pompeii. In: 2020 IMEKO TC-4 international conference on metrology for archaeology and cultural heritage Trento, Italy, Oct 22–24

15. Malcom C (1985) Observation on Ammannati's Neptune fountain: 1565 and 1575. In: Morrogh A, Superbi Gioffredi F, Morselli P, Borsook E (eds) Renaissance Studies in honour of Craig Hugh Smyth. II, Giunti, Firenze Italy, pp 113–136
16. Poli G, Peccerillo A (2016) The Upper Miocene magmatism of the Island of Elba (Central Italy): compositional characteristics, petrogenesis and implications for the origin of theTuscany Magmatic Province. Min Petrol 110:421–445